The Role of the Lysine Demethylases

KDM5 and KDM6 in Bone Malignancies



Edward Samuel Hookway

A thesis submitted for the degree of

Doctor of Philosophy

Lincoln College

Nuffield Department of Orthopaedics, Rheumatology and Musculoskeletal Sciences

University of Oxford

Trinity 2016

The Role of the Lysine Demethylases KDM5 and KDM6 in Bone Malignancies

Edward Samuel Hookway

Lincoln College

Doctor of Philosophy, Trinity 2016

ABSTRACT

Methylation of histone lysine residues functions as a dynamic, reversible mechanism for regulating gene expression and aberrations in this process have been linked with the development of cancer. Members of the lysine demethylase (KDM) family remove methyl marks from histones. KDM5B removes methyl marks from histone H3 lysine 4 (H3K4) whereas KDM6A and KDM6B remove methyl marks from histone H3 lysine 27 (H3K27).

In this thesis, GSK-J4, an inhibitor of KDM5B, KDM6A and KDM6B, is shown to impair viability in a range of cancers affecting bone including multiple myeloma, Ewing sarcoma and chordoma. GSK-J4 induces a biphasic transcriptional response, characterized by an early, massive rise in the expression of a number of cysteine-rich metallothionein genes followed by induction of ATF4 via phosphorylation of eIF2α by GCN2. Induction of ATF4 leads to apoptosis in myeloma cells and cell cycle arrest in Ewing sarcoma. Ectopic overexpression of metallothioneins is shown to be sufficient to induce the ATF4 response. GSK-J4 is shown to alters cellular metabolism by impairing glutaminolysis. ChIPseq demonstrates a global increased H3K27me3 in response to treatment with GSK-J4 with a decrease in H3K4me3 around transcription start sites of genes not involved in the ATF4 response. Combined knockdown of KDM6A and KDM6B recapitulates the cellular response to GSK-J4 whereas inhibition of KDM5B is not sufficient to reproduce the effect.

A model is presented suggesting that the increased requirement for incorporation of cysteine into protein due to the expression of metallothioneins leads to the presence of uncharged cysteinyl-tRNA molecules that are sensed by GCN2 leading to activation of an ATF4-driven integrated stress response.

ACKNOWLEDGMENTS

I would like to thank Professor Nick Athanasou and Professor Udo Oppermann for their support and supervision. Thanks also to present and former postdoctoral researchers in the Oppermann group who have helped guide me including James Dunford, Martin Philpott, Deborah Brotherton and Peter Cain. The assistance of Takeshi Kashima, whose untimely illness and death was a great loss to the bone community in Oxford, is also greatly appreciated.

I would also like to extend my thanks to other members of the Oppermann group who have helped with the work of this thesis including but not limited to Laurynas Pliuškys, Graham Wells and Na Wu.

A final word of thanks to all those who supported and encouraged me in my transition away from clinical medicine and into academia.

The work in this thesis has been supported by the Bone Cancer Research Trust.

CONTENTS

Acknowledgments ii

Contents iii

Table of Figures xi

Table of Tables xiv

Abbreviations xiv

Introduction 1

1.1 General Introduction to Epigenetics in Cancer Biology 1

1.1.1 Epigenetics and development 2

1.1.2 Molecular mechanisms of epigenetic regulation 4

1.1.3 DNA structure and organisation 4

1.1.4 Histone modification and the "histone code" 7

1.1.5 DNA base modification 18

1.1.6 Non-coding RNAs 29

1.2 Cancer and bone 32

1.3 Epidemiology and Pathogenesis of Multiple Myeloma 32

1.4 Epidemiology and Pathogenesis of Ewing Sarcoma 41

1.5 GSK-J4 is a small molecule iinhibitor of KDM5B, KDM6A and KDM6B 48

1.6 The lysine demethylase families KDM5 and KDM6 50

1.7 The KDM5 subfamily 50
1.7.1 KDM5B - JARID1B 51
1.8 The KDM6 subfamily 52
1.8.1 KDM6A (UTX) 52
1.8.2 KDM6B (JMJD3) 53
1.9 Outline of thesis 54
2 Materials and methods 55
2.1 Cell Culture 55
2.1.1 Multiple Myeloma cells 55
2.1.2 Ewing Sarcoma Cell Lines 55
2.1.3 Mycoplasma testing 56
2.2 Viability Assay 57
2.3 RNA extraction 57
2.4 cDNA synthesis 57
2.5 Quantitative PCR 58
2.6 Preparation of RNA for microarray expression analysis 58
2.7 Knock-down with Locked Nucleic Acid (LNA) anti-sense molecules 59
2.8 Next Generation Sequencing 59
2.8.1 RNA extraction and library preparation for Next Generation Sequencing ... 59
2.8.2 Chromatin Immunoprecipitation and Next Generation Sequencing 61

2.8.3 Antibodies 62

2.8.4 Library Pooling and Quantification for Sequencing 63

2.8.5 Sequencing 63

2.9 SPRI-beads production 64

2.10 Flow cytometry methods 64

2.10.1 Cell cycle analysis – Propidium iodide staining. 64

2.10.2 Apoptosis Detection – Annexin V 65

2.10.3 Cellular proliferation – BrdU incorporation 65

2.11 Buffers 65

2.12 Chapter 3 specific methods 66

2.12.1 Screening of the ability of small molecule inhibitors of chromatin enzymes to reduce cell viability 66

2.12.2 IC_{50} determination 67

2.12.3 Microarray analysis of transcriptomic response to GSK-J4 67

2.12.4 Motif analysis of promoter region 68

2.12.5 Analysis of the Integrated stress response 68

2.12.6 Fluorescence microscopy to measure free intracellular zinc 68

2.13 Chapter 4 specific methods 69

2.13.1 ATP assay 69

2.13.2 Determination of NADP(H) levels 69

2.13.3 Oxygen consumption assay 69

2.13.4 Glutamate dehydrogenase activity assay 70

2.13.5 Metabolomic analysis by Nuclear Magnetic Resonance spectroscopy 70

2.14 Chapter 5 specific methods 71

2.14.1 Quantitative ChIP sample preperation 71

2.14.2 Quantitative ChIP data processing 71

2.14.3 RNAseq data processing 72

2.14.4 Motif analysis and GO analysis 72

3 Cell based screening and identification of GSK-J4 as a potent inhibitor of bone cancer viability 73

3.1 Overview 73

3.2 Introduction 74

3.2.1 Cell based screening using a focused library of small molecule inhibitors against epigenetic target classes 74

3.2.2 Locked Nucleic Acids 76

3.2.3 Activating Transcription Factor 4 (ATF4) and the integrated stress response 77

3.3 Results 80

3.3.1 A screen of small molecules identifies GSK-J4 as reducing cell viability in cancers of bone 80

3.3.2 GSK-J4 has an IC_{50} in the low micromolar range in cancer cell lines 83

3.3.3 GSK-J4 reduces viability in patient-derived primary tissue 85

3.3.4 Treatment with GSK-J4 results in apoptosis in myeloma cells and a cell cycle arrest in Ewing sarcoma 91

3.3.5 GSK-J4 induces an ATF4 and metallothionein transcriptomic response 93

3.3.6 The transciptomic response to GSK-J4 observed in the microarray is consistent across a range of myeloma and Ewing sarcoma cell lines. 96

3.3.7 Locked Nucleic Acids are taken-up by multiple myeloma cells 97

3.3.8 Simultaneous targeting of KDM6A and KDM6B by LNAs recapitulate the phenotypic effect of GSK-J4 in JJN3 cells 98

3.3.9 GSK-J4 acts through ATF4 activation 102

3.3.10 GSK-J4 activates the ATF4 pathway via the stress kinase GCN2 105

3.3.11 Intracellular free zinc increases in response to GSK-J4 108

3.3.12 Overexpression of metallothioneins induces the ATF4 response 108

3.4 Discussion 113

4 GSK-J4 reprograms cellular metabolism and inhibits glutamine utilization 117

4.1 Overview 117

4.2 Introduction 118

4.2.1 Metabolism in cancer 118

4.2.2 Metabolic profiling using Nuclear Magnetic Resonance 120

4.3 Results 122

4.3.1 GSK-J4 reduces cellular ATP levels, alters the ratio of NADPH:NADP+ and induces reactive oxygen species. 122

4.3.2 GSK-J4 reduces cellular oxygen consumption 123

4.3.3 GSK-J4 treatment leads to an accumulation of intracellular glutamine with a decreased level of glutamate 124

4.3.4 Glutaminolysis is inhibited by GSK-J4 126

4.3.5 Dimethyl-2-oxoglutarate temporarily rescues cells from the effect of GSK-J4 128

4.3.6 GSK-J4 induces different metabolic changes compared to conventional myeloma treatments 129

4.3.7 The glutaminase inhibitor compound 968 does not mimic the effect of GSK-J4 129

4.3.8 GSK-J4 does not directly inhibit enzymes involved in glutaminolysis 130

4.3.9 GSK-J4 causes transcriptional changes in genes associated with metabolism as measured by qPCR 131

4.4 Discussion 133

5 GSK-J4 globally alters H3K4me3 and H3K27me3 as measured by ChIPseq 137

5.1 Overview 137

5.2 Introduction 137

5.2.1 Chromatin precipitation and next generation sequencing 137

5.2.2 Epigenetic data visualization 140

5.3 Results 142

5.3.1 Draft assembly of the SF9 genome 142

5.3.2 GSK-J4 causes a global increase in H3K27me3 144

5.3.3 GSK-J4 causes a generalized decrease in H3K4me3 with sparing of ATF4 target genes 145

5.3.4 RNAseq confirms a large induction of metallothioneins and ATF4 response 150

5.4 Discussion 156

6 Specific inhibition of KDM5B in multiple myeloma cell lines 160

6.1 Overview 160

6.2 Introduction 160

6.3 Results 164

6.3.1 Inhibition of KDM5B inhibits myeloma cell line MM1S proliferation 164

6.3.2 Inhibition of KDM5B does not inhibit proliferation in other myeloma cell lines. 165

6.3.3 Inhibition of KDM5B leads to cell cycle arrest and does not induce apoptosis in MM1S multiple myeloma cells 165

6.3.4 Inhibition of KDM5B causes a global increase in H3K4me3 in MM1S cells 166

6.4 Discussion 169

7 Discussion and Future Perspectives 171

8 References 176

9 Appendices 234

9.1 List of Primers 234

9.2 Code for heatmap function 237

9.3 H3K4me3 peaks near Transcription start sites not downregulated 238

9.4 Publications 244

TABLE OF FIGURES

Figure 1 Post-translational modification of histone tails 8

Figure 2 Phylogenetic tree of the human iron and 2-oxoglutarate dependent oxyygenases 16

Figure 3 Mechanisms of action of lysine demethylases 18

Figure 4 Cytosine base modification 28

Figure 5 microRNA processing 31

Figure 6 Structures of GSK-J4 and related molecules..... 48

Figure 7 Overview of KDM5 and KDM6 protein archtecture 50

Figure 8 Structure of a Locked Nucleic Acid 76

Figure 9 Translation Regulation of ATF4 78

Figure 10 Small molecule screening in cancer cell lines. 81

Figure 11 Viability of cancer cell lines treated with GSK-J4 or GSK-J5..... 82

Figure 12 GSK-J4 inhibits proliferation in Ewing Sarcoma..... 82

Figure 13 Dose response curves for GSK-J4 and GSK-J5 in Ewing Sarcoma..... 83

Figure 14 GSK-J4 reduces viability in primary Ewings cells 87

Figure 15 GSK-J4 decreases primary myeloma cell viability. 88

Figure 16 Histology of Melanocytic Neuroectodermal Tumour of Infancy..... 90

Figure 17 GSK-J4 reduces viability in Melanotic Neuroectodermal Tumour of Infancy ... 91

Figure 18 Cell cycle analysis and induction of apoptosis in JJN3 and TC71 cells 92

Figure 19 Microarray analysis of the transcriptional response to GSK-J4 in myeloma and Ewings cells. 94

Figure 20 Motif analysis of promoter region of genes regulated by GSK-J4..... 95

Figure 21 qPCR validation of genes identified by microarray 97

Figure 22 Locked Nucleic Acids are taken-up by JJN3 myeloma cells 98
Figure 23 LNA screening targeting KDM6A and KDM6B 100
Figure 24 Correlation between knockdown of KDM5 and KDM6 family members 101
Figure 25 LNAs targeting KDM5B 102
Figure 26 Induction of ATF4 in response to treatment with GSK-J4 103
Figure 27 ISRIB attenuates the ATF4 response to GSK-J4 103
Figure 28 Knockdown of ATF4 reduces the phenotypic response to GSK-J4 104
Figure 29 GSK-J4 does not activate ATF4 through PERK or PKR 105
Figure 30 Knockdown of GCN2 with LNAs 106
Figure 31 LNAs targeting GCN2 reduce the cellular response to GSK-J4 107
Figure 32 GSK-J4 causes a transient increase in free intracellular zinc 108
Figure 33 Time course of transcriptional response to GSK-J4 in JJN3 cells 109
Figure 34 Plasmid map containing the “metallothionein ubergene”. 110
Figure 35 Expression of the “metallothionein ubergene” (4xMT) induces the ATF4 response 111
Figure 36 Metallothionein ubergene expression induces an ATF4 response 111
Figure 37 GSK-J4 reduces intracellular ATP content 122
Figure 38 GSK-J4 increases cellular reactive oxygen species 123
Figure 39 GSK-J4 reduces oxygen consumption 124
Figure 40 GSK-J4 causes changes in metabolites in JJN3 myeloma cells 125
Figure 41 Alteration of metabolic pathways in JJN3 upon GSK-J4 treatment 127
Figure 42 Dimethyl-2-oxoglutarate protects cells from GSK-J4 effects and metabolic perturbations after inhibitor treatments 128

Figure 43 GSK-J4 does not inhibit glutamate dehydrogenase activity 131
Figure 44 Expression level of metabolomic enzymes changes with GSK-J4 treatment ... 132
Figure 45 Hilbert Curves of increasing interation 141
Figure 46 Statistics of draft assembly of SF9 genome 143
Figure 47 Hilbert Visualization of H3K27me3 coverage in JJN3 cells 144
Figure 48 Hilbert Visualization of fold-changes in H3K27me3 coverage. 145
Figure 49 GSK-J4 reduces H3K4me3 coverage 146
Figure 50 ChIP profiles of the metallothionein cluster and ASS1 148
Figure 51 H3K4me3 and RNAseq coverage around the metallothionein cluster and ASS1 149
Figure 52 MA plot of changes in gene expression 151
Figure 53 Volcano plot of regulated genes 152
Figure 54 Gene Ontology analysis of regulated genes 153
Figure 55 Increased expression of KDM5B is associated with lower overall survival in multiple myeloma 161
Figure 56: Structures of KDM5-C49 and KDM5-C70 162
Figure 57 Structure of KDOAM25 162
Figure 58: Dose-response curves of KDOAM25 and KDM5-C70 in MM1S cells..... 164
Figure 59: Dose response curves for KDOAM25 in other myeloma cell lines. 165
Figure 60 Inhibition of KDM5B causes cell cycle arrest in MM1S cells..... 166
Figure 61 KDOAM25 increases H3K4me3 in MM1S myeloma cells 167
Figure 62 Increased H3K4me3 at transcription start sites in KDOAM25 treated MM1A. 168

TABLE OF TABLES

Table 1 Risk stratification in patients with multiple myeloma 35

Table 2 Translocations observed in multiple myeloma 37

Table 3 Chromosomal translocations found in Ewing Sarcoma 43

Table 4 Small molecules used in cell-based screening. 75

Table 5 IC50 value for GSK-J4 in various cancer cell lines 84

Table 6 Statistics of draft assembly of SF9 genome 143

Table 7 50 top upregulated genes 154

Table 8 50 top downregulated genes 155

Table 9 IC_{50} values of compounds against KDM family members 163

ABBREVIATIONS

5AZA	5-aza-2'deoxycytidine
5-caC	5-carboxylcytosine
5-fC	5-Formylcystosine
5-hmC	5-Hydroxymethylcytosine
5-mC	5-Methylcytosine
7AAD	7-aminoactinomycin
A	Adenine
AID	Activation-Induced Deaminase
AML	Acute Myeloid Leukaemia
ARID	AT-Rich Interaction Domain
ASCT	Autologous Stem Cell Transplant
ASH2L	ASH2-like Histone Lysxtine Methyltransferase Complex Subunit
ASNS	Aspargine Synthetase
ASS1	Arginosuccinate Synthetase
ATF4	Activating Transcription Factor 4
ATP	Adenosine Triphosphate
BCR	B Cell Receptor
BRD4	Bromodomain Containing Protein 4

BTZ	Bortezomib
C	Cytosine
CBX	Chromobox Protein
ChIP	Chromatin Immunoprecipitation
ChIPseq	Chromatin Immunoprecipitation followed by Next Gen Sequencing
CNS	Central Nervous System
CRBN	Cereblon
CRL4	Cullin-RING E4 Ubiquitin Ligase 4
D2HG	D-2-Hydroxygluterate
D2OG	Dimethyl-2-Oxogluterate
DDIT3	DNA Damage-Induced Transcript 3
DMSO	Dimethylsulfoxide
DNA	Deoxyribose Nucleic Acid
DNMT	DNA Methyltransferase
DPPA4	Development Pluripotency Associated 3
ECM	Extracellular Matrix
eIF2α	Eukaryotic Initiation Factor 2α
ESFT	Ewing Sarcoma Family of Tumours
EZH1/2	Enhancer of Zeste 1/2
FAD	Flavin Adenine Dinucleotide
FGFR	Fibroblast Growth Factor Receptor
G	Guanine
GCN2	General Control Nonrepressible 2 (EIF2AK4)
GDH	Glutamate Dehydrogenase
GLS1/2	Glutaminase 1/2
GLUL	Glutamate Ammonia Ligase
GO	Gene Ontology
Gol3P	Glycerol-3-Phosphate
GTP	Guanosine Triphosphate
H2A	Histone 2A
H2B	Histone 2B
H3	Histone 3
H4	Histone 4
HAT	Histone Acetyltransferase
HDAC	Histone Deacetylase
HDACi	Histone Deacetylase inhibitor
HSC	Haematopoietic Stem Cells
IDH1/2	Isocitrate Dehydrogenase 1/2
ISS	International Staging System
JmjC	Jumonji-domain containing
JMJD3	Jumonji-domain containing 3 /KDM6B
KDM	Lysine Demethylase
KMT	Lysine Methyltransferase

LNA	Locked Nucleic Acid
lncRNA	long non-coding RNA
LOX	Lysyl Oxidase
MBD	Methyl-CpG Binding Domain
MGUS	Monoclonal Gammopathy of Undetermined Significance
miRISC	mi-RNA Induced Silencing Complex
miRNA	microRNA
MLL	Mixed Lineage Leukaemia
MM	Multiple Myeloma
MNTI	Melanotic Neuroectodermal Tumour of Infancy
mRNA	messenger ribose nucleic acid
MT1X	Metallothionein 1X
NAD+	Nictonamide Adenine Dinucleotide
NADPH	Nictonamide Adenine Dinucleotide Phosphate
ncRAN	Non-coding RNA
NMC	NUT Midline Carcinoma
NMR	Nuclear Magnetic Resonance
nuRD	Nuclear Remodeling Deacethylase
NUT	Nuclear Protein in Testis
OCR	Oxygen Consumption Rate
PBS	Phosphate Buffered Saline
PcG	Polycomb Group
PCK2	Phosphoenolpyruvate carbokinase 2
PCNA	Prolifating Cell Nuclear Antigen
PERK	Protein Kinase R-like ER Kinase
PET	Positron Emission Tomography
PHD	Plant Homeodomain
PI	Propidium Iodide
piRNA	piwi-interacting RNA
PKR	Protein Kinase R
PNET	Peripheral Neuroectodermal Tumour
PRC1/2	Polycomb Repressive Complex 1/2
P-TEFb	Positive-Transcription Elongation Factor b
qPCR	Quantitative PCR
RBBP5	Retinoblastoma Binding Protein 5
RIN	RNA Integrity Number
RING1A/1 B	Ring FingerProtein 1A/1B
R-ISS	Revised International Staging System
RNAse H	Ribonuclease H
RNAseq	RNA sequencing
RPM	Read Per Million Mapped Reads
SAM	S-Adenosyl Methionein

SEM	Standard Error of the Mean
SGC	Structural Genomics Consortium
SMM	Smoldering Multiple Myeloma
T	Thymine
TCA	Tricarboxylic Acid
TDG	Thymidine DNA Glycosylase
TET	Ten-Eleven Translocation
TP53	Tumour Protein P53
TPM	Transcripts Per Million
tRNA	Transfer RNA
TxG	Trithorax Group
uORF	Upstream Open Reading Frame
UTX	Ubiquitously-Transcribed X Chromosome Tetratricopeptide Repeat Protein/KDM6A
VCAM1	Vascular Cell Adhesion Molecule 1
WDR5	WD repeat Domain 5
WHSC1	Wolf-Hirschorn Syndrome Candidate 1/ MMSET
XBP-1	X-Box Protein 1
XIST	X-Inactivation Specific Trnascript

INTRODUCTION

1.1 GENERAL INTRODUCTION TO EPIGENETICS IN CANCER BIOLOGY

The classical paradigm in cancer biology has been that a change in DNA leads to an alteration of the transcribed mRNA resulting in a change of function of a protein that contributes to the development of the cancer phenotype with its characteristic hallmarks such as proliferative signalling, evasion of growth suppression, resistance to cell death, replicative immortality, angiogenesis, and metastasis (Hanahan and Weinberg 2000). For example, the underlying change in the DNA can include point mutations that lead to either a gain of function in an oncogene, such as the V600E mutation in *BRAF* causing increased kinase activity in some melanomas (Kumar et al. 2004); deletions of DNA leading to the loss of tumour suppressor genes such as *TP53*; or chromosomal translocations resulting in the expression of fusion proteins that drive cancer development as in Ewing Sarcoma (Delattre et al. 1992).

In addition, dysregulated expression of a normal protein without any underlying DNA mutation is implicated in cancer development and maintenance of cancer. A cell that inappropriately does not express a functioning tumour suppressor is equivalent to a cell expressing a mutant tumour suppressor, which has lost its activity: in both examples the cells are lacking a functional protein.

Epigenetics is now recognized as an important contributor to cancer and depicts a broad term that encompasses many diverse processes that are important within the cell for regulating the level of expression of genes and controlling the phenotype of the cell. The term derives from

the Greek "epi" meaning "above" or "over" and signifies the position of epigenetics being "above the genome" and in a position to control gene expression. The term “epigenetics” wasloosely defined at a Cold Spring Harbour conference as a "stable, heritable phenotype that is not caused by a change in the underlying DNA sequence" (Berger et al. 2009), However, it is often used to describe modifications of DNA and chromatin, chromatin remodelling and interactions with non-coding RNAs.

In this chapter I will describe underlying molecular and structural biology behind epigenetic processes and discuss the implications of these mechanisms in cancer biology.

1.1.1 Epigenetics and development

With the exception of gamete cells produced by meiosis and immune cells that have undergone somatic recombination, every cell in the body contains the same DNA sequence from the moment of conception until death. Despite containing the same DNA 'blueprint', an individual eukaryotic organism displays many different cell types with different transcriptional profiles over its life span. Recent advances in sequencing technology have allowed the transcriptomes of individual cells to be accurately recorded and this has demonstrated that at any given time only a small proportion of the genome is being actively transcribed (Djebali et al. 2012). Therefore, it is clear that mechanisms exist, which tightly control gene expression both in a cell-type specific and a temporal manner.

Many insights into this process of gene expression control have been gained from the study of embryogenesis and developmental biology. All cells are derived from the zygote and within five days the undifferentiated totipotent cells of the morula give rise to distinct cell populations in the blastocyst of the trophopblast and pluripotent cells of the inner cell mass and trophoblast (De Paepe et al. 2014). As embryogenesis progresses, cells becoming

increasingly differentiated and specialised, losing their ability to differentiate into any cell type. Multipotent stem cells, such as the mesenchymal stem cell, are able to differentiate into a limited number of related cell types (Kokabu, Lowery, and Jimi 2016) whereas terminally differentiated cells have lost the ability to change into any other cell type under normal physiological conditions.

The developmental biologist C H Waddington developed the metaphor of the "epigenetic landscape" to describe the process of cell differentiation (Waddington 1942). He imagined a hill with many valleys, representing different epigenetic changes, with a ball at the top representing an undifferentiated cell in its totipotent state. As the ball rolls down the hill into a valley it loses the ability to cross over into other valleys, indicating the increasing specialisation and differentiation of the cell, until it finally comes to rest at the bottom in a terminally differentiated state. Each differentiated state is intricately associated with a different "landscape" as the nature of the landscape prevents the ball from transitioning into a different valley, just as a cell that has terminally differentiated into a hepatocyte does not spontaneously become a neuron.

One feature associated with the development of cancer is the loss of cellular differentiation where cancer cells lose phenotypic features associated with their cell of origin. Using Waddington's analogy, the epigenetic landscape has changed so the ball is able to escape from its terminally differentiated state at the bottom of a valley. Alterations of epigenetic or chromatin components can be one of the causes of the development of the cancer, as in the case of NUT-midline carcinoma (discussed below), or can be secondary to other driver mutations within the cell. The ability to target epigenetic processes, to change the transcriptomic profile of a cancer cell and cause inappropriately silenced tumour suppressor

genes to become re-expressed or decrease the expression of oncogenes, offers a mechanism for treating cancer cells by targeting the underlying molecular mechanisms that have led to cancer development instead of relying on cytotoxic chemotherapy (Azad et al. 2013).

1.1.2 Molecular mechanisms of epigenetic regulation

The diverse range of epigenetic mechanisms can be split into two broad categories: firstly, mechanisms involving modification to the structure of DNA and chromatin and, secondly, mechanisms involving the expression of regulatory RNA sequences. It is important to appreciate that any individual epigenetic modification cannot truly be considered in isolation as there exists a complex interplay between the different mechanisms (Murr 2010; Vaissière, Sawan, and Herceg 2008). Whilst some of the interactions have been documented, it is likely that in this emerging field of cancer biology there are further interactions that have yet to be discovered, let alone be fully understood.

1.1.3 DNA structure and organisation

Many mechanisms of epigenetic regulation are dependent on the structure of DNA and how it is organised within the cell nucleus. The image of DNA made famous by Watson and Crick is of a double helix formed from two antiparallel strands of DNA (J. D. Watson and Crick 1953). Each strand contains a backbone formed from alternating a phosphate group with a deoxyribose sugar and also attached to the deoxyribose is one of the four nitrogen-containing bases: adenine (A), thymine (T), guanine (G) and cytosine (C). Between the two strands of DNA, bases form non-covalent hydrogen bonds with their partner such that adenine binds thymine and guanine binds cytosine, referred to as Chargaff's rules (Chargaff, Lipshitz, and Green 1952) . Each turn of the helix comprises 10 base pairs with the distance between each pair being 3.4 Angstrom (equal to 0.34nm or $3.4x10^{-10}$m). Whilst this may

seem at first glance to be a very small distance, when it is considered that the length of the human genome is approximately 3 billion base pairs long and somatic cells contain two copies of the genome this results in a total length of several meters of DNA per cell. An estimate of the number of human cells in the "average" human body of 40 trillion cells ($4x10^{13}$) (Bianconi et al. 2016) therefore gives a total length of DNA equivalent to the distance from the sun to Pluto and back again. Clearly a mechanism is needed for efficiently packing this amount of DNA in a cell nucleus.

Double stranded DNA interacts with proteins and RNA within the cell nucleus to form chromatin, a more condensed and structured molecule that allows the long lengths of DNA be packaged within the cell. One of the core components of chromatin are the histone proteins. There are 5 major families of histone protein and these are highly conserved through evolution. Heterodimers are formed between H2A and H2B, and H3 and H4 and then two each of these dimers join together to form an octamer consisting of two copies each of H2A, H2B, H3 and H4. This histone octamer forms a core region, around which 147 base pairs of DNA wrap around 1.67 times forming a nucleosome. In between adjacent beads on the string is a section of linker DNA approximately 80bp long. The wrapping of DNA around the core of histone proteins has been referred to as having a "bead on a string" appearance when viewed under an electron microscope with a diameter of approximately 10nm.

Histone 1 does not form part of the core complex of histones around which DNA wraps but interacts with the DNA wrapped around the nucleosome and in the linker region to help stabilize the structure and form an even more compact structure where multiple histones wrap around each other to form a 30nm wide fibre (Orthaus et al. 2009). During cell division,

further protein interaction occurs leading to even further condensation of the chromatin, resulting in the appearance of chromosomes as seen during metaphase.

The packaging of DNA and the structure of chromatin have important implications for gene expression. When the chromatin is in the more open "beads on a string" configuration, referred to as euchromatin, transcription factors and RNA polymerases can bind to the DNA and therefore euchromatin is normally observed in areas of the genome that are actively transcribed. Chromatin that is in the more densely packed 30nm fibre conformation, referred to as heterochromatin, is less able to bind the protein machinery necessary for transcription and is therefore associated with areas not associated with active gene transcription. Areas of heterochromatin can either be constitutive or facultative (Saksouk et al. 2015). Constitutive heterochromatin is associated with areas of the genome that are not usually transcribed such as regions around centromeres and telomeres or consists of highly repetitive areas such as microsatellites or tandem repeats. Facultative heterochromatin is found in areas of the genome where transcription of the underlying DNA occurs in a cell-type specific manner, meaning it may be transcribed at some points in development in certain cell types but not in others.

Modulating the structure of chromatin from the open euchromatin to closed heterochromatin therefore offers a mechanism of controlling the level of gene expression and an explanation for gene silencing: a cell may express the necessary transcription factors for the expression of a particular gene but if it is located in an area of heterochromatin it may not be actively transcribed.

1.1.4 Histone modification and the "histone code"

Post-translation modification of histone proteins is one of the major mechanisms of epigenetic regulation (D. J. Patel and Wang 2013; Kouzarides 2007). Each of the histone proteins that participate in the formation of the hetero-octamer contains a globular C-terminal domain around which the DNA wraps itself but also contains an N-terminal tail that protrudes outwards from the core. Each of the N-terminal tails contains multiple amino acids that can be subjected to a range of post-translational modifications and enzymes have been identified capable of e.g. methylation (Zhang and Reinberg 2001), acetylation (Sterner and Berger 2000), phosphorylation (Nowak and Corces 2004), sumoylation (Nathan et al. 2006), poly-ADP ribosylation (Hassa et al. 2006), deamination (Cuthbert et al. 2004) and ubiquitination (Gutiérrez et al. 2012). To add to the complexity, it is possible for multiple different post-translational modifications to occur on any given histone tail and some modifications, such as methylation can occur up to three times on a lysine residue. The multiple permutations of different modifications which can act to either enhance or repress transcription has given rise to what is referred to as the "histone code" (Jenuwein and Allis 2001). It is also important to remember that there are multiple interactions between different types of epigenetic modifications: repressive histone marks are often associated with DNA methylation which also acts to repress transcription (Rose and Klose 2014).

An example of the importance of histone tails in tumour biology has been demonstrated through large-scale sequence analyses discovering mutations in histone proteins, referred to as “oncohistones: for example, in chondroblastoma, a rare tumour that occurs in the epiphysis of long bones, a mutation was found in 95% of cases coding for the same residue in the tail of a subtype of histone 3 (Behjati et al. 2013). When referring to histone modification it is

conventional to refer to the histone number first, the single letter amino acid code of the residue being modified second, the position of the residue third and then finally any modification. The mutation resulted in the change on histone 3 lysine 36 (H3K36), which can normally be post-translationally modified by methylation. Whilst it is unclear of the exact mechanistic implications of this mutation, its near universal prevalence in a rare tumour type suggests it must have important downstream implications. Similarly, oncogenic histone mutations have been found in pontine glioma (Lewis et al. 2013), chondrosarcoma (Behjati et al. 2013) and giant cell tumour of the bone (Amary et al. 2016), underlining again the importance of chromatin structure in oncogenic processes.

Proteins which are involved in the "histone code" are divided into three categories: "writers", which are responsible for adding marks to histones; "erasers", responsible for removing marks; and "readers" that recognise the presence of modification and help recruit other proteins to that location.

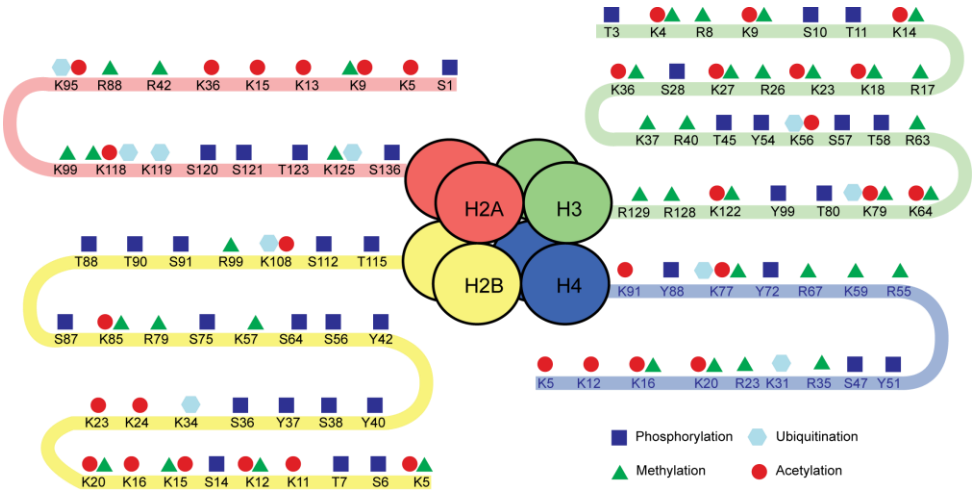


Figure 1 Post-translational modification of histone tails

Amino acids that are post-translationally modified by either phosphorylation, ubiquitination, methylation or acetylation are indicated. Further modifications as described in the text also occur.

1.1.4.1 Histone acetylation

One of the earliest post-translational modification of histones discovered was acetylation (Allfrey and Mirsky 1964). Acetyl marks are added to the positively charged lysine residues in histone tails by histone acetyltransferases (HATs) using acetyl-coenzyme A as a substrate. The negatively charged phosphate backbone of DNA normally interacts with the positively charged lysine residues, and acetylation removes the positively charged group from the lysine, reducing the strength of the interaction between the DNA and the nucleosome and therefore makes the DNA more accessible for the transcriptional machinery to bind. Histone acetylation is therefore commonly associated with areas of active gene transcription (Sterner and Berger 2000).

There are more than 30 enzymes in humans with histone acetyltransferase activity and they can be categorised either on the basis of their subcellular localisation or overall protein structure and function of the catalytic domain (Wapenaar and Dekker 2016). Located in the nucleus, Type A HATs are responsible for interaction with chromatin whereas Type B HATs are located within the cytoplasm and interact with newly synthesised histone molecules before they become integrated into chromatin (K. K. Lee and Workman 2007). Residues in all four of the core histones are able to be acetylated but transcriptional activation is particularly associated with acetylation of H3K9 and H3K14 (Karmodiya et al. 2012). Many HATs can be considered to be promiscuous in that they have a wide range of targets which will be acetylated both within histones and in other proteins (Friedmann and Marmorstein 2013). It may therefore be more appropriate to refer to these proteins as "lysine acetyltransferases".

Histone deacetylases (HDACs) are responsible for the removal of acetyl marks from lysine residues on histones and a range of proteins (Delcuve et al. 2012). There are approximately 20 HDACs found in humans and can be separated into those which use zinc as a cofactor, the so-called called HDACs, and those that use NAD+, the sirtuins (Carafa et al. 2016). Deacetylation of histones is associated with an increased interaction between DNA and the histone and is therefore associated with transcriptional repression (Sterner and Berger 2000). An example of the interaction between different epigenetic mechanisms is the interplay between DNA methylation and histone deacetylation, both repressive marks, via the methyl-CpG binding domain (MBD) protein family (discussed further below) which are able to recruit HDACs (Saito and Ishikawa 2002).

A number of HDAC inhibitors (HDACi) have been licensed for clinical use against a range of cancers. Cutaneous T cell lymphoma was the first cancer for which an HDACi, vorinostat, was approved (Mann et al. 2007) and the HDACi panobinostat is now approved for multiple myeloma in Europe (Laubach et al. 2015). Clinical trials are underway in a range of haematological malignancies and solid tumours (A. C. West et al. 2014).

Bromodomains are "readers" of acetylated lysine residues and are found in over 40 proteins in humans including HATs and HDACs (Filippakopoulos and Knapp 2014). An important example in cancer biology of a bromodomain-containing protein is involved in the rare NUT midline carcinoma (NMC), an aggressive cancer with poor prognosis. In NMC, a chromosomal translocation occurs creating a fusion protein between the Nuclear Protein in Testis (NUT) gene on chromosome 15 with the Bromodomain containing Protein 4 (BRD4) on chromosome 19 (French et al. 2004). The fusion protein is oncogenic and normally found in isolation from other mutations. BRD4 contains two bromodomains and can interact with

acetylated lysine in the promoter region of genes, recruiting Positive-Transcription Elongation Factor b (P-TEFb) and leading to transcriptional activation. BRD4 also binds extensively to enhancer and so-called super-enhancer regions of DNA, which can lead to the upregulation of other oncogenic genes. Inhibitors, which disrupt the ability of BRD4 and other members of the BET bromodomain family from binding to acetylated lysine residues, have proven very effective in animal models at inhibiting the growth of cancer cells containing the NUT-BRD4 fusion and have been advanced into clinical trials in several malignancies. Inhibition of BRD4 has also been shown to decrease the expression of MYC which is often overexpressed in cancers leading to the possibility that inhibitors of bromodomain containing proteins may be more generally useful in the treatment of cancers (Grayson et al. 2014).

BRD4 also plays an important role in epigenetics due to its function as a "mitotic bookmark" (Dey et al. 2000). During mitosis, many proteins normally associated with chromatin are removed but BRD4 remains bound to H4K5ac around the site of genes that were being actively transcribed immediately prior to mitosis (R. Zhao et al. 2011). BRD4 also recruits the transcription machinery to these bookmarked sites after mitosis by binding positive translation elongation factor b (PTEFb) which is required for phosphorylation of RNA polymerase and activation of transcription (Jang et al. 2005).

1.1.4.2 Histone Lysine Methylation

In addition to acetylation, lysine residues in histone tails can also be methylated. Lysine methyltransferases (KMT) are enzymes that add methyl marks to the ε-nitrogen of lysine residues using S-adenosyl methionine (SAM) as the methyl donor. Lysine demethylases (KDM) remove the methyl marks from lysine residues and are discussed in detail below.

Methylated lysines can exist in three different methylation states, which have been associated with different functions: mono-methyl (me1), di-methyl (me2) and tri-methyl (me3).

Histone lysine methylation plays an important role in development and the function of many of the proteins involved were first elucidated by studying embryogenesis and development in the fruit fly Drosophila (Black, Van Rechem, and Whetstine 2012). Proteins belonging to the Trithorax Group (TxG) are associated with activation of gene transcription (Schuettengruber et al. 2011) whereas proteins in the Polycomb group (PcG) are associated with transcriptional repression (Steffen and Ringrose 2014).

PcG proteins join together to form transient multimeric Polycomb Repressive Complex 1 and 2 (PRC1/2) that have different actions but work together to cause gene silencing. PRC2 contains either *Enhancer of Zeste 1 or 2 (*EZH1/2) a lysine methyltransferase that is specifically able to add methyl groups to H3K27, forming the repressive histone marks H3K27me2 and H3K27me3. EZH2 overexpression or gain of function mutations have been detected in a wide range of malignancies where it causes dysregulation of H3K27me3 and therefore alters gene expression (Yamaguchi and Hung 2014). Mutations in two other proteins that form part of PRC2, SUZ12 and EED result in deficiency of H3K27me3 and are associated with malignant peripheral nerve sheath tumours (William Lee et al. 2014). PRC1 is a multimeric protein complex that can be composed of a number of different subunits (Schwartz and Pirrotta 2013). The chromobox proteins (CBX) represent a group of evolutionary conserved proteins that are associated with heterochromatin and hence transcriptional repression and function as a reader domain for H3K27me3 and the repressive mark H3K9me3. A number of closely related CBX proteins (CBX2/5/7/8) can be part of the PRC1 complex, and changes in the expression of CBX proteins has been shown to play an

important role in differentiation (Ren, Vincenz, and Kerppola 2008). The role of different CBX proteins in cancer is an active area of research. CBX7 downregulation has been associated with poor prognosis in various cancers, including anaplastic thyroid cancer (Pallante et al. 2008), but overexpression of CBX7 has been documented in lymphomas (Scott et al. 2007).

Also in the PRC1 complex is Ring Finger Protein 1A or 1B (RING1A/1B) which acts to ubiquitinylate H2AK119, a modification that leads to further compaction of chromatin and therefore transcriptional repression (Cao, Tsukada, and Zhang 2005; Wang et al. 2004).

The method by which polycomb complexes are targeted to the genome in humans remains under active study. The canonical model involves PRC2 initiating the repression by methylating H3K27 at an unmethylated CpG island with subsequent recruitment of PRC1 via its chromobox containing proteins to maintain the repression by ubiquitinylating H2AK119 (Di Croce and Helin 2013). In *Drosophila*, PRC2 is targeted to PRC response elements in DNA but due to the larger complexity of PRCs in humans the mechanism is not so clear (Frey et al. 2016).

One mechanism by which PRC2 can be recruited is via interacting with non-coding RNAs. An example of ncRNA recruiting PRC2 occurs in X-chromosome inactivation. X-inactivation specific transcript (XIST) is transcribed from the X inactivation centre of the chromosome that is to be silenced producing an RNA that is capped, spliced and polyadenylated but not translated. XIST diffuses down the length of the X chromosome where it interacts with the SUZ12 component of PRC2, recruiting the complex and cause H3K27me3 deposition via the action of EZH1/2 (Hernández-Muñoz et al. 2005).

A further example of ncRNA being implicated in the recruitment of PRC2 is that of HOTAIR, a 2kb non-coding RNA transcribed from chromosome 12 that has been reported to be involved in transcriptional silencing of genes on other chromosomes through the recruitment of PRC2 (Gupta et al. 2010). HOTAIR has been shown to be overexpressed in a wide range of solid tumours including gliomas, urothelial tumours and breast cancers (Y. Wu et al. 2014). More recent studies have however cast doubt upon the specificity of the interaction of PRC2 with HOTAIR as it has been demonstrated that RNA is bound promiscuously both by individual members of PRC2 such as EZH2 and SUZ12 bind RNA promiscuously (Betancur and Tomari 2015) as well as to the assembled PRC2 complex (Davidovich et al. 2015) .

An alternative explanation for the recruitment of PRC to DNA differs from the canonical explanation by having a modified PRC1 responsible for the initial event. PRC1 containing KDM2B recognises unmethylated CpG island and using the RING1A/B subunit of PRC1 causes ubiquination of H2AK119. PRC2 is then recruited to this site of the ubiquitination through the action of AE binding protein 2 (AEBP2) which interacts with several members of the PRC2 family leading to trimethylation of H3K27 (X. Wu, Johansen, and Helin 2013; Rose and Klose 2014; Grijzenhout et al. 2016).

The importance of H3K27 in controlling gene expression is observed in glioblastoma multiforme where the mutation from a lysine to a methionine at position 27 in H3F3A is a common mutation (see above, “oncohistones”) (Sturm et al. 2012; Schwartzentruber et al. 2012). This mutation has been associated with decreased levels of H3K27me3 globally and aberrant gene expression (Lewis et al. 2013; Chan et al. 2013). The same mutation has subsequently been identified in a range of central nervous system tumours including high grade astrocytomas (Shankar et al. 2016) and midline gliomas (Aihara et al. 2014).

Counteracting the polycomb group proteins are members of the trithorax group associated with the maintenance of activation of gene expression via histone modification by methylation of H3K4, H3K36 and ATP-dependent chromatin remodelling. Genes that are being activetly transcriped have H3K4me3 around their transcription start site.. Proteins of the trithorax group form multi-subunit complexes comprising proteins with a range of functions including "writer", "eraser" and "reader" domains and these are largely conserved in eukaryotic organisms (Schuettengruber et al. 2011). The trithorax complex contains a protein with methyltransferase activity of either the SET1-family or mixed lineage leukaemia (MLL) family in complex with ASH2-like histone lysine methyltransferase complex subunit (ASH2L), WD repeat domain 5 (WDR5), retinoblastoma binding protein 5 (RBBP5) and DPY-30. A key component of the trithorax group of proteins is the Mixed Lineage Leukaemia (MLL) family of genes that contain methyltransferase activity with the ability to mono-, di- and tri- methylate H3K4. MLL genes are often involved in chromosomal translocations in haematological malignancies (DiMartino and Cleary 1999). ASH2L is known to modulate the methyltransferase activity towards H3K4 of the trithorax complex and has been found to be overexpressed in certain oestrogen receptor positive breast cancers (Qi et al. 2014). WDR5 is important in the formation of multimeric protein complexes and its overexpression in bladder cancers has been associated with increased H3K4me3 (Chen et al. 2015). Retinoblastoma (Rb) Binding Protein 5 (RBBP5) binds Rb, a key regulator of cell cycle progression. Overexpression of DPY-30 has been implicated in increasing proliferation in gastric cancer cells (Y. J. Lee et al. 2015).

Other than the core components of the trithorax complex, additional proteins have been noted to bind to certain forms of the complex in different cell types. For example, the histone

demethylase UTX which is able to demethylate the repressive H3K27me3 mark has been found in complexes with MLL2/3 (Schuettengruber et al. 2011). This complex will therefore have the dual activity of increasing the permissive mark H3K4me3 and reducing H3K27me3. DOT1L is a histone methyltransferase that is responsible for methylation of H3K79 and interacts with MLL-AF9 fusion proteins associated with the development of leukaemia (Nguyen et al. 2011).

Some gene loci are marked by both H3K27me3 and H3K4me3 – so-called bivalent or poised promoters. Bivalent promoters are often found associated with genes during development that are required to be rapidly expressed when required but remain repressed until then (Voigt, Tee, and Reinberg 2013). It has been suggested that loss of the repressive H3K27me3 mark from bivalent promoters may be associated with activation of oncogenes and the initiation or propagation of cancer (Martinez-Garcia and Licht 2010).

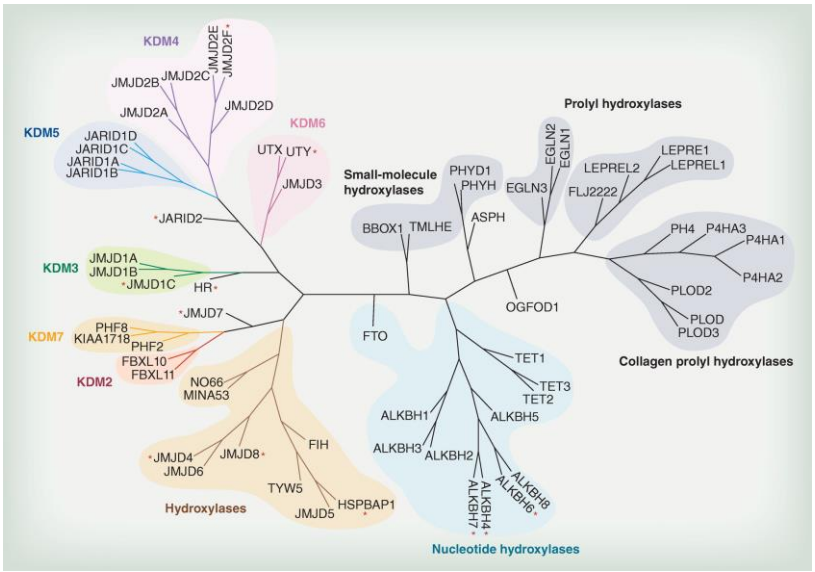


Figure 2 Phylogenetic tree of the human iron and 2-oxoglutarate dependent oxyygenases

Lysine demethylases located within the larger family of 2-oxogutarate (2-OG) dependent oxygenases. From (Johansson et al. 2014).

Histone methyl marks can be removed by enzymes of the histone demethylase family (KDM), a part of the larger family of iron and 2-oxyglutarate-dependent oxygenases (Figure 2). Demethylation occurs via two distinct mechanisms involving either a FAD-dependent amine oxygenase in the KMD1 family, which is able to remove mono- and di- methyl but not trimethyl groups from H3K4 and H3K9 (Zheng et al. 2015). Removal of the trimethyl modification occurs via the Jumonji-domain containing (JmjC) proteins that use alpha-ketoglutarate and iron as cofactors for the demethylation reaction(Johansson et al. 2014) Like the lysine methyltransferases, the demethylase family is important during embryogenesis and development.Several identified mutations and deletions in lysine demethylase genes have been reported to lead to developmentally abnormal phenotypes (Nottke, Colaiácovo, and Shi 2009). Possibly due to the fact that lysine methylation is associated with both activation of gene expression, for example H3K4me3, and the repression of expression with marks such as H3K27me3, both over and under-expression of various KDMs have been associated with a cancer phenotype (Johansson et al. 2014). It is likely that the phenotypic effect of aberrant expression or mutation in the KDMs is highly dependent on the cell type of origin and the presence of any other mutations present.

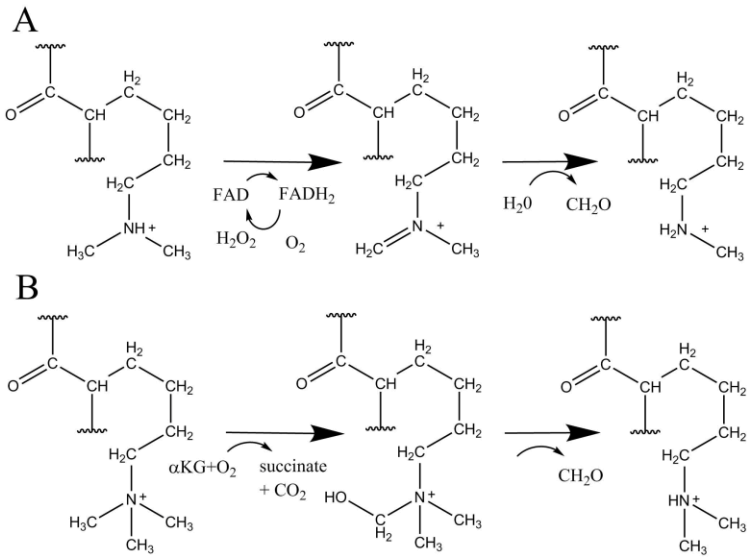


Figure 3 Mechanisms of action of lysine demethylases

(A) KDM1 uses FAD as a cofactor and (B) JmjC enzymes use α-ketoglutarate (αKG)

1.1.5 DNA base modification

An epigenetic modification is one that is stable and heritable but does not depend on a change to the underlying DNA sequence consisting of the four nitrogen-containing bases (adenine (A), thymine (T), guanine (G) and cytosine (C)) attached to a deoxyribose-phosphate backbone. A chemical modification to a base, which causes a change in the interaction of proteins involved with transcription but does not change how the base is read and copied during DNA replication, is therefore able to exert an epigenetic effect. In prokaryotes, modification to both adenine and cytosine has been recorded (Sánchez-Romero, Cota, and Casadesús 2015), whereas in eukaryotic organisms methylation of cytosine is most frequently observed, and more recently methylation of adenine has been discovered. (references).

The major form of modification to DNA observed is the addition of a methyl group to cytosine resulting in 5-methylcytosine (5-mC). When found in promoter regions of a gene, 5-mC is associated with silencing of that gene by inhibiting transcription (Doerfler 1983; Bird 2002; Suzuki and Bird 2008). This inhibition of transcription has an important role in cancer biology as, if the promoter of a tumour suppressor gene is hypermethyated, there will be a lack of functional protein produced (Laird and Jaenisch 1996; Esteller 2007; Baylin and Herman 2000). As discussed above, a wild-type protein that is not expressed by a cell is in many ways equivalent to an expressed mutant protein that has lost the ability to perform its normal tumour suppressor role: in both situations there is the lack of a functioning protein within the cell. Aberrant methylation patterns in cancer has been noted in the 1980ies, and it is now recognized that hypermethylation of tumour suppressor promoter regions is a common mechanism found in many different cancer types including haematological malignancies, carcinomas and sarcomas.

There are several related mechanisms by which DNA methylation in the promoter of a gene leads to decreased transcription. Part of the inhibitory effect on transcription may be explained by the methyl group of the 5-mC projecting into the major groove of the DNA helix interfering with the binding of transcription factors and other proteins necessary for transcription (Dantas Machado et al. 2015). More important in mediating the effect of methylated DNA on gene silencing is the interaction between 5-mC and the Methyl-CpG Binding Proteins (MBD), proteins which selectively bind to methylated DNA and have low affinity to DNA that is not methylated (Q. Du et al. 2015). The presence of proteins bound to the 5-mC helps to physically prevent the binding of transcription factors that will reduce the level of transcription. MBDs consist of a family of proteins that in addition to containing

domains that allow recognition of methylated DNA are able to affect chromatin structure, another important epigenetic mechanism discussed below. Some MBDs contain domains that allow them to directly alter chromatin structure, such as SETDB1 and SETDB2, which contain a histone methyltransferase domain that increases H3K9 trimethyl levels associated with transcriptional repression and heterochromatin formation. Other MBDs, such as MBD1-4 and MeCP2 interact with histone deacetylases (HDACs) that also results in the formation of heterochromatin associated with decreased transcription.

5-methylcystosine is formed by enzymes of the DNA 5-cytosine Methyltransferase family (DNMT) using S-adenosyl methionine (SAM) as their methyl donor. The activity of the DNMTs is not equal for all cytosine molecules within DNA and has a preference for a cytosine molecule immediately upstream of a guanine (Jeltsch 2016), commonly referred to as a CpG dinucleotide where the 'p' represents the phosphate group of the DNA backbone. The convention of referring to a CpG dinucleotide is to distinguish it from a cytosine and guanine base pairs on opposite strands of DNA that are connected via hydrogen bonding.

The CpG dinucleotide occurs at approximately one quarter of the frequency in mammalian genomes than would be expected given their overall GC content however, compared to other eukaryotic organisms, mammals have a significantly higher rate of methylation at CpG nucleotides (Han et al. 2008). A suggested reason for the lower than expected lever of CpG is that when a methylated cytosine spontaneously deaminates it forms a thymine and whilst there exists an enzyme that can detect a thymine/guanine mismatch, thymine DNA glycosylase (TDG), the enzyme is not completely efficient. Over evolutionary time, this would result in the transition of 5-methylcytosine to thymine leading to a C : G to A : T mutation. MBD4, mentioned above as a methylated DNA binding protein, also contains

glycosylase activity that is able to repair deamination from 5-methylcystosine to thymine and therefore plays an important role in preventing mutations at the site of CpG (Yoon et al. 2003). MBD4 itself is subject to epigenetic regulation and is found to be transcriptionally silenced as an early event in many colorectal adenocarcinomas (Neri and Lucci-Cordisco 2009). MBD4 mutations also occur in colorectal cancers with microsatellite instability and defects in mismatch repair (Bader et al. 1999).

The distribution of CpG dinucleotides across the vertebrate genome is uneven, with large areas between genes containing very few CpGs followed by a much higher density found in the promoter regions of many genes – referred to as "CpG islands" (Varriale and Bernardi 2010). CpG islands are regions at least 200 base pairs long which contain greater than 50% GC content and an observed to expected CpG ratio greater than 60%. In contrast to promoters with a high level of DNA methylation that are associated with transcriptional silencing, promoters of actively expressed genes contain a larger number of unmethylated CpGs. The increased frequency of CpG islands in gene promoters may be explained firstly by the decreased deamination rate of unmethylated cytosine to uracil which occurs compared to that of 5mC to thymine and secondly by the improved detection and repair of U: G by base excision repair appears compared to that of T:G.

There are three catalytically active members of the DNMT family: DNMT1, DNMT3a and DNMT3b (Subramaniam et al. 2014). The enzyme originally named DNMT2 was found not to methylate cytosines in DNA but instead to methylate a specific cytosine in the tRNA of aspartic acid so it was renamed tRNA Cytosine-5 methyltransferase - (TRDMT1) (Goll et al. 2006). DNMT1 is important in maintaining the methylation pattern when DNA is replicated. As DNA polymerase replicates the complementary strand, the appropriate bases are

faithfully replicated but the newly synthesized strand of DNA will not contain any methylated bases. DNMT1 has a high activity for methylating cytosine in CpG dinucleotides when the double stranded DNA is hemimethylated – that is one strand contains a methylated cytosine and the other strand does not as occurs immediately after DNA replication (Jeltsch 2016). DNMT1 interacts with Proliferating Cell Nuclear Antigen (PCNA) and is localized at the replication fork allowing the methylation pattern to be propagated (Iida et al. 2002). Importantly, the activity of DNMT1 explains how DNA methylation is an epigenetic mark that can be inherited from parent to daughter cells.

The hemimethylated status of newly replicated DNA is used as a way of the organism to detect which strand is newly synthesised and is important for the correct functioning of the mismatch repair (MMR) system in prokaryotes (Fukui and Fukui 2010). Although the MMR system is evolutionarily highly conserved, the presence or absence of methylated bases does not appear to be used as a detection mechanism for newly synthesized DNA in eukaryotes yet DNMT1 appears to play a crucial role in this pathway. The interaction of DNMT1 with PCNA brings it into contact with many other proteins of the MMR system and studies where DNMT1 has been knocked-down have indicated that this results in increased microsatellite instability, a hallmark of deficient MMR that is not related to DNA methylation (Loughery et al. 2011).

Compared to the activity at hemimethylated sites, the activity of DNMT1 for *de novo* methylation, adding a methyl group to a cytosine when neither strand contains an existing methyl group is much lower under physiological conditions (Bird et al. 1999). Overexpression of DNMT1 though has been shown to induce *de novo* promoter methylation

and aberrant regulation of DNMT1 in cancer cells may play an important role in gene silencing (Etoh et al. 2004).

Members of the DNMT3 family (DNMT3a, DNMT3b and DNMT3L, a catalytically inactive accessory protein) are associated with *de novo* methylation and in contrast to DNMT1, are able to methylate cytosine when the opposite strand is not methylated with the same efficiency as they can methylated cytosine in hemimethylated DNA (Bird et al. 1999). Whilst DNMT3s show a preference for methylation at CpG sites they are also able to methylate cytosines in other contexts including CpA dinucleotides at very low levels. DNMT3 are important for methylating areas of repetitive DNA, which may represent transposable elements and the methylation and silencing of these regions are important for maintaining genomic stability. DNMT3s therefore plays an important role in establishing the methylation pattern within the cell.

In a further example of interaction between different mechanisms of epigenetic control, DNTM3a is known to interact with proteins associated with repressive chromatin marks. DNMT3a interacts via its PHD domain with unmethylated histone 3 lysine 4, a mark associated with gene repression (Otani et al. 2009). EZH2, the catalytically active histone methyltransferase subunit of PRC2, is also associated with repression of transcription and interacts with DNMT3 linking the repressive marks of DNA methylation and histone modifications (Viré et al. 2006).

Genome editing studies using a human embryonic stem cell line have shown that removal of both DNMT3a and DNMT3b, either singularly or together, is not fatal in these cells and does not diminish their pluripotency. Silencing of DNMT1 however was fatal in these cells (J.

Liao et al. 2015). This is in contrast to studies in mice where double-knockout of DNMT3a and b was embryonically lethal (Okano et al. 1999).

DNMT3a appears to be particularly important in the haematological malignancies, especially Acute Myeloid Leukaemia (AML), in which up to 22% of cases have a mutation in the gene (Ley et al. 2010). In mouse haematopoietic stem cells (HSC), mutations in DNMT3a have been associated with an advantage in self-renewal. As HSCs survive for many decades in human, mutations in DNMT3a may be an early event which when coupled to an advantage in self-renewal can lead to an increasing prevalence of HSCs containing the mutation over a lifetime. Extensive genomic sequencing studies of thousands of individuals without haematological malignancies have shown that over time HSCs become increasingly clonal with 5-10% of 70 year olds relying on only one clone for almost all parts of haematopoiesis (Jaiswal et al. 2014; Genovese et al. 2014; M. Xie et al. 2014). These same sequencing studies have demonstrated the prevalence of mutations in DNMT3a in hematopoietic stem cells. The exact mechanism by which the mutations in DNMT3a lead to haematological malignancy is not clear and in many cases secondary mutations are also found, but these studies indicate the importance of DNMT3 in maintaining genomic stability and preventing malignant development (Yang, Rau, and Goodell 2015).

DNA methylation also plays an important role in other epigenetic mechanisms implicated in cancer biology such as X-chromosome inactivation and genetic imprinting. Genetic imprinting is an epigenetic process by which the parental origin of a particular allele is maintained in daughter cells. For imprinted genes normally only those inherited from a particular parent are expressed but this can lead to disease for a number of reasons. One situation is when there is a mutation in a gene that is expressed whilst its unmated partner

allele is silenced. Errors in meiosis can result in a daughter cell receiving two copies of a gene from the same parent instead of the usual situation in which one allele is received from each, a situation referred to as uniparental diosymy. If a gene normally expresses the maternal copy of the gene but both copies have come from the father this will result in disease.

An example of imprinting in cancer biology is the GTP-binding protein Di-Ras3 (DIRAS3, also known as ARHI and NOEY2). The DIRAS3 gene is maternally imprinted meaning that only the paternal allele is expressed (Y Yu et al. 1999). DIRAS3 is a tumour suppressor, found normally expressed in breast and ovarian tissue but is absent in cancerous tissue (Yinhua Yu et al. 2003). Unlike most tumour suppressor genes which require "two hits" to deactivate them, because of the two copies contained within the cell, DIRAS3 only requires "one hit" due to the silencing of the imprinted maternal gene. DIRAS3 is a further example of the interplay between different mechanisms of epigenetic regulation. The "hit" observed in preventing gene function is often due to promoter methylation by DNMT of the un-imprinted paternal allele leading to gene silencing. Furthermore, in certain breast cancers it has been shown that the microRNA miR-221 is upregulated and by binding to the 3' untranslated region of the DIRAS3 mRNA it can lead to degradation and therefore a decrease in protein expression levels (Y. Li et al. 2013).

Demethylation of cytosine bases is the reverse process of methylation, and the balance between the two is important for regulating the methylation pattern within the cell. DNA demethylation can happen either actively or passively. As during each round of DNA replication the methylation pattern has to be re-established on the newly synthesized strand by the action of DNMT1, as discussed above, inhibiting the process of maintenance methylation will result in a global decrease in the methylation level of the cells over multiple

cell divisions. Two drugs are licenced approved for clinical use that work by inhibiting methylation of the newly synthesized strand of DNA, 5-Azacitidine and 5-Azadeoxycitidine. They are used in the treatment of myelodysplastic syndrome and other haematological malignancies such as acute myeloid leukaemia and chronic myeloid leukaemia (Gros et al. 2012). Both are cytidine analogues containing a nitrogen in the 5' position of the heterocycle, the position to which DNMTs would normally attach the methyl group. After activation by intracellular kinases, the trinucleotide can be incorporated into DNA in place of a dCTP where the hemimethylated CpG is recognised by DNMT1, as described above, and the process of methylation begins with the enzyme forming a covalent adduct to the base. The presence of the nitrogen in the 5 position of the nitrogenous ring means that the DNTM1 is unable to complete the methylation reaction and so becomes permanently attached to the base, which is subsequently removed by DNA repair machinery leading to degradation of DNMT1 and depletion of intracellular levels.

DNA methylation can also be an active process catalysed by enzymes of the Ten-Eleven Translocation (TET) family of enzymes, originally discovered as a fusion partner to MLL in acute myeloid leukaemia (Ono et al. 2002). An interesting observation is that MLL, also known as Lysine Methyltransferase 2A (KMT2A) is responsible for Histone 3 Lysine 4 methylation, a mark of transcriptional activation. There are three members of the TET family in humans all containing an oxygenase domain preceded by a cysteine rich area and TET1 and TET3 also contain a CXXC domain, important for binding to methylated CpG dinucleotides. The TET family of proteins results in the oxidation of 5-methylcytosine to 5-hydroxymethylcytosine (5hmC) using molecular oxygen as a substrate and requiring alpha-ketoglutarate as a co-factor. Further oxidation using the same mechanism is possible from

5hmC to 5-formylcytosine (5fC) and then to 5-carboxylcystosine (5caC). Following the activation oxidation from 5mC to 5hmC using the TET enzymes, passive dilution of the methylated cytosine mark occurs as subsequent rounds of DNA replication occur without the methyl mark being replaced by DNMT as it does not recognise the 5hmC as a mark to indicate that the newly synthesized strand should be methylated. Like 5hmC, 5fC and 5caC also undergo passive dilution following DNA synthesis; it can also be actively repaired by removal of the oxidized base using thymidine DNA glycosylase (TDG) followed by repair using the base excision repair system (Hashimoto et al. 2012).

The ability of TET family enzymes to demethylate cytosine is important in early embryogenesis and for establishing the methylation pattern of the new organism and consolidating the methylation states of the maternal and paternal genomes (H. Zhao and Chen 2013). TET3 rapidly oxidizes the 5mC to 5hmC in the paternal genome but appears to be excluded from the maternal genome and certain areas of the paternal genome that remain methylated as part of genomic imprinting, as discussed above. The maternal genome is rich in the histone mark H3K9me2 to which additional proteins such as Development Pluripotency Associated 3 (DPPA3, also known as STELLA or PGC7) are recruited, excluding TET3 and therefore preventing the active demethylation by oxidation (Nakashima et al. 2013). Areas of the paternal genome that are imprinted appear to use the same mechanisms in preventing demethylation.

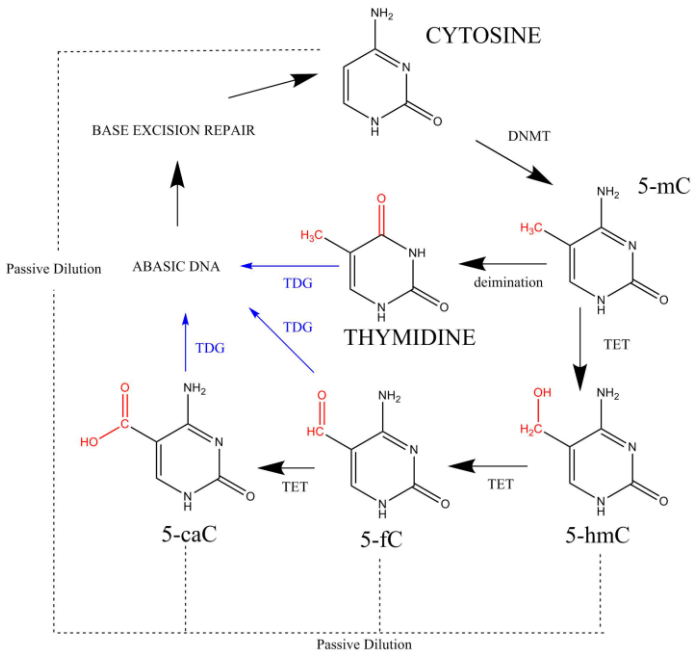


Figure 4 Cytosine base modification

Schematic representation of modification of cytosine bases in DNA. For details see text. DNMT, 5-mC 5-methylcytosine, 5-hmC 5-hydroxymethylcytosine, 5-fC 5-formylcytosine, 5-caC 5-carboxylcytosine

In addition to the role of TET1 in association with MLL in the fusion gene associated with AML, TET2 is overexpressed in a wide range of both solid tumours and haematological malignancies (Delhommeau et al. 2009). TET2 mutations have been found in a number of cancers resulting in increased levels of 5mC and decreased levels of 5hmC. It has been observed that in *de novo* AML, mutations in TET2 and isocitrate dehydrogenase 1 or 2 (IDH1/IDH2) appear to be mutually exclusive (Figueroa et al. 2010). IDH is an enzyme of the tricarboxylic acid cycle that catalyses the oxidative decarboxylation of isocitrate to alpha-ketoglutarate, the cofactor required for TET2 protein function. Mutations in IDH can lead to the production of alpha-hydroxyglutarate, which inhibits the activity of TET2. Therefore

mutations in either IDH or TET2 result in an aberrant chromatin methylation pattern within the cell and in this manner contributes to the cancer phenotype.

1.1.6 Non-coding RNAs

A further mechanism of epigenetic control is through the expression of non-coding RNAs (ncRNA). Non-coding RNAs are transcribed from the genome and often undergo post-transcriptional processing such as polyadenylation or splicing but do not result in a protein product being formed. Studies by the ENCODE consortium have suggested that many areas of the genome not traditionally associated with protein-coding are transcribed at very low rates but this does not necessarily imply that all of these transcripts have a function (Djebali et al. 2012). Several examples of non-coding RNAs have been discussed above in relation to the role they play in the recruitment of polycomb complex to DNA during X-inactivation. In the context of epigenetics, "non-coding RNAs" is used to refer to those RNA that have a regulatory effect on other genes especially the long non-coding RNAs (lncRNA) which are over 200nt long (Kung, Colognori, and Lee 2013) and short non-coding RNAs, such as microRNAs (miRNA) and piwi-interacting RNAs (piRNAs), but it must be remembered that ribosomal RNA and tRNAs transcribed at high levels in the cell also do not get translated to form a protein product.

MicroRNAs (miRNA) are 22bp RNAs that can alter gene expression by binding to the 3' untranslated region of mRNAs leading to their destabilisation and degradation (He and Hannon 2004). Primary miRNAs are transcribed from DNA by RNA polymerase 2 and are processed within the nucleus by the microprocessor complex that includes DROSHA, a ribonuclease enzyme and DiGeorge Critical Region 8 (DGCR8, also known as pasha) to form a stem-loop structured pre-miRNA of 70-80bp in length (Denli et al. 2004). The

processed pre-miRNA is exported to the cytoplasm where it is processed by DICER1 which removes the loop leaving a mature double-stranded miRNA (Hutvágner et al. 2001). One strand of the miRNA is then attached to an Argonaut protein to form the miRNA-induced silencing complex (miRISC), which is able to bind via complementary base pairing with the 3'UTR of the target protein. Binding of the miRISC complex directs the mRNA:miRNA complex to the processing bodies (P-body) where the mRNA is degraded preventing further translation. Therefore, increased levels of a particular miRNA than targets a given mRNA will lead to decreased levels of the mRNA and therefore reduce expression of the protein.

Disruption of the miRNA system has been observed in many cancer types either by aberrant transcription of the primary miRNA (Jansson and Lund 2012) or dysregulation of the processing system (Palanichamy and Rao 2014) with either over- or under- expression of proteins involved leading to a change in the level of mature miRNA and therefore altered gene expression.

Piwi (in Drosophilla P-element induced wimpy testis) RNAs (piRNA) are longer than miRNAs at approximately 30bp long and were originally discovered as important in development in *Drosophila* (Juliano, Wang, and Lin 2011). Expression of piRNAs in cancerous tissues appears to differ from that of healthy tissue of the same origin (Martinez et al. 2015). The exact role and mechanism of action of piRNAs is a topic of active research.

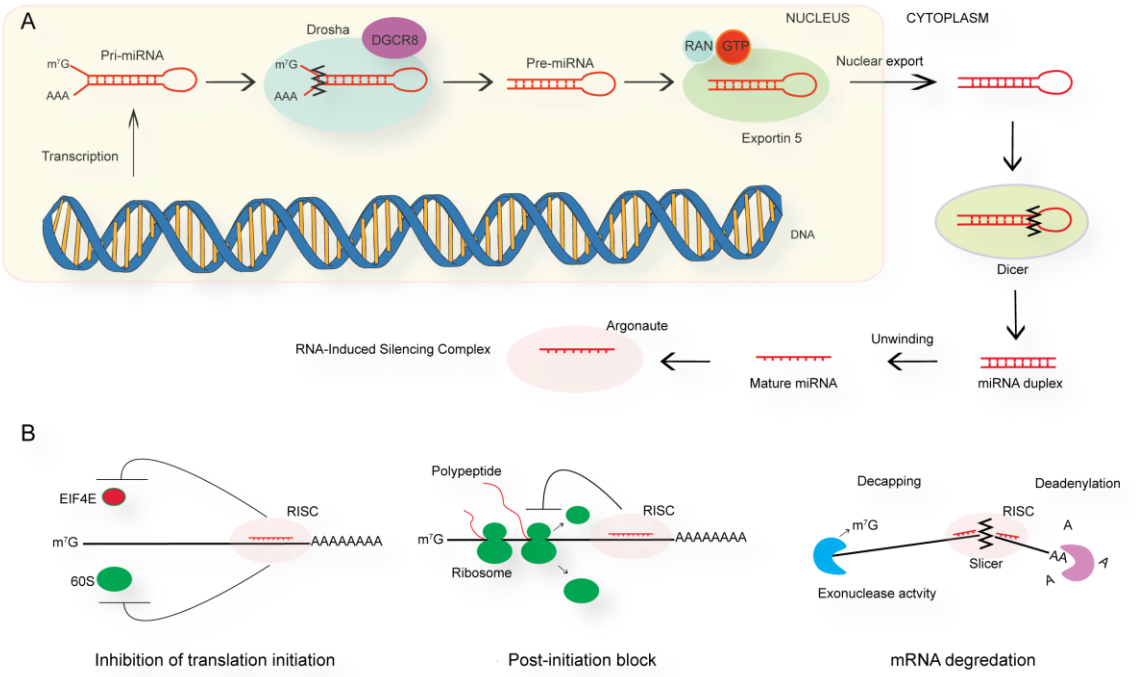


Figure 5 microRNA processing

(A) *miRNA genes are transcribed by RNA polymerase 2 or 3 and the produced transcript, referred to as* ***pri-miRNA****, forms a double-stranded hairprin structure and contains a 5' cap and 3' polyadenylation. The pri-miRNA is recognised by DiGeorge Syndrome Critical Region 8 (DRCG8, also known as "pasha") and processed by Drosha to remove the 5' cap and poly A tail, forming a* ***pre-miRNA****. The pre-miRNA is exported to the cytoplasm by exportin 5 in complex with RAN-GTP. In the cytoplasm, the pre-miRNA is further processed by Dicer to remove the loop structure leaving a miRNA duplex. Following unwinding of the duplex, one strand is incorporated into the RNA-Induced Silencing Complex (RISC) in association with proteins of the Argonaut family.*

(B) *miRNA associated with RISC can modify protein expression by interfering with the initiation of translation via inhibiting binding of either the 60S ribosomal subunit of EIF4E. Polypeptide elongation can also be inhibited by causing ribosomes to disengage prematurely from the mRNA transcript. miRNA-RISC can also lead to mRNA degradation by interacting with proteins that result in decapping and deadenylation promoting degredation of the transcript through exonucleases. The interaction of miRNA and RNA forming a double stranded RNA is the substrate for the argonaute protein Slicer that results in mRNA cleavage.*

1.2 CANCER AND BONE

Cancer in bone can be separated into primary cancer that is a cancer, which originates in the bone tissue, and secondary cancer, which have spread to the bone by metastasis from distant sites. Certain cancers show a predilection for metastasis to bone including cancers originating in the thyroid, lung, kidney, prostate and breast. The "seed and soil" hypothesis first promulgated by Paget in the 1880s (Paget 1889) proposes that for metastasis to occur there must be permissive factors both in the original cancer, the "seed", and in the microenvironment of the distant organ to which the cancer has metastasized, "soil". Although secondary cancers will not be further discussed in this thesis, the capacity for bone to act as a permissive microenvironmental "soil" for cancer growth is important in the pathogenesis of multiple myeloma (MM), a haematological malignancy of post-germinal centre plasma cells that were investigated in more detail in this thesis work.

1.3 EPIDEMIOLOGY AND PATHOGENESIS OF MULTIPLE MYELOMA

Multiple myeloma is a malignancy of plasma cells characterized by clonal expansion, excess production of aberrant monoclonal immunoglobulin proteins, detectable in either blood or urine, where it is referred to as Bence Jones protein, and end organ dysfunction. It is predominantly a disease of older age with a median age at diagnosis of 70 years. Multiple myeloma accounts for approximately 2% of all cancer diagnoses and 14% of haematological malignancies and has an age-adjusted incidence of 5.6 cases per 100,000 per year.

The clinical course of multiple myeloma progresses through several distinct phases. Monoclonal Gammopathy of Undetermined Significance (MGUS) is a condition present in

approximately 5% of people over the age of 50 and progresses to myeloma at a rate of about 1% per year. MGUS is differentiated from myeloma by the absence of end organ damage, less than 10% plasma cells in the bone marrow and a paraprotein concentration of lower than 3g/dL. Patients with MGUS are asymptomatic although the accumulation of Ig light chains can result in the development of amyloidosis. MGUS itself can be subdivided into a number of categories based on the nature of the expressed paraprotein.

Smouldering Multiple Myeloma (SMM) is a progression from MGUS in which there is greater evidence of disease burden. The risk of progression to myeloma is higher than with MGUS, with a rate of approximately 10% per year in the first five years after diagnosis. SMM is characterized by greater than 10% plasma cells in bone marrow and/or a paraprotein concentration above 3g/dL but no evidence of end organ damage or a "myeloma defining event". The concept of a myeloma defining event was introduced by the International Myeloma Working Group in 2014 (Rajkumar et al. 2014) to account for a cohort of patients that had previously not met the criteria for diagnosis, and therefore treatment of myeloma but were at greater than 80% risk of progressing within two years. Myeloma defining events include plasma cells comprising greater than 60% of bone marrow, evidence of more than one bone lesion upon MRI or a ratio of involved to uninvolved free chains greater than 100.

Myeloma is diagnosed when one of the myeloma defining criteria mentioned above is met or there is evidence of end organ damage attributable to the clonal expansion of plasma cells. Evidence of end organ damage include hypercalcaemia, anaemia, renal dysfunction or bone disease, comprising of either lytic lesions, pathological fractures or osteoporosis due to the disease. In the early stages of myeloma, plasma cells may be confined to the bone marrow but in certain cases the disease progresses to extramedullary sites such as the spleen.

Aggressive cases of myeloma can progress to a plasma cell leukaemia where malignant plasma cells are found to exceed 20% of the circulating leukocytes in the blood.

Staging of myeloma was previously performed using the Durie Salmon staging system (Durie and Salmon 1975) that used factors including levels of haemoglobin, serum calcium, presence of bone lesions, level of paraprotein production and degree of renal impairment. The International Staging System (ISS) (Greipp et al. 2005) is a simplified system involving only levels of albumin and beta-2 microglobulin (B2M). In stage 1, albumin is above 3.5mg/dL and B2M below 3.5mg/dL, stage 3 requires B2M above 5.5mg/dL and the intermediate stage 2 for patients that fall into neither stage 1 or 3. Median survival is quoted as 62 months for stage 1 disease, 44 months for stage 2 and 29 months for stage 3. However, these figures should be viewed with caution as they originate from the original publication on the ISS system, which is now 11 years old and there has been advances in treatment since this time.

The International Myeloma Working Group published further data on risk stratification (W J Chng et al. 2014) that in addition to the ISS system uses cytogenetic information assessed by Fluorescent In Situ Hybridization (FISH) for three markers: t(4;14), 17p13 (the genomic location of TP53) and 1q21.

A further refinement to the staging system was promulgated in 2015 by the International Myeloma Working Group combing the ISS and various cytogenetic markers in addition to the level of serum lactate dehydrogenase (LDH) to give the Revised International Staging System (R-ISS) (A. Palumbo et al. 2015). In the R-ISS, high risk cytogenetic markers include t(4;14), t(14;16) and del(17p). Stage 1 of the new R-ISS requires a normal serum LDH and the absence high-risk cytogenetic changes in addition to the stage 1 criteria of ISS. Stage 3

includes ISS stage 3 with either a high-risk chromosomal abnormality or a high LDH. Stage 2 R-ISS includes all disease that is neither stage 1 nor 3. Overall survival at 5 years was 82%, 60% and 40% for R-ISS stage 1 to 3 respectively in a meta-analysis of 4445 patients from 11 international myeloma trials.

	High-risk	Standard-risk	Low-risk
Parameter	ISS 2/3 t(4;14) or 17p13	Others	ISS 1/2 and absence of t(4;14), del(17p13) +1q21 Age <55
Median Overall Survival	2 years	7 years	>10 years
Percent Patients	20%	60%	20%

Table 1 Risk stratification in patients with multiple myeloma

Abbreviations: ISS International Staging System. Table modified from (W J Chng et al. 2014)

There are two distinct primary molecular events that are associated with the transition of a normal plasma cell to one that has the potential to develop into myeloma: hyperdiploidy with trisomies of odd numbered chromosomes and translocations involving the immunoglobulin heavy chain locus (IGH) (Morgan, Walker, and Davies 2012). These two mechanisms are each responsible for approximately 50% of cases of myeloma and a small number of cases are found to have both mutations concurrently (Prideaux et al. 2014). A common mechanism of dysregulation of the G1/S checkpoint and cyclin D unifies the two distinct types of underlying molecular abnormalities in myeloma by overexpression of genes either being

driven by the IGH promoter in translocation or by copy number variation in hyperdiploid myelomas (Wee J Chng et al. 2007) .

The presence of chromosomal translocations in multiple myeloma can be partially explained by the normal process by which a functional antibody-secreting plasma cell is developed. B cells are derived from a haematopoetic stem cell found in bone marrow via a common multi-potent progenitor cell and the common lymphoid progenitor cell (Kondo 2010). Whilst in the bone marrow, a series of carefully orchestrated DNA editing events occur in the immunoglobulin heavy chain locus where rearrangement of segments of DNA referred to a Variable (V), Diversity (D) and Junction (J) followed by similar events in the light chain locus (although these lack the diversity segments found in the heavy chain). This editing leads to the production of either a mature B cell with a cell surface B cell receptor (BCR) or, if the process fails, apoptosis of the cell. Mature B cells then migrate to the lymphoid organs where they await activation by presentation of an antigen that can bind to their BCR resulting in their rapid proliferation leading to the formation of a germinal centre. During the rapid proliferation, B cells undergo a process of somatic hypermutation, in order to increase the affinity of any antibody produced for its target, and class switch recombination leading to the production of different classes of immunoglobulins. Both of these processes require the DNA editing enzyme activation-induced deaminase (AID) and lead to the formation of double-stranded DNA breaks (González et al. 2007). Whilst normally these double-stranded breaks are repaired locally, it is possible for recombination to occur at sites of other double-stranded breaks leading to chromosomal translocations.

In myeloma, several translocation partners are regularly observed with the IGH locus including cyclin D1, cyclin D3, the MAF transcription factor, and jointly to Wolf-Hirschhorn

syndrome candidate 1 (WHSC1, also known as MMSET) and fibroblast growth factor receptor 3 (FGFR3).

Translocation partner	Location	Prevalance
Cyclin D1	t(11;14)	15%
Cyclin D3	t(6;14)	2%
MAF/MAFB	t(14;16) t(14;20)	10%
WHSCI1/FGFR3	t(4;14)	15%

Table 2 Translocations observed in multiple myeloma

Prevalence figures as given in (Prideaux et al. 2014)

The t(4;14) translocation is one of the high-risk chromosomal abnormalities discussed in staging of myeloma, as described above. The translocation leads in all cases to over-expression of WHSC1, a SET-domain containing lysine methyltransferase and in 70% of cases to over-expression of FGFR3. The 30% of cases with a t(4;14) translocation that do not express FGFR3 have no survival benefit over those which do express FGFR3 suggesting that it is the fusion with WHSC1 that is important in the pathogenesis of myeloma (Keats et al. 2005). WHSC1 has catalytic activity to mono- and di-methylate histone 3 lysine 36 (H3K36) in vivo (Kuo et al. 2011) although in vitro using peptides as substrates activity has been demonstrated for a wider range of targets (Morishita, Mevius, and di Luccio 2014). Increased expression of WHSC1 has a range of effects within myeloma cells including overexpression of SLAMF7 (Z. Xie et al. 2013) and regulation of genes involved in cell cycle control and cellular adhesion (Brito et al. 2009). WHSC1 also includes the H/ACA

box RNA ACA11 in intron 20 which is also overexpressed in t(4;14) myeloma cells that may play a role in the pathogenesis of the disease (Mirabella et al. 2013).

An important consideration in the pathogenesis of multiple myeloma is the role played by the bone marrow microenvironment. In early myeloma and its precursor conditions, myeloma cells are restricted to growth within the bone marrow. It is only when the disease progresses and accumulates more mutations that malignant cells are able to survive outside the supporting niche of the bone marrow (Varettoni et al. 2010). The bone marrow microenvironment consists of a cellular compartment, including the haematopoetic cells, bone marrow stromal cells, immune cells, adipocytes, osteoblasts and osteoclasts. A complex interaction between these cells leads to conditions that are permissive for myeloma growth (Kawano et al. 2015). The non-cell compartment of the bone marrow microenvironment, consisting of the extracellular matrix (ECM), is also important in disease pathogenesis. Changes to the composition of the ECM are observed during myeloma development (Slany et al. 2014) and binding to ECM components alter the susceptibility of myeloma cell lines to apoptosis (Damiano et al. 1999).

Treatment options for myeloma depend largely on whether or not a patient is considered fit for an Autologous Stem Cell Transplant (ASCT) which has been demonstrated to increase median overall survival by 12 months (Attal et al. 1996). Fitness for ASCT is determined by the presence of other medical morbidities and the age of the patient with a cut-off of 70 years being often used. ASCT is preceded by induction chemotherapy followed by high-dose chemotherapy to ablate bone marrow prior to the transplant and followed by maintenance therapy. There are a large number of individual therapeutic options in use and under investigation in clinical trials and as they can be used in combination there are

currently a vast number of permutations of drugs being actively used (Moreau et al. 2015; Rajkumar 2016).

Corticosteroids including prednisolone and dexamethasone have been long used as treatment for myeloma and other heamatological malignancies. High-dose corticosteroids can also directly induce apoptosis in myeloma cells. Corticosteroids are associated with a range of side-effects including osteoporosis, which limits their tolerability and duration of use. Recent studies have suggested that the use of lower doses of dexamethasone in combination with lenalidomide provide a survival advantage over high-dose dexamethasone and lenalidomide (Rajkumar et al. 2010).

Bortezomib (also known commercially as Velcade) reversibly inhibits the proteasome activity of myeloma cells and is effective in myeloma cells not only due to the single-agent action of inducing apoptosis (G. Lu, Punj, and Chaudhary 2008) but also by sensitizing cells to other chemotherapeutic agents (Nikrad et al. 2005). Bortezomib stabilises IκB, a regulatory subunit of nuclear factor kappa B (NF-κB) and therefore prevents the expression of anti-apoptotic proteins such as BCL2, the proliferative cyclin D and adhesion molecules such as Vascular Cell Adhesion Molecule 1 (VCAM1) (Hideshima et al. 2002; Z.-W. Li et al. 2008). Bortezomib is also known to induce the unfolded protein response in myeloma cells (Obeng et al. 2006). Bortezomib was first approved for use by the Federal Drug Administration (FDA) in 2003 for refractory myeloma and has since been approved as first-line therapy in combination with a range of drugs including dexamethasone and lenolidamide (Painuly and Kumar 2013). Other proteasome inhibitors in clinical use include carfilzomib and the orally available compound ixazomib.

Immunomodulatory drugs including thalidomide and the closely related molecules lenolidamide and pomalidamide are also used in the treatment of multiple myeloma. The stated rationale behind the first trials involving thalidomide was that the known anti-angiogenic action of the compounds would be beneficial in myeloma where there is an increase seen in marrow vascularity (Singhal et al. 1999). However, it has become clear that the mechanism of action of these compounds is more complex and relies not only upon the effects on the myeloma cells but also on other cells in the bone marrow microenvironment.

The molecular target for the thalidomide-derived class of compounds is cereblon (CRBN), the substrate adaptor for Cullin-RING E3 ubiquitin ligase 4 (CRL4) (Ito et al. 2010). Thalidomide modulates the proteins targeted for ubiquitination and subsequent degradation and leads to rapid degradation of Ikaros family Zinc Finger protein 1 (IKZF1) and IKZF3, transcription factors necessary for B cell development. These are expressed in myeloma cells, and their proteolytic degradation leads to myeloma cell death (Krönke et al. 2014). The same mechanism of action applies to modulation of other immune cells within the bone marrow microenvironment thereby producing beneficial effects for the treatment of myeloma (Görgün et al. 2010).

Two monoclonal antibodies have been approved for treatment in multiple myeloma. Elotuzumab is a humanized antibody that targets signalling lymphocytic activation molecule family member 7 (SLAM7) found highly expressed in myeloma cells but is also present on natural killer cells. Elotuzumab leads to activation of NK cells and destruction of myeloma cells via antibody-mediated cell-dependent cytotoxicity (Collins et al. 2013; Guo et al. 2015) and has been demonstrated in combination with lenalidomide and low doses dexamethasone to have activity in patients with relapsed myeloma (Mateos et al. 2016).

Daratumumab is a monoclonal antibody against CD38, which is highly expressed in myeloma cells. In contrast to elotuzumab, daratumumab has shown efficacy as a single agent in patients with relapsed myeloma (Lokhorst et al. 2015; Antonio Palumbo et al. 2016).

The pan-histone deacetylase inhibitor panobinostat has demonstrated effectiveness in clinical trials in patients with refractory myeloma who have already been treated with a proteasome inhibitor (Ibragimova et al. 2013) and an immunomodulatory drug (Laubach et al. 2015). The first-generation HDAC inhibitor Vorinostat (SAHA) has demonstrated efficacy in clinical trials of myeloma patients (Siegel et al. 2014) although currently it is not licensed for the treatment of myeloma.

1.4 Epidemiology and Pathogenesis of Ewing Sarcoma

The Ewing sarcoma family of tumours comprises the clinical entities formally classified as Ewing Sarcoma, Peripheral Neuroepithelioma (PNET), or Ashkin's Tumour. These tumours show a similar morphology when examined by light microscopy, being composed of small, round cells with "malignant" nuclei. Distinction between the members of the family was previously made on the basis of neuroectodermal differentiation as assessed by markers such as Neuron-Specific Enolase (NSE), differentiating PNET from Ewing Sarcoma, or the location of the tumour, the Ashkin's Tumour being found within the chest wall, typically in the paravertebral region. Molecular biology techniques have identified that Ewing sarcoma share one of several common chromosomal translocations involving EWS RNA binding protein 1 (EWSR1) and a member of the ETS transcription factor family.

The United Kingdom cancer registry data show that between 1985 and 2009, 1458 cases of Ewing sarcoma were diagnosed, representing 15% of all primary bone cancers (National

Cancer Intelligence Network 2012). There is a predilection for young age with 85% of Ewing sarcoma occurring in those under 30 with the peak age-specific rate occurring in males aged between 15 and 19. There is a significantly increased rate of the disease in males with an incidence of 1.5 per million compared with the rate of 1.0 per million in females. Approximately half of the cases of Ewing sarcoma are diagnosed in the appendicular skeleton although the disease can arise in any bone and cases of extra-osseous Ewing sarcoma have also been described (Zagar, Triche, and Kinsella 2008). Five-year survival remained largely unchanged between 1985 and 2004 at 50%, with better survival demonstrated in cases with the primary tumour arising in the extremities.

The most common symptom of primary bone cancers including Ewing sarcoma is bone pain and the presence of night pain is a "red-flag" for diagnosis. Initial diagnosis includes plain X-ray imaging looking for evidence of lytic lesions, new bone formation, periosteal reaction or soft tissue swelling. In the United Kingdom, further investigation and management in the case of a suspected primary bone tumour is performed in specialist centres under a multidisciplinary team (Gerrand et al. 2016). Biopsy for diagnosis should only be performed at specialist centres due to the risk of compromising definitive treatment by poorly performed biopsies (Mankin, Lange, and Spanier 1982; Andreou et al. 2011). Diagnosis of Ewing sarcoma based on its histological appearance and expression of the surface marker CD99 is confirmed by the use of cytogenetics demonstrating a chromosomal break in the region of the EWSR1 gene on chromosome 22.

Imaging studies performed in the staging of Ewing sarcoma include CT scans to assess for the presence of soft tissue metastasis, especially to the lungs, and bone scan for assessment of metastasis to distant bones. Current UK recommendations include performing a bone

marrow biopsy in cases of Ewing sarcoma (Gerrand et al. 2016) although an American study has suggested that the concordance between evidence of local disease only by imaging and absence of bone marrow involvement is excellent and may negate the need for bone marrow biopsy in patients with local disease only (Kopp et al. 2015).

Treatment of localized Ewing sarcoma consists of three to six cycles of neoadjuvant chemotherapy, local treatment by either surgery, radiotherapy or a combination of the two, followed by further adjuvant chemotherapy. Chemotherapeutic agents used include vincristine, ifosfamide, doxorubicin and etoposide (Juergens et al. 2006) and several clinical trials are currently studying the optimum treatment regimen (Gaspar et al. 2015).

The most common translocation, accounting for approximately 85% of cases, fuses the long arm of chromosome 11 to the long arm of chromosome 22 (t(11;22)(q24;q12)) creating a fusion protein between EWSR1 and the FLi1 proto-oncogene (FLI1) (Turc-Carel et al. 1988). Other fusion partners are listed in Table 3.

Translocation	Gene Fusion	Incidence
t(11;22)(q24;q12)	EWS-FLI1	85%
t(21;22)(q22;q12)	EWS-ERG	5-10%
t(7;22)(p22;q12)	EWS-ETV	Rare
t(17;22)(q12;q12)	EWS-EIAF	Rare
t(2;22)(q33;q12)	EWS-FEV	Rare

Table 3 Chromosomal translocations found in Ewing Sarcoma

Data adapted from (Savita Sankar and Lessnick 2011)

Knockdown studies of the EWS-FLI1 fusion has shown that it is essential for cell growth in Ewing sarcoma cell lines (Tanaka et al. 1997) and mouse models of Ewing sarcoma (Hu-Lieskovan et al. 2005). Studies involving ectopic expression of the fusion protein have been confounded by the unclear nature of the cell of origin of Ewing sarcoma. Overexpression in the murine fibroblast line NIH3T3 results in transformation and a change in the transcriptomic profile (May et al. 1993). However, certain genes subsequently determined to be necessary for Ewing sarcoma growth are not found to be up-regulated in this system (Braunreiter et al. 2006) and conversely the system depends on the up-regulation of other genes such as platelet derived growth factor receptor 3 that are not necessary for Ewing sarcoma growth in vivo (Uren et al. 2003). Ectopic expression of the fusion protein in immortalized human fibroblasts leads to a transcriptional profile with similarity to that found in tumours (Hancock and Lessnick 2008) as does ectopic expression in human mesenchymal stem cells (Riggi et al. 2008).

The EWS-FLI1 fusion protein has been demonstrated to both activate and repress transcription of specific genes (Smith et al. 2006) and both are important in the pathogenesis of the disease. Activation of genes may occur due to the EWS-FLI1 transcript acting directly as a transcription factor (Zwerner et al. 2008). EWS-FLI1 is also known to directly interact with multiple proteins involved in transcription such as the RNA polymerase core unit hsRBP7 (Petermann et al. 1998), RNA helicase A (RNA) (Toretsky et al. 2006), BRCA1-associated RING domain protein 1 (BARD1) (Spahn et al. 2002), c-Jun (Kim, Denny, and Wisdom 2006), ELK4 (also known as SAP1) (D. K. Watson et al. 1997) and CBP/p300 (Nakatani et al. 2003).

One gene regulated directly by the EWS-FLI1 leading to increased expression is the histone methyltransferase enhancer of Zester, Drosophilla homologue 2 (EZH2). As discussed above, EZH2 is part of the polycomb repressive complex 2 (PCR2) and mediates transcriptional repression via methylation of histone 3 lysine 27 (Burdach et al. 2009). Knockdown of EZH2 in Ewing sarcoma cell lines led to the increase in genes associated with differentiation including epithelial membrane protein 1 (EMP1), Ephrin receptor B2 (EPHB2), glial fibrillary acidic protein (GFAP), growth associated protein 43 (GAP43) and protocadherin 7 (PCDH7) (Richter et al. 2009). These results suggest that EZH2 overexpression leads to maintenance of stemness via polycomb-mediated repression of differentiation genes. A small study of soft tissue sarcomas including 6 cases of extra-osseous Ewing sarcoma suggests that higher levels of expression of EZH2 are associated with a higher risk of metastatic disease and reduced overall survival (Ramaglia et al. 2016).

In addition to EZH2, the polycomb component BMI1 proto-oncogene, polycomb ring finger (BMI1) is also up-regulated in Ewing sarcoma (Douglas et al. 2008). BMI1 has been implicated in repression of cyclin dependent kinase inhibitor 2a (CDKN2A) (Jacobs et al. 1999) but its role in Ewing sarcoma is independent of this effect and appears to be mediated by repression of genes involved in cellular differentiation in a mechanism analogous to that seen with EZH2.

Other key genes up-regulated by EWS-FLI1 and implicated in pathogenesis of Ewing sarcoma include NK2 homeobox 2 (NK2.2) (Smith et al. 2006), nuclear receptor subfamily 0 group B member 1 (NR0B1) (Kinsey, Smith, and Lessnick 2006) and GLI family zinc finger 1 (GLI1) (Zwerner et al. 2008).

Repression of genes by the EWS-FLI1 fusion protein is mediated through recruitment of inhibitory complexes such as the nuclear remodeling deacetylase (nuRD) complex to gene promoter regions (S Sankar et al. 2013). These inhibitor complexes contain histone deacetylases, lysine specific demethylase 1 (LSD1/KDM1A) and methylated DNA binding proteins, which act as described earlier to repress active gene transcription. Genes which are directly inhibited in this manner in Ewing sarcoma include transforming growth factor beta receptor 2 (TGFRB2) and lysyl oxidase (LOX), both of which are necessary for Ewing sarcoma proliferation (S Sankar et al. 2013).

The role of the insulin-like growth factor pathway has been studied in Ewing sarcoma and led to several clinical trials. Insulin-like growth factor receptor one and two (IGF-R1, IGF-R2) are cell surface tyrosine kinase receptors that upon activation homodimerise and activate downstream signaling pathways. These include the mitogen-activated protein kinase (MAPK) and phosphoinositide 3-kinase (PI3K) pathways resulting in increased cellular proliferation and resistance to apoptosis (LeRoith and Roberts 2003). Ewing sarcoma cells both express IGF1 and its receptor and accordingly are able to stimulate their own growth in an autocrine fashion (Yee et al. 1990). Inhibition of IGF-1R using either a monoclonal antibody or the small molecule inhibitor lisitinib was shown to have a synergistic effect the DNA minor groove binding compound trabectedin in both cell lines and a mouse xenograft model, possibly through a mechanism whereby trabectedin promotes expression of IGF-1R via increasing the affinity of the EWS-FLI1 fusion protein to the promoter region of the gene (Amaral et al. 2015). Despite preclinical data suggesting the efficacy of compounds targeting the IGF pathway, clinical trials have been overall disappointing although a small minority (0.7%) of patients have demonstrated a complete response (van Maldegem et al. 2016). This

may suggest that targeting IGFR1 may be a valid approach but only in a selected cohort of patients.

Poly-ADP-ribose polymerase (PARP) inhibition has also been examined as a therapeutic modality in Ewing sarcoma. PARP is required for the repair of DNA damage including single-stranded breaks and its inhibition potentiates the deleterious effects of DNA damaging agents (Cipak and Jantova 2010). Ewing sarcoma was identified as being particular sensitive to PARP inhibition in a large screen of cancer cells lines (Garnett et al. 2012) and a phase 2 trial resulted in stable disease in 4 out of 12 patients treated with the PARP inhibitor olaparib (Norris et al. 2014).

Hypermethylation of DNA promoter regions has also been demonstrated in Ewing sarcoma and is implicated in the pathogenesis of the disease (N. Patel et al. 2012). A total of 36 genes were identified as being hypermethylated when compared to human mesenchymal stem cells, the suggested progenitor cell for Ewing sarcoma. The list of affected genes includes several involved in differentiation such as versican (VCAN) and collagen 1A1 (COL1A1) both of which are required for extracellular matrix formation and the nerve growth factor receptor (NGFR). Treatment with the DNA methyltransferase inhibitor 5-aza-2'deoxycytidine (5AZA) was able to increase the expression of these genes and previous studies has demonstrated that 5AZA reduces proliferation in Ewing sarcoma (Hurtubise, Bernstein, and Momparler 2008).

Recent in vitro data demonstrate that Ewing sarcoma is also susceptible to inhibition of BET bromodomains using the small molecule JQ1 (Hensel et al. 2016). JQ1 treatment was able to reduce expression of the EWS-FLI1 fusion protein and reduces proliferation of Ewing sarcoma cell lines.

1.5 GSK-J4 IS A SMALL MOLECULE IINHIBITOR OF KDM5B, KDM6A AND KDM6B

A tool compound used throughout this thesis is the small molecule inhibitor GSK-J4. GSK-J4 was described originally as an inhibitor of 2-oxoglutarate dependent oxygenases KDM6A and KDM6B (Kruidenier et al. 2012) and has subsequently been confirmed to also have activity against KDM5B (Heinemann et al. 2014), however with a 5-30-fold less inhibitory activity. GSK-J4 is the cell permeable pro-drug of GSK-J1 and is activated intracellularly by removal of an ester group masking a carboxylic acid. A prodrug is a compound that lacks activity itself but is the precursor of an active compound. It is believed that the presence of the carboxylate reduces the cell permeability but is required for activity due to mimicking the 2-oxoglutarate. GSK-J5 is a pyridine regio-isomer of GSK-J4, which has greatly reduced ability to inhibit the activity of the enzymes and is used in these experiments as a control compound. A further derivative, KDOBA67 replaces the carboxylic acid with an alcohol group, therefore is cell-permeable and does not require an activation step with intracellular esterases.

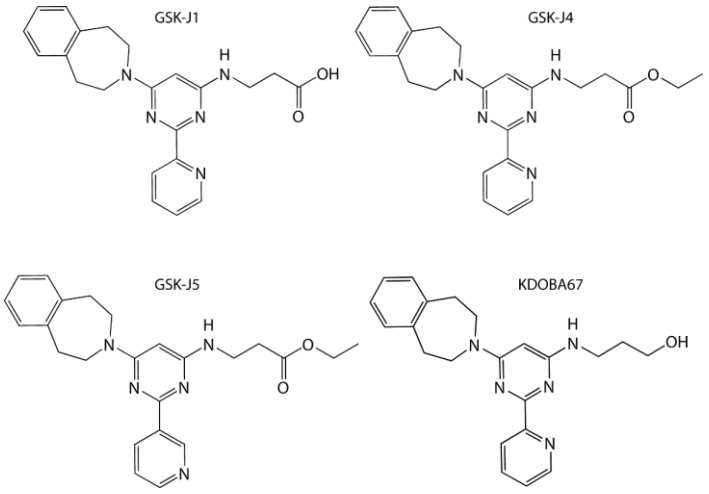


Figure 6 Structures of GSK-J4 and related molecules

GSK-J4 has been used to investigate a variety of processes including embryogenesis (B. Xie et al. 2016; Kamikawa and Donohoe 2015; Inoue et al. 2014), immune cell differentiation and regulation (Liu et al. 2015; Doñas et al. 2016; Kruidenier et al. 2012), as well as chondrogenesis (Yapp et al. 2016).

Three published studies have investigated the role of GSK-J4 in cancers. In the first, the authors investigated the role of KDM6A and KDM6B in the haematological malignancy T cell acute lymphoblastic leukaemia(T-ALL) (Ntziachristos et al. 2014). This paper demonstrated that KDM6B was required for disease initiation yet KDM6A acted as a tumour suppressor and is frequently inactivated through mutation in T-ALL. GSK-J4 was able to inhibit T-ALL cell growth in vitro with an IC_{50} of 2μM by inducing cell cycle arrest and apoptosis.

In paediatric brainstem gliomas, GSK-J4 was able to inhibit cell growth and to induce apoptosis in cells containing a lysine to methionine mutation at position 27 of histone 3 (referred to as H3K27M) (Hashizume et al. 2014). The authors report no activity in cells with wild-type H3K27 although the maximum concentration of GSK-J4 used was only 8μM. Xenograft models where human tumours were implanted into the brain stem of mice showed that GSK-J4 was able to reduce the growth of these tumours. Analysis of the CNS of mice treated with GSK-J4 indicated the presence of both GSK-J4 and GSK-J1 indicating that GSK-J4 was able to cross the blood brain barrier and be activated in this system.

GSK-J4 has also been demonstrated to induce apoptosis and reduce the tumour initiating capacity of cancer stem cells derived from the ovarian cancer cell line A2780 (Sakaki et al. 2015).

1.6 THE LYSINE DEMETHYLASE FAMILIES KDM5 AND KDM6

The focus of work in this thesis is directed towards the members of the KDM5 and KDM6 family so a more detailed background to these proteins will be given in order to complement the general background provided above. An overview of the architecture and substrates for these families members is shown is Figure 7.

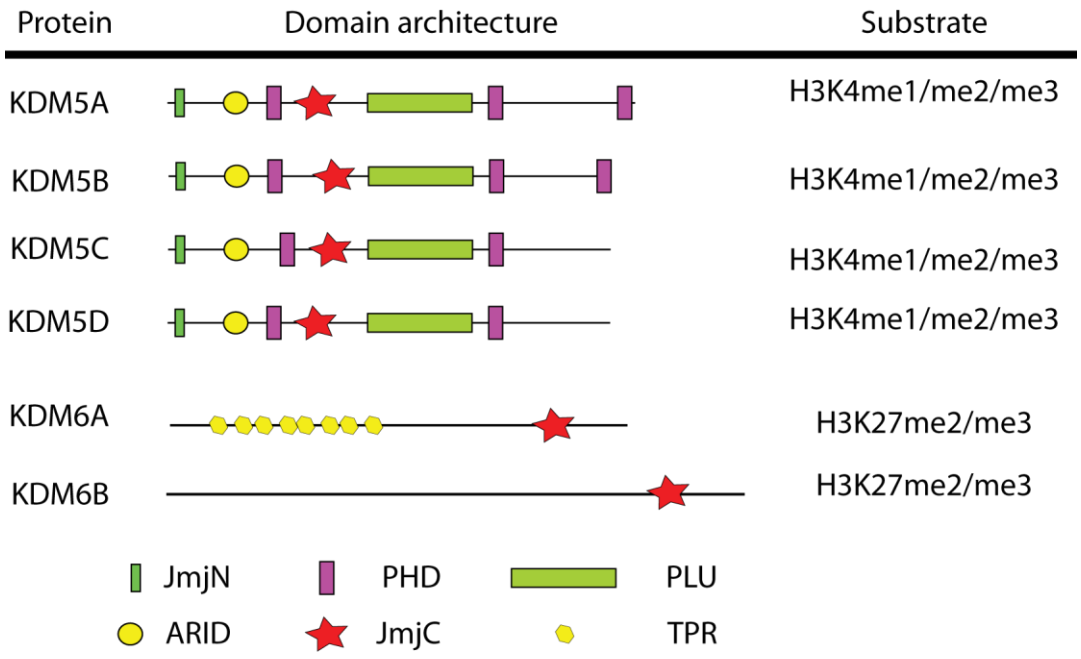


Figure 7 Overview of KDM5 and KDM6 protein archtecture

1.7 THE KDM5 SUBFAMILY

KDM5 is an evolutionary-conserved family of KDMs with orthologues found in species including C. elegans, where it is known as RBR2, Drosophila melanogaster, known as LID and yeast, Jhd2p. In humans, the family consists of four members (KDM5A-D). All KDM5 proteins contain five conserved domains: a JmjC domain which is required for the demethylase activity; a JmjN domain which has been implicated in maintaining protein

stability (Huang et al. 2010); an AT-Rich Interaction Domain (ARID), involved with DNA-binding; the zinc-finger C5HC2 zinc finger and a Plant Homeo Domain (PHD), an epigenetic reader which recognises methylated lysine residues on histones. KDM5 has been demonstrated to demethylate methylated lysine 4 of Histone H3 (H3K4) (Xiang et al. 2007) when in the di- and tri-methyl state. The H3K4me3 is associated with active gene transcription and inhibition of KDM5 has been postulated to play a role in tumourigenesis (Blair et al. 2011).

1.7.1 KDM5B - JARID1B

KDM5B is a 176kDa protein encoded by a gene found at chromosomal position 1q32.1. Two alternatively spliced isoforms exists although no difference in function has been reported between the two. KDM5B (also known as JARID1B and PLU1) was first identified in breast cancer cell lines when it was identified as being down-regulated in cells treated with an antibody against the Human Epidermal Growth Factor Receptor 2 (HER2, also known as Neu, ErbB-2) (P. J. Lu et al. 1999). It was also demonstrated by the same group that KDM5B was conspicuously over-expressed in breast cancer and has a restricted expression pattern in normal human tissues (Barrett et al. 2002). KDM5B interacts with KDM1 to reduce the expression of CCL14, decreasing the angiogenic and metastatic potential of breast cancer cells in vivo (Q. Li et al. 2011). Over-expression of KDM5B in breast cancer cell lines is associated with down-regulation of CDKN1A, promoting cellular proliferation (Wong et al. 2012). KDM5B has also been implicated in the pathogenesis of melanoma (Kuzbicki et al. 2013), colorectal cancer (Ohta et al. 2013) and lung cancer (Rao et al. 2011).

1.8 THE KDM6 SUBFAMILY

The KDM6 family of lysine demethylases consists in humans of KDM6A (Ubiquitously-transcribed TPR protein on the X chromosome (UTX)), KDM6B (JMJD3) and KDM6C (Ubiquitously-transcribed TPR protein on the Y chromosome (UTY)). KDM6A and KDM6B have been long established as having demethylase activity (Hong et al. 2007) with KDM6C having more recently been demonstrated to be active (Walport et al. 2014). All members of the KDM6 family contain a single JmjC domain, which is important for the demethylase activity. KDM6A and KDM6C also contain six copies of the Tetraticopeptide Repeat (TPR) domain which is important for protein-protein or protein-RNA interactions (Blatch and Lässle 1999). KDM6A and B enzymes are able to remove the di- and tri-methyl marks from histone 3 lysine 27 (H3K27), a mark normally associated with transcriptional repression. KDM6 enzymes antagonise the activity of the Polycomb Repressive Complex 2 (PRC2), which acts to trimethylate H3K27. The importance of control of H3K27 methylation during embyonic development appears conserved across species and accordingly orthologues of KDM6 are found throughout the vertebrate kingdom. Abberant methylation of H3K27 has also been associated with cancer (Martinez-Garcia and Licht 2010) and can be due to either over-activity of methyltransferase genes (Morin et al. 2010) or inactivity of one of the KDM genes (van Haaften et al. 2009).

1.8.1 KDM6A (UTX)

KDM6A is a 154kDa protein encoded by a gene at chromosomal position Xp11.2. There are 14 confirmed splice variants of which 11 are known to produce a protein product. It is one of the few genes on the X-chromosome not to undergo inactivation (Greenfield et al. 1998)

and this has been suggested as important for murine development of sex-specific reproductive organs through regulation of homeobox genes (Berletch et al. 2013). Complete deletion of KDM6A is fatal during embryonic development (Copur and Müller 2013) but in mice with mutated KDM6A that lack demethylase activity embryos are viable but display a distinct phenotype (Shpargel et al. 2012) suggesting that non-catalytic functions are also important. In humans, germ-line microdeletions of the catalytic portion of the KDM6A gene have been found to be responsible for a small number of cases of Kabuki Syndrome (Lederer et al. 2012). KDM6A has been implicated in several cancers in humans, including multiple myeloma, in which one study showed in-activitng mutations in 10% of cases (van Haaften et al. 2009), oesophageal squamous cell carcinomas and clear cell carcinomas of the kidney. No association has been made between mutated KDM6A and ESFT.

1.8.2 KDM6B (JMJD3)

KDM6B (also known as JmjD3) is a 176kDa protein encoded by a gene at chromosomal position 17p13.1. Two alternatively spliced isoforms of the gene exist although there is no known difference in function. Like KDM6A, KDM6B is known to be important in the developing embryo and plays a particular role in neurological development (Akizu et al. 2010; Estarás et al. 2012). There are several established relationships between KDM6B and cancer. Expression of the tumour suppressor locus INK4b-ARF-INK4a is suppressed by PC2 (Gil and Peters 2006; Bracken et al. 2007) and activated by KDM6B (Agger et al. 2009). KDM6B has been shown to be over-expressed in Hodgkin Lymphoma and in B cells exposed to Epstein Barr Virus (Anderton et al. 2011). In cervical cancer cells exposed to the Human Papilloma Virus (HPV) protein E7, KDM6B is increased and knockdown of KDM6B leads

to reduced proliferation (McLaughlin-Drubin et al. 2011). KDM6B has been shown to have reduced expression in lung cancers and liver cancer when compared with corresponding normal tissue (Agger et al. 2009).

1.9 OUTLINE OF THESIS

In this thesis, I will be investigating the effect of inhibition of KDM5B, KDM6A and KDM6B in a range of cancers that affect bone using the epigenetic tool compound GSK-J4.

Chapter 2 contains the methods used throughout the thesis.

Chapter 3 reports the results of cell-based assays using GSK-J4 and locked nucleic acids in which it is shown that a large metallothionein response is induced followed by the activation of the ATF4 integrated stress pathway via the kinase GCN2

Chapter 4 investigates the metabolomics changes that result from treatment with GSK-J4, revealing a perturbation of glutamate utilization and disruption of oxidative phosphorylation.

Chapter 5 shows the results of ChIPseq and RNAseq using GSK-J4, indicating global changes in H3K4me3 and H3K27me3 marks, in keeping with the postulated mechanism of action of GSK-J4.

Chapter 6 demonstrates the result of using a selective KDM5B inhibitor, showing that the phenotypic response is different to that achieved with dual inhibition of KDM5B and KDM6.

Chapter 7 summarises the presented work and discusses future directions of study.

2 MATERIALS AND METHODS

2.1 CELL CULTURE

2.1.1 Multiple Myeloma cells

The human multiple myeloma cell lines JJN3, RPMI-8226, MM1R, MN-60, MINO, ARH-77, NCI-H929 were gifts from Dr Claire Edwards, NDORMS, University of Oxford. The cell lines JIM3, MM1S, KMS11 and U266 were gifts from Professor Gareth Morgan, Institute of Cancer Research, London.

All myeloma cell lines with the exception of JJN3 were cultured in RPMI (Sigma) with the addition of 10% heat inactivated Fetal Calf Serum (FCS) (Invitrogen) and the supplementation of 2mmol/L glutamine (Sigma). JJN3 cells were cultured in a 50:50 mix of RPMI and Iscove's Modified Dulbecco's Media (IMDM), supplemented with 20% FCS and 4mmol/L glutamine. Cell culture media were not supplemented with antibiotics.

MM cell lines were cultured in humidified incubators at 37°C with 5% carbon dioxide (CO_2). Cells grew either in suspension or lightly attached to the bottom surface of the flask. Cells were passaged twice a week. For passaging, flasks were gently tapped to loosen any cells attached to the bottom of the flask and then split in a ratio of 1:3 for JJN3, MM1R, MM1S, MN-60, MINO,ARH-77, NCI_H929 and U266 and 1:10 for other cell lines.

2.1.2 Ewing Sarcoma Cell Lines

The cell lines TC71, A673, CHIP100, RM82, STA-ET1, STA-ET10, SK-N-MC and RDES were obtained from Professor Nick Athanasou and Professor Bass Hassan, University of Oxford, as part of the EuroBoNet network.

All ESFT cell lines were cultured in RPMI with the addition of 10% heat inactivated FCS and 2mmol/L glutamine with the exception of TC71 that was cultured in IMDM supplemented with 10% FCS and 4mmol/L glutamine. Cell culture media were not supplemented with antibiotics.

ESFT cell lines were cultured in humidified incubators at 37°C with 5% CO_2. All ESFT cell lines grew adherent to the bottom surface of the flask. For routine growth, cells were passaged twice a week. Cell media was removed, the cell monolayer washed twice with phosphate buffered saline (PBS) and then 5ml of 0.5% trypsin (Sigma) was added. Flasks were incubated at 37°C for 10 mins to allow cells to detach. 5ml of media containing FCS was added to flasks to quench the activity of trypsin and the cells were centrifuged at 400g for 3 minutes. Cells were split 1:5 for SK-N-MC, RDES, STA-ET10; 1:10 for CHIP100, RM82 and STA-ET1 and 1:20 for TC71 and A673.

2.1.3 Mycoplasma testing

To ensure that cultured cells remained clear of infection by mycoplasma species, routine surveillance by PCR was performed. 1ml of media from growing cultures was removed and centrifuged at 500g for 3 minutes to pellet cell debris. 500µl of supernatant was then removed, placed into a clean Eppendorf tube and centrifuged at 20,000g for 5 mins. The supernatant was discarded and 50µl of TE buffer added before heating to 95°C for 5 minutes. PCR (40 cycles) was performed using the forward primer 5'GTGGGGAGCAAAYAGGATTAGA3' (including the "wobble" base Y, an equal mix of C and T) and the reverse primer 5'GGCATGATGATTTGACGTCRT3' with an annealing temperature of 60°C and extension temperature of 72°C. PCR products were analysed on a

1% agarose gel and a band visualized at approximately 450bp indicates the presence of mycoplasma infection, the exact size depending on the species of mycoplasma present.

2.2 VIABILITY ASSAY

Cell viability was measured using the resazurine -based PrestoBlue assay (Thermo Fisher) according to the manufacturer's instructions. Briefly, 10µl of PrestoBlue was added to 100µl of media containing cells and incubated for 30 minutes at 37°C. Plates were read on a FLUOstar Optima (BMG) with excitation filter at 535nm and emission filter at 615nm. Values were corrected for plate blanks and normalized to vehicle control from the same plate.

2.3 RNA EXTRACTION

Cells were lysed in 350µl of TRIzol (Invitrogen) and stored at -80°C until required. RNA was extracted using the Direct-zol RNA MiniPrep kit (Zymo) according to the manufacturer's instruction. Briefly, to 350µl of TRIzol an equal volume of 100% ethanol was added, mixed well and then added to the column. The column was spun for 30s at 8000g, washed once with 400µl pre-wash buffer followed by incubation for 15 minutes incubation with 30 units DNAse I, washed a second time with pre-wash buffer followed by a 700µl of wash buffer. Columns were dry-spun at 8000g for 3 minutes to remove all traces of wash buffer then RNA eluted in 30µl nuclease-free water.

2.4 cDNA SYNTHESIS

RNA extracted from cells was quantitated on the NanoDrop 1000 (Thermo Scientific) and assessed for purity by measurement of the ratio of absorbance at 260:280nm and 260:230nm, a ratio above 1.8 being deemed satisfactory. Up to 2ug of RNA was then converted to cDNA

using the High-Capacity cDNA Reverse Transcription Kit (Applied Biosystems) according to the manufacturer's instructions.

2.5 QUANTITATIVE PCR

Quantitative PCR (qPCR) was performed on the Viia 7 Real Time PCR machine (Applied Biosystems) using Fast SYBR Green Master Mix (Applied Biosystems), primers at a final concentration of 225nM and 20ng starting cDNA in a final volume of 10ul. Measurements were performed in technical triplicates for each sample. Standard cycling parameters for fast SYBR chemistry including a melt curve were used: 10 second initial denaturation at 95°C followed by 40 cycles of 1 second at 95°C followed by 20 seconds at 60°C with a final melt curve rising from 60°C to 95°C at 0.05°C per second.

Data analysis was performed using the -ΔΔCT method using the endogenous controls as described for each experiment in the text.

Intron-spanning primers were designed with an annealing temperature above 60°C. Prior to use, each primer pair was validated to ensure that only one peak was present in the melt curve and that the primer amplified with an efficiency of between 90% and 110%. A full table of primers used is included in Appendix A.

2.6 PREPARATION OF RNA FOR MICROARRAY EXPRESSION ANALYSIS

RNA for microarray studies was prepared using a traditional phenol:chloroform extraction protocol. Cells were lysed in 1ml of TRIzol to which was added 200µl of chloroform. The sample was well mixed, followed by centrifugation at 12,000g for 3 minutes. The aqueous phase was removed and transferred to a clean tube where 500µl of propan-2-ol was added to

precipitate the RNA. Samples were incubated for 10 minutes then centrifuged at 12,000g at 4°C for 10 minutes. The supernatant was removed, the RNA pellet washed twice in 80% ethanol then re-suspended in 50µl of nuclease-free water. RNA was quantitated on the Nandrop, as described above, and 1µg transferred to Cambridge Genomic Services, Cambridge, UK, a commercial organisation that further processed the samples and hybridized them using the HumanHT-12V4 BeadChip (Illumina), returning raw intensity values that were processed as described in the appropriate section.

2.7 KNOCK-DOWN WITH LOCKED NUCLEIC ACID (LNA) ANTI-SENSE MOLECULES

$6x10^4$ cells in 1 ml of media were seeded into a 24-well plate and Locked Nucleic Acid molecules were added to a final concentration of 5µM. On day 4, a further 1 ml of LNA-containing media was added to each well. On day 7, proliferation was measured by removing 100µl of cell suspension (in quadruplet) and adding 10µl PrestoBlue reagent and measured as described above. Data were normalised to cells treated with a scrambled LNA. RNA was extracted from the remaining cells as described above.

2.8 NEXT GENERATION SEQUENCING

2.8.1 RNA extraction and library preparation for Next Generation Sequencing

RNA was extracted as described above. In addition to quality control by means of the Nanodrop, RNA integrity was assessed on a Tape Station 2100 (Agilent) using High Sensitivity RNA screentape (Agilent) according to the manufacturer's instructions. Briefly, 1µl of RNA was added to 2µl of high sensitivity sample buffer, heated to 72°C for 3 minutes,

placed on ice for 2 minutes before being loaded into the Tape Station. Quality was assessed by inspection of the electropherogram obtained and derived RNA Integrity Number (RIN) (Schroeder et al. 2006). Unless otherwise stated, RIN values were always above 8 for processed samples.

Poly-adenylated RNA was enriched from extracted RNA using the NEBNext Poly(A) mRNA magnetic isolation module (New England Biolabs) according to the manufacturer's instructions. Poly A-enriched RNA was then used as the input to the NEBNext Ultra Directional RNA Library Prep Kit for Illumina (New England Biolabs) with modifications to the fragmentation time, adaptor concentration, number of PCR cycles and magnetic beads used for clean-up steps.

Fragmentation time was reduced from 15 minutes to 12 minutes based on the observation that even with high RIN numbers (indicating intact RNA), 15 minutes of fragmentation tended to result in a mean fragment size below the 200bp that is desired.

The concentration of the adaptor added was reduced from the recommended 1.5µM to 750nM due to the presence of excessive adaptor-dimers at the recommended concentration. Adaptor dimers are able to bind to the flow cell during sequencing and reduce the number of reads per library.

The number of PCR cycles was reduced by 2-fold from the recommendation of the manufacturer. Following manufacturer recommendations, final library concentrations of 25-100nM were being obtained which was in excess of the amount needed for sequencing and increased the risk of PCR duplicates.

Finally, in place of the Ampure XP beads (Beckman Coluter) recommended by the manufacturer, an in-house SPRI-bead product was used, the details of which appear below.

2.8.2 Chromatin Immunoprecipitation and Next Generation Sequencing

For adherent cell lines, cells were first scraped into solution. Cells were pelleted by centrifugation at 400g for 5 minutes at 4°C and then re-suspended in 1% formaldehyde (Sigma) for 8 minutes, after which glycine was added in excess to stop cross-linking. Cells were spun at 400g for 5 minutes at 4°C, the supernatant removed and the cell pellet re-suspended in up to 300µl chip lysis buffer (details of all buffers used below) containing freshly added protease inhibitor cocktail (Roche). Sonication was performed in a Bioruptor Pico (Diagenode) sonicator for 3 rounds consisting of 10 cycles of 30 seconds on and 30 seconds off with a brief vortex performed between each round of sonication. Sonication efficiency was confirmed by reversal of crosslinking of a 2µl sample at 90°C for 30 minutes in 1M sodium chloride, analyzed on a 1% agarose gel.

A 50:50 mix of protein A and protein G Sepharose beads (Thermo Fisher) was washed three times with chip dilution buffer and then re-suspended in chip dilution buffer containing an equal volume to the beads of 10mg/ml bovine serum albumin (Sigma, UK) and 20µl of 10mg/ml yeast tRNA (Ambion) and allowed to rotate at 4°C for one hour. After incubation, beads were washed twice in chip dilution buffer prior to use.

Sonicated chromatin was diluted to a volume of 1ml using chip dilution buffer and to this 50µl of Sepharose beads was added. After 1 hour incubation at 4°C, samples were centrifuged at 400g for 3 minutes at 4°C and the supernatant transferred to a clean tube. Antibody, as described below, was added to the tube and incubated on a rotor overnight at

4°C. After the overnight incubation, 50µl of pre-blocked sepharose beads were added to each sample and allowed to incubate for 1 hour on a rotor at 4°C.

Sepharose beads were washed sequentially in the following buffers on ice: low salt buffer (twice), high salt buffer, lithium cholride buffer and TE buffer (twice). Finally, 300µl of chip elution buffer was added to each sample, vortexed and then heated at 65°C overnight. Following overnight incubation, supernatants were transferred to clean tubes and 10µl of 20mg/ml proteinase K (Thermo Fisher) added and incubated at 55°C for 2 hours. Pulled-down DNA was recovered using SPRI beads with a ratio of 1.8 (approximately 540µl) and eluted in 20µl of 0.1x TE. Samples were analyzed on the High Sensitivity D1000 tape on the Tape Station 2100 (Agilent) according to the manufacturer's instructions to investigate the size distribution and amount of recovered DNA.

Illumina-compatible libraries were produced using the NEBNext Ultra DNA library prep kit for Illumina (New England Biolabs) according to the manufacturer's instructions but with the same modifications as described above for the preparation of RNAseq libraries.

2.8.3 Antibodies

The following antibodies were used:

Anti-H3K27me3	Millpore Catalogue 07-449 Lot 2455635. 10µg per IP.
Anti-H3K4me3	Millpore Catalogue 07-473 Lot 2207281. 1 µg per IP.

2.8.4 Library Pooling and Quantification for Sequencing

The molarity of each library to be pooled was determined on the Tape Station. The volume of each individual library to be added to the final pool was determined based on the reciprocal of the molarity and the final proportion of the total number of sequencing reads required for each library. The final pooled library was then analysed on the Tape Station again to determine the final concentration and size-distribution of the final pool.

The pooled library was also quantitated by qPCR using the Kapa Library Quantification Kit (Kapa Biosystems) according to manufacturer's instructions with two different dilutions of the final library. Using the mean library size for the pool determined earlier on the Tape Station, a size adjustment was performed on the measured quantity to obtain the size-adjusted quantity.

Finally, concentrations measured by the two different methods were compared to ensure that the results were consistent with each other. When compared to the clustering achieved on the sequencer, quantitation from the Tape Station consistently underestimated the molarity of the pool whereas quantitation by qPCR overestimated the molarity so a mean value of the two obtained molarities was used as the final concentration of the pool.

2.8.5 Sequencing

All sequencing was performed on a NextSeq 500 (Illumina) using version 2 chemistry. Pooled libraries were loaded into the sequencer according to the manufacturer's instructions: briefly, libraries were denatured with an equal volume of 0.2M sodium hydroxide for 5 minutes at room temperature, mixed with an equal volume 0.2M Tris buffer pH 8 then diluted using HT1 buffer (Illumina) to 1ml resulting in libraries at 20pM. To 1183µl of HT1 buffer,

117µl of the 20pM dilution was added resulting in a final library concentration of 1.8pM in 1300µl, all of which was loaded into the reagent cartridge.

For RNAseq, 80bp paired-end reads were obtained. For ChIPseq and ATACseq, 40bp paired-end reads were obtained unless otherwise stated for individual experiments.

2.9 SPRI-BEADS PRODUCTION

In place of using commercial Beckman Coulter Ampure XP beads, an in-house alternative was used. Sera-Mag Speedbeads Carboxyl Magnetic Beads (hydrophobic) were purchased from GE Healthcare and 1ml of re-suspended beads was washed three times in 0.5M EDTA. SPRI-buffer (details below) was freshly produced and the pre-washed magnetic beads were re-suspended into a volume of 50ml. Beads were rotated at room temperature for 1 hour prior to use.

2.10 FLOW CYTOMETRY METHODS

Experiments were performed on a LSRFortessa (BD) instrument running FACSDiva Software version 6 with 10^4 events recorded for each experiment.

2.10.1 Cell cycle analysis – Propidium iodide staining.

Sub-confluent cultures of cells were treated with compounds at the IC80 value for between 6 and 36 hours. Cells were harvested, washed once in PBS and counted. $2x10^5$ cells were fixed overnight in 70% ethanol in PBS at -20°C. Fixed cells were centrifuged at 400g for 5 minutes and washed with PBS for 15 minutes after which they were centrifuged again. Cells were re-suspended in 200µL of PBS containing 0.1% sodium citrate, 0.1% Nonidet P40,

25µg/ml propidium iodide and 12.5µg/ml RNAse and incubated in the dark for 30 minutes before being analysed.

2.10.2 Apoptosis Detection – Annexin V

Apoptosis was determined by detecting phosphatidylserine by FITC-conjugated annexin V using the Apoptosis Detection Kit (Abcam). Briefly, following compound treatment as above, cells were harvested, washed once in PBS and 2x105 cells re-suspended in 500µl of binding buffer containing 5µL Annexin V-FITC and 5ul Propidium Iodide (50µg/ml). Cells were incubated in the dark for 10 minutes before being analysed.

2.10.3 Cellular proliferation – BrdU incorporation

Cellular proliferation was measured using the FITC BrdU Flow Kit (BD Pharminagen). Briefly, cells were treated with compound for 24 hours. BrdU was added at a final concentration of 10uM and cells were harvested after 30 minutes, 1hour and 3 hours. Cells were fixed and permeabiiized and stored at -80°C in 90% FCS, 10% DMSO. To stain, cells were thawed, washed and re-permeabilized prior to incubation with DNase 30µg/ 106 cells for 1 hour. FITC-labelled anti-BrdU was added to cells for 20 mins and total DNA stained with 7-aminoactinomycin D (7AAD). Samples were kept in the dark prior to analysis.

2.11 BUFFERS

The following buffers have been used:

Chip Lysis Buffer pH 8.1: 5ml SDS 10%, 1ml EDTA 0.5M, 5ml Tris-HCl 0.5M, pH adjusted with ammonium hydroxide and volume adjusted to 50ml with water.

ChIP Dilution buffer: 50µl SDS 10%, 120µl EDTA 0,5M, 1.67ml Tris-Hcl 0.5M pH 8.1, 1.57ml NaCl 5M, 550 Triton-X-100 100%, adjusted to 50ml with water

ChIP Low Salt Wash Buffer: 500µl SDS 10%, 500µl Triton-X-100 100%, 200µl EDTA 0.5M, 2ml Tris-Hcl 0.5M pH 8.1, 1.5ml NaCl 5M, adjusted to 50ml with water

ChIP High Salt Wash Buffer: 500µl SDS 10%, 500µl Triton-X-100 100%, 200µl EDTA 0.5M, 2ml Tris-Hcl 0.5M pH 8.1, 5ml NaCl 5M, adjusted to 50ml with water

ChIP Lithium Chloride Wash Buffer: 25ml LiCl 0.5M, 500µl Nonident P-40, 100µl EDTA 0.5M, 1ml Tris-Hcl 0.5M pH 8.1, 5ml Deoxycholate 10%, adjusted to 50ml with water

2.12 CHAPTER 3 SPECIFIC METHODS

2.12.1 Screening of the ability of small molecule inhibitors of chromatin enzymes to reduce cell viability

On Day -1, 3000 per well were plated in 96 well plates in 90µl of media and allowed to adhere or equilibrate overnight. Compounds were added in 10µl media. Solvent controls were performed at 0.1% (v/v) reflecting the concentration of the solvent used for dissolving the compounds. Treated plates were incubated for 72 hours in a humidifed incubator at 37°C and 5% CO_2 and cell viability was measured by means of the PrestoBlue assay as described above. Viability was calculated as the percentage of the DMSO-only treated cells. Screening was completed in triplicate and the arithmetic mean was calculated for each treatment and cell type. Data were plotted as a heatmap in R using a custom package function (initially

based on the "Pretty Heatmap" package *pheatmap*), the code of which can be found in Appendix B.

2.12.2 IC_{50} determination

Cells were plated as above and a ten point serial, 2-fold dilution series of the compound of interest was created ranging from a top dose of 50μM to a bottom dose of 97.6nM. Plates were incubated for 72 hours in a humidified incubator at 37°C and 5% CO_2 and cell viability was measured by means of the PrestoBlue assay as described in Chapter 2. Data were normalised to the vehicle-only treated cells on each plate. Technical quadruplets were included on each plate and three biological replicates of each dose response curve were generated. Normalised data were plotted in Prism 5.03 (Graphpad Software). A curve was automatically fitted to the data using the equation $y = bottom + \frac{(top-bottom)}{(1+10^{(logIC50*Hill\ Slope)})}$ and the fitted IC_{50} value extracted.

2.12.3 Microarray analysis of transcriptomic response to GSK-J4

JJN3 and RPMI 8226 MM cells and A673 and TC71 ESFT cells were treated at their respective IC_{80} values of GSK-J4, or an equimolar concentration of the inactive regional-isomer GSK-J5 or with 0.1% (v/v) DMSO for 6 hours. In addition, JJN3 cells were treated with the clinical proteasome inhibitor bortezomib (Velcade) at 5nM and with GSK-J4 at a sub-IC_{50} concentration of 500nM for the same time. RNA was then collected and samples were processed as described in Chapter 2.

On return of the raw data from Cambridge Genomics Services, data were processed using the R package "lumi" (P. Du, Kibbe, and Lin 2008). Briefly, data were normalised using the Robsust Spline Normalisation routine prior to performing a variance stabilising

transformation. Fold-change values were compared to vehicle treated cells and calculated as $2^{(\text{Expression in treatment condition} - \text{Expression in DMSO condition})}$.

2.12.4 Motif analysis of promoter region

Genes of interest identified from the analysis of the microarray data were analysed using Homer (version 4.6) using the genome build hg19 version and the default promoter region of each gene equating to the 2000 base pairs upstream of the transcription start site.

2.12.5 Analysis of the Integrated stress response

ISRIB (also known as Integrated Stress Response Inhibitor, trans-N,N′-(Cyclohexane-1,4-diyl)bis(2-(4-chlorophenoxy)acetamide, trans-N,N′-1,4-Cyclohexanediylbis[2-(4-chlorophenoxy)-acetamide) was purchased from Sigma. ISRIB (at 50nM) was added to cells 1 hour prior to treatment with GSK-J4. Cellular responses were analysed by qPCR as

2.12.6 Fluorescence microscopy to measure free intracellular zinc

Cells were treated with Fluozin-3 AM (Life Technologies), a cell-permeable fluorescent dye with specificity for zinc over other divalent cations. 5μM Fluozin-3 was added to cell media and incubated at 37°C for 60 minutes. Cells were washed 3 times with PBS and then incubated for a further 60 minutes prior to treatment with GSK-J4. Images were obtained every 2 minutes using a Zeiss Axio microscope and images analysed using ZEN Lite software (Zeiss)

2.13 CHAPTER 4 SPECIFIC METHODS

2.13.1 ATP assay

10^4 cells were treated with compound for the desired time. Cellular ATP content was measured using Cell Titre Glo Reagent (Promega). The reagent was reconstituted as recommended by the manufacturer and then diluted 1:6 with PBS. 100µl of diluted Reagent was added. Luminescence was measured using a Micro BetaTrilux 1650 scintillation counter (PerkinElmer).

2.13.2 Determination of NADP(H) levels

10^4 cells were treated with compound for the desired time. The ratio of oxidised to reduced nicotinamide adenine dinucleotide phosphates was determined using the NADP+/NADPH-Glo Assay (Promega) according to the manufacturer's instructions.

2.13.3 Oxygen consumption assay

Oxygen consumption was measured using the Mito_ID Extracellular O2 Sensor Kit (High Sensitivity) from Enzo Life Sciences. $5x10^4$ cells in 150µl of media were treated with compound for 24 hrs after which 10µl of sensor probe was added. Plates were read on a FLUOstar OPTIMA (BMG). Oxygen consumption is measured using a dual delay time of 30 µs and 70 µs, time resolved fluorescence (TR-F).The TR-F is converted to phosphorescence lifetime values using the Lifetime = t2-t1/Ln(D1/D2) were t=delay time and D=measured intensity value. From this equation a lifetime curve is generated where time (x-axis) and TR-F intensity (y-axis) are plotted which enables the calculation of oxygen consumption rate (OCR).

2.13.4 Glutamate dehydrogenase activity assay

Glutamate dehydrogenase (GDH) activity was measured using the GDH Activity Assay Kit (Sigma) according to the manufacturer's instructions. Activity is measured using a coupled reaction that produces NADH, the accumulation of which was measured calorimetrically using the absorbance at 450nm on a FLUOstar Optima plate reader (BMG). Change in absorbance at 450nm was measured for 20 minutes in the presence and absence of inhibitors at a range of concentration. The relative activity of the inhibitor-treated specimens relative to the controls was then calculated.

2.13.5 Metabolomic analysis by Nuclear Magnetic Resonance spectroscopy

Cell treatment: $7.5x10^6$ cells were treated with compound for the desired length of time. For flux experiments, 3 hrs prior to the end of treatment the media was removed and replaced with media containing either 10mM glucose-1,2-^{13}C2 or 2mM L-Glutamine-3-^{13}C. For metabolite extraction treated cells were washed twice with PBS and transferred to 1.8ml glass vials (Fisher), vials were centrifuged at 500g for 5 min, the supernatant discarded and the cell pellet was frozen at -80oC. Metabolites were extracted using methanol, chloroform and water in a ratio of 2:2:1.8. The aqueous layer was removed into a clean glass vial and solvent was removed by vacuum centrifugation. Freeze-dried aqueous phase samples, previously kept at -80°C, were re-suspended in 60µl NMR buffer (100mM sodium phosphate, 500µM TMSP, 10% D_2O, pH7.0) with vortexing, and 40µl of supernatant was transferred to champagne vials. 35µl supernatant was then transferred to 1.7mm NMR tubes and kept at 4°C prior to NMR. Spectra were acquired on a Bruker 600MHz spectrometer with a TCI 1.7mm z-PFG cryogenic probe using a Bruker SampleJet autosampler at 300K. In all experiments, the ^{1}H carrier was on the water frequency and the ^{1}H 90° pulse was calibrated

at a power of 0.326W. Processing of the NMR ouput was performed by Professor Ulrich Guenther and Dr Michelle Thompson at the Wellcome Trust Center for Biomolecular NMR at the University of Birmingham who returned values for each metabolite at different time points for further analysis.

2.14 CHAPTER 5 SPECIFIC METHODS

2.14.1 Quantitative ChIP sample preperation

ChIP was performed as described above with the additional step of spiking-in exogenous chromatin from SF9 cells. Prior to fixation, cells were counted with a haemocytometer and one sixth of the total number of SF9 cells added.

2.14.2 Quantitative ChIP data processing

Sequenced reads were aligned to a concatenated genome containing the human reference genome GRCh38 and the assembled SF9 genome. Reads were mapped using HISAT2 (Pertea et al. 2016) and the number of reads mapping uniquely to the SF9 determined for each sample. Bedtools version 2.2.24 (Quinlan and Hall 2010) was used to generated bedgraph files from the mapped BAM files using the scaling factor derived from the SF9 read count. Averaged tracks for each condition were produced representing the mean of the scaled values for biological replicates. The produced bedgraphs were then used as a source to create Homer tag directories (Heinz et al. 2010) using the -raw option to avoid automatic normalization. Homer was subsequently used to produce counts for metagenomics profiles around the TSS. Bedtools was also used to produce 5kb bins across the genome and filled with the median K27me3 coverage in that bin for data visualization using the HilbertVis package (version 1.30.0) in R (Anders 2009).

2.14.3 RNAseq data processing

Samples were mapped as above and the number of SF9 reads counted. A read count matrix was generated using featureCounts (Y. Liao, Smyth, and Shi 2014) using the GRCh28 GTF file as reference. The read counts matrix was processed using DESeq2 (Love et al. 2014) with scaling factors produced from the SF9 counts being used as the measure of library size in place of the automatically estimated size based on read counts. Abundance Estimates in Transcripts Per Million (TPM) were calculated using StringTie (version 1.24.0) (Pertea et al. 2016).

2.14.4 Motif analysis and GO analysis

Transcription factor motif analysis and gene ontology analysis was performed from within Homer V4.3 (Heinz et al. 2010).

3 Cell based screening and identification of GSK-J4 as a potent inhibitor of bone cancer viability

3.1 OVERVIEW

In this chapter, I will present results demonstrating the identification of GSK-J4, a small molecule inhibitor of KDM5B, KDM6A and KDM6B, as a potent inhibitor of viability in multiple myeloma (MM), the Ewing Sarcoma family of tumours (ESFT) and chordoma. The differing results of inhibition with GSK-J4 on cellular proliferation and induction of apoptosis in MM and ESFT will be shown. Transcriptomic analysis of the effect of GSK-J4 on MM and ESFT through microarray analysis demonstrating a common induction of a large metallothionein response involving the Activating Transcription Factor 4 (ATF4) pathway will be presented. Data implicating the eIF2α kinase General Control Nonrepressible 2 (GCN2, gene symbol EIF2AK4) as the kinase responsible for activation will be shown. Evidence will then be presented that the observed effect with GSK-J4 is specific by demonstrating that the phenotype can be recapitulated by achieving a knockdown of the target pattern involving KDM5B, KDM6A and KDM6B and that is necessary for all three targets to be reduced for the same phenotypic response.

3.2 INTRODUCTION

3.2.1 Cell based screening using a focused library of small molecule inhibitors against epigenetic target classes

As described in the general introduction, dysregulation of epigenetic processes is being increasingly recognised as one of the hallmarks of cancer. The complex interaction both between different epigenetic processes, such as DNA methylation and histone modifications, and between epigenetic processes and other dysregulated functions within cancer cells such as cell cycle control and the induction of apoptosis has made it difficult to predict which individual epigenetic processes will be important in any specific cancer type.

Through the efforts of organisations such as the Structural Genomics Consortium (SGC) and their associated industrial pharmaceutical partners, efforts have been made to develop high-quality, small molecule tool compounds that inhibit specifically a given family of proteins involved in a given epigenetic process, a smaller subset of that family or even individual members. The SGC have developed criteria for such tool compounds including the demonstration of inhibition of the target enzyme in the low nanomolar range, evidence of specificity by having a greater than 30-fold specificity over other families of epigenetic proteins and the demonstration of cellular activity *in vitro* in the low micromolar range (Arrowsmith et al. 2015).

Class/Target	Compound	µM	Class/Target	Compound	µM
Bromodomains - BRD2, BRD3, BRD4, BRDT (BET)	(+)-JQ1	1	Histone methyltransferase - EZH2 and EZH1	CPI-360	10
Bromodomains - Negative control	(-)-JQ1 (inactive)	1	Histone methyltransferase - EZH2 and EZH1	CPI-413	10
Bromodomains - BRD2, BRD3, BRD4, BRDT (BET)	PFI-1	5	Histone methyltransferase - G9a, GLP	UNC0638	1
Bromodomains - BRD2/3/4	I-BET	1	Histone methyltransferase - G9a, GLP	UNC0642	1
Bromodomains - pan-Bromodomain	Bromosporine	1	Histone methyltransferase - G9a, GLP	A-366	2
Bromodomains - CBP, BRD4(1)	CBP/BRD4 (0383)	5	Histone methyltransferase - SUV39H1	Chaetocin	0.05
Bromodomains - CREBBP, EP300	SGC-CBP30	1	Histone methyltransferase - SETD7	PFI-2	2
Bromodomains - CREBBP, EP300	I-CBP112	1	Histone methyltransferase - DOT1L	SGC0946	7.5
Bromodomains - BRD2, BRD3, BRD4, BRDT (BET, BD2)	RVX-208	5	Histone methyltransferase - EZH2	GSK343	3
Bromodomains - SMARCA, PB1	SMARCA	2.5	Histone methyltransferase - EZH2	UNC1999	1
Bromodomains - SMARCA, PB1	PB1/SMARCA	2.5	Histone methyltransferase - SMYD2	LLY-507	1
Bromodomains - SMARCA2/4, PB1(5)	PFI-3	1	Arginine methyltransferase - PRMT3	SGC707	1
Bromodomains - BAZ2A, BAZ2B	GSK2801	1	Lysine demethylases - LSD1	Tranylcypromine	20
Bromodomains - BRPF1B	PFI-4	1	Lysine demethylases - LSD1	GSK-LSD1 (irreversible)	0.5
Bromodomains - TRIM24/BRPF	TRIM24/BRPF	10	Lysine demethylases - LSD1	GSK-LSD1 (reversible)	5
Bromodomains - pan-BRPF	OF-1	5	Lysine demethylases - JMJD3, UTX, JARID1B	GSK J4	10
Bromodomains - BAZ2A, BAZ2B	BAZ2-ICR	1	Lysine demethylases - Negative control	GSK J5 (inactive)	10
Bromodomains - pan-BRPF	NI-57	1	Lysine demethylases - pan-2-OG	IOX1 (5-carboxy-8HQ)	40
Bromodomains - BRD9, BRD7	LP99	1	Lysine demethylases - JMJD3, UTX, JARID1B	UR-4	10
HDAC - hydroxamic acids	Belinostat	5	Lysine demethylases - JARID	KDOAM-25a	1
HDAC -	CXD101	1	Histone demethylase	Methylstat (Ester)	2.5
HDAC - aliphatic acid compounds	Valproic acid	1000	Histone demethylase - Pan JmjC	(E)-JIB-04	0.05
HDAC - ortho-amino anilides	Entinostat	0.5	Histone demethylase - JMJD2E	ML324	5
HDAC - hydroxamic acids	SAHA	2.5	Histone demethylase	KDOBA67	10
HDAC - hydroxamic acids - Class I & II	Trichostatin A	0.5	Histone demethylase - JARID1	KDM5-C70	10
HDAC - SIRT1 (indirect?) activator	SRT1720	1	Prolyl-Hydroxylases - PHD2 (EGLN1)	IOX2	10
HDAC - SIRT1	EX 527	1	Methyl Lysine Binder? - WDR5	OICR-9429	1
HDAC - 1,2,3,(8)	CI-994	1	Methyl Lysine Binder - L3MBTL3	UNC1215	5
HDAC - HDAC3	RGFP966	10	DNA methyltransferase (DNMT) -	5-Azacitidine	10
HDAC - HDAC8	PCI-34051	5	DNA methyltransferase (DNMT) - DNMT1/3	5-Azadeoxycitidine	5
HDAC - HDAC6	Rocilinostat	10	Poly ADP ribose polymerase (PARP)	Olaparib	1
HDAC - HDAC6	Tubastatin A HCl	10	Poly ADP ribose polymerase (PARP)	Rucaparib	10
tRNA loading inhibitor	MAZ1805	1	Kinase inhibitor - ATP competitive - PIM	K00135	1
tRNA loading inhibitor	MAZ1392	1	Kinase inhibitor - ATP mimetic - Haspin	5-Iodotubercidin	1
Peptidyl arginine deiminase (PADI4)	GSK484	1	Histone acetyltransferase (HAT) p300/CBP	C646	1

Table 4 Small molecules used in cell-based screening.

The concentration given is the final concentration used in cells for screening purposes

A library consisting of approximately 100 small molecule tool compounds for probing epigenetic process is available within the laboratory, the details of which are presented in Table 4. This library includes some compounds which have demonstrated activity *in vivo* and have been used clinically in humans, such as valproic acid, belinostat and SAHA, but also includes other compounds with undemonstrated *in vivo* activity. It is probable that several of these compounds would never be successful as "drugs" but this does not detract from their utility as probes for epigenetic processes within a tissue culture environment.

3.2.2 Locked Nucleic Acids

Locked Nucleic Acids (LNAs) are modified, synthetic oligonucleotides containing a phosphorothioate bond and a bridging bond between the 2' oxygen and 4' carbon of the pentose ring (Orum and Wengel 2001). The modification to the LNA structure renders them resistant to degradation by both endo- and exonucleases within the cell. LNAs are able to enter cells without the need for transfection reagents or other techniques such as electroporation through a process called gymnotic delivery in which the LNAs are taken up by the cell. LNAs designed with sequences complementary to mRNA can be used to efficiently silence gene expression by forming a double-stranded LNA:RNA molecule leading to degradation of the RNA component through the action of ribonuclease H (Maláč and Barvík 2013); the modifications to the LNA prevent degradation by RNAse H meaning that one molecule of LNA can lead to the destruction of multiple copies of the target mRNA(Stein et al. 2010).

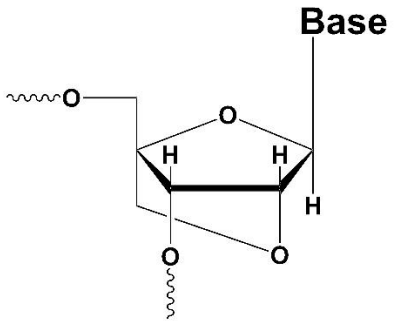


Figure 8 Structure of a Locked Nucleic Acid

3.2.3 Activating Transcription Factor 4 (ATF4) and the integrated stress response

Activating Transcription Factor 4 (ATF4) acts as a transcription factor to mediate a common set of responses to various cellular stress situations. This is due to the fact that ATF4 translation, and the translation of its target genes, is increased in response to eukaryotic initiation factor 2 alpha (eIF2α) phosphorylation at serine 51 whereas the majority of non-ATF4 target genes shows decreased translation in response to eIF2α phosphorylation.

The eIF2 α molecule is essential for the initiation of translation and binds the methionine tRNA in a GTP-dependent manner and facilitates binding of the ribosomal 40S subunit and recognition of the translation start site. Following initiation of translation, eIF2α is released from the translation initiation complex and the guanine nucleotide exchange factor EIF2B is able to exchange the GDP bound to eIF2 with a molecule of GTP, allowing binding to $tRNA^{Met}$ and further initiation of translation. When phosphorylated at serine 51, eIF2α is able to bind EIF2B with high affinity but prevents the exchange of GDP for GTP. Due to the relative abundance of eIF2α and EIF2B in the cell, with EIF2B being present at much lower concentrations, even small levels of phosphorylation of eIF2α lead to sequestration of EIF2B preventing formation of the translation initiation complex and therefore causes protein translation to be greatly reduced.

In contrast, translation of ATF4 and its target genes is enhanced by phosphorylation of eIF2α. The ATF4 mRNA contains two upstream open reading frames (uORF) before the start codon of the gene. Under non-stressed conditions, translation begins at the most 5' uORF (uORF1) and following its translation the ribosome continues scanning along the mRNA where it can quickly bind eIF2-$tRNA^{Met}$ and be ready to translate the distal 3' uORF (uORF2). Following

translation, the ribosome dissociates from the mRNA and therefore translation of the ATF4 gene itself does not occur. When eIF2α is phosphorylated the level of eIF2-tRNA^{Met} is low, translation of uORF1 occurs and ribosomal scanning along the transcript continues but as it has not been able to bind an eIF2-tRNA^{Met} complex by the time it reaches uORF2 it is not translated. Since translation of uORF2 leads to the dissociation between ribosome and mRNA, the ribosome can continue until it reaches the start codon of ATF4, resulting in its translation.

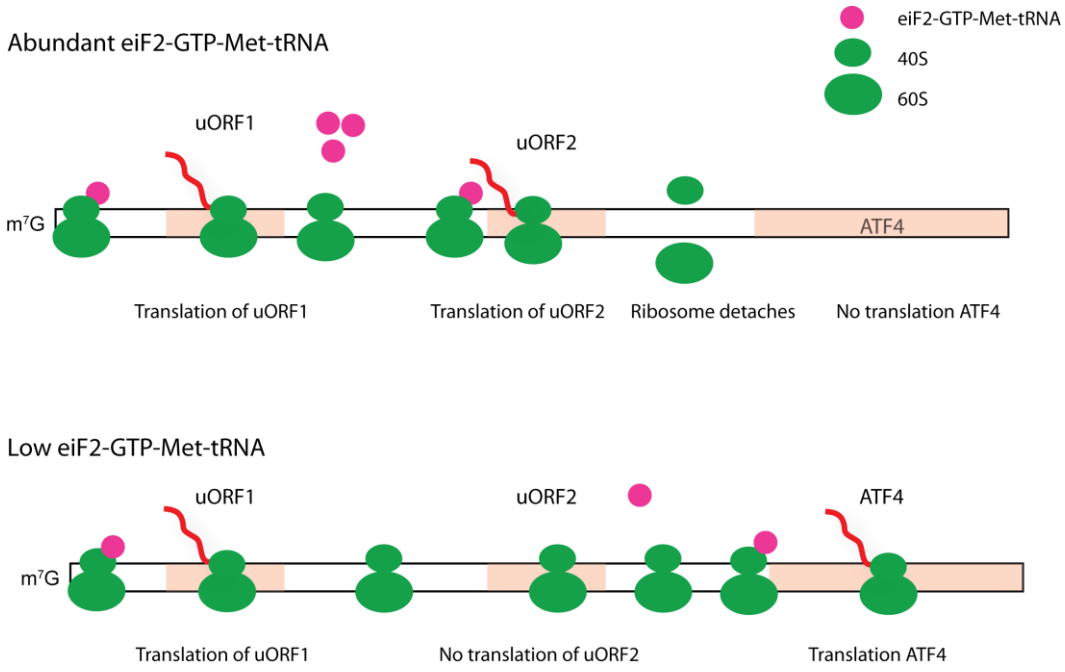


Figure 9 Translation Regulation of ATF4

Under normal conditions, abundant eIF2-tRNA^{Met} leads to rapid recharging of the scanning ribosome after translation of uORF1 resulting in translation of uORF2 and detachment of the ribosome prior to reaching the ATF4 coding region. When eIF2-tRNA^{Met} is limited, ribosomes are not reliably recharged prior to uORF2, so translation does not occur and ribosomes do not detach. A proportion of the scanning ribosomes will bind eIF2-tRNA^{Met} prior to reaching the ATF4 coding region, resulting in its translation.

The activated stress kinases able to phosphorylate eIF2α sense different forms of cellular stress situations although it appears that there is overlap for example in oxidative stress, across the kinases. Eukaryotic translation Iniating Factor 2a Kinase 1 (EIF2AK1, also known as Heme Regulated Inhibitor (HRI)) responds to low levels of heme and is important in cells of the erythroid line. EIF2AK2 (also known as Protein Kinase R (PKR)) is activated by autophosphorylation when bound to double stranded RNA as found in viral infections. EIF2AK3 (Protein kinase R-like ER Kinase, (PERK)) is bound to the endoplasmic reticulum membrane and responds to unfolded protein stress. Finally, EIF2AK4 (General Control Nonrepressible 2, (GCN2)) senses deficiency in amino acids within the cell.

3.3 RESULTS

3.3.1 A screen of small molecules identifies GSK-J4 as reducing cell viability in cancers of bone

Using a set of approximately 100 small molecule inhibitors of proteins associated with chromatin biology, the inhibitor GSK-J4 reduces cell viability across a range of cancers of bone including chordoma, multiple myeloma and Ewing Sarcoma (Figure 10). In the screen, cell viability is not reduced by GSK-J5, an inactive region-isomer of GSK-J4 (Figure 11). Direct visualisation by light microscopy of the adherent Ewing sarcoma cell lines TC71 treated with GSK-J4 for 72 hours shows that there are far fewer cells after treatment than when the same number of cells are seeded and treated with vehicle only (Figure 12)

The closely related compound KDOBA67, in which a hydroxyl moiety replaces the carboxylic acid group found in GSK-J1 and allows the compound to be cell permeable without activation by intracellular esterases, however loses in vitro potency by 20-30 fold compared to GSK-J1. KDOBA67 has an effect on cell viability in the chordoma cell lines with decreased viability observable on day 3 whereas a clear response to GSK-J4 is only observed on day 6. This may suggest that the chordoma cells are slower at converting the pro-drug GSK-J4 to the active GSK-J1 than the other cell lines studied.

The combined results of inhibition of viability by both the GSK-J4 and KDOBA67 compounds, and the absence of decreased viability with treatment by GSK-J5 support the hypothesis that the observed phenotypic effect of GSK-J4 in reducing cell viability is due to on-target effects and not due to a generalised toxicity of the molecule. Data presented later in the chapter also demonstrates that certain non-bone cancer cell types do not

undergo reduction in viability at the concentrations used in this screening experiment.

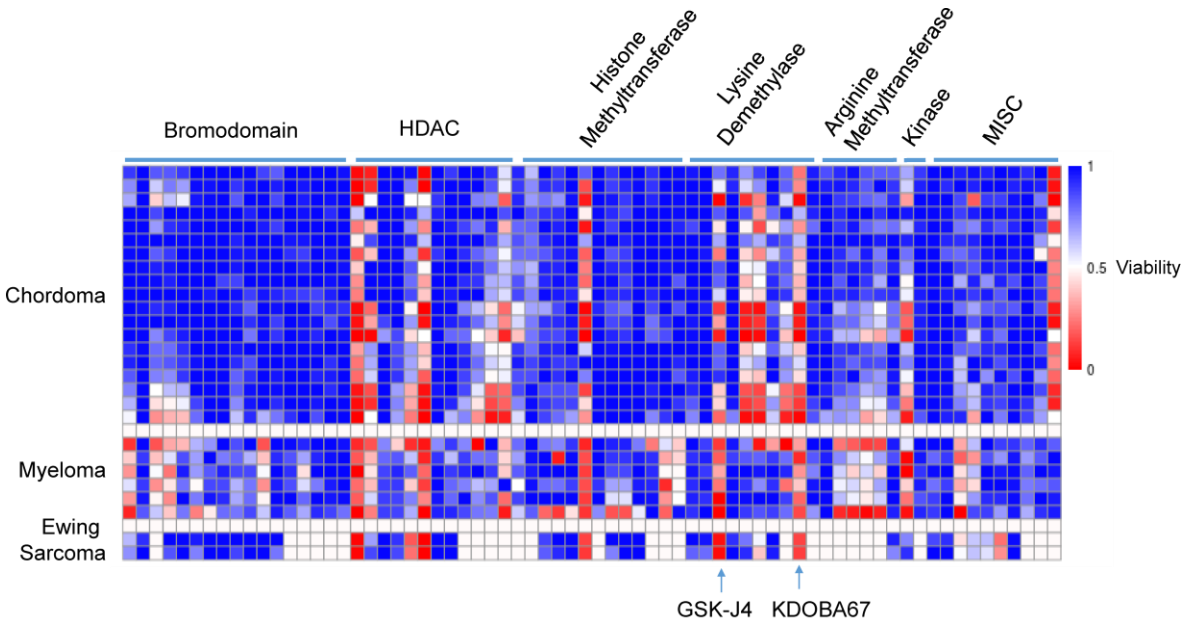


Figure 10 Small molecule screening in cancer cell lines.

Each data point represents a specific cell line, time point and drug treatment. The small molecules used in the screening and the concentration can be found in Table 4. Data plotted represents the viability in the specific condition as a fraction of the vehicle-only treated control. Each data point represents the mean of at least two biological experiments. As the compound library has increased over time, a full data-set is not available for the Ewing Sarcoma cell lines screened. This figure includes data generated by team members Graham Wells, Na Wu and Jack Worlidge.

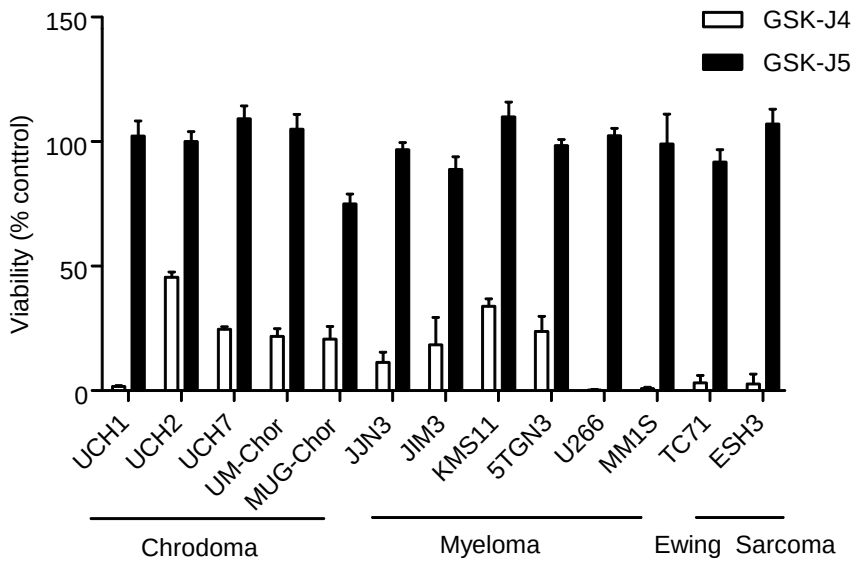


Figure 11 Viability of cancer cell lines treated with GSK-J4 or GSK-J5

Each data point in this figure represents the values from Figure 10 for treatment with 10μM GSK-J4 or GSK-J5 on day 6 for chordoma cell lines and day 3 for myeloma and Ewing sarcoma cell lines. Plotted values represent the mean ± SEM for at least 3 biological replicates.

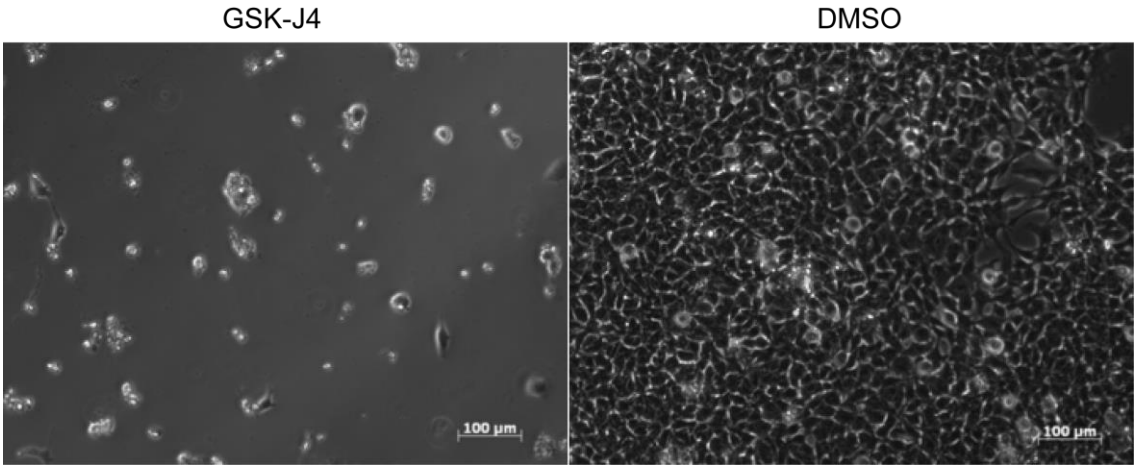


Figure 12 GSK-J4 inhibits proliferation in Ewing Sarcoma

TC71 Ewing sarcoma cells seeded at the same density were treated with either 10μM GSK-J4 (left) or DMSO (right) and imaged after 72 hours. The rapidly growing cells have become confluent in the vehicle treated cells but remain sparse in the GSK-J4 treated sample.

3.3.2 GSK-J4 has an IC_{50} in the low micromolar range in cancer cell lines

Having identified GSK-J4 as a potent inhibitor of viability in bone cancer cells in a screening experiment, the IC_{50} of GSK-J4 and GSK-J5 at 72h was determined.

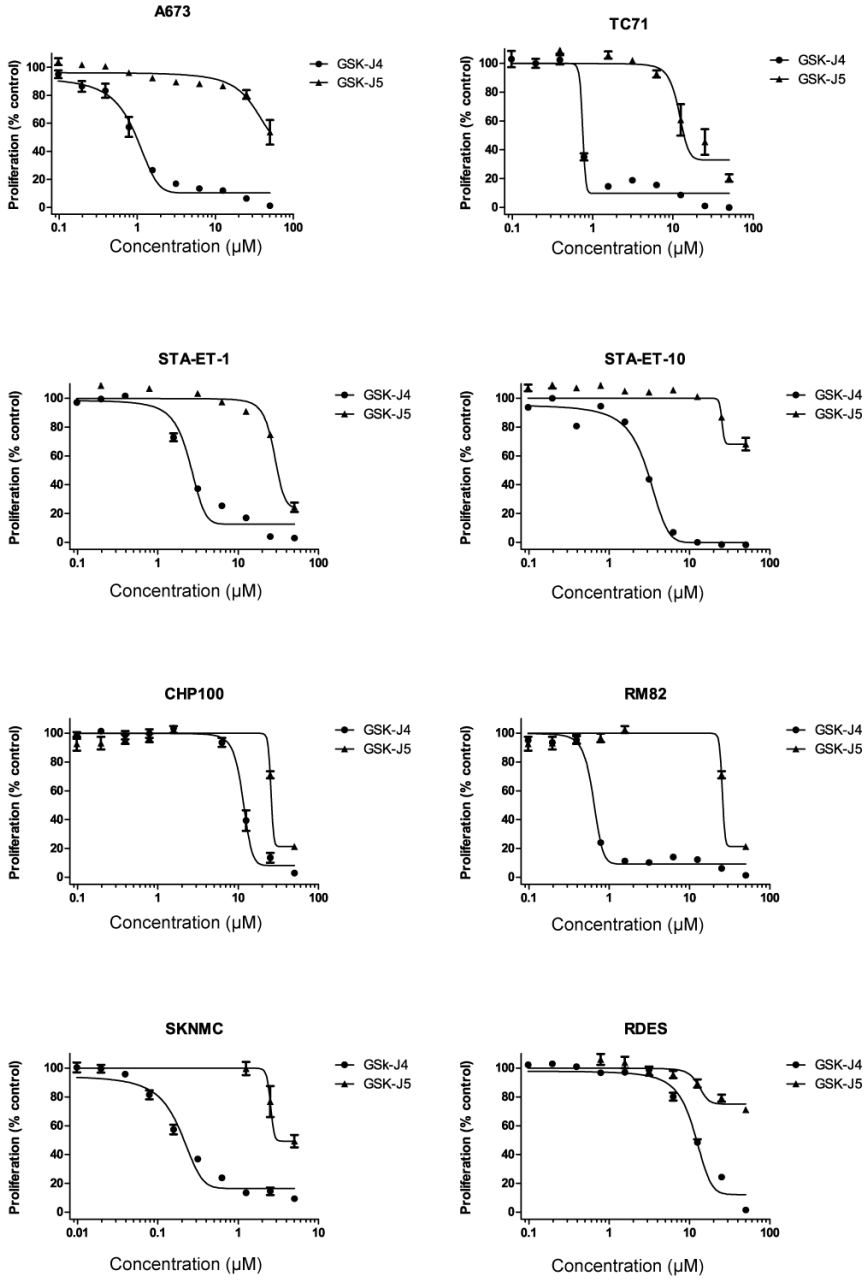


Figure 13 Dose response curves for GSK-J4 and GSK-J5 in Ewing Sarcoma

Data plotted represent the mean ± SEM for each point. n=3

Figure 13 demonstrates the dose-response curves obtained in Ewing Sarcoma cell lines showing sensitivity to GSK-J4 with an IC_{50} in the low micromolar range and only small response to GSK-J5 at concentrations of 50μM. A summary of IC_{50} values obtained in a range of cell lines is shown in Table 5.

Type	Cell line	IC50 (μM)	Standard Deviation
Ewing Sarcoma	A673	2.9	0.5
	TC71	2.7	0.1
	RDES	13.8	2.5
	SKNMC	0.2	0.1
	CHP100	11.6	3.7
	STA-ET-1	2.3	0.1
	STA-ET-10	3.1	0.1
	RM82	0.6	0.3
Myeloma	JJN3	1	0.7
	RPMI8226	1	0.2
	KMS11	2.3	1.1
	U266	1.6	0.2
	JIM3	1	0.1
	MM1R	0.5	0.1
	MM1S	1.9	0.3
	LP1	2.1	0.2
	KMM1	1.2	0.3
	ARH77	2	1.5
B Cell Lymphoma	MINO	0.7	0.1
B Cell Leukaemia	MN60	0.4	0.2
Colorectal	LS411N	6.3	0.7
	SW620	1	0.2
	LS174T	3.8	1.1
	HCT-15	0.4	0.3
	LSS13	2.7	0.7
Stromal Cells	HSS	16	2.8
Prostate Cancer	DU145	43	11.8

Table 5 IC50 value for GSK-J4 in various cancer cell lines

The data in Table 5 demonstrates the activity of GSK-J4 in a range of cancers affecting bone and include members of the Ewing sarcoma family of tumours and the plasma cell malignancy multiple myeloma. Activity is also demonstrated in cell lines derived from other malignancies of B cells such as B cell lymphoma and B cell leukaemia. Activity in the low micromolar range is also shown for cancers of colorectal origin showing that the activity of GSK-J4 is not limited solely to cancers of mesenchymal origin. In contrast, DU145, the sole prostate cancer cell line screened shows an appreciably higher IC_{50} of 43μM, approaching the level at which the "inactive" control compound GSK-J5 can be seen to start to have an effect on viability.

Further evidence that the reduction in cell viability seen with GSK-J4 is not due to general cytotoxic effects has been obtained within the group where GSK-J4 is used in other biological systems, such as investigating T cell differentiation, without any reduction in cell viability observed. GSK-J4 has also been tested on the DiscoveRx platform in which a compound is tested against a range of primary human tissues and is not found to be generally cytotoxic (data not shown).

3.3.3 GSK-J4 reduces viability in patient-derived primary tissue

In order to confirm that the reduction in viability in cancer cell lines seen with GSK-J4 translates to diseases under study and is not merely a phenomenon associated with continuous growth of cells in culture, the effect of GSK-J4 on material derived directly from patients was examined.

3.3.3.1 Ewing Sarcoma

For Ewing sarcoma, a fresh tissue sample was obtained from a biopsy of a pelvic lesion in a 10 year old male that was subsequently confirmed histologically and cytogenetically to be a Ewing sarcoma. Within 1 hour of biopsy, a sample approximately $5mm^3$ in size was placed into tissue culture medium prior to further manipulation. Approximately half of the sample was mechanically disrupted by dissection with scalpels before overnight collagenase digestion to yield a single-cell suspension. The next day, the suspension was passaged into tissue culture flasks and cells were allowed to adhere and were observed for any growth. After a brief growth of some cells with a fibroblast-like morphology there appeared to be no further growth and this half of the culture was discarded.

The other half of the original specimen was dissected into smaller masses of tissue, approximately $1mm^3$ and was placed into tissue culture-coated $60mm^2$ plates. Samples were observed for outgrowth of cells from the original tumour mass. After approximately 3 days, small, polygonal cells were observed growing from one of the tumour masses (Figure 12).

Cells were allowed to proliferate from the tumour mass for approximately 10 days before being trypsinised and passaged onto a larger surface. Further proliferation was allowed to occur and cells were passaged initially at a ratio of 1:5 every week. At passage 5, a homogenous population of cells similar in appearance to the original cells growing out of the tumour mass was observed. Cells were confirmed to be of Ewing Sarcoma origin by PCR for the EWS-FLI1 fusion transcript. Cells have grown in continuous culture for greater than 6 months and for over 50 passages and the derived cell line was named ESH3.

Sensitivity of ESH3 to GSK-J4 was measured by performing a dose-response curve as with other cell lines described earlier, resulting in an IC_{50} of 3.35μM

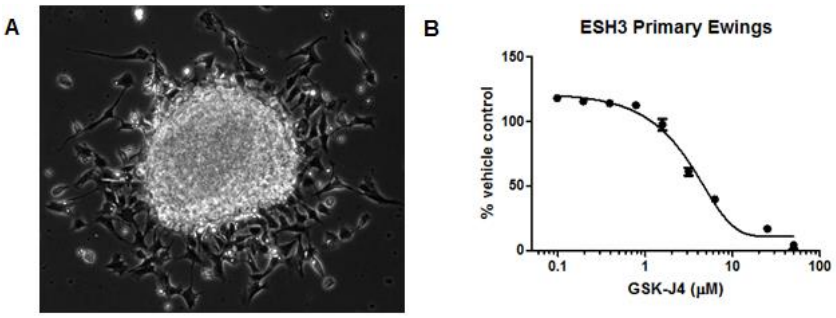


Figure 14 GSK-J4 reduces viability in primary Ewings cells

(A) *Small, polygonal cells can be seen arising from an explanted Ewing Sarcoma tissue sample that form the cell line ESH3. (B) Dose- response of ESH3 cells to GSK-J4 (n=3)*

3.3.3.2 Multiple Myeloma

In collaboration with Dr Charlotte Pawlyn at the Institute of Cancer Research, London, the effect of GSK-J4 on patient-derived myeloma cells was investigated. Following bone marrow aspirates, CD138 positive malignant plasma cells were purified using antibody-based magnetic separation. Cells were cultured either alone or in a 5:1 ratio with a GFP-expressing stromal cell feeder line. Following treatment with GSK-J4, cell viability was measured by flow cytometry using annexin/PI staining as described in chapter 2. To only measure the myeloma cells in the co-culture experiment, the feeder cells expressing GFP were subtracted by appropriate gating.

GSK-J4 causes a dose-dependent decrease in cell viability in primary human myeloma cells in the low micromolar range in keeping with the effect observed in myeloma cell lines (Figure 15). Not surprisingly, the decrease in viability observed in myeloma cells was more pronounced in cells grown in isolation when compared to cells grown in a stromal cell co-culture system.

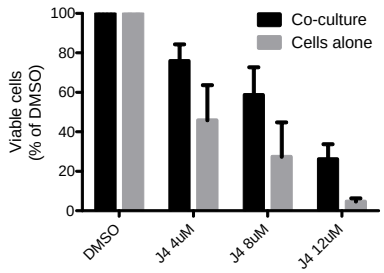


Figure 15 GSK-J4 decreases primary myeloma cell viability.

CD138 positive myeloma cells were cultured in the presence or absence of a stromal cell feeder line. In both cases, GSK-J4 treatment produces a dose-dependent decrease in cell viability, with a greater reduction seen in cells cultured without the feeder cells present. Data represent the mean ± SEM of three biological replicates.

3.3.3.3 Melanotic Neuroectomdermal Tumour of Infancy

Melanotic Neuroectodermal Tumour of Infancy (MNTI, also known as Pigmented Neuroectodermal Tumour of Infancy, PNTI) is a very rare sarcoma that commonly affects the head and neck region of infants (Kruse-Lösler et al. 2006). A 2-months old child presented to the Nuffield Orthopaedic Centre with a swelling of the fibula. A 5x2.5x2.5cm pigmented lesion was excised and was diagnosed as a MNTI. Histologically, melanin deposits were noted within some cells of the tumour (Figure 16A,B,C) and some cells expressed CD99 (Figure 16 D) and HMB45 (Figure 16 E). A full description of the histology and genetics of the tumour is presented in (Barnes et al. 2016).

A $5mm^3$ sample of the tumour was dissected to remove all non-tumour tissue and after mechanical disruption cells were treated overnight with collagenase prior to plating in tissue culture-treated vessels. Initially, under bright field microscopy two distinct cell types can be seen (Figure 16 E): one containing large deposits of melanin and the other small and round in shape. After growth in culture for five passages, melanin-containing cells were no longer visible and a single cell type with an elongated cell body became dominant in culture (Figure 16 G). These cells continued to express HMB45 and neuron- specific enolase (Figure 16 H&I) in keeping with the histology of the primary tumour. The cell line derived from the MNTI tumour continued to grow in culture for over 6 months and has been named ESH1.

ESH1 cells were screened against a range of histone demethylase inhibitors including GSK-J4 (details in Table 4) and the single concentration of 10μM reduced viability to approximately 60% after 3 days and 20% after 7 days. Treatment with an equimolar concentration of the inactive control compound GSK-J5 showed no decrease in viability when compared to the vehicle only control.

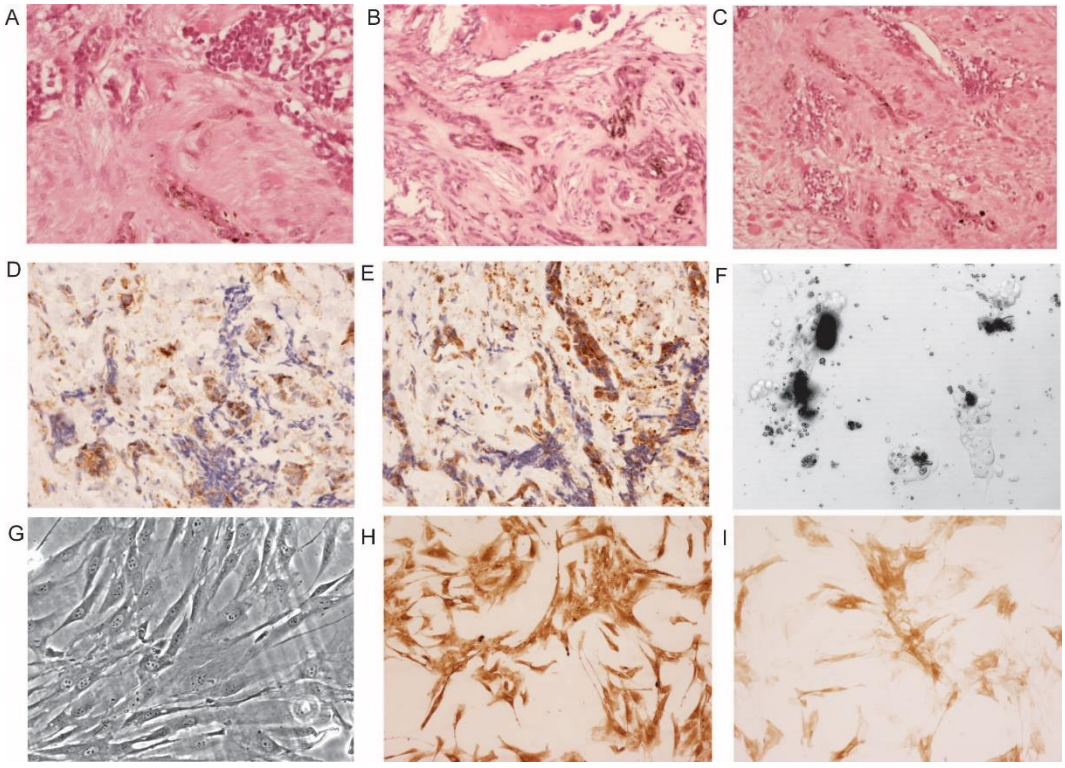


Figure 16 Histology of Melanocytic Neuroectodermal Tumour of Infancy

(A) Haematoxylin and eosin-stained section from the tumour. The two main tumour cell types are readily apparent: nests of small round cells with scant cytoplasm and hyperchromatic nuclei (top) and cords of polygonal, 'epithelial-like' cells containing speckles of melanin (bottom centre).

(B) Scattered pigment-containg tumour cell in bone.

(C) MNET tumour cells in soft tissue with residual muscle fibres evident .

Tumour cells staining positive for CD99 (D) and HMB45 (E)

(F) Bright- field images of the cell line derived from the MNTI at passage 2 produced copious amounts of melanin causing cell clumps to appear black.

(G) Phase contrast image of passage 7 cells

Cells in culture showing positive staining for HMB45 (H) and NSE (I)

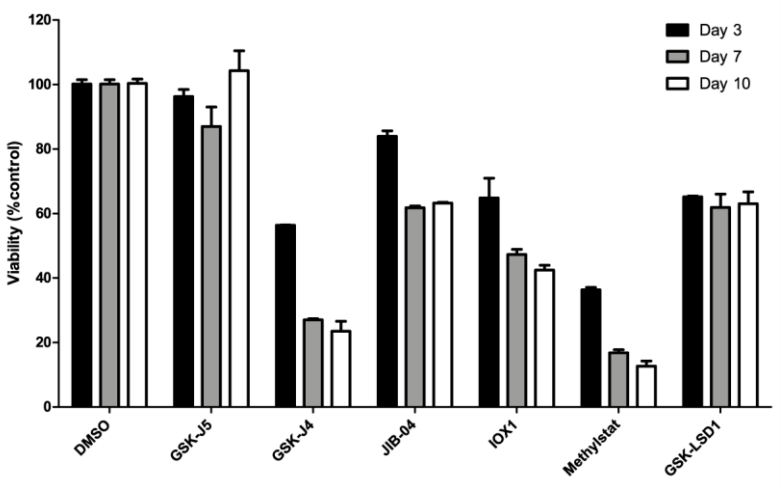


Figure 17 GSK-J4 reduces viability in Melanotic Neuroectodermal Tumour of Infancy

Plotted values represent the mean ± SEM for each point. n=3

3.3.4 Treatment with GSK-J4 results in apoptosis in myeloma cells and a cell cycle arrest in Ewing sarcoma

To further examine the effect that GSK-J4 treatment has on cancers of bone, the myeloma cell line JJN3 and the Ewing sarcoma cell line TC71 were investigated. In both cases, cells were treated for 24 hours with 5μM GSK-J4, a concentration equating to approximately IC_{80}. In JJN3 cells, treatment with GSK-J4 induces apoptosis, with an increase in the sub-G1 population, a reduction in the percentage of cells incorporating BrDU and an increase of cells staining positive for annexin V and propidium iodide (PI) (Figure 18 Cell cycle analysis and induction of apoptosis in JJN3 and TC71 cells). In contrast, in the Ewing sarcoma cell line TC71 there is a large increase in the proportion of cells in the G1 phase of the cell cycle, with no increase in the sub-G1 population or increased annexin V/PI staining. The proportion of cells incorporating BrDU into DNA decreases from 43% to less than 1%. To ensure that apoptosis was not just beginning later in the TC71 cells, incubation with GSK-J4

was extended to 72h with no evidence by flow cytometry of induction of apoptosis (data not shown).

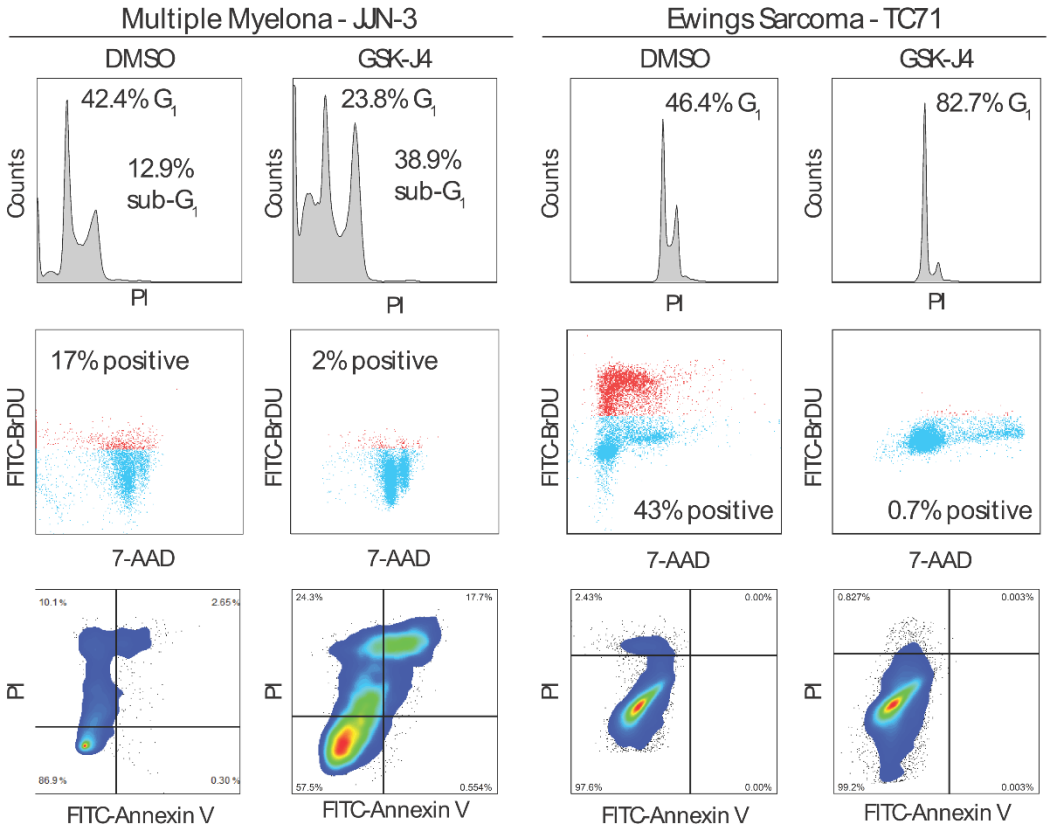


Figure 18 Cell cycle analysis and induction of apoptosis in JJN3 and TC71 cells

Top panel: Cell cycle analysis with propidium iodide in JJN3 cells (left) and TC71 cells (right). Middle panel: Incorporation of BrDU (red) or not (blue). Bottom panel: measurement of induction of apoptosis.

3.3.5 GSK-J4 induces an ATF4 and metallothionein transcriptomic response

In order to further explore the transcriptomic response of cells to treatment with GSK-J4, microarray analysis was undertaken for both myeloma and Ewing sarcoma cells treated with GSK-J4, GSK-J5 and the conventional myeloma treatment bortezomib (Figure 19).

It is striking when examining the transcriptomic response to GSK-J4 that a very similar profile is obtained in both the multiple myeloma cells and Ewing sarcoma cells examined and that only a relatively small number of genes, approximately 50, are regulated by greater than 2-fold at the 6 hour time point. The transcriptomic response appears to consist of two different elements. Firstly, clustered at the top of the genes for response to GSK-J4, are several members of the metallothionein family. To represent the data in the heatmap of Figure 19, fold-changes greater than 10 have been limited to this value in order to better demonstrate smaller fold-changes but the fold-change between the GSK-J4 and vehicle treated samples was greater than several hundred fold. JJN3 cells treated will much lower concentrations of GSK-J4 also still induce the metallothionein response but do not appear to induce the other components of the transcriptomic response observed. It is also notable that the conventional myeloma treatment bortezomib does not induce the metallothionein response in the JJN3 cells in which it was tested but otherwise appears to induce a similar profile of genes as GSK-J4.

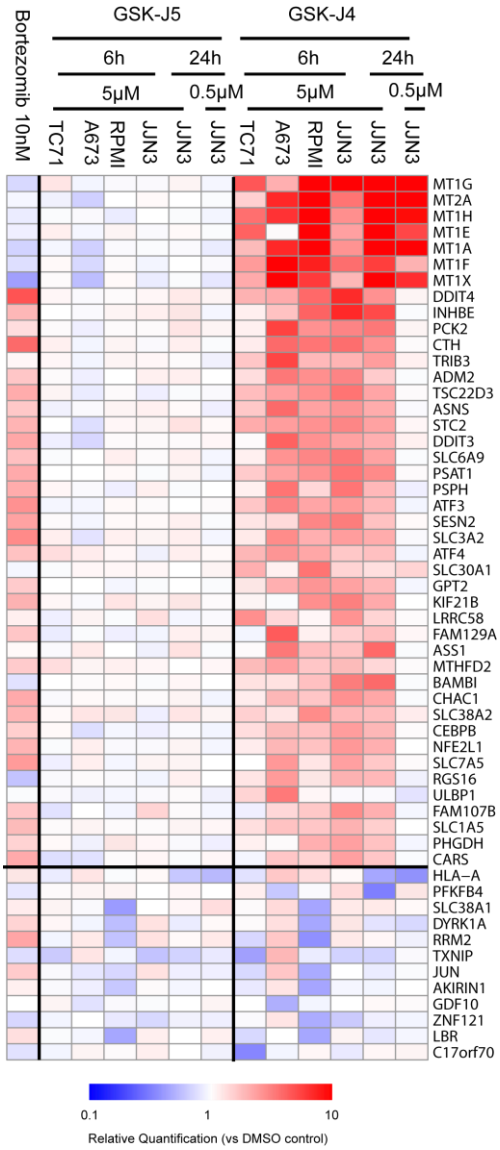


Figure 19 Microarray analysis of the transcriptional response to GSK-J4 in myeloma and Ewings cells.

Each data point represents the fold-change for the given transcript compared to the vehicle-only treatment. Values greater than a 10-fold change have been limited to 10 in order to demonstrate effectively small differences in fold-change and ordered by the mean fold-change observed in the GSK-J4 treated samples. TC71 and A673 are Ewing sarcoma cell lines, RPMI and JJN3 myeloma cell lines. JJN3 cells treated with bortezomib are included for comparison.

The second component of the transcriptomic response observed in response to GSK-J4 is notable for containing a large number of genes involved in metabolism, such as asparagine synthetase (ASNS), arginosuccinate synthetase (ASS1) and phosphoenolpyruvate carboxykinase 2 (PCK2). Performing a motif analysis of the promoter region of the non-metallothionein genes that were regulated in the microarray analysis indicates that the two most highly enriched motifs were for Activating Transcription Factor 4 (ATF4) and DNA Damage Inducible 3 (DDIT3, also known as CHOP) (Figure 20). The ATF4 gene itself is also found to be up-regulated by treatment with GSK-J4.

Rank	Motif	Name	Target Sequences (%)	Background Sequences (%)	p value
1		ATF4	20.70	2.40	$1x10^{-10}$
2		DDIT3	17.07	1.58	$1x10^{-10}$
3		CEBP	19.51	5.50	$1x10^{-5}$
4		NFY	40.24	24.25	$1x10^{-2}$

Figure 20 Motif analysis of promoter region of genes regulated by GSK-J4

Motif analysis of the top 100 regulated genes in the microarray experiment reveal that the two most significantly enriched motifs belong to ATF4 and DDIT3

From the microarray analysis, it is also possible to see that treatment with GSK-J5 led to no changes in gene expression, consistent across the conditions examined, a result in keeping with its role as an "inactive" control compound.

3.3.6 The transciptomic response to GSK-J4 observed in the microarray is consistent across a range of myeloma and Ewing sarcoma cell lines.

To confirm that the transcriptional response observed in the microarray experiment was consistent across a range of cell lines, a panel of myeloma and Ewing sarcoma cell lines was selected and the expression of genes determined to be regulated by the microarray experiment were measured by qPCR after 6h and 24h of treatment with a cell-line specific IC_{80} of GSK-J4 (Figure 21).

Metallothionein 1X (MT1X) was chosen as a representative of the metallothionein genes as a single product could be amplified specifically during qPCR. Other genes were chosen to represent ATF4 and its downstream pathways, including genes involved in metabolism such as ASNS, ASS1 and PCK2 mentioned above and DDIT3 and genes downstream to it.

Across the range of cell lines tested, GSK-J4 induced a large metallothionein response as measured by the expression of MT1X at 6h. The magnitude of the response was in the order of greater than a 100-fold induction for the majority of the cells examined but in the Ewing sarcoma cell line SKNMC greater than 1000-fold increase in the level of expression was noted. By 24 hours, the expression of MT1X had decreased from the high level noted at 6 hours in all cell lines, returning almost to baseline expression levels in Ewing sarcoma cell lines but remaining elevated in myeloma cell lines.

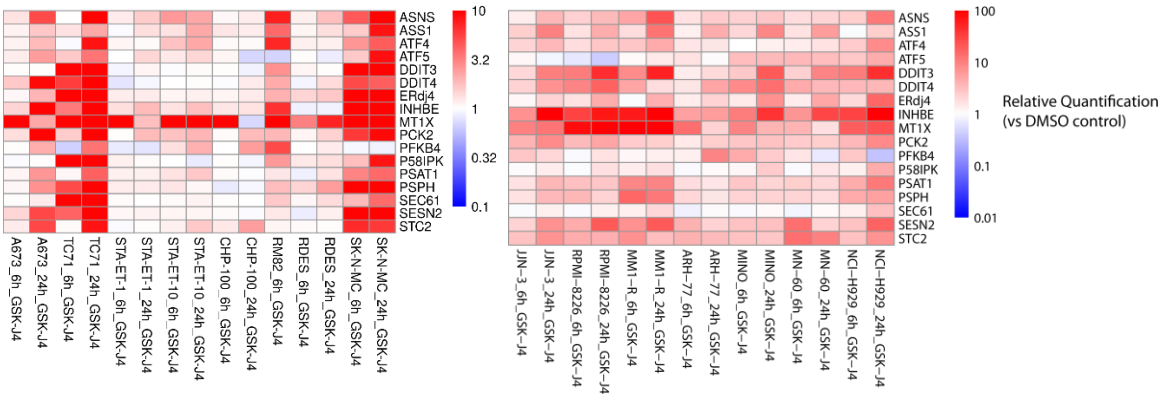


Figure 21 qPCR validation of genes identified by microarray

Results represent qPCR data for Ewing sarcoma cell lines (left) and myeloma cell lines (right) at either 6h or 24h post treatment with GSK-J4 at a dose equivalent to the IC_{80} of the cell line. Due to the extreme range of values, in order to better visualize smaller changes, values above 10 for Ewing sarcoma and 100 for myeloma have been censored at these values. Each data point represents the mean value of three biological replicates.

3.3.7 Locked Nucleic Acids are taken-up by multiple myeloma cells

In order to test the ability of LNAs to enter myeloma cells, JJN3 cells were treated with a scrambled (control) LNA conjugated to a 6-carboxyfluorescin (FAM) fluorophore, allowing detection of cells into which LNAs have entered both by microscopy and by flow cytometry. Labelled-LNA was added to culture media of growing cells to a final concentration of 5µM and the culture was incubated for 24 hours. Analysis by flow cytometry demonstrated that almost 100% of cells were positive for intracellular LNAs and accumulation of LNA can be seen by microscopy (Figure 22).

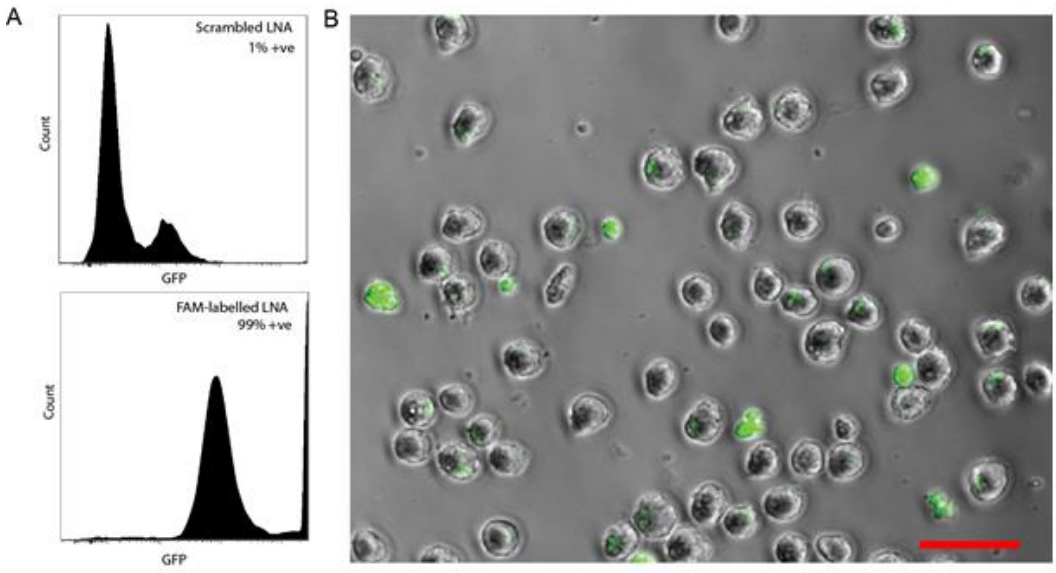


Figure 22 Locked Nucleic Acids are taken-up by JJN3 myeloma cells

(A) Flow cytometry demonstrates that 99% of cells treated with FAM-conjugated LNA are positive after 24 hours (lower panel). (B) Small inclusions of LNAs visible in multiple cells. Cells that are entirely green are likely dead and have lost membrane permeability. Scale bar 50μM

3.3.8 Simultaneous targeting of KDM6A and KDM6B by LNAs recapitulate the phenotypic effect of GSK-J4 in JJN3 cells

In an attempt to dissect which of the enzymes inhibited by GSK-J4 were responsible for the observed phenotype of decreasing viability, inducing expression of metallothioneins and activating an ATF4 driven response, knock-down studies using LNAs targeting the enzymes individually and in combination were performed.

LNAs were the tool of choice for this exercise due to the difficulty associated with transfecting myeloma cells with either shRNAs or siRNAs. LNAs were designed by collaborators from Santaris (Copenhagen, Denmark). To put the LNA experiments into the historical context in which they were performed, when the initial LNA experiments were

conducted the action of GSK-J4 on KDM5B had not been recognized and it was thought that GSK-J4 inhibited only the members of the KDM6 family. Therefore, in the design of the LNAs for knockdown the only targets considered in the initial experiments were KDM6A, KDM6B and an LNA designed to knockdown both KDM6A and KDM6B. Suspicion had been raised that GSK-J4 may be having an effect on targets other than KDM6A and KDM6B as, mechanistically, it would be expected that inhibition of these enzymes would result in an increase in the level of H3K27me3, a mark traditionally associated with gene silencing, and the vast majority of the regulated gene expression seen from the microarray experiment had shown up-regulation of gene expression. Furthermore, previous studies had implicated KDM5B in the regulation of expression of metallothioneins (Scibetta et al. 2007) and in the context of both KDM5 and KDM6 being members of the same family of iron and alpha-ketoglutarate-dependent oxidoreductases suggested that GSK-J4 may be having "off-target" effects on members of the KDM5 family.

JJN3 cells were incubated with 5μM LNAs targeted against either KDM6A (numbers 0-23), KDM6B(24-48) or dual-targeted (49-61) for 7 days as described earlier. Control cells were incubated with a non-targeted "scramble" LNA. After 7 days, cell viability was measured with PrestoBlue and RNA extracted for qPCR to determine the expression level of KDM5A, B and C, KDM6A and B and MT1X as a marker of transcriptional response seen with GSK-J4.

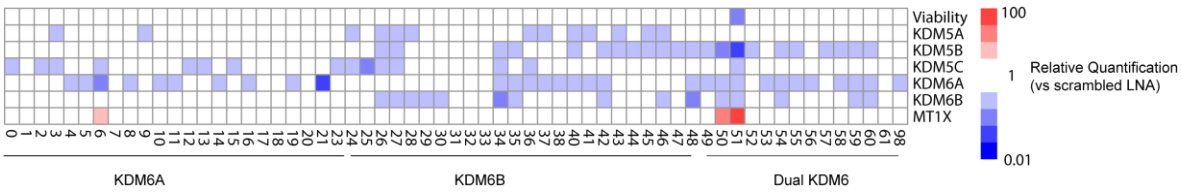


Figure 23 LNA screening targeting KDM6A and KDM6B

Screening of LNAs to assess for knockdown of KDM5, KDM6, induction of metallothioneins and reduction in viability. Viability data normalized to a value of 1 for control cells treated with scrambled LNA. qPCR data expressed as the relative quantification of data in LNA-treated condition versus scrambled control. Plotted values represent the mean of 2 biological replicates

Several interesting observations can be made from the initial screen of the LNA library displayed in Figure 23. Treatment with none of the individually target LNAs was able to reproduce the phenotype of GSK-J4 of expression of MT1X and decreased cell viability. LNA 51, targeted against both KDM6A and KDM6B resulted in a decrease in cell viability and a large expression of MT1X (60-fold increased expression when compared to the scrambled control). The level of knockdown achieved with LNA 51 for KDM6 targets is not as good as achieved by some of the individually targeted LNAs, for example LNA 21 decreases expression of KDM6A to a relative quantification (RQ) of 0.047 without affecting the expression of KDM6B whereas KDM6A expression with LNA 51 results in a RQ 0.34 with LNA 51.

Intriguingly, LNA 51 also led to a profound decrease in the expression of KDM5B to an RQ of 0.04. LNA 50 can also be observed to have a knockdown of all three of the enzymes of interest, albeit to a lesser degree than with LNA 51, and a mild induction of MT1X is also observed in this case although there is not a decrease in cell viability. The sequence of LNAs 50 and 51 have not been disclosed but analysis by Santaris who produced the LNAs has indicated that the effect on KDM5B by LNA 50 and 51 is not a direct effect, suggesting that

the decrease in its level of expression is as a downstream consequence of the down-regulation of either KDM6A and 6B.

Analysis of the expression levels of KDM5 and KDM6 family members in JJN3 cells treated with all LNAs reveals that there is a strong correlation between the expression level of KDM6B and KDM5B (Spearman rho 0.78, p-value $2.26x10^{-16}$) with no strong association between other pairs (Figure 24). This observation would suggest that knockdown of KDM6B also leads to a reduction in KDM5B expression.

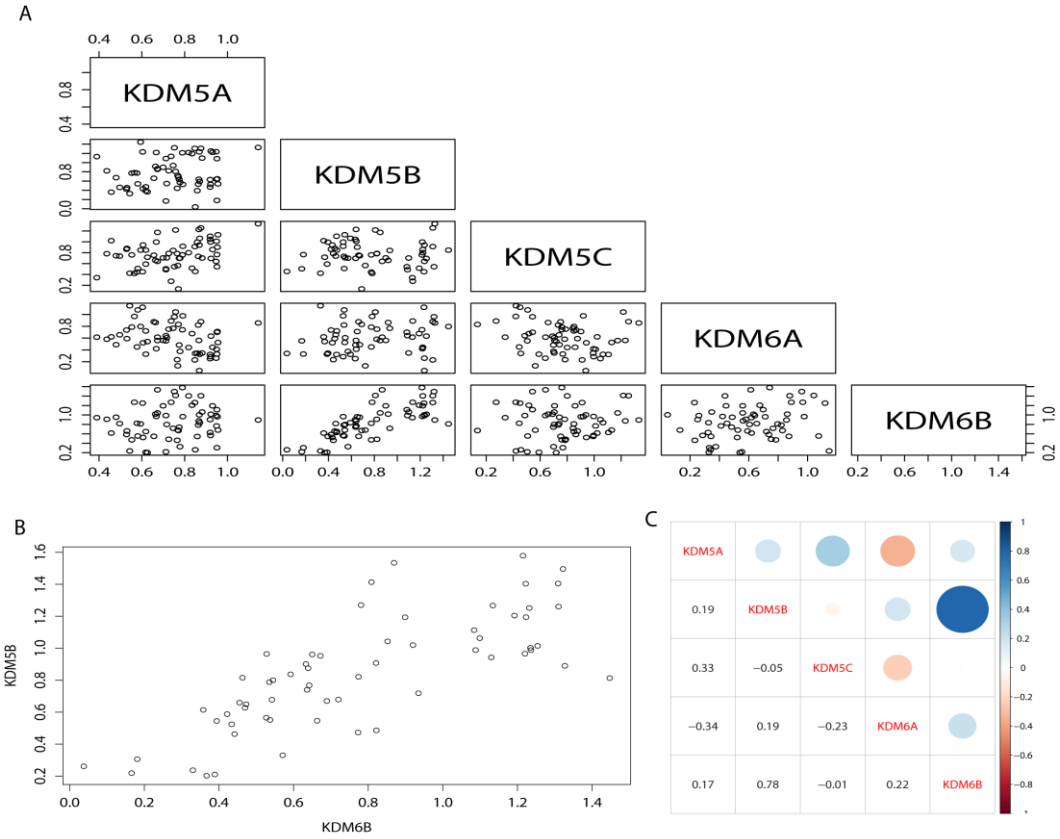


Figure 24 Correlation between knockdown of KDM5 and KDM6 family members

(A) Pairwise plotting of expression levels of KDM5 and KDM6 family members in LNA-treated JJN3 cells. (B) Enhanced view of the relationship between KDM5B and KDM6B expression. (C) Pairwise correlation matrix displaying the Spearman rho value in the bottom half and a graphical indication of the size of the correlation in the upper half.

To confirm that the observed phenotype was not related to the effect of knocking down KDM5B alone, new LNAs were designed to assess the response on the cell to the single knockdown of KDM5B without affecting KDM6A and 6B. Whilst good knockdown was achieved with several LNAs, although not to the level of knockdown achieved with LNA 51, there was no observed decrease in cell viability or an increase in the expression of metallothioneins suggesting that the action of KDM6B alone is not responsible for the observed phenotype.

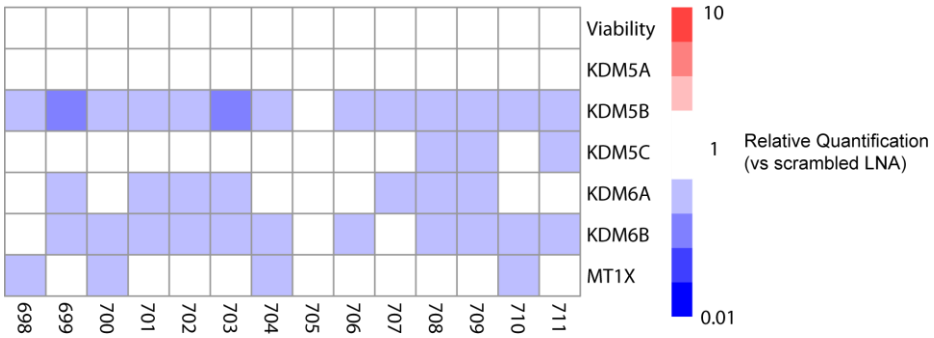


Figure 25 LNAs targeting KDM5B

Viability data normalized to a value of 1 for control cells treated with scrambled LNA. qPCR data expressed as the relative quantification of data in LNA-treated condition versus scrambled control. Data represent the mean of 2 biological replicates

3.3.9 GSK-J4 acts through ATF4 activation

To confirm that the action of GSK-J4 was occurring through the ATF4 pathway, as suggested by the microarray (Figure 19) and subsequent motif analysis (Figure 20), further investigation of ATF4 activation was undertaken.

In a time-course experiment, GSK-J4 is shown to increase phosphorylation of Eukaryotic translation Initiation Factor 2a (eIF2α), to induce ATF4 and its downstream target CHOP

(the protein product of the DDIT3 gene) and to induce apoptosis starting at 6 hours post-treatment with an increase up to 24 hours (Figure 26).

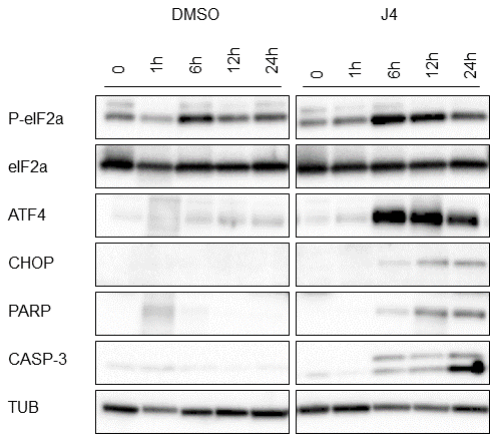


Figure 26 Induction of ATF4 in response to treatment with GSK-J4

Western blots showing induction of ATF and CHOP, eIF2α phosphorylation and cleavage of caspase 3 and PARP in response to GSK-J4. Data shown are representative of 3 biological replicates. Western blots were performed in collaboration with Federica Lari in the laboratory of John Christianson, Ludwig Institute of Cancer Research, University of Oxford.

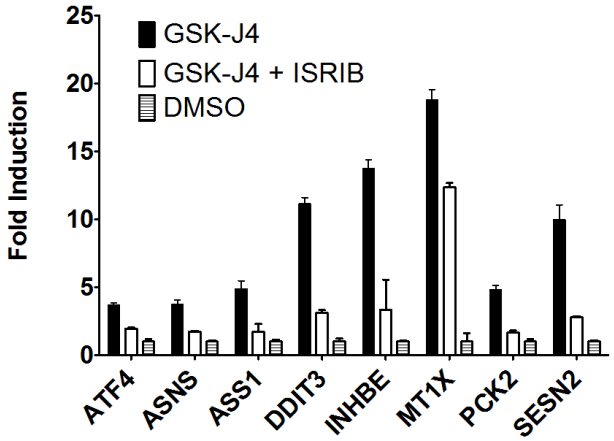


Figure 27 ISRIB attenuates the ATF4 response to GSK-J4

JJN3 cells were pre-incubated with 50nM ISRIB for 1 hour then treated with 5μM GSK-J4 for 24 hours. Data is shown as fold-induction of cells incubated with ISRIB alone. Plotted values represent the mean ± SEM of 3 biological replicates. T-tests indicate all values significant $p<0.05$

Pre-incubation with the ISRIB inhibitor (Sidrauski et al. 2013) was able to attenuate the transcriptional response to GSK-J4 as measured after 24 hours (Figure 27) indicating a clear involvement of the canonical integrated stress response.

LNA knockdown of ATF4 using two separate LNAs (referred to as LNA 16 and 19 (ATF4) which are different from the LNAs referred to in Figure 23) was also able to lead to an attenuation of the transcriptomic profile seen with GSK-J4 at 24 hours and reduce the degree to which cell viability decreased when cells were exposed to GSK-J4 at 48 hours Figure 28.

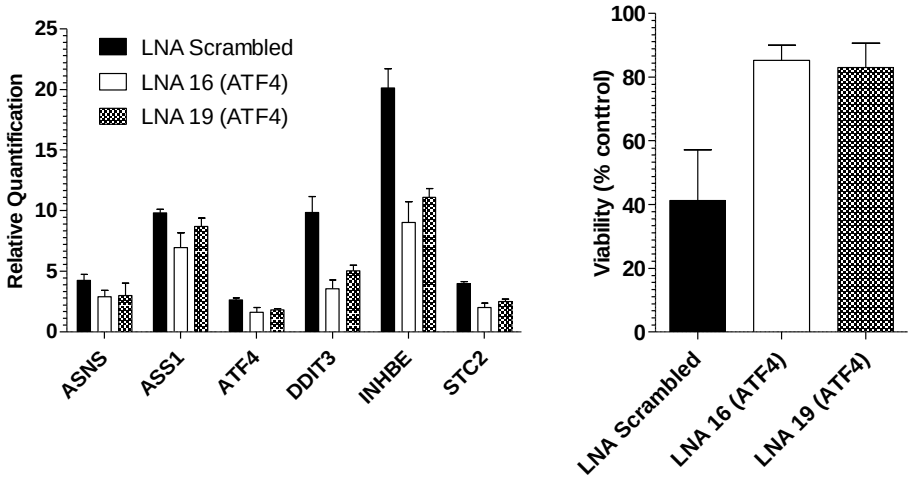


Figure 28 Knockdown of ATF4 reduces the phenotypic response to GSK-J4

(Left) Knockdown of ATF4 attenuates the transcriptional response to GSK-J4 and (right) reduces the decrease in viability to GSK-J4 at 48 hours. Plotted values represent the mean ± SEM of 2 biological replicates.

3.3.10 GSK-J4 activates the ATF4 pathway via the stress kinase GCN2

In order to determine which of the four kinases of eIF2α was responsible for the activation of ATF4 pathway in response to GSK-J4, each was systematically examined.

In multiple myeloma, in which there is a large production of immunoglobulin chains, the endoplasmic reticulum (ER) is under "stress" so it was postulated that ATF4 activation was occurring via activation of PERK. However, GSK-J4 did not induce splicing of X-Box Protein 1 (XBP-1) (Figure 29), a marker of ER stress and the unfolded protein response (Yoshida et al. 2001). In addition, the small molecule inhibitor of PERK GSK2606414 (PERKi) (Atkins et al. 2013) was unable to prevent the phosphorylation of eIF2α or induction of ATF4, CHOP and apoptosis in response to GSK-J4 but did prevent these in cells treated with the ER stress-inducing agent tunicamycin (Figure 29).

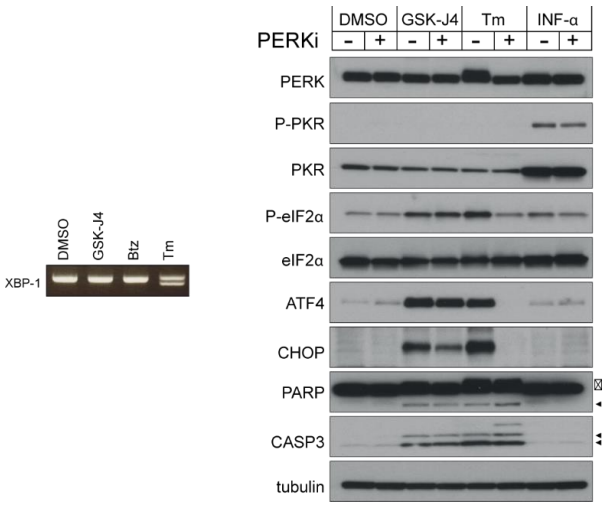


Figure 29 GSK-J4 does not activate ATF4 through PERK or PKR

(Left) GSK-J4 does not induce splicing of XBP-1 in JJN3 multiple myeloma cells. (Right) PERKi does not inhibit the ATF4-driven response to GSK-J4 but does inhibit the response to the known ER-stress inducer tunicamycin (TM). GSK-J4 does not induce autophosphorylation of PKR in contrast to interferon alpha (INFα). Western blots were performed in collaboration with Federica Lari in the laboratory of Dr John Christianson, University of Oxford.

Figure 29 also demonstrates that upon treatment with interferon alpha (IFNα), a known activator of PKR, phosphorylation of PKR occurs with an increase in phosphor-eIF2α and induction of ATF4. Phosphorylation of PKR does not occur upon treatment with GSK-J4 indicating that it is not activating the ATF4 pathway through this kinase.

Investigation of the role of GCN2 is made more difficult by the lack of small molecule inhibitors of its kinase activity. To this end, a knockdown approach with LNAs was performed. Measuring the magnitude of the knockdown with a range of LNAs indicated that no single LNA provided a sufficiently large knockdown so the two best performing LNAs (57 and 63) were pooled together and in combination were able to obtain a knockdown to a RQ of 0.125 (Figure 30)

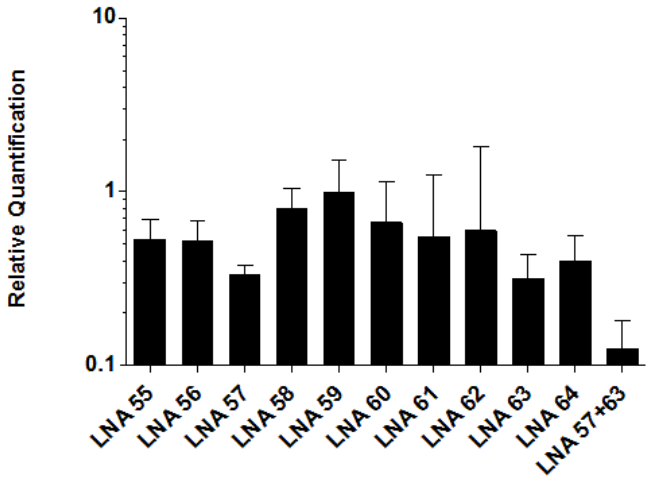


Figure 30 Knockdown of GCN2 with LNAs

JJN3 cells were treated with LNA at 5µM concentration for 7 days and then relative quantification of GCN2 expression was measured by qPCR. Plotted data represents the mean ± SEM of 2 biological replicates.

The ability of the pool of GCCN2 LNAs was then assessed for its ability to attenuate the cellular response to treatment with GSK-J4. Cells were treated with LNAs for 7 days prior to treatment with GSK-J4 after which cell viability was measured using PrestoBlue and RNA extracted for qPCR of genes associated with the ATF4 response. Treatment with the pool of GCN2 LNAs was able to blunt the transcriptional response to GSK-J4 with a decrease in the induction of expression of genes such as DDIT3 (CHOP) INHBE and ASS1. GCN2 LNAs were also able to reduce the decrease in cell viability upon treatment with GSK-J4 (Figure 31).

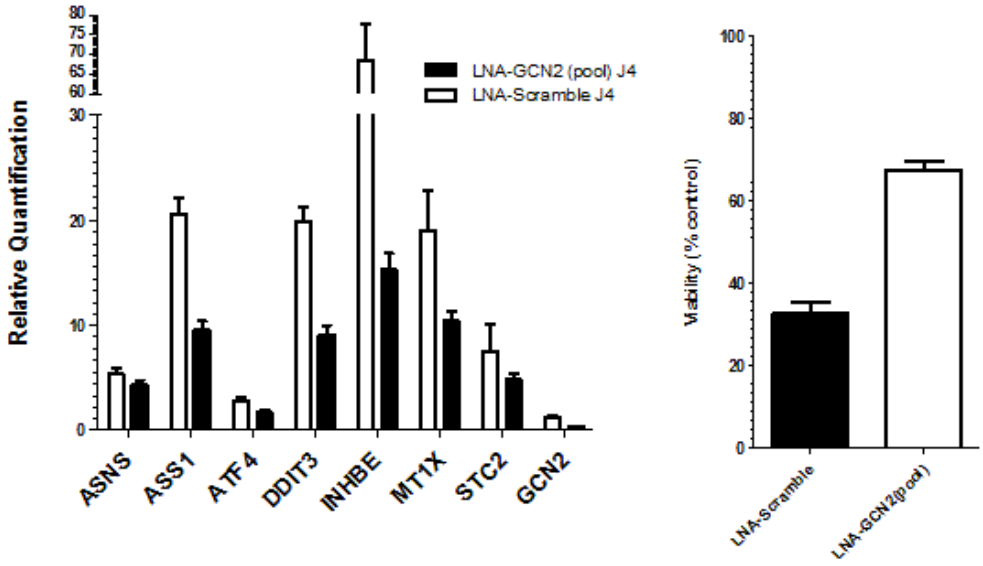


Figure 31 LNAs targeting GCN2 reduce the cellular response to GSK-J4

(Left) Knockdown of GCN2 attenuates the transcriptional response to 5μM GSK-J4 and (right) reduces the decrease in viability to GSK-J4 at 48 hours. Plotted values represent the mean ± SEM of 2 biological replicates.

3.3.11 Intracellular free zinc increases in response to GSK-J4

In order to attempt to understand why there is a large induction of metallothioneins in response to GSK-J4, relative levels of intracellular free zinc were measured using the fluorescent dye Fluozin-3AM. In response to GSK-J4, there is a rapid rise in the level of intracellular free zinc, peaking after approximately 50 minutes with a return to approaching baseline by 2 hours.

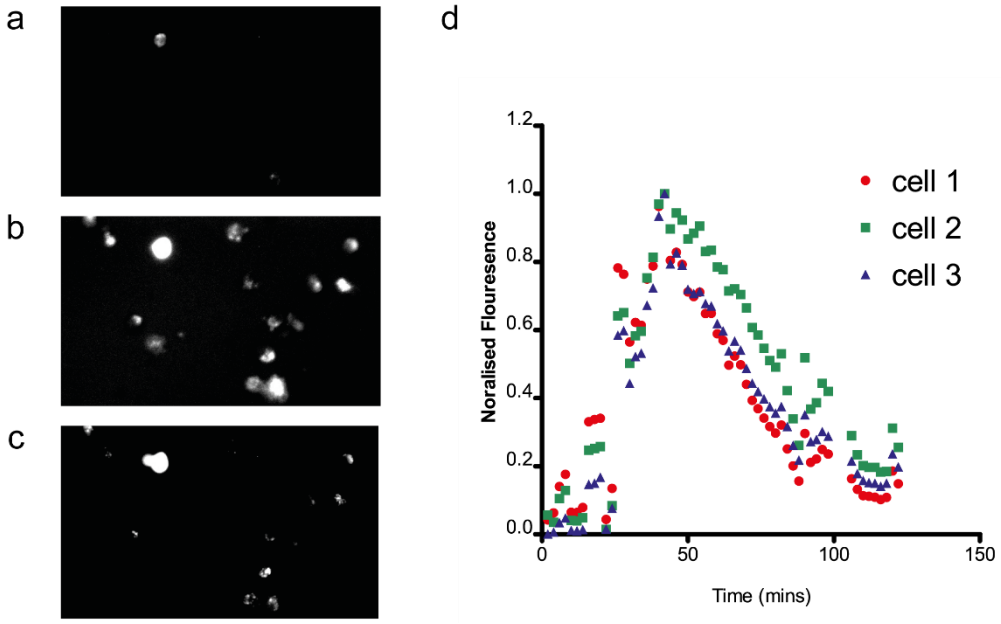


Figure 32 GSK-J4 causes a transient increase in free intracellular zinc

(Left) Images from baseline (a), 48 minutes (b) and 120 (c) after treatment with 5μM GSK-J4 showing fluorescence intensity in cells loaded with Fluozin-1 AM. (Right) Fluorescence intensity for three cells over time normalized to the level of the highest intensity.

3.3.12 Overexpression of metallothioneins induces the ATF4 response

Examining a time-course of the response to GSK-J4 indicates that the metallothionein response starts within 2h of exposure with the ATF4-driven response being detectable by 6 hours and more prominent at 24 hours (Figure 33).

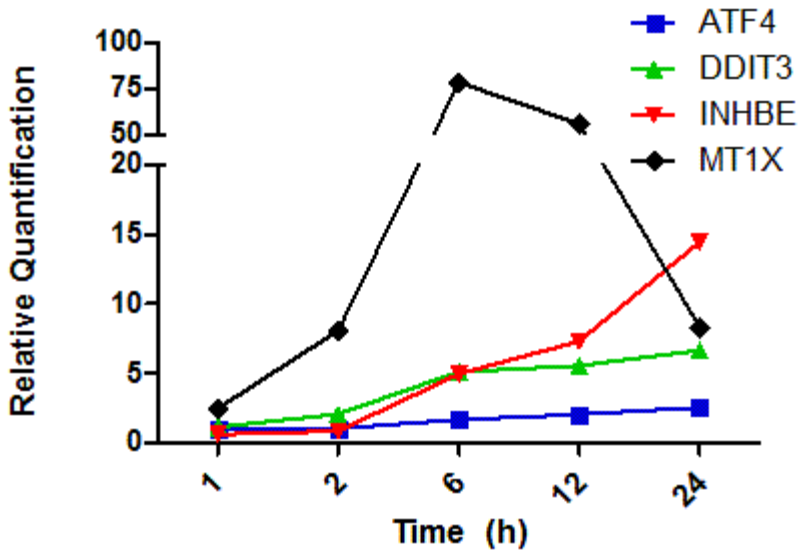


Figure 33 Time course of transcriptional response to GSK-J4 in JJN3 cells

JJN3 myeloma cells were treated with 5μM GSK-J4 and the relative quantification of the metallothionein MT1X, ATF4 and downstream ATF4 targets INHBE and DDIT3 were measured by qPCR at the times indicated.

It was hypothesized that the induction of metallothionein genes may in themselves be responsible for the activation of the ATF4, an association that has not previously been made within the literature.

To test this hypothesis, an artificial construct coding for four metallothionein (MT1G, MT1H, MT1X and MT2A) genes separated by the self-cleaving porcine teschovirus-1 2A (p2A) peptide sequence (termed the "metallothionein übergene", Figure 34) was generated by team member Dr Martin Philpott and transfected into a doxycycline-inducible flip-in HEK293 cell line. This was done after having first confirmed that HEK cells respond in a similar manner to GSK-J4 as the other bone cancer cells under investigation with a metallothionein response and induction of the ATF4-driven integrated stress response.

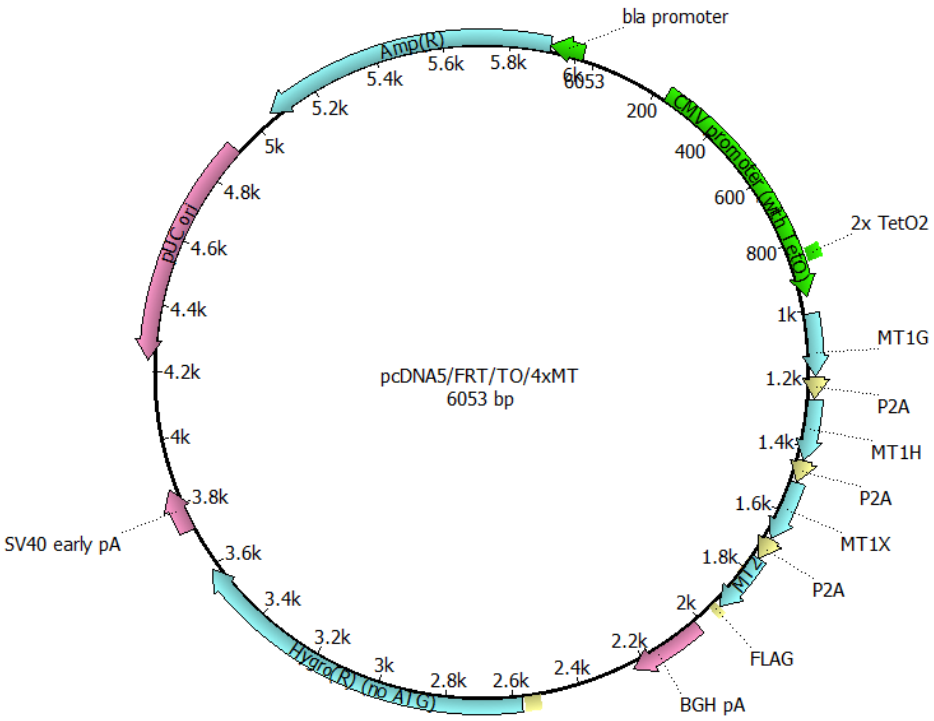


Figure 34 Plasmid map containing the "metallothionein ubergene".

A plasmid containing Metal Regulatory Transcription factor 1 (MTF1), the transcription factor that controls the expression of metallothioneins was also obtained and used in transient transfection experiments to test if over-expression of the transcription factor driving metallothionein expression could lead to the induction of the ATF4 response.

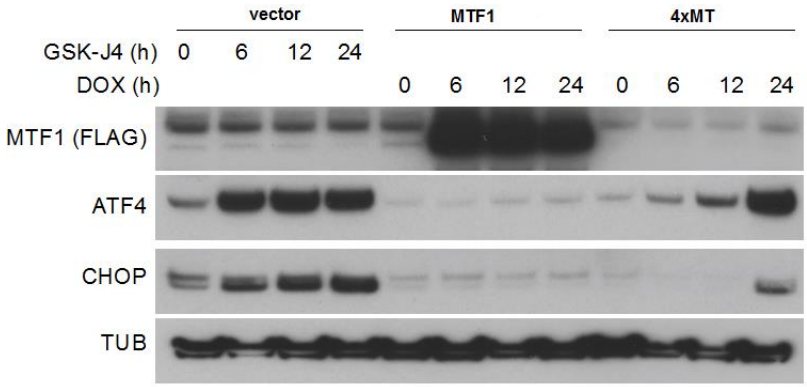


Figure 35 Expression of the "metallothionein ubergene" (4xMT) induces the ATF4 response

Induction of the "metallothionein übergene" but not the transcription factor MTF1 induces the ATF4 response in HEK293 cells. Blot is representative of three biological replicates.

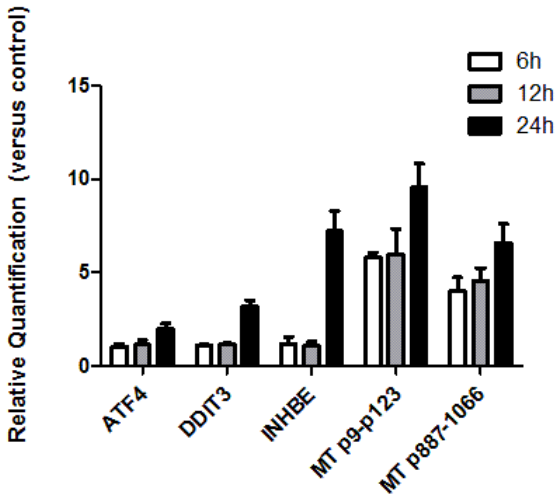


Figure 36 Metallothionein ubergene expression induces an ATF4 response

HEK293 cells with the integrated metallothionein übergene were exposed to doxycycline for 6,12 and 24h and relative expression of ATF4, DDIT3 and INHBE was measured by qPCR. P9-p123 and p887-1066 refer to the metallothioneine übergene under doxycycline control. Data represent the mean and SEM for three biological replicates.

Transient transfection with MTF1 led to a relatively small induction of metallothioneins (as measured by qPCR for MT1X) but did not cause an induction of the ATF4 response as measured by Western blots (Figure 35). In contrast, exposure of the flip-in HEK293 cells containing the "metallothionein übergene" to doxycycline led to expression of metallothioneins from the construct (measured by qPCR using primers directed against the two ends of the construct transcript) and induction of the ATF4 response as measured both by qPCR (Figure 36) and by Western blotting (Figure 35).

3.4 DISCUSSION

In this chapter, the small molecule inhibitor GSK-J4 has been shown to inhibit proliferation in a range of cancers that affect bone including multiple myeloma, Ewing sarcoma and chordoma. The similar phenotypic response obtained using the structurally-related molecule KDOBA67 and the lack of activity of GSK-J5, an isomer of GSK-J4 without inhibitory activity, add support to the effect observed being due to on-target inhibition of the targets of GSK-J4 KDM5B, KDM6A and KDM6B.

Knockdown experiments using locked nucleic acids have demonstrated that a LNA that targets both KDM6A and KDM6B is able to reproduce the phenotypic effect of GSK-J4. Using the same LNA, it is observed that there is a profound knockdown of KDM5B that is not a direct result of LNA-mediated mRNA reduction. Across the range of LNAs used, knockdown of KDM6B correlates with knockdown of KDM5B. Only in cases where there are reduced levels of all three enzymes is induction of metallothioneins and reduced viability observed. Targeted reduction of KDM5B alone with an LNA does not reproduce the phenotype observed with GSK-J4. Although GSK-J1 has KDM5B inhibitory activity in vitro, the IC50 of 550nM brings into question the biological relevance of this action when compounds are being used at a low micromolar range in cell culture. It may be that the predominant effect on KDM5B may be its downregulation as a result of inhibitory effects on KDM6B, either by small molecule in the case of GSK-J4 or knockdown in the case of the LNAs.

Activity of GSK-J4 has been shown in cell lines for myeloma, chordoma and Ewing sarcoma and also in primary patient-derived material, in the case of Ewing sarcoma and the rare

Melanotic Neuroectodermal Tumour of Infancy in primary cell lines that have been established during the course of this study.

GSK-J4 induces a distinct transcriptional profile in the cell types studied and is characterized by a large induction of a range of metallothionein genes followed by an ATF4-driven integrated stress response working through the eIF2α kinase GCN2. However, although in both Ewing sarcoma and myeloma the ATF4 response is induced, the downstream consequences differ in the two cancer types with a cell cycle arrest observed in Ewing sarcoma and programmed cell death in multiple myeloma. The reasons for the two differing responses to the ATF4 response are unclear but could be due to the fundamental difference in the biology between the two cancers.

Metallothioneins are evolutionary conserved, small proteins (approximately 60 amino acids in length) containing a large number of cysteine residues. Metallothioneins were first identified in the cortex of horse kidneys, induced by cadmium intoxication (Margoshes and Vallee 1957). The large number of cysteine residues, accounting for roughly 30% of the total proteins, enable metallothioneins to sequester divalent heavy metal ions such as mercury, zinc and copper and hence the role of metallothioneins in the toxicology of heavy metals has been extensively studied. Metallothionein expression is controlled both positively and negatively by a range of factors (Takahashi 2015). Positive regulation occurs via MTF-1 and other transcripton factors including upstream factor 1 (USF1) and nuclear factor 1 (NF1) although the exact mechanism by which the excess of free heavy metal is detected is not well understood in eukaryotes (Waldron and Robinson 2009). In addition to the positive regulation of metallothioneins there are several well-characterised negative regulatory factors including DNA methylation by DNMT3A and remodeling of chromatin by the action

of methylated-DNA binding proteins interacting with histone deacetylases (Ghoshal et al. 2002). A further known negative regulator of metallothionein expression is PU.1 (the gene product of SPI1), an ETS-family transcription factor that has been implicated in B cell development (Imoto et al. 2010). However, PU.1 is downregulated in myeloma cells, and recent studies suggest that one of the mechanisms of immunomodulatory drug action in myeloma is through up-regulation of PU.1 (Endo et al. 2016).

Experimental data show that there is an increase in the amount of free zinc in the cell, peaking in the hour after treatment (Figure 32). It remains unclear whether the observed zinc is a cause of the increase in metallothionein expression or occurs as a consequence of it. If the zinc is the cause of the increase in metallothionein response, it is not known whether the zinc is entering the cell from outside or being released from intracellular stores. It is possible that expression of metallothioneins which have a high affinity for zinc could sequester the zinc which is attached with lower affinity to other proteins and during the process of the transfer the zinc enters for a time a "free" state that activates the fluorescent dye.

Considering the speed of the response with increase in free zinc levels being observable after time points as short as 10 minutes after addition of GSK-J4 it is difficult to identify a mechanism by which GSK-J4 could cause the zinc to enter the cell as quickly as observed. Zinc transfer across the cell membrane is facilitated by specific transporters and up-regulation of such channels is observed in the microarray data (Figure 19) such as SLC30A1 but this gene is itself regulated by MTF1 that canonically is activated in response to excess heavy metal. Indeed, the up-regulation of SLC30A1 is likely acting as a channel for the egress of zinc from the cell that would help to restore the homeostatic balance following excess free zinc within the cell.

Another consideration that was given to explain the metallothionein response was that there may be contamination with a heavy metal (palladium) that was used during the synthesis of GSK-J4. However, quality control checks have identified that this is not the case. A further explanation was that the nitrogen atoms present in the structure of GSK-J4 could chelate zinc on the outside of the cell and transport it across the plasma membrane. Both of these last points are however contradicted by the fact that the experiments with LNA 51, which mimics the effect of GSK-J4, also leads to an induction of the metallothionein response so it is very unlikely to be due to an off-target effect of GSK-J4. Furthermore, the observation that the overexpression of the metallothionein ubergene was able to induce the ATF4 response supports the notion that GSK-J4 directly controls metallothionein expression, which in turn leads to an ATF4 response. Overexpression of metallothioneins has been associated with a large number of tumours (JASANI and SCHMID 1997), with heavy metal exposure (Margoshes and Vallee 1957), resistance to platinum-based chemotherapy agents such as cisplatin (Schilder et al. 1990), protection from insulin-dependent diabetes (Cai 2004) and protection from neurodegeneration (A. K. West et al. 2008): in general, the expression of metallothioneins is associated with a protective effect for the cell against a stressor such as heavy metals and reactive oxygen species (X. Li, Chen, and Epstein 2004). As the ATF4 response is itself protective against a range of stressors such as viral infection, the unfolded protein response and nutritional deficiency it may ostensibly seem reasonable that there is a connection between the two separate pathways. However, no previous study has indicated a connection between expression of metallothioneins and the induction of the ATF4 response. A possible explanation for this observation will be provided in chapter seven.

4 GSK-J4 REPROGRAMS CELLULAR METABOLISM AND INHIBITS GLUTAMINE UTILIZATION

4.1 OVERVIEW

In the previous chapter it was shown that GSK-J4 induces the ATF4 response via the kinase GCN2 that is characteristically associated with responding to nutritional stress within the cell such as amino acid starvation. In this chapter, the metabolic response to GSK-J4 will be examined in multiple myeloma and Ewing sarcoma cells. Data will show that the redox environment of the cell is altered on exposure to GSK-J4 and that there is an induction of reactive oxygen species (ROS). Furthermore, GSK-J4 alters oxygen consumption and oxidative phosphorylation with a decrease of intracellular ATP levels. Using Nuclear Magnetic Resonance (NMR) techniques, the baseline metabolic state of JJN3 cells will be described showing that these cells use glutamine as the source of carbon for the tricarboxylic acid (TCA) cycle and the process of glutaminolysis is inhibited by treatment with GSK-J4. The metabolic response to GSK-J4 will be compared to that of other myeloma treatments and shown to be different. Finally, it will be shown that the use of dimethyl-ketoglutarate, a cell-permeable form of alpha-ketoglutarate, is able to temporarily rescue GSK-J4 treated cells from apoptosis.

4.2 INTRODUCTION

4.2.1 Metabolism in cancer

Alteration of metabolism in proliferating cells has been a longstanding observation since the work of Warburg in the 1930s and was included as one of "the next generation hallmarks" of cancer by Hanahan and Weinberg (Hanahan and Weinberg 2011).

The Warburg Effect in oncology is the observation that rapidly proliferating cells use the anaerobic glycolytic pathway as their main source of energy even under normoxic conditions. In order to produce an equivalent amount of ATP using the glycolytic pathway and conversion of pyruvate to lactate as opposed to entry of pyruvate to the TCA cycle and oxidative phosphorylation requires a much greater flux through the glycolytic pathway and an increase in the overall consumption of glucose by the cell. The increase in glucose passage through the glycolytic pathway may be beneficial for the rapidly proliferating cells as glucose can be diverted through the pentose phosphate shunt leading to the production of necessary reducing equivalents in the form of NADPH. The pentose phosphate pathway is also necessary for the production of ribulose-5-phosphate, a necessary precursor for nucleotide synthesis and therefore DNA replication. This increased use of glucose observed by cancer cells is a rational for the use of ^{18}fluorine-labelled glucose as a "tracer" for position emission tomography (PET) scanning used clinically in the diagnosis of cancers.

Loss of function mutations within enzymes of the TCA cycle have been associated with various cancer syndromes. Mutations in succinate dehydrogenase subunit A (SDHA) is found in approximately 5% of phaeochromocytomas and paragangliomas (Burnichon et al. 2010). Mutations in fumarate hydratase (FH) is associated with hereditary leiomyomatosis

and renal cell carcinoma syndrome (HLRCC). In both cases it is thought that accumulation of intermediates of the TCA cycle can lead to competitive inhibition of enzymes involved in epigenetic processes such as the TET enzymes and Jumonji-domain containing demethylases (Xiao et al. 2012). Accumulation of fumarate is able to react with free thiol groups in cysteine residues through a non-enzymatic nucleophilic reaction resulting in protein-succination that leads to dysregulation of protein function (Llamas-Velasco et al. 2016; Blatnik, Thorpe, and Baynes 2008).

Gain of function mutations in the isocitrate dehyrdrogenase enzymes have been shown to lead to the accumulation of high levels of D-2-hydroxyglutarate (D2HG) (Dang et al. 2009), a metabolite normally only found in cells at very low levels that can interfere with the alpha-ketoglutarate dependent demethylase enzymes (Figueroa et al. 2010). Mutation of IDH has been associated with a number of different malignancies and tumour syndromes including glioma (Parsons et al. 2008), acute myeloid leukaemia (Mardis et al. 2009) and multiple enchondromatosis (Pansuriya et al. 2011).

In multiple myeloma, observations have been made that there are characteristic changes in the metabolomic profile of cells (Ludwig et al. 2015) with notably an altered ratio of xanthine to hydroxyxanthine. These changes were noted in samples from the bone marrow microenvironment of not only myeloma but also from patients with the pre-malignant monoclonal gammopathy of undermined significance (MGUS) suggesting that the change is likely to occur early in the history of the disease. Specific changes in metabolism have also been discovered in cells resistant to the proteasome inhibitor bortezomib including alterations in activity of lactate dehydrogenase A (LDHA) and HIF1A (Maiso et al. 2015).

4.2.2 Metabolic profiling using Nuclear Magnetic Resonance

One of the techniques used in this chapter for the investigation of the metabolic profile of cells is that of nuclear magnetic resonance (NMR) metabolomics. NMR relies upon fundamental physical properties of atoms in molecules and the way that these atoms behave in a magnetic field when pulsed with electromagnetic radiation of a given frequency. For an atom to be detectable in NMR, it has to have an uneven number of protons and/or neutrons leading to a property called half-integer spin. Therefore the hydrogen atom with a single proton has a half-integer spin and is detectable by NMR but carbon-12 (^{12}C), with six protons and six neutrons, is not detectable by NMR. The ^{13}C isotope, containing an extra neutron when compared to ^{12}C, is however detectable by NMR, a property that will be exploited for some of the experiments described herein. Atoms with half integer spin have a small magnetic momentum and when placed into an external magnetic field the momentums will align. The alignment with the magnetic field can be in either a low-energy state (where it is aligned with the external field) or a high-energy state where, in effect, the north pole of the nuclear magnetic moment is closest to the north pole of the external field. Application of an external electromagnetic pulse at a specific frequency is able to flip the alignment from the low to the high-energy state and by measuring the frequency generate when the atom "relaxes" on the removal of the electromagnetic field it is possible to discern information about the chemical environment of atoms generating the signal. Many factors can influence the frequency of the emitted signal, including the presence of carbon-carbon double and triple bonds, aromatic cycles and other hydrogen atoms in proximity to a given atom. These many factors lead to characteristic frequency spectra for different macromolecules and, importantly for NMR metabolomics, different molecules and relative quantities can be identified when

in a mixture. Therefore, using NMR metabolomics allows identification on many different biomolecules at once and so therefore is useful for monitoring the overall metabolic state of the cell.

The properties of NMR can be exploited by adding to growing cells metabolites which have been labelled in specific positions with ^{13}C isotopes. ^{13}C is present at an abundancy of approximately 1% in nature and so is poorly detected in unlabeled experiments. By replacing all of a specific metabolite present in cell media with metabolites labelled with ^{13}C, the carbon molecules can be detected by NMR and used to identify the downstream metabolites that have been formed. Using this information, one can trace the metabolic pathways within the cells from a given starting molecule. ^{13}C labelling of glutamine and glucose has been used in this chapter to explore the cellular metabolic profile and the influence GSK-J4 treatment has on it.

4.3 RESULTS

4.3.1 GSK-J4 reduces cellular ATP levels, alters the ratio of NADPH:NADP+ and induces reactive oxygen species.

TC71 Ewing sarcoma and JJN3 cells treated with a GSK-J4 at a concentration equivalent to an IC_{80} value for 24h had a reduction in the level of intracellular ATP. The ratio of reduced to oxidized nicotinamide adenine dinucleotide phosphate (NADPH:NADP+) was significantly reduced following 24 hours of treatment with GSK-J4 in both JJN3 and TC71 cells (Figure 37). Treatment with GSK-J4 can also be seen to induce reactive oxygen species in both JJN3 and TC71 cell lines Figure 38.

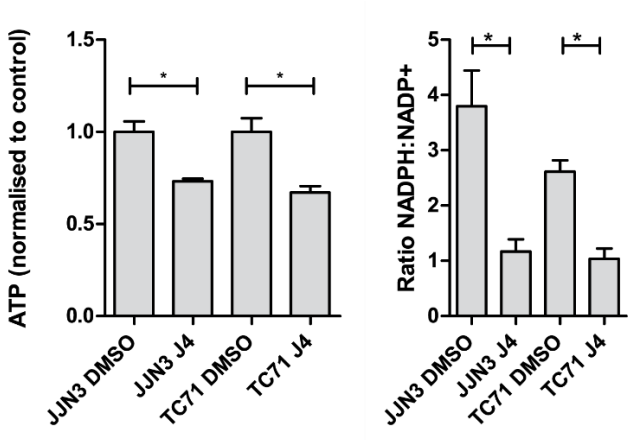


Figure 37 GSK-J4 reduces intracellular ATP content

Cellular ATP content and the NAPDH:NADP+ ratio were measured after 24 hours treatment with 5μM GSK-J4. Values obtained were corrected for cell number and normalized to the vehicle-only control. Data represent the mean±SEM of 4 biological replicates. Significance was calculated using the Mann-Whitney U Test with a $p<0.05$ indicating significance.

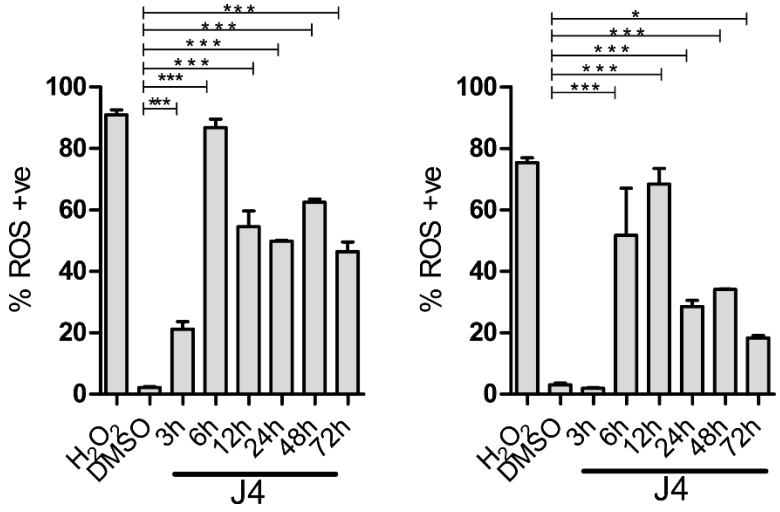


Figure 38 GSK-J4 increases cellular reactive oxygen species

*The number of cells positive for reactive oxygen species as determined by increased fluorescence of the CellROX Green dye after treatment with 5μM GSK-J4 in either TC71 Ewing sarcoma cells (Left) or JJN3 multiple myeloma cells (Right). No change over time was seen in cells treated with vehicle only (data not shown). Data plotted as mean±SEM of 4 biological replicates. Significance was calculated using the Mann-Whitney U Test with * representing $p<0.05$, ** $p<0.01$ and *** $p<0.001$.*

4.3.2 GSK-J4 reduces cellular oxygen consumption

Oxygen consumption by TC71 and JJN3 was measured using a fluorescence assay in which the intensity of a fluorescent probe changes with the partial pressure of oxygen within the cell media. The probe is added to a culture of growing cells followed by the addition of a layer of gas-impermeable oil meaning that any oxygen used by cellular respiration within the culture will reduce the amount of oxygen present in the media (as it is unable to equilibrate with the atmosphere) and therefore changes the fluorescence intensity.

In TC71 Ewing sarcoma cells, under baseline conditions there is a high oxygen consumption rate (OCR) that is reduced to about half of the initial value after 6 hours exposure to GSK-J4 and reduced further to a very low rate after 24 hours exposure. In contrast, the JJN3 myeloma cells have a very low OCR in their baseline condition that does not alter

significantly following treatment with GSK-J4. These finding are consistent with the Ewing sarcoma cell line having a high rate of oxidative phosphorylation in its basal state that is significantly reduced upon treatment with GSK-J4. In contrast JJN3 myeloma cells have a significantly lower OCR in its basal state suggesting that oxidative phosphorylation is not used as the primary source of energy production.

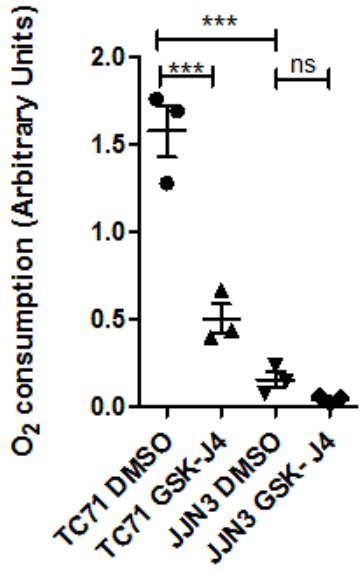


Figure 39 GSK-J4 reduces oxygen consumption

*Oxygen consumption was calculated for an equal number of cells of TC71 Ewing sarcoma and JJN3 myeloma in cells treated with either DMSO of GSK-J4. Significance was calculated using a T-test (***, $p<0.001$)*

4.3.3 GSK-J4 treatment leads to an accumulation of intracellular glutamine with a decreased level of glutamate

To investigate the changing composition of metabolites following treatment with GSK-J4, cell extracts were measured by one-dimensional nuclear magnetic resonance spectroscopy at different time-points after addition of the compound. Analysis reveals a decrease in a

number of TCA cycle intermediates such as fumarate and a decrease in amino acids such as aspartate, an amino acid formed from oxaloacetate. The level of glutamine can be seen to increase over time whereas the level of glutamate is seen to decrease in response to GSK-J4, as does the level of proline, an amino acid formed from glutamate. In addition to the increase in glutamine, also an increase in the level of other amino acids such as tyrosine, valine or isoleucine is noted.

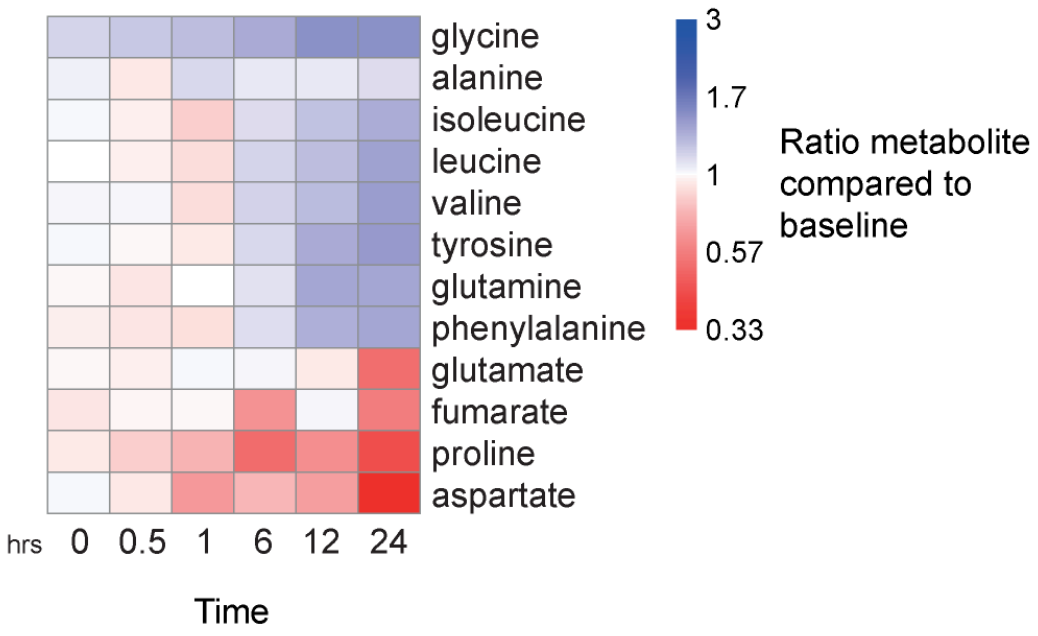


Figure 40 GSK-J4 causes changes in metabolites in JJN3 myeloma cells

The level of metabolites in JJN3 cells was measured by 1D NMR at time points indicated following treatment with 5μM GSK-J4 and the ratio of the level of the metabolite to the corresponding level in the vehicle-treated control was calculated. Data represents the mean value of 3 biological replicates.

4.3.4 Glutaminolysis is inhibited by GSK-J4

Using glucose and glutamine labelled with ^{13}C it is possible to follow the labelled carbon through metabolic pathways and identify incorporation into different metabolic pathways. In the baseline state of JJN3 myeloma cells, glucose is converted into lactate with very low amounts of glucose metabolites entering into the TCA cycle. A significant amount of glucose is metabolized into riboses (pentose phosphate pathway) and is used to form the precursors for nucleic acid synthesis, NADPH generation and glycosylation pathways. Glutamine is converted via glutaminolysis to glutamate, metabolized to alpha-ketoglutarate and feeds the TCA cycle. Clear labeling of carbons originating from labeled glutamine are observed in TCA intermediates such as succinate, fumarate and malate as well as amino acids that are formed from TCA cycle intermediates.

In cells treated with GSK-J4, a significant change in the metabolic profile can be observed. The amount of labelled carbon passing from glutamine is reduced such that the level in glutamate is decreased compared to the control condition and labelled carbon atoms no longer enter the TCA cycle. There is consequently a reduced incorporation of carbon atoms originating from glutamine into TCA cycle intermediates and the amino acids that are formed from them. Glucose continues to feed the glycolytic pathway and be converted to lactate with no apparent compensatory entry to the TCA cycle following the decrease of entry of carbons from glutamine. Also observed is a large increase in the amount of carbon originating in glucose being incorporated into glycerol-3-phospahte (Gol3P). Gol3P is formed from the reduction of dihydroxyacetone phosphate through the action of the enzyme glycerol-3-phosphate dehydrogenase using NADH and H^+ to generate NAD^+ necessary for other metabolic processes. The production of Gol3P is also important in maintaining the

mitochondrial membrane production through the glycerol-3-phosphate shuttle, a series of coupled reactions in which Gol3P and dihydroxyacetone phosphate are sequentially oxidized and reduced, with Gol3P accepting electrons from flavin adenine dinucleotide (FAD) as a cofactor. Gol3P is also important for the biosynthesis of lipids.

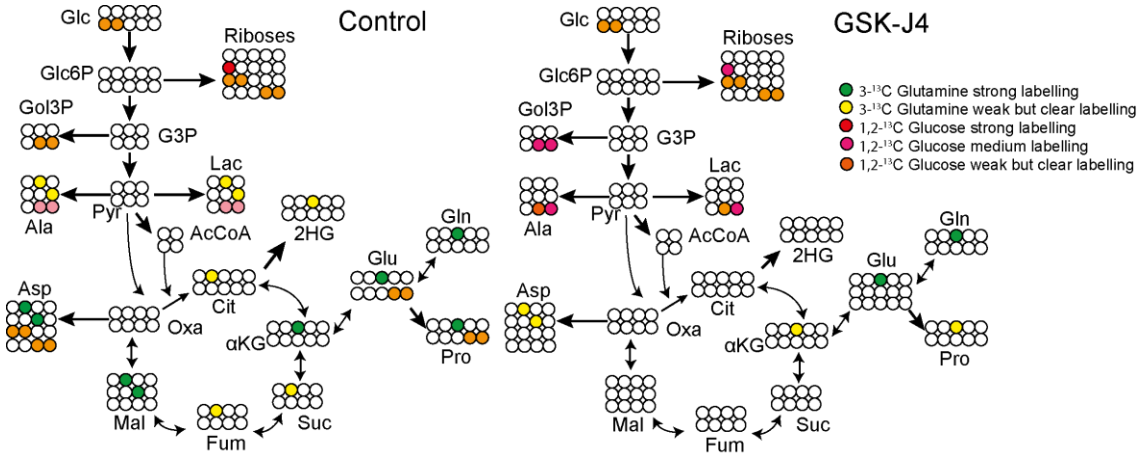


Figure 41 Alteration of metabolic pathways in JJN3 upon GSK-J4 treatment

A representation of the metabolism of glucose and glutamine in JJN3 cells under normal conditions (left) and 24h after treatment with 5μM GSK-J4 (right). Each circle represents an unlabelled carbon atom that was not detected during NMR. Coloured circles indicate species identified by 2D NMR and an indication of the amount present. Data represent the consensus of 3 separate biological experiments. Abbreviations: Glc glucose, Glc6P glucose-6-phsophate, Gol3P glycerol-3-phosphate, G3P glyceraldehyde-3-phosphate, Ala alanine, Pyr pyruvate, Lac lactate, AcCoE acetyl-coenzyme A, Cit citrate, 2HG, 2 hydroxygluterate, aKG alpha-ketogluterate, Suc succinate, Fum fuemarate, Mal malate, Asp aspartate, Oxa oxaloacetate, Glu glutamate, Gln glutamine, Pro prolime

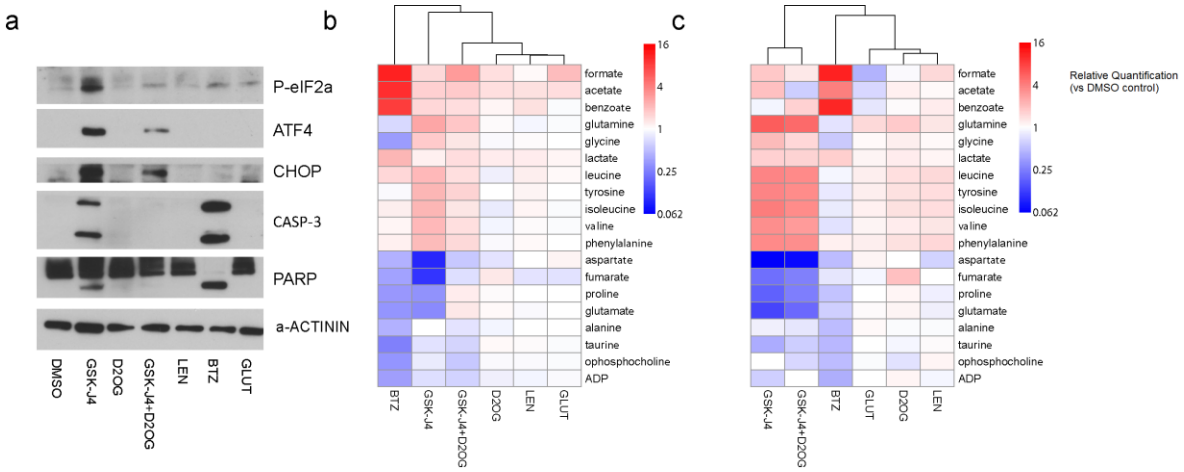


Figure 42 Dimethyl-2-oxoglutarate protects cells from GSK-J4 effects and metabolic perturbations after inhibitor treatments

(a) Western blot indicating that D2OG prevents GSK-J4 eIF2a phosphorylation, reduces the expression of ATF4 and CHOP and prevents cleavage of caspase 3 and PARP at 24h post treatment. (b) 24 hours following treatment with GSK-J4, the presence of D2OG ameliorates the metabolomics changes induced by GSK-J4 with a reversal of the decrease in glutamate observed and (c) 48 hours post exposure to GSK-J4, cells treated in addition with D2OG show a very similar metabolic profile to cells that did not receive D2OG. Data represent the mean value of three biological replicates compared to the vehicle only control at each time point. Relationship between samples was calculated using an unsupervised hierarchical clustering approach. D20G dimethyl-2-oxogluterate, BTZ bortezomib, LEN lenalidomide, GLUT glutaminase inhibitor compound 968.

4.3.5 Dimethyl-2-oxoglutarate temporarily rescues cells from the effect of GSK-J4

Supplementation of cell media with the cell-permeable alpha-ketoglutarate analogue dimethyl-2-oxoglutarate (D2OG) temporarily protects cells treated with GSK-J4 from the induction of the ATF4 response and apoptosis and reverses the metabolic changes observed after 24 hours (Figure 42). Specifically, it can be seen that in contrast to cells treated with GSK-J4 but not D2OG there is a decrease in the level of glutamate at 24h which is reversed in the cells that have also received D2OG supplementation. After 48 hours, the metabolomics

profile of JJN3 cells treated with GSK-J4 alone and with D2OG are similar to each other, indicating that the effect was only temporary and likely limited to the available supply of D2OG.

4.3.6 GSK-J4 induces different metabolic changes compared to conventional myeloma treatments

In order to compare the effect of GSK-J4 on the metabolic profile of JJN3 cells with other commonly used treatments for myeloma, 1D spectra of cells treated with bortezomib (BTZ) and lenalidomide (Len) were obtained following 24 hours with a dose equivalent to the IC_{80} in each case. Notable changes exist between the profiles obtained for each of the conventional treatments when compared to GSK-J4. For bortezomib treated cells, a large amount of intracellular formate and acetate was observed and, in contrast to treatment with GSK-J4 the level of intracellular glutamine was seen to decrease. Treatment with lenalidomide produced subtle metabolomics changes after 24 hours and the response seen is different to that obtained with GSK-J4.

4.3.7 The glutaminase inhibitor compound 968 does not mimic the effect of GSK-J4

In order to ascertain if the effect of GSK-J4 was mediated via direct inhibition of glutaminolysis, JJN3 cells were treated with the glutaminase inhibitor compound 968 at a dose equivalent to the IC_{80} for either 24 or 48 hours followed by extraction of metabolites for analysis by NMR. Cells were also assessed after 24 hours for the ability of the compound

to induce the ATF4 response and apoptosis. The glutaminase inhibitor induced neither the ATF4 response nor apoptosis and did not have a similar metabolic profile to that obtained with GSK-J4 lending support to the conclusion that the method of action is not through either a direct inhibition or regulation of intracellular glutaminases.

4.3.8 GSK-J4 does not directly inhibit enzymes involved in glutaminolysis

In a further attempt to explain the observed changes in the intracellular amount of glutamine and glutamate, GSK-J4 was tested for its ability to directly inhibit enzymes involved in the process of glutaminolysis. Using a commercially available colorimetric assay for the activity of glutamate dehydrogenase (GDH) neither GSK-J4 nor GSK-J1, the carboxylic acid derivative of GSK-J4 that is active against the lysine demethylase enzymes, was observed to impair that activity of enzyme. Further enzymatic assays were performed by Dr James Dunford in the group and no inhibition for glutaminase, isocitrate dehydrogenase 1 or 2 or alpha-ketoglutarate dehydrogenase for either GSK-J4 or GSK-J1 was observed, indicating that GSK-J1, the intracellularly active metabolite of GSK-J4 has no observable off-target effects on these metabolic glutamine utilizing pathways.

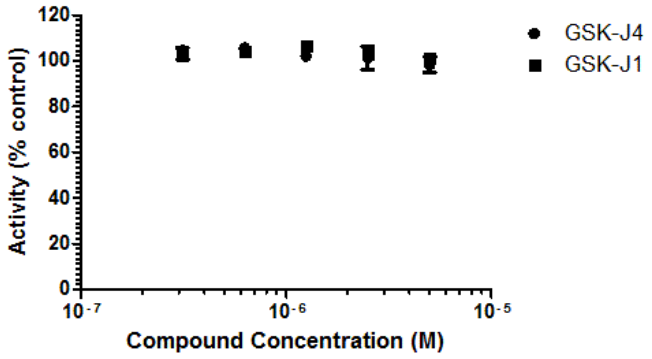


Figure 43 GSK-J4 does not inhibit glutamate dehydrogenase activity

The activity of glutamate dehydrogenase was measured in varying concentrations of 5μM GSK-J4 and GSK-J1 and compared to the activity of GDH in the absence of inhibitor. Data represent the mean±SEM for three biological replicates.

4.3.9 GSK-J4 causes transcriptional changes in genes associated with metabolism as measured by qPCR

In order to better understand the metabolic changes observed in the NMR flux experiments, and to link the ATF4 response to these metabolic perturbations, a qPCR panel of approximately 50 genes associated with metabolism was generated. This panel includes genes for enzymes in the glycolytic pathway, tricarboxylic acid cycle and genes associated with amino acid metabolism (Figure 44). Treatment with GSK-J4 causes a large change in the transcriptional profile with up-regulation of several anabolic genes in keeping with the known activation of the ATF4 pathway mediated by GCN2. This up-regulation of genes includes many enzymes directly involved in the synthesis of amino acids such as aspargine synthetase (ASNS) and phosphoserine phosphatase (PSPH). The profile of the transcriptional changes of metabolic enzymes to GSK-J4 is similar in both the TC71 Ewing Sarcoma and JJN3 myeloma cell lines, as was previously seen in the microarray experiment

and is in keeping with the predominant response observed being driven by the induction of the ATF4 pathway.

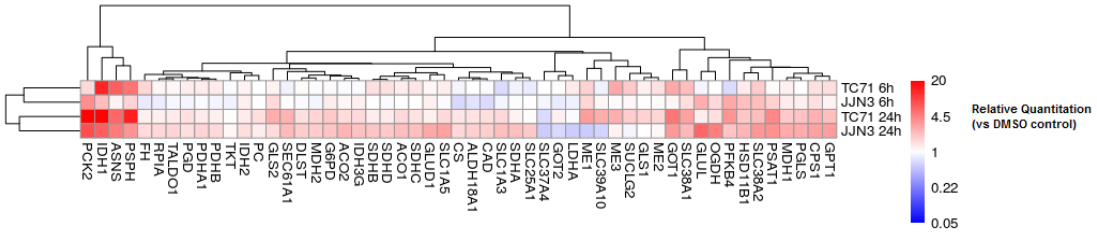


Figure 44 Expression level of metabolomic enzymes changes with GSK-J4 treatment

Expression of genes involved in metabolic processes expressed as a fold change in JJN3 and TC71 cells treated with 5μM GSK-J4 compared to vehicle only treated cells Data represent the mean of 3 independent experiments.

4.4 DISCUSSION

The observation that there is a reduction in the ratio of NADPH:NAPD+, an increase in cells positive for reactive oxygen species and the observation from the previous chapter that there is a large induction in metallothioneins is indicative that treatment with GSK-J4 leads to an increased oxidative stress within cells. Whilst metallothioneins are normally associated with cellular response to heavy metals, induction of metallothioneins is also observed when cells are under oxidative stress induced by other causes (Chiaverini and De Ley 2010). NADPH plays an important role in protecting cells from oxidative stress by providing reducing equivalents for the regeneration of reduced glutathione, peroxiredoxins and for the activity of thioredoxin reductase. The oxidative phase of the pentose phosphaste pathway in which glucose 6-phosphate is converted to ribulose 5-phosphate with the generation of NADPH is an important cellular mechanism for regeneration of the pool of NADPH. The initial step of the pentose phosphate pathway is catalysed by the enzyme glucose 6-phosphate dehydrogenase which is allosterically activated by NADP+ leading to increased use of the pathway and therefore generation of NADPH (Barcia-Vieitez and Ramos-Martínez 2014; Stanton 2012; Fabregat et al. 1985). From the 2 dimensional metabolomic data it can be seen that in the JJN3 myeloma cells there is a large utilization of the pentose phosphate pathway even in the base state. The pentose phosphate pathway is highly active in many cancers (Patra and Hay 2014) for the production of nucleotides and for lipid synthesis and due to the key regulation of the first step by the NADPH:NADP+ ratio suggests that such cells are already under a degree of oxidative stress.

Isocitrate dehydrogenase uses NADP+ as a cofactor for the oxidation and decarboxylation of isocitrate to alpha ketoglutarate generating NADPH in the process. The large increase in

expression of IDH1 observed in both the Ewing sarcoma and multiple myeloma cell lines may represent a further cellular response to the increased oxidative stress generated by GSK-J4 (Itsumi et al. 2015) in addition to a cellular attempt to increase flux through the TCA cycle for the production of amino acids and lipids.

The 2D metabolomics studies involving the flux of labelled glutamine and glucose reveal that the JJN3 myeloma cells in their basal state display many of the features of the Warburg effect. Despite the abundance of oxygen available to the cells in the culture environment glucose is predominantly metabolized anaerobically forming lactate. These data are supported by the oxygen consumption assays which indicate that JJN3 myeloma cells have a very low level of oxygen consumption in their basal state, suggesting that oxidative phosphorylation is not being used as the primary source of ATP generation within these cells. The NMR data also demonstrate that glutamine is used as a source of carbons for the TCA cycle and that carbon originating in glutamine is incorporated into lactate, demonstrating that malate must be exported from the mitochondria into the cytoplasm where malic enzyme 1 (ME1) is able to convert malate to pyruvate which is then converted lactate. The metabolic conversion of glutamine to lactate also leads to the generation of NADPH and NAD+ that are necessary for other cellular processes. These observations are in keeping with those made in glioblastoma cells in which glutamine and not glucose was seen to predominantly fuel the TCA cycle (DeBerardinis et al. 2007) and is now considered a hallmark of Myc driven metabolic changes in cancers.

The observed response to GSK-J4 in cells is analogous to the effect seen in neuroblastoma cells upon acute depletion of glutamine (Qing et al. 2012). In this work, glutamine, which is normally present in abundance within cells and in cell culture medium was removed, and the

authors observed the induction of an ATF4 response and the up-regulation of pro-apoptotic genes such as PUMA and NOXA. These changes are seen upon treatment with GSK-J4 despite the abundance of glutamine as determined by NMR. Qing et al. also report that pharmacological inhibition of glutamine metabolism leads to a similar phenotype as the acute glutamine deprivation, a finding that was not replicated in this study using the glutaminase inhibitor Compound 968, however in their study the pharmacological inhibition was directed against enzymes involved in the conversion of glutamate to alpha-ketoglutarate and not the glutaminases which may explain the difference observed.

Examination of the enzymes involved in glutamine metabolism do not present an obvious explanation for the observed inhibition of glutaminolysis. The expression of both isoforms of glutaminase (GLS1 and GLS2) can be seen to increase in response to GSK-J4 in both myeloma and Ewing sarcoma cell lines. The level of expression of glutamate ammonia ligase (GLUL), the enzyme that is responsible for the formation of glutamine from glutamate and ammonia in an ATP-dependent fashion, is up-regulated to an even greater degree than the change in expression observed of both GLS1 and GLS2.

The fact that supplementation of the cells with DMOG was able to temporarily reverse the effects of GSK-J4, both in the metabolic profile observed and in the prevention of the induction of the ATF4 response and the decreased glutamate and increased glutamine observed strongly suggests that the limiting factor in the system is the conversion of glutamine to glutamate. However, there is, as measured by qPCR, upregulation of the glutaminase enzymes and no evidence of direct inhibition by GSK-J1 or GSK-J4. A possible explanation observed is that the level of glutamate ammonia ligase (GLUL), the enzyme that is responsible for the formation of glutamine from glutamate and ammonia in an ATP-

dependent fashion, is up-regulated to an even greater degree than the change in expression observed of both isoforms of GLS. It is therefore possible that the change in the relative expression of the enzymes alters the dynamic equilibrium between glutamine and glutamate found in cells resulting in larger concentrations of glutamine. From the data available it is unclear whether the ATF4 response is being induced as a result of the observed changes in the metabolism within the cell, such as reduction in the level of aspartate, or whether the observed phenotype is as a consequence of ATF4 induction.

5 GSK-J4 GLOBALLY ALTERS H3K4ME3 AND H3K27ME3 AS MEASURED BY CHIPSEQ

5.1 OVERVIEW

In this chapter, chromatin immunoprecipitation followed by next generation sequencing (ChIPseq) will be used to describe the distribution and changes of H3K4me3 and H3K27me3 levels in the multiple myeloma cell line JJN3 upon GSK-J4 treatment. A quantitative approach to ChIPseq normalization, requiring as technical pre-requisite genome assembly of the SF9 genome, demonstrates that treatment with GSK-J4 leads to a global increase in H3K27me3 with a decrease in the level of H3K4me3 except for a small subset of genes. RNA sequencing of JJN3 cells treated with GSK-J4 confirms the original observations obtained in the microarray experiments with induction of metallothioneins and an AT4-driven response.

5.2 INTRODUCTION

5.2.1 Chromatin precipitation and next generation sequencing

ChIPseq is a powerful tool for examining the interaction of proteins such as histones and transcription factors with DNA (Johnson et al. 2007). Fragmentation of chromatin, containing genomic DNA, is followed by immunoprecipitation of the protein of interest causing co-precipitation DNA that is interacting with the protein. Following purification, the short fragments of precipitated DNA are converted into sequencing libraries and millions of these fragments are sequenced in parallel. By aligning the sequences to a reference

genome it is possible to draw inferences about the genomic binding location of the protein of interest.

Two key features can be obtained from ChIPseq data: the physical location of the peak on the reference genome and the magnitude of the size of the peak. Although early attempts are made in the field of single-cell ChIPseq (Rotem et al. 2015), the vast majority of ChIPseq experiments reported to date have required the use of large numbers of cells resulting in a profile that represents an amalgamation of the cell population under study. Factors such as stage in the cell cycle will alter the interaction between protein and DNA and therefore even in a homogenous population of cells it is unlikely that at any given time all of the peaks identified in the population will be represented in any given cell. In this context, a peak of increased size at a given location will therefore indicate that, on average, a greater proportion of cells within the population are having the mark in question.

A difficulty in the interpretation of ChIPseq experiments occurs in normalizing the raw data between difference samples. It has long been appreciated that if one sample is sequenced more deeply than a second sample, all others factors being equal, the sample sequenced to a higher depth will appear to have larger peaks. Therefore, it has been common practice to normalize samples to reads per million mapped reads (RPM) to account for the difference in sequencing depth. RPM normalization does not, however, account for differences in biological complexity between samples. If one sample contains only half the amount of protein-DNA interaction compared to a second sample at the same genomic locations, following normalization for sequencing depth it would appear that both samples were equivalent whereas in reality the less complex sample has been sequenced to twice the effective depth of the more complex sample. In experiments where the location of peaks is

the main feature of interest this is less of a problem as it only has a limited effect on the ability to call a peak as present or absent. However, when examining global changes the issue of complexity is problematic.

In order to overcome the issue of sample complexity, the process of quantitative ChIPseq has recently been introduced (Orlando et al. 2014). Quantitative ChIPseq exploits a spike-in of exogenous chromatin from a second species to act as a reference for the complexity of the chromatin under study. By adding chromatin in a fixed ratio to the original number of cells, and assuming that the efficiency of the immunoprecipitation is the same in all cases, samples can be normalized to each other by scaling to the reciprocal of the number of reads from the spiked-in species. By scaling samples in such a manner, account is taken for both the complexity of the original sample and the depth of sequencing.

A basic requirement for the quantitative ChIPseq method to work is that the antibody being used has to recognize the protein of interest in both species. It is not a requirement that the antibody has the same affinity for the antigen in both species, only that the experimental conditions are kept constant and that the efficiency of the pull-down for both species is similar for every each sample. For histone modifications, which are evolutionarily highly conserved, there is a large degree of reactivity across species.

A second requirement for quantitative ChIPseq is that the organism being used as a spike-in has a reference genome against which reads can be aligned. For the method to work efficiently, it is beneficial that the genomes are dissimilar to reduce the possibility of ambiguously mapping any given read to the wrong species. Whilst one could take the approach that any reads not mapping to the reference genome of the first species must belong to the second, this would not account for reads that can map to either genome and ignores

the fact that mapping to the reference genome never occurs with 100% accuracy. While the initial quantitative CHIPseq study (Orlando et al. 2014) used the Drosophila genome as reference genome, employing spike-in from the S2 cell line, it was decided for this work to use the Spodoptera genome by addition of SF9 cells as this is a cell line in regular use within the laboratory. The SF9 cell line was established as a clonal isolate of the parental cell line IPLB-Sf-21-AE (also called SF21), originating from the ovary of the fall armyworm *Spodoptera frugiperda*. SF9 cells are extensively used in biology laboratories in process of protein production, are easy to cultivate and rapidly dividing and therefore provide an enticing option for cells to use for spike-in normalization. Whilst there has been a limited effort to sequence and annotate the transcriptome of SF9 cells (Landais et al. 2003; Nègre et al. 2006), to date no publication has described a draft genome suitable for use in quantitative ChIPseq normalization. Therefore a genome draft for SF9 cells needed to be generated before continuing with further experiments.

5.2.2 Epigenetic data visualization

A key challenge in epigenetic studies is finding methods to adequately display and convey the huge amounts of data experimentally generated (Marx 2015). For certain epigenetic marks, such as H3K4me3 that are located around transcription start sites, it is possible to build up meta-genomic profiles where the coverage around all transcription start sites is measured individually and then an average coverage calculated. A more challenging problem is the visualization of broad marks which are not so tightly associated with particular features such as transcription start sites and that may expand over many kilobases.

One method of visualization that will be employed in this thesis is the space-filling Hilbert curve (Hilbert 1891). As the curve goes through increasing iterations, as demonstrated in

Figure 45, the length of the line increases but it always remains bound with the same two-dimensional space. This property of the Hilbert curve can be exploited to visualize very long vectors of data such as those needed to visualize the genome. By applying a colour scale to the plotted line differences in coverage of a particular epigenetic mark within the genome can be displayed.

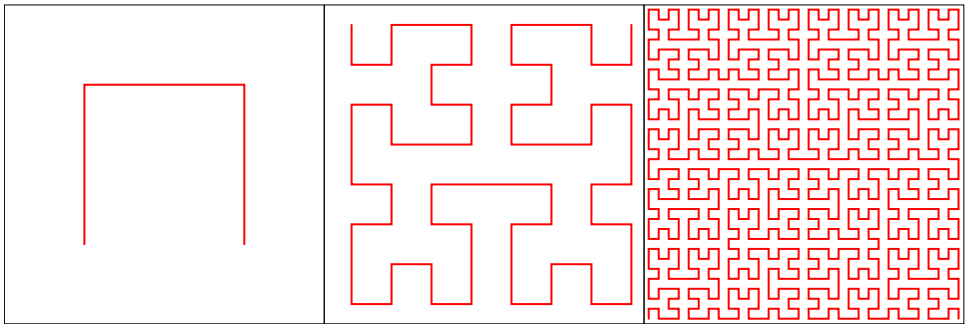


Figure 45 Hilbert Curves of increasing interation

Whilst the Hilbert curve is not a conventionally used visualization for epigenetics, it has been employed in this thesis as many of the global changes in histone methylation that will be displayed later within the chapter are not easily appreciated when using other graphical approaches. Graphical representation of ChIP data often focus on individual gene features, such as the transcription start site, however displaying changes which are occurring throughout the genome and not specifically in relation to an easily identifiable feature is otherwise a challenge. The Hilbert curve helps to overcome some of these challenges by providing a view of the entire length of the genome in one image.

5.3 RESULTS

5.3.1 Draft assembly of the SF9 genome

In order to generate a genome assembly, genomic DNA from 10 million SF9 cells was isolated, fragmented to a size of approximately 350bp and then used to prepare libraries compatible with Illumina sequencing. Paired-end sequencing with a read length of 83bp was performed on a Nextseq 500. Following trimming for quality and adaptors, reads were error corrected using Fiona (Schulz et al. 2014) prior to being divided into groups of 100 million pairs of reads. Each group of 100 million reads was used to generate a genome assembly using SPAdes (Bankevich et al. 2012). A consensus assembly between the two de novo assemblies was created using AMOS and MUMmer (Kurtz et al. 2004). Statistics were generated using QUAST (Gurevich et al. 2013). Full details of the methodology used to produce the SF9 genome assembly is given in Chapter 2.

Table 6 details statistics of the genome assembly produced. When considering contigs over 250bp in length, a total genome length of 319MB is obtained with a GC content of 35.1%. The largest contig is 169244bp long. The N50 value, the length of contig above which 50% of the assembly can be produced is 13109 and the L50 value, the number of contigs required to produced 50% of the genome 6385.

Graphs displaying the cumulative length of the assembly and GC content across the genome are shown in Figure 46.

Contigs	53174
Contigs (>= 0 bp)	53232
Contigs (>= 1000 bp)	40833
Contigs (>= 5000 bp)	17936
Contigs (>= 10000 bp)	9100
Contigs (>= 25000 bp)	2133
Contigs (>= 50000 bp)	357
Largest contig	169244
Total length	319112353
Total length (>= 0 bp)	319124978
Total length (>= 1000 bp)	311052735
Total length (>= 5000 bp)	253296027
Total length (>= 10000 bp)	190665688
Total length (>= 25000 bp)	84139975
Total length (>= 50000 bp)	24664717
N50	13109
N75	5991
L50	6385
L75	15385
GC (%)	35.91

Table 6 Statistics of draft assembly of SF9 genome

Summary statistics of the assembled SF9 genome. N50/N75 is the contig length required such that using contigs this length or longer produces 50%/75% of bases for the genome. L50/75 is the minimum number of contigs required to produce 50%/75% of the genome.

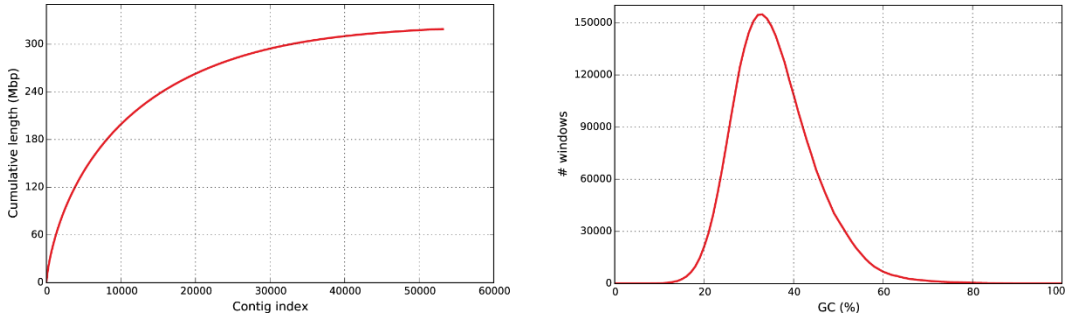


Figure 46 Statistics of draft assembly of SF9 genome

(Left) Cumulative length of assembly obtained with increased numbers of contigs. (Right) GC content of the genome obtained by binning the assembly into 100bp windows.

5.3.2 GSK-J4 causes a global increase in H3K27me3

In keeping with its role as an inhibitor of the H3K27 demethylases KDM6A and KDM6B, treatment with GSK-J4 in the multiple myeloma cell line JJN3 leads to a global increase in the level of H3K27me3 after 24 hours. Figure 47 demonstrates Hilbert visualizations of the genome showing the averaged, normalized coverage of H3K27me3 in DMSO-treated cells and in those treated with GSK-J4. It can be seen that the distribution of H3K27me3 throughout the genome is similar in both cases but the magnitude of the coverage is increased with GSK-J4. Figure 48 demonstrates the log fold change between coverage in cells treated with GSK-J4 or DMSO confirming that in the vast majority of locations within the genome there is an increase in the level of H3K27me3.

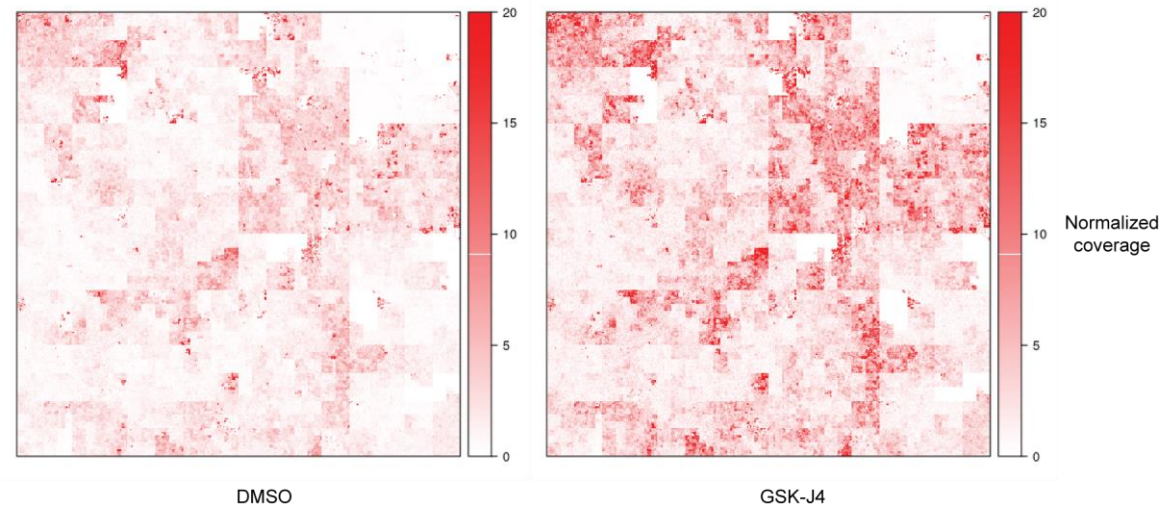


Figure 47 Hilbert Visualization of H3K27me3 coverage in JJN3 cells

Hilbert Visualisations represent the average, normalized coverage of 2 replicates of JJN3 cells treated with either DMSO (left) or GSK-J4 (right) for 24 hours. The genome was divided into bins of 5kb in length and the median coverage for each bin plotted.

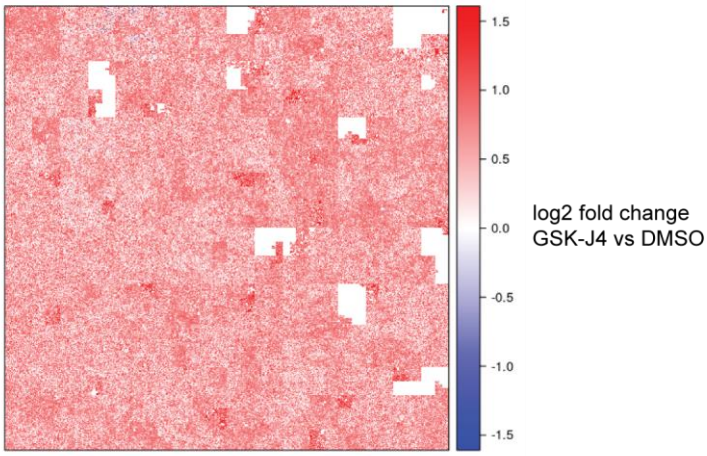


Figure 48 Hilbert Visualization of fold-changes in H3K27me3 coverage.

The log2 fold change of each region of the genome as determined in Figure 47 was calculated and plotted as a Hilbert Curve.

An interesting side note of using Hilbert visualization to display epigenetic data is that there are regions of Figure 48 displaying blank areas where there is no H3K27me3 coverage data. These areas likely represent chromosomal deletions or, as is the case for the area in the top right hand corner of figure 4, the Y chromosome, which is absent in JJN3 cells.

5.3.3 GSK-J4 causes a generalized decrease in H3K4me3 with sparing of ATF4 target genes

In contrast to the increase in H3K27me3, treatment with GSK-J4 leads to a generalized decrease in the coverage of H3K4me3 as demonstrated by a decrease in the average coverage around the transcription start site of all genes.

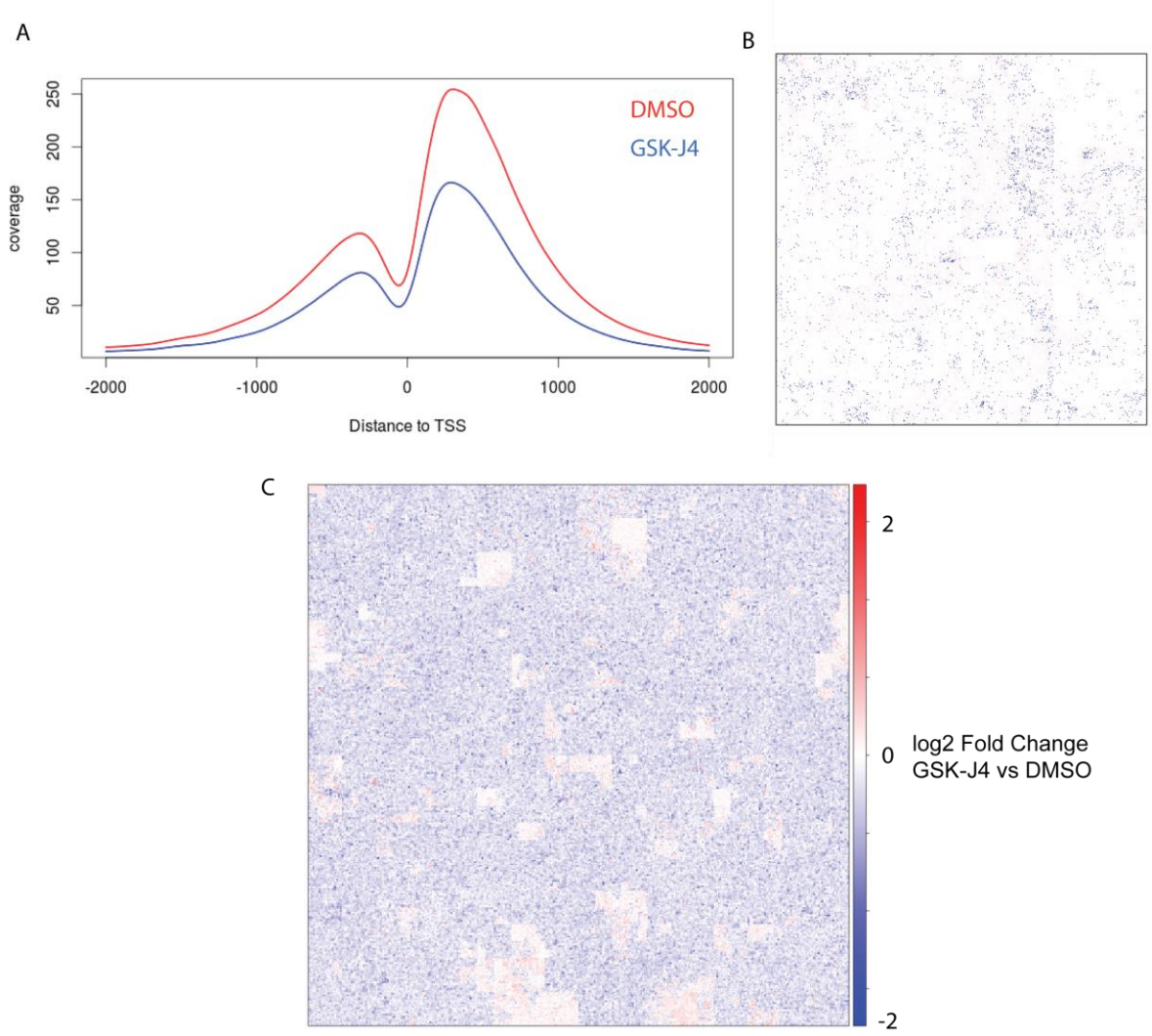


Figure 49 GSK-J4 reduces H3K4me3 coverage

(A) Profile of H3K4me3 coverage at transcription start sites in DMSO (red) and GSK-J4 (blue) treated cells. (B) Hilbert plot demonstrating distribution of H3K4me3 peaks throughout the genome. (C) Log2 fold change in H3K4me3 coverage with intervening genomic regions removed.

As compared to H3K27me3, H3K4me3 can be seen distributed in a concentrated manner and as defined peaks throughout the genome (

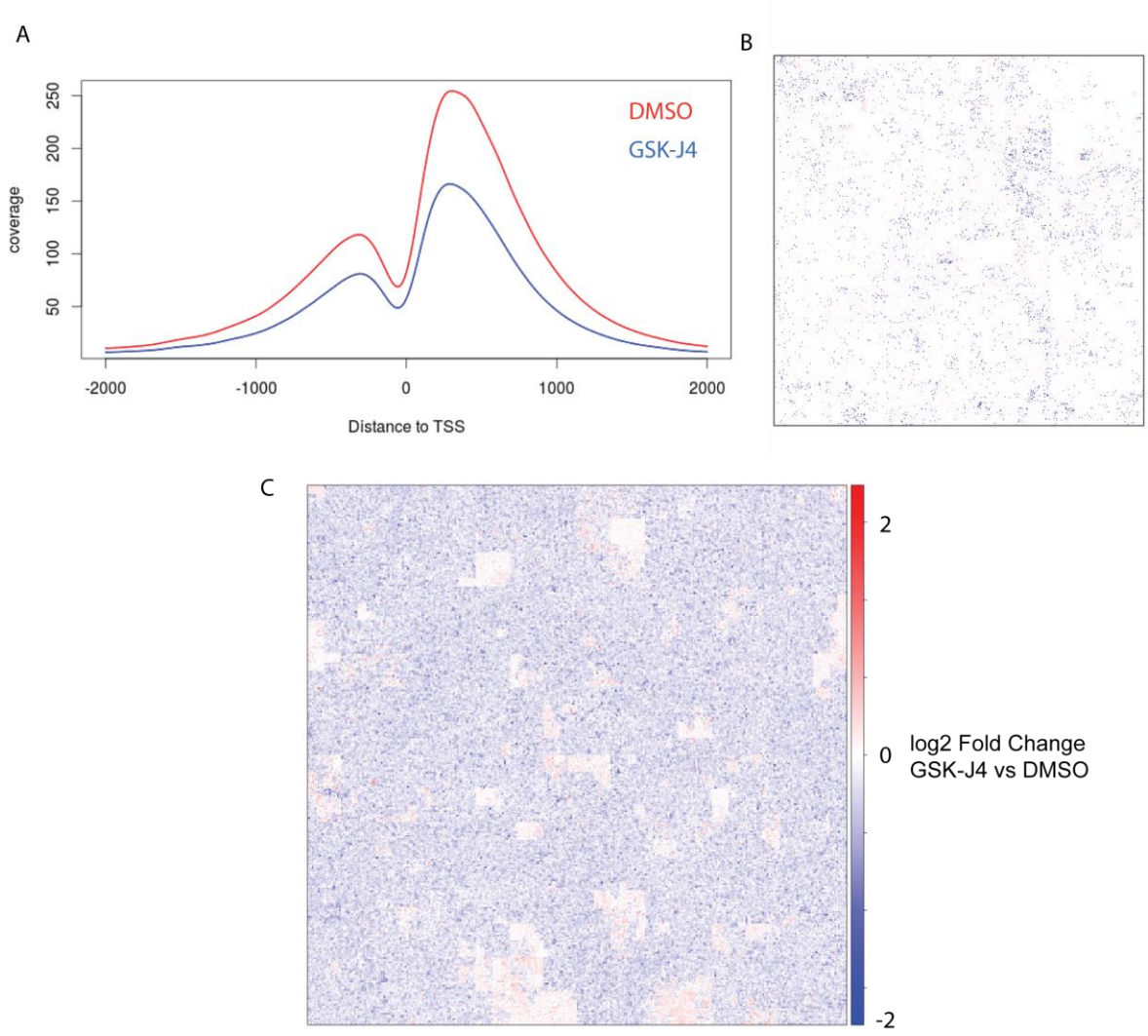


Figure 49B). When the intervening genomic regions are removed and the log2 fold change between the GSK-J4 and DMSO conditions are visualized, it can be seen that the vast majority of changes observed in H3K4me3 levels result in decreases in coverage in the GSK-J4 treated samples

(

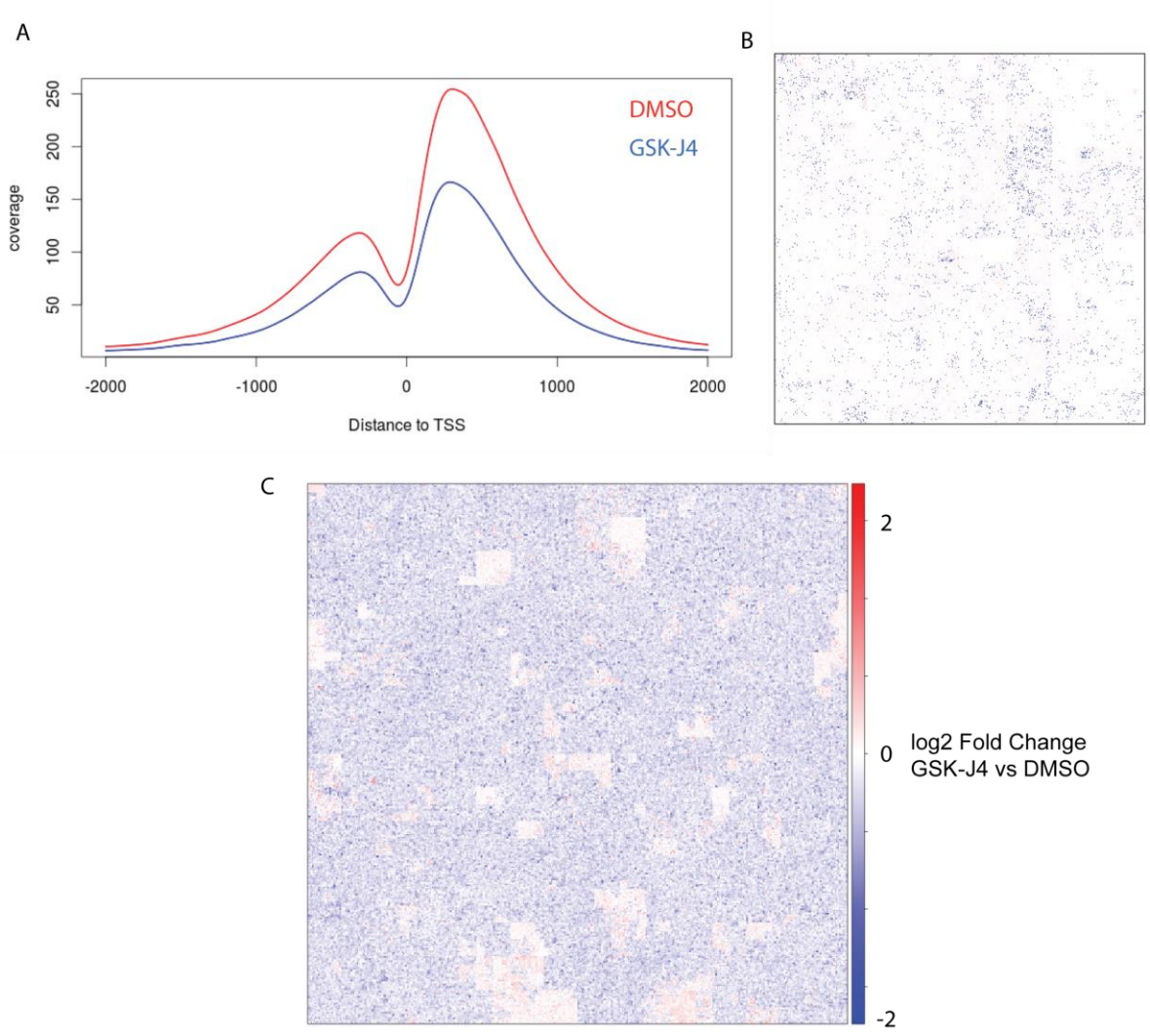


Figure 49C). However, in addition to a generalized decrease in observed H3K4me3 levels, there are discrete areas where the level of coverage remains constant or is seen to increase. 446 genes are identified as having increased H3K4me3 levels in GSK-J4 treated cells for at least 100bp with a log-likelihood ratio of greater than 5 within 2kb either side of the transcription start site (Appendix C). Inspection of this list reveals ATF4 target genes such as ASS1, BBC3, CHAC1, INHBE and SESN2 and several genes in the metallothionein cluster including MT1G, MT1H and MT1M.

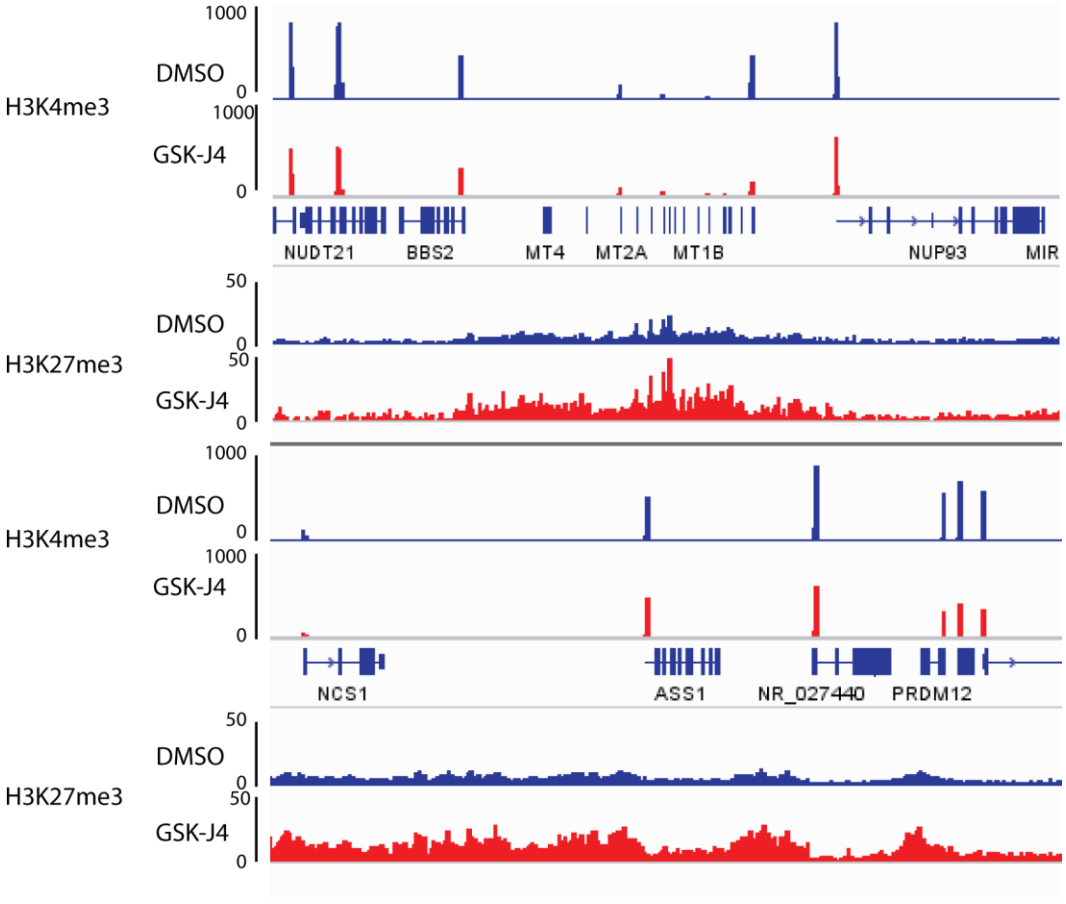


Figure 50 ChIP profiles of the metallothionein cluster and ASS1

Profiles of H3K4me3 and H3K27me3 focused on the metallothionein cluster (top) and the ATF4 target gene ASS1 (bottom).

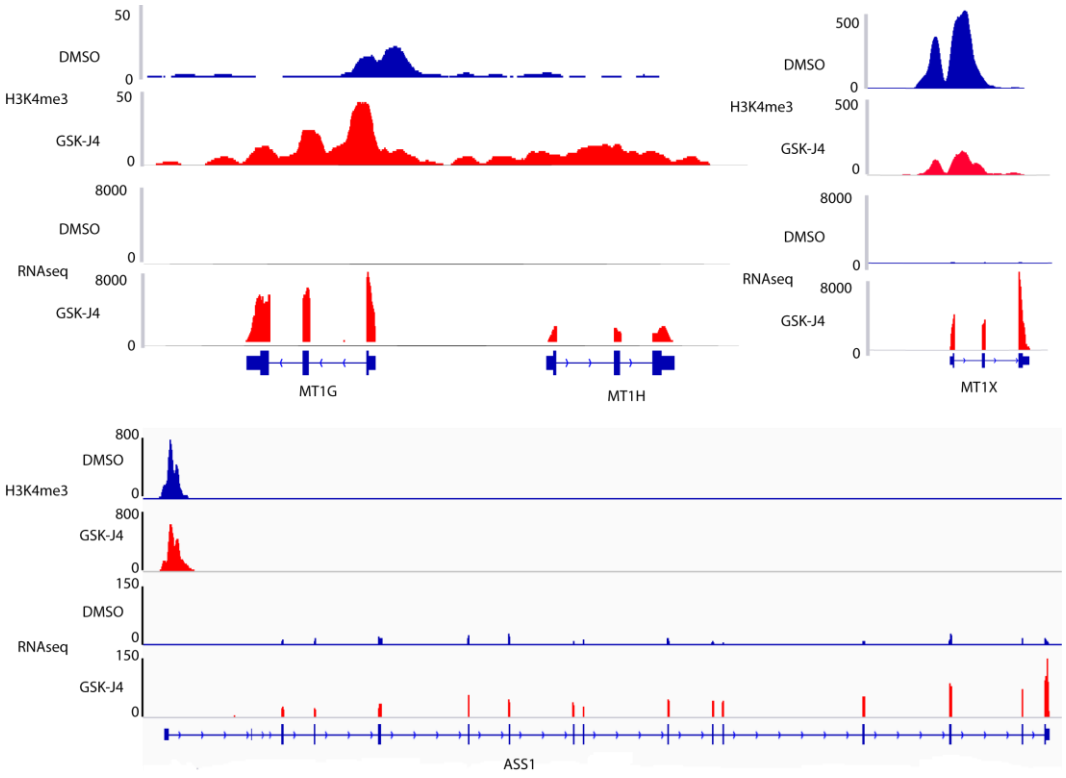


Figure 51 H3K4me3 and RNAseq coverage around the metallothionein cluster and ASS1

Local view of three metallothionein gene sand ASS1 demonstrating H3K4me3 profile and RNAseq coverage for JJN3 cells treated with GSK-J4 or DMSO.

Figure 50 demonstrates two regions of interest in the response to GSK-J4. In the top panel, the image is centered on the metallothionein cluster, which demonstrates a broad enrichment of H3K27me3 in both the control cells and, to a greater extent, cells treated with GSK-J4. The narrow peaks of H3K4me3 can also be observed at the transcription start site of genes. In contrast, in the bottom panel there is a relative paucity of H3K27me3 marks compared to the surrounding area in both the DMSO and GSK-J4 treated cells with, again, a peak of H3K4me3 centered on the transcription start site.

A localized view of the H3K4me3 profile around three metallothionein genes and ASS1 is shown in Figure 51. For the metallothionein genes MT1G and MT1H, increased H3K4me3 can be seen in the GSK-J4 treated condition with both an increase in the size and breadth of the peaks. This is associated with an extremely large induction of approximately 8000 fold of MT1G with a smaller but still significant increase in the level of expression of MT1H. This is in contrast to the H3K4me3 peak observed around MT1X in which there is a large peak seen in the DMSO condition (note change in scale) although little active transcription. In GSK-J4 treated cells, there is reduced H3K4me3 compared to the DMSO condition, to a level about that seen around MT1H and MT1G, but evidence of a large amount of transcription from RNAseq data. The transcription start site of ASS1 shows a mild broadening of the H3K4me3 associated with increased transcription in GSK-J4 treated cells compared to controls.

5.3.4 RNAseq confirms a large induction of metallothioneins and ATF4 response

In order to expand on the microarray data that has already been presented in chapter 3 demonstrating the response to GSK-J4 treatment at a 6 hour time point, RNAseq was performed following treatment for 24 hours. In total 2547 genes were significantly regulated with an adjusted p value below 0.05. Of the 2547 genes regulated, 1398 genes were down-regulated and 1149 genes up-regulated (Figure 52 and Figure 53). The top up-regulated genes (Table 7) include all members of the previously identified metallothionein family and a large number of ATF4 target genes including ASS1, INHBE, DDIT3 and DDIT4 and protein phosphatase 1 regulatory subunit 15A (PPP1R15A, also known as GADD34). A large up-regulation is also observed of the tumour suppressor gene CDKN1C.

Examining Transcript Per Million (TPM) values, in GSK-J4 treated samples the sum of the TPMs of the metallothionein genes is 28,083 compared to 101 in the DMSO condition, indicating that metallothionein genes represent approximately 2.8% of all transcripts in the GSK-J4 condition after 24h treatment.

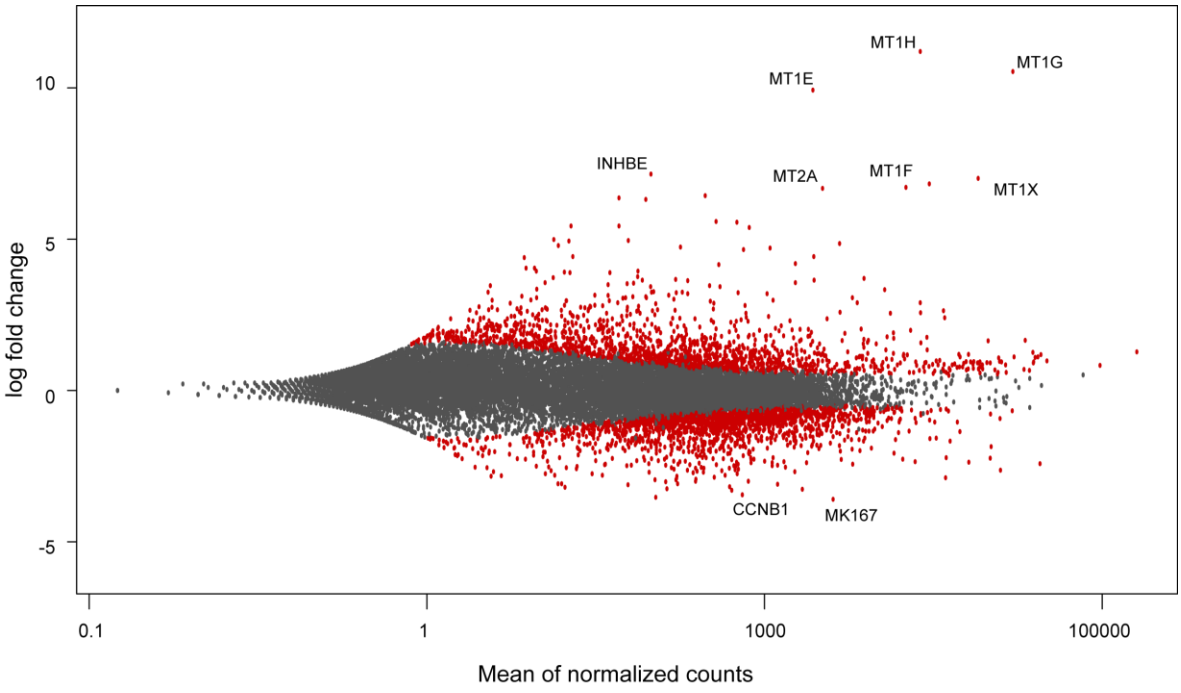


Figure 52 MA plot of changes in gene expression

Log fold change in gene expression between GSK-J4 and DMSO treated cells plotted against the mean expression between conditions. Genes which are significantly regulated (adjusted p value <0.05) are coloured in red.

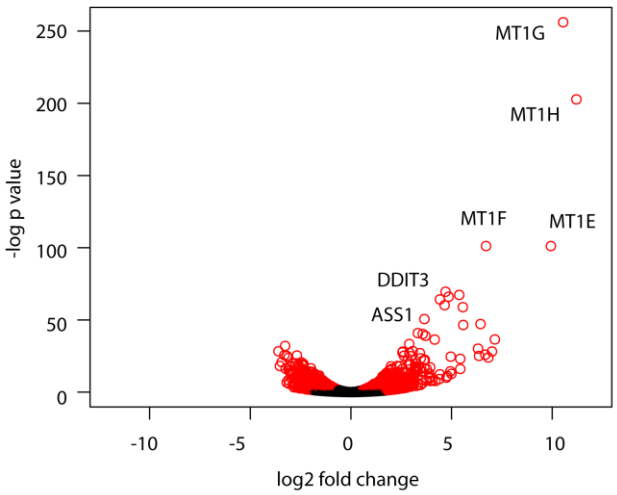


Figure 53 Volcano plot of regulated genes

The negative logarithm of the adjusted p value plotted against log2 fold-change for JJN3 cells treated with GSK-J4 compared to DMSO treated cells. Certain metallothionein transcripts and ATF4-target genes such as DDIT3 and ASS1 are indicated.

The top down-regulated genes (Table 8) include many involved in cell cycle regulation and progression such as cyclin B, cyclin A2, MKI67 and aurora kinase A. These observations are in keeping with the decrease in viability and proliferation described in chapter 3.

Gene ontology analysis of the down-regulated genes reveals an enrichment of terms associated with cell cycle progression (Figure 54). Pathways associated with the up-regulated genes include terms associated with cellular stress and apoptotic signaling pathways. Motif analysis of the down-regulated genes shows enrichment of promoters containing binding sites for the E2F family of transcription factor in keeping with the gene ontology analysis showing regulation of pathways involved in cell cycle control and progression. Upregulated genes show enrichment for binding sites of ATF3, ATF4 and DDIT3 as observed also in the microarray experiment.

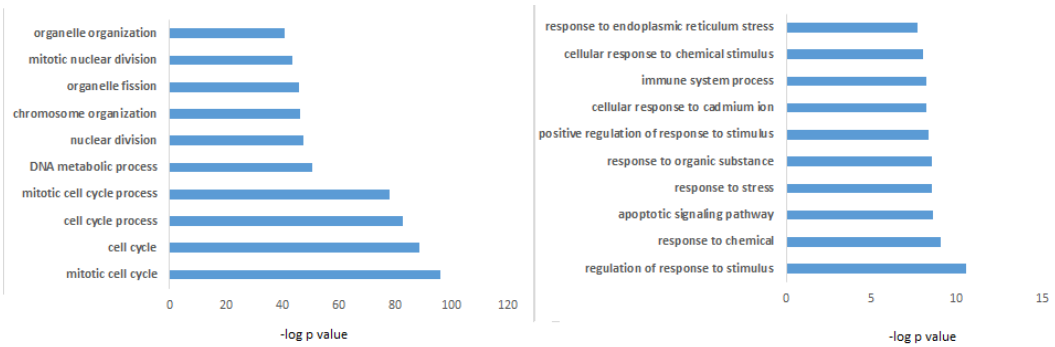


Figure 54 Gene Ontology analysis of regulated genes

Top 10 gene ontology pathways associated with the down-regulated (left) and up-regulated (right) genes.

Symbol	Description	log2FoldChange	padj
MT1H	metallothionein 1H [Source:HGNC Symbol;Acc:HGNC:7400]	11.20392311	1.8848E-203
MT1G	metallothionein 1G [Source:HGNC Symbol;Acc:HGNC:7399]	10.54488032	7.5064E-257
MT1E	metallothionein 1E [Source:HGNC Symbol;Acc:HGNC:7397]	9.934526211	6.852E-102
MT1L	metallothionein 1L (gene/pseudogene) [Source:HGNC Symbol;Acc:HGNC:7404]	7.152480381	3.30596E-37
MT2A	metallothionein 2A [Source:HGNC Symbol;Acc:HGNC:7406]	7.008617455	7.89726E-29
MT1M	metallothionein 1M [Source:HGNC Symbol;Acc:HGNC:14296]	6.831609407	1.05013E-24
MT1X	metallothionein 1X [Source:HGNC Symbol;Acc:HGNC:7405]	6.7134322	6.852E-102
MT1F	metallothionein 1F [Source:HGNC Symbol;Acc:HGNC:7398]	6.678442056	1.17942E-26
INHBE	inhibin beta E subunit [Source:HGNC Symbol;Acc:HGNC:24029]	6.439087199	7.21374E-48
MT1JP	metallothionein 1J, pseudogene [Source:HGNC Symbol;Acc:HGNC:7402]	6.365604378	8.26561E-26
MT2P1	metallothionein 2 pseudogene 1 [Source:HGNC Symbol;Acc:HGNC:7407]	6.314462174	8.46528E-31
EGR1	early growth response 1 [Source:HGNC Symbol;Acc:HGNC:3238]	5.581233968	3.10325E-47
CHAC1	ChaC glutathione specific gamma-glutamylcyclotransferase 1 [Source:HGNC Symbol;Acc:HGNC:28680]	5.560729289	1.42931E-59
MT1HL1	metallothionein 1H-like 1 [Source:HGNC Symbol;Acc:HGNC:31864]	5.433408312	8.82093E-17
HSPA7	heat shock protein family A (Hsp70) member 7 [Source:HGNC Symbol;Acc:HGNC:5240]	5.432105922	8.79684E-24
CCL3L3	C-C motif chemokine ligand 3 like 3 [Source:HGNC Symbol;Acc:HGNC:30554]	5.382100243	5.01602E-68
MT1DP	metallothionein 1D, pseudogene [Source:HGNC Symbol;Acc:HGNC:7396]	4.994374671	2.17643E-13
MAP1B	microtubule associated protein 1B [Source:HGNC Symbol;Acc:HGNC:6836]	4.959931798	2.76181E-25
BEX2	brain expressed X-linked 2 [Source:HGNC Symbol;Acc:HGNC:30933]	4.938481165	4.2074E-15
CCL3	C-C motif chemokine ligand 3 [Source:HGNC Symbol;Acc:HGNC:10627]	4.854560181	9.04592E-67
DPPA2P4	developmental pluripotency associated 2 pseudogene 4 [Source:HGNC Symbol;Acc:HGNC:44629]	4.791287128	8.13412E-12
MT1A	metallothionein 1A [Source:HGNC Symbol;Acc:HGNC:7393]	4.74196449	1.0019E-10
HMOX1	heme oxygenase 1 [Source:HGNC Symbol;Acc:HGNC:5013]	4.703091855	3.04506E-70
DDIT3	DNA damage inducible transcript 3 [Source:HGNC Symbol;Acc:HGNC:2726]	4.656455428	6.44257E-61
ASS1	argininosuccinate synthase 1 [Source:HGNC Symbol;Acc:HGNC:758]	4.421666947	6.86137E-65
MT1XP1	metallothionein 1X pseudogene 1 [Source:HGNC Symbol;Acc:HGNC:7442]	4.421414874	4.76714E-13
GDF15	growth differentiation factor 15 [Source:HGNC Symbol;Acc:HGNC:30142]	4.392103303	9.43946E-10
HSPA6	heat shock protein family A (Hsp70) member 6 [Source:HGNC Symbol;Acc:HGNC:5239]	4.19997701	2.00571E-08
CDKN1C	cyclin dependent kinase inhibitor 1C [Source:HGNC Symbol;Acc:HGNC:1786]	4.161687956	3.94987E-37
SPRR2D	small proline rich protein 2D [Source:HGNC Symbol;Acc:HGNC:11264]	4.049265773	1.3619E-08
UNC5B	unc-5 netrin receptor B [Source:HGNC Symbol;Acc:HGNC:12568]	4.046807955	8.57785E-09
OSGIN1	oxidative stress induced growth inhibitor 1 [Source:HGNC Symbol;Acc:HGNC:30093]	3.939118286	1.92896E-08
SMIM14	small integral membrane protein 14 [Source:HGNC Symbol;Acc:HGNC:27321]	3.93788764	7.38119E-18
LINC01229	long intergenic non-protein coding RNA 1229 [Source:HGNC Symbol;Acc:HGNC:49682]	3.912949546	2.97835E-10
SERINC2	serine incorporator 2 [Source:HGNC Symbol;Acc:HGNC:23231]	3.898850149	3.84306E-11
FTH1P16	ferritin heavy chain 1 pseudogene 16 [Source:HGNC Symbol;Acc:HGNC:3986]	3.896015807	1.7195E-13
ISG20	interferon stimulated exonuclease gene 20 [Source:HGNC Symbol;Acc:HGNC:6130]	3.763661641	9.24447E-17
TMTC1	transmembrane and tetratricopeptide repeat containing 1 [Source:HGNC Symbol;Acc:HGNC:24099]	3.731416784	8.3524E-09
SLC30A1	solute carrier family 30 member 1 [Source:HGNC Symbol;Acc:HGNC:11012]	3.704745716	1.1291E-39
FTH1P2	ferritin heavy chain 1 pseudogene 2 [Source:HGNC Symbol;Acc:HGNC:3989]	3.671345209	3.83582E-23
PPP1R15A	protein phosphatase 1 regulatory subunit 15A [Source:HGNC Symbol;Acc:HGNC:14375]	3.652504119	2.5628E-51
FTH1P5	ferritin heavy chain 1 pseudogene 5 [Source:HGNC Symbol;Acc:HGNC:3996]	3.649798418	2.2025E-17
ATF3	activating transcription factor 3 [Source:HGNC Symbol;Acc:HGNC:785]	3.62411431	6.95221E-23
DDIT4	DNA damage inducible transcript 4 [Source:HGNC Symbol;Acc:HGNC:24944]	3.568645516	5.62284E-41
TPSAB1	tryptase alpha/beta 1 [Source:HGNC Symbol;Acc:HGNC:12019]	3.556440231	5.83807E-07
FTH1P20	ferritin heavy chain 1 pseudogene 20 [Source:HGNC Symbol;Acc:HGNC:37639]	3.526110164	6.74368E-15
SLFN5	schlafen family member 5 [Source:HGNC Symbol;Acc:HGNC:28286]	3.503202647	3.08602E-09

Table 7 50 top upregulated genes

Symbol	Description	log2FoldChange	padj
MT-ND4L	mitochondrially encoded NADH:ubiquinone oxidoreductase core subunit 4L [Source:HGNC Symbo	-3.599749582	5.54E-29
FAM72C	family with sequence similarity 72 member C [Source:HGNC Symbol;Acc:HGNC:30602]	-3.528523502	7.93E-19
CCNB1	cyclin B1 [Source:HGNC Symbol;Acc:HGNC:1579]	-3.4400717	1.6E-21
KIF18B	kinesin family member 18B [Source:HGNC Symbol;Acc:HGNC:27102]	-3.305069454	2.62E-26
MKI67	marker of proliferation Ki-67 [Source:HGNC Symbol;Acc:HGNC:7107]	-3.269396919	1.04E-32
FAM72D	family with sequence similarity 72 member D [Source:HGNC Symbol;Acc:HGNC:33593]	-3.245957261	5.8E-17
HMGN1P36	high mobility group nucleosome binding domain 1 pseudogene 36 [Source:HGNC Symbol;Acc:HG	-3.192380318	1.94E-07
KIF23	kinesin family member 23 [Source:HGNC Symbol;Acc:HGNC:6392]	-3.181454643	9.56E-26
SORD2P	sorbitol dehydrogenase 2, pseudogene [Source:HGNC Symbol;Acc:HGNC:49919]	-3.10792569	4.55E-09
CDC20	cell division cycle 20 [Source:HGNC Symbol;Acc:HGNC:1723]	-3.103382987	1.92E-24
DEPDC1	DEP domain containing 1 [Source:HGNC Symbol;Acc:HGNC:22949]	-3.076225634	1.94E-15
CDC25C	cell division cycle 25C [Source:HGNC Symbol;Acc:HGNC:1727]	-3.075907879	6.69E-07
GPR68	G protein-coupled receptor 68 [Source:HGNC Symbol;Acc:HGNC:4519]	-3.075204798	1.49E-06
TICRR	TOPBP1 interacting checkpoint and replication regulator [Source:HGNC Symbol;Acc:HGNC:28704	-3.02371966	8.84E-16
CDCA2	cell division cycle associated 2 [Source:HGNC Symbol;Acc:HGNC:14623]	-3.001441546	2.57E-14
PLK1	polo like kinase 1 [Source:HGNC Symbol;Acc:HGNC:9077]	-2.993993885	8.11E-19
LRFN1	leucine rich repeat and fibronectin type III domain containing 1 [Source:HGNC Symbol;Acc:HGNC:	-2.951976787	1.35E-13
KIF14	kinesin family member 14 [Source:HGNC Symbol;Acc:HGNC:19181]	-2.941906917	5.46E-10
HMMR	hyaluronan mediated motility receptor [Source:HGNC Symbol;Acc:HGNC:5012]	-2.930631434	1.74E-12
FAM72A	family with sequence similarity 72 member A [Source:HGNC Symbol;Acc:HGNC:24044]	-2.897365888	4.47E-14
MT-ND5	mitochondrially encoded NADH:ubiquinone oxidoreductase core subunit 5 [Source:HGNC Symbo	-2.88631692	2.59E-06
AURKA	aurora kinase A [Source:HGNC Symbol;Acc:HGNC:11393]	-2.870776665	9.56E-21
ANLN	anillin actin binding protein [Source:HGNC Symbol;Acc:HGNC:14082]	-2.834013701	3.31E-15
MT-TS2	mitochondrially encoded tRNA serine 2 (AGU/C) [Source:HGNC Symbol;Acc:HGNC:7498]	-2.83070476	0.00048
MT-TG	mitochondrially encoded tRNA glycine [Source:HGNC Symbol;Acc:HGNC:7486]	-2.823331195	0.000337
AMPD1	adenosine monophosphate deaminase 1 [Source:HGNC Symbol;Acc:HGNC:468]	-2.805270549	4.71E-08
CENPV	centromere protein V [Source:HGNC Symbol;Acc:HGNC:29920]	-2.798115093	1.62E-05
SPAG5	sperm associated antigen 5 [Source:HGNC Symbol;Acc:HGNC:13452]	-2.794123428	1.92E-18
HMGN2P15	high mobility group nucleosomal binding domain 2 pseudogene 15 [Source:HGNC Symbol;Acc:HG	-2.749727913	7.05E-05
BUB1B	BUB1 mitotic checkpoint serine/threonine kinase B [Source:HGNC Symbol;Acc:HGNC:1149]	-2.749720812	1.06E-20
MT-TY	mitochondrially encoded tRNA tyrosine [Source:HGNC Symbol;Acc:HGNC:7502]	-2.743223468	9.03E-07
KIF15	kinesin family member 15 [Source:HGNC Symbol;Acc:HGNC:17273]	-2.725052185	2.77E-15
DEPDC1B	DEP domain containing 1B [Source:HGNC Symbol;Acc:HGNC:24902]	-2.697985078	2.27E-11
FOXM1	forkhead box M1 [Source:HGNC Symbol;Acc:HGNC:3818]	-2.694678988	1.75E-12
TPX2	TPX2, microtubule nucleation factor [Source:HGNC Symbol;Acc:HGNC:1249]	-2.680989185	4.38E-26
POLQ	polymerase (DNA) theta [Source:HGNC Symbol;Acc:HGNC:9186]	-2.661508005	2.09E-13
PGAP1	post-GPI attachment to proteins 1 [Source:HGNC Symbol;Acc:HGNC:25712]	-2.652788409	0.000127
CCNB2	cyclin B2 [Source:HGNC Symbol;Acc:HGNC:1580]	-2.648159988	1.18E-18
TTK	TTK protein kinase [Source:HGNC Symbol;Acc:HGNC:12401]	-2.632900464	1.17E-14
MT-ND4	mitochondrially encoded NADH:ubiquinone oxidoreductase core subunit 4 [Source:HGNC Symbo	-2.632220292	0.000175
CCNA2	cyclin A2 [Source:HGNC Symbol;Acc:HGNC:1578]	-2.612490618	1.2E-19
KIF20A	kinesin family member 20A [Source:HGNC Symbol;Acc:HGNC:9787]	-2.600616579	2.12E-10
PRC1	protein regulator of cytokinesis 1 [Source:HGNC Symbol;Acc:HGNC:9341]	-2.599799747	9.96E-19
CGN	cingulin [Source:HGNC Symbol;Acc:HGNC:17429]	-2.582332487	4.43E-05
NCAPG	non-SMC condensin I complex subunit G [Source:HGNC Symbol;Acc:HGNC:24304]	-2.571352282	2.2E-17
PRR11	proline rich 11 [Source:HGNC Symbol;Acc:HGNC:25619]	-2.567636602	9.74E-11
HJURP	Holliday junction recognition protein [Source:HGNC Symbol;Acc:HGNC:25444]	-2.563719775	2.3E-10
CKS1BP3	CDC28 protein kinase regulatory subunit 1B pseudogene 3 [Source:HGNC Symbol;Acc:HGNC:242	-2.55197259	7.18E-05
ITPRIPL1	inositol 1,4,5-trisphosphate receptor interacting protein-like 1 [Source:HGNC Symbol;Acc:HGNC:	-2.550803229	1.76E-10

Table 8 50 top downregulated genes

5.4 DISCUSSION

This chapter has documented the results of next generation sequencing techniques including ChIPseq and RNAseq to further dissect the effect of GSK-J4 on multiple myeloma cells. A key tool needed for this analysis has been the use of a quantitative approach to sequencing normalization. This was accomplished by the addition of exogenous chromatin or RNA from the SF9 insect cell line requiring the assembly of a draft genome to use as a reference. The process of assembling a high quality genome in which there is full resolution of repeat regions and a continuous sequence for the length of a chromosome is complicated and was beyond the scope of this thesis. Alternative sequencing methodology such as the use of mate-paired reads or extra-long reads using in conjunction with short paired-end reads can be helpful in improving the quality of the assembly (Wetzel, Kingsford, and Pop 2011; van Heesch et al. 2013). In addition, the use of transcriptomic data can also aid in the process of scaffolding contigs together into the correct order (Xue et al. 2013). An indication of the complexity of the task is that the most recent release of the human genome, hg38, contains in addition to the canonical chromosome sequences over 400 alternative and unknown sequences that cannot be accurately located to within a chromosome. Therefore, whilst it may seem that 50,000 contigs for a genome only 320MB long is suboptimal, the reference sequenced produced for the SF9 was sufficient to perform the required purpose of distinguishing exogenous DNA from that of the sample of interest.

The ChIPseq results obtained for H3K27me3 is in keeping with the known-mechanism of action of GSK-J4 in inhibiting the demethylases KDM6A and KDM6B leading to a global accumulation of H2K27me3. The results obtained for H3K4me3 were less expected as it had initially been anticipated that the inhibitory action of GSK-J4 on KDM5B would lead to

an accumulation of H3K4me3 in a similar manner to that seen with H3K27me3. The suspicion that an overall increase in H3K4me3 marks might be seen was heightened by early observations that the predominant transcriptional effect of GSK-J4 was to lead to a rapid increase in transcription of a number of genes. A possible explanation for the observed result is the relative potency that GSK-J4 has for the KDM6 family and KDM5B, with the latter being approximately 5-10- fold lower. Therefore, whilst in vitro GSK-J1, the intracellular active GSK-J4 metabolite is seen to have inhibitory activity towards KDM5B, the in vivo activity may predominantly be through the activity against KDM6A and 6B.

The histone methylation profiles around the metallothionein cluster of genes shows the presence of a broad region of H2K27me3 over the whole cluster in both DMSO-treated cells and significantly elevated after 24h of treatment with GSK-J4. In addition, both conditions show the presence of the H3K4me3 mark at the transcription start sites of the metallothionein genes, in the case of MT1G and MT1H at a higher coverage than in the DMSO control but in the case of MT1X the H3K4me3 peak is reduced in absolute terms compared to the control condition. The observation of similar marks present in both conditions is difficult to correlate with the current paradigm of H3Kme3 and H3K27me3 as indicators of transcription, when the RNAseq data, and earlier microarray data, show almost no transcription of metallothionein RNA in the control conditions yet very highly up-regulated in cells treated with GSK-J4. One possible explanation for this observation is that the chromatin state has not been examined at the relevant time. In chapter 3 it was demonstrated that the induction of transcription of metallothioneins occurs rapidly after treatment with GSK-J4, peaks after approximately 12 hours and then starts to decline. It is therefore possible that a change in chromatin state involving a reduction in the level of H3K27me3 occurs rapidly in response

to GSK-J4 treatment and by 24 hours has returned to its baseline state. The half-life of the mRNA transcripts for metallothioneins is unknown so it is possible that the measured mRNA levels at 24h were transcribed earlier and that there is little active transcription at this time point. These points can be addressed experimentally by performing analysis of newly synthesized RNA at the 24h time point and by profiling the chromatin landscape at earlier time points.

A second possible explanation for the apparent discrepancy between the ChIP profiles of the metallothionein genes and the transcriptomic data is the existence of distinct populations of cells responding heterogeneously to GSK-J4. The techniques used to investigate the ChIP profiles and transcriptomic response to GSK-J4 all lead to a result that is the population average of the effect being observed. It is possible that in the cell population there is a subset of cells that are actively transcribing metallothionein genes and this is associated with increased H3K4me3 and decreased H3K27me3. A second population not transcribing metallothioneins may have high H3K27me3 and low H3K4me3. The averaged result that is measured therefore results in a superposition of these two states leading to both high H3K4me3, high H3K27me3 and evidence of active transcription. With current technology it is difficult to assess the histone profiles at single cell resolution but the use of emerging single cell sequencing techniques would be able to detect if there are populations of cells differing in their expression of metallothioneins that could be used to further probe this idea.

A further method to examine the possibility of a heterogeneous population of cells would be by performing double-ChIP experiments in which H3K27me3 and H3K4me3 are initially pulled down followed by a second immunoprecipitation using an antibody against DNA polymerase II. If there was no evidence of DNA polymerase II following an initial

H3K27me3 ChIP this would be suggestive of there being a population of cells in which the metallothionein cluster is marked with H3K27me3 and that transcription is not occurring. In contrast, it would be expected that following H3K4me3 pull down that it would also be possible to immunoprecipitate DNA polymerase II indicating that active transcription is underway in these cells.

The analysis of the RNAseq data was largely in keeping with what was expected from the previous microarray experiments and cell based assays as presented in chapter 3. There is an up-regulation of the metallothionein cluster and induction of a number of ATF4 target genes. One gene that is highly up-regulated in the RNAseq samples but was not detected in the microarray experiment is PPP1R15A which is an ATF-4 target gene and involved in the regulation of EIF2alpha phosphorylation through its interaction with protein phosphatase 1 (Brush, Weiser, and Shenolikar 2003). Increased expression of PPP1R15A can lead to a decrease in the overall level of phosphorylation of EIF2alpha resulting in a release of the translational block and then leading to apoptosis. Up-regulation is also seen for C-C motif chemokine ligand 3 (CCL3, also known as MIP-1A), a protein associated with myeloma-induced bone disease through activation of osteoclastogenesis (Oba et al. 2005) and inhibiting the function of osteoblasts (Vallet et al. 2011).

Down-regulated transcripts included a large number of genes involved in cell cycle progression. It is likely that the decrease in expression of these genes is a secondary consequence of the ATF4-driven response to the cellular stress that GSK-J4 induces and not the primary cause for the decrease in proliferation observed.

A hypothesis of the mechanism of action of GSK-J4 will be presented in chapter 7 following presentation of data related to the selective inhibition of KDM5B in chapter 6.

6 SPECIFIC INHIBITION OF KDM5B IN MULTIPLE MYELOMA CELL LINES

6.1 OVERVIEW

In this chapter the effect of specific inhibition of KDM5B will be described. Using small molecule inhibitors designed to specifically target the KDM5 family it will be shown that only one multiple myeloma cell line, MM1S, undergoes cell-cycle arrest after a delay of several days. This is in contrast to the effect of GSK-J4 in which apoptosis is induced within 24 hours in all myeloma cell lines treated. The cell cycle arrest is accompanied by a global increase in H3K4me3.

6.2 INTRODUCTION

The data presented so far have focused on the activity of GSK-J4, a compound that has affinity for both KDM6A/B and approximately 5-30 -fold lower affinity for KDM5 members (Heinemann et al. 2014; Johansson et al. 2016). In the previous chapter, it has been shown that the predominant effect seen in cells treated with GSK-J4 is an increase in H3K27me3 marks associated with the inhibitory action of GSK-J4 on the KDM6 family. Only a small number of genes associated with the ATF4 response demonstrated an increase in H3K4me3 marks around their transcription start site.

In addition to the work presented involving the use of GSK-J4, interest in the specific role of KDM5B in myeloma had been generated by clinical data obtained by collaborators at the Institute of Cancer Research, London. In three large multiple myeloma trials, a univariate

analysis revealed that the expression level of KDM5B was measured on enrollment and those with the highest quartile of expression were found to have significantly worse overall survival compared to those in the lower three quartiles. In contrast, there was no association found with either KDM6A or KDM6B. A multivariate analysis on the data from the Myeloma 1X trial indicates that the highest quartile of KDM5B expression at diagnosis remains associated with a statistically worse outcome compared to lower KDM5B expression (p=0.039).

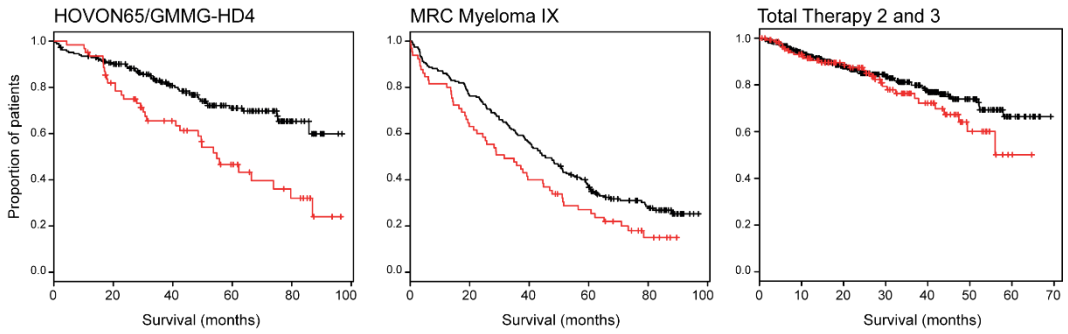
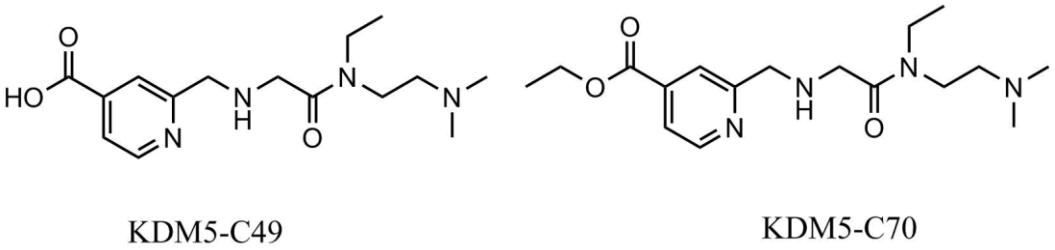


Figure 55 Increased expression of KDM5B is associated with lower overall survival in multiple myeloma

Data from Affymetrix gene expression analysis with linked survival was available from 3 large datasets of myeloma patients at diagnosis (Hovon65/GMMG-HD4 trial (n=246, GSE19784), MRC Myeloma IX trial (n=259), Total Therapy 2 and 3 trials (n=559, GSE2658)). Results for the probeset 201548_s_at (KDM5B) are shown as Kaplan-Meier survival curves for patients comparing those with the highest quartile of expression (red) of KDM5B to all others (black). Data kindly provided by Doctors F Davies, G Morgan, C Pawlyn (Institute of Cancer Research, London).

In order to better understand the role of KDM5B in multiple myeloma studies have been performed using a range of small molecule inhibitors specifically designed to target KDM5 whilst having only limited activity against other lysine demethylases. The compound KDM5-C49 was first described in the patent literature (PCT WO2014053491A1) and further

characterization has been provided in a paper including work from this thesis (Johansson et al. 2016). In a manner similar to GSK-J1, KDM5-C49 contains a polar carboxylic acid group rendering it poorly cell-permeable and therefore an ethyl-ester derivative KDM5-C70 is used for cell-based experiments.

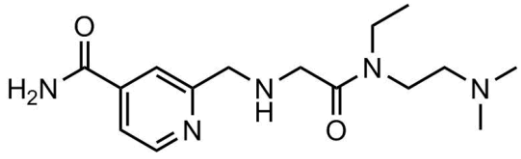


KDM5-C49 KDM5-C70

Figure 56: Structures of KDM5-C49 and KDM5-C70

Using the AlphaScreen assay (Eglen et al. 2008), KDM5-C49 has an IC_{50} of 4nM against KDM5B and approximately 10nM against other members of the KDM5 family (Johansson et al, 2016). The IC_{50} against the next closest KDM was 200nM against KDM4C and the IC50 for KDM6B was 1.4µM.

Also investigated was an experimental compound KDOAM25. This compound is similar to KDM5-C49 but with a modification to the carboxylic acid group forming an amide.



KDOAM25

Figure 57 Structure of KDOAM25

KDOAM25 is less potent against KDM5B compared to KDM5-C49 with an IC_{50} of 19nM however it is more selective against other members of the histone demethylase family with an IC50 against KDM4C of 4.8µM.

A summary of the IC_{50} of the compounds discussed in this chapter is presented in Table 9.

	KDM-C49	KDOAM25	GSK-J1
KDM5A	0.007	0.079	3.9
KDM5B	0.004	0.019	0.55
KDM5C	0.013	0.063	1.5
KDM5D	0.015	0.063	1.5
KDM4C	0.21	4.8	64.9
KDM6B	1.4	100	0.16

Table 9 IC_{50} values of compounds against KDM family members

IC_{50} values (µM) for the compounds used in this chapter against members of the KDM family. Values for KDM-C59 and GSK-J1 are taken from (Johansson et al. 2016) and for KDOAM25 from Dr Anthony Tumber, Structural Genomics Consortium.

6.3 RESULTS

6.3.1 Inhibition of KDM5B inhibits myeloma cell line MM1S proliferation

Treatment of the multiple myeloma cell line MM1S with either KDM5-C70 or KDOAM25 led to a dose-dependent decrease in viability. The effect of the decrease of viability was not evident after 3 days of treatment but became apparent after 5 days and was more pronounced at 7 days (Figure 58). Calculation of EC50 demonstrates values of 200nM for KDM5-C70 and 30μM for KDOAM25.

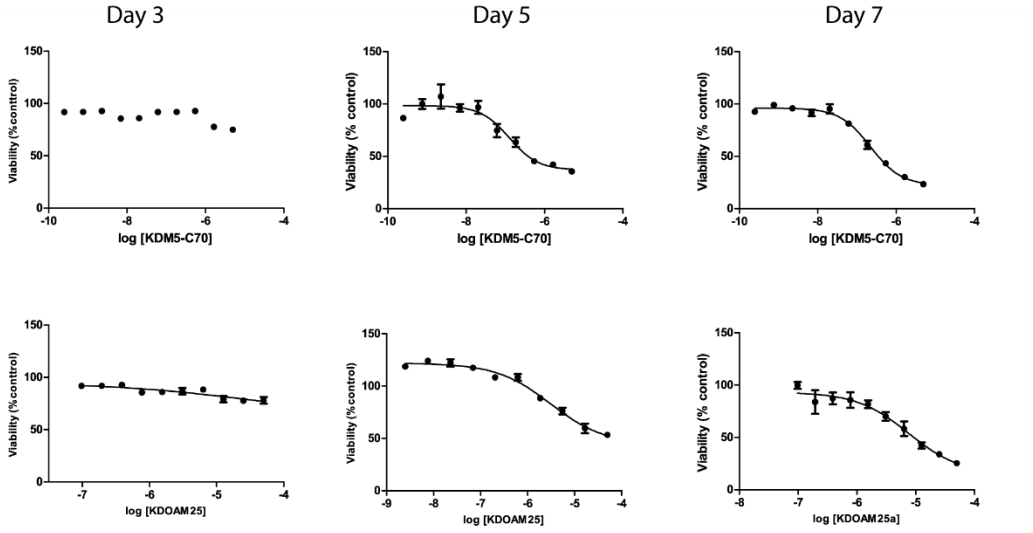


Figure 58: Dose-response curves of KDOAM25 and KDM5-C70 in MM1S cells

MM1S cells were treated for either 3,5 or 7 days with either KDM5-C70 or KDOAM25 and viability was measured by PrestoBlue assay. Data plotted represent the mean±SEM of 3 biological replicates.

6.3.2 Inhibition of KDM5B does not inhibit proliferation in other myeloma cell lines.

In a range of other myeloma cell lines including JJN3, KMS11, U266 and JIM3 there is no decrease in viability upon treatment with either KDM5-C70 or KDOAM25 for 7 days (Figure *59*).

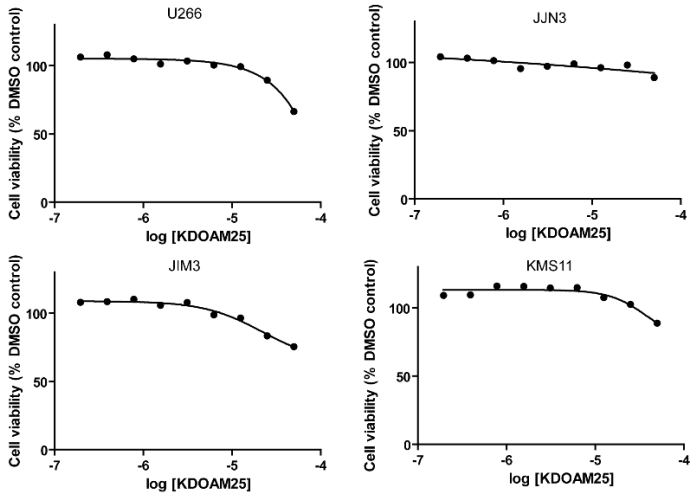


Figure 59: Dose response curves for KDOAM25 in other myeloma cell lines.

Myeloma cell lines were treated with KDOAM25 for 7 days and viability was measured by PrestoBlue assay. Data plotted represent the mean±SEM of 3 biological replicates.

6.3.3 Inhibition of KDM5B leads to cell cycle arrest and does not induce apoptosis in MM1S multiple myeloma cells

Treatment of MM1S cells with 50µM of KDOAM25 increased the proportion of cells in G1 from 62% to 78% whilst decreasing the proportion of cells in G2 from 22% to 11%. There was no increase in the sub-G1 population nor induction of annexin V as determined by flow cytometry indicating no induction of apoptosis.

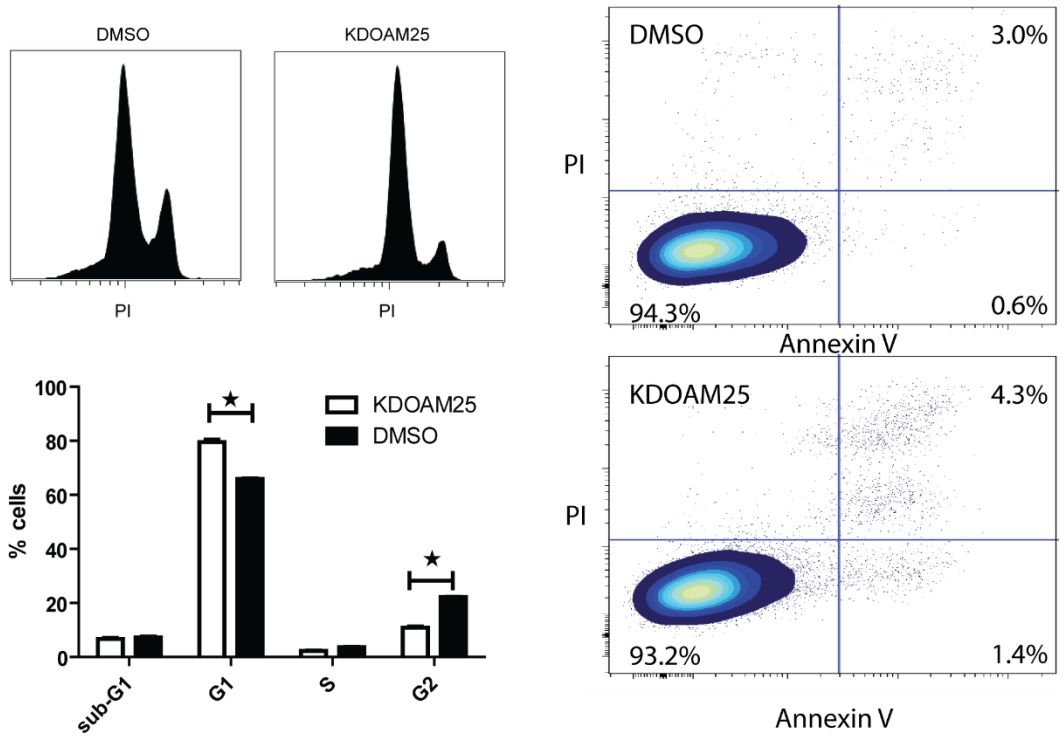


Figure 60 Inhibition of KDM5B causes cell cycle arrest in MM1S cells

(Left) KDOAM25 alters the cell cycle profile of MM1S cells as measured by propidium iodide staining using flow cytometry. Cells were treated with 50μM for 7 days. Data in the bar chart represent the mean±SEM of 4 biological replicates. Significance was calculated using the Mann-Whitney U test. (Right). KDOAM25 does not increase the percentage of MM1S cells positive for annexin V after 7 days. Data representative of 3 biological replicates.

6.3.4 Inhibition of KDM5B causes a global increase in H3K4me3 in MM1S cells

Treatment of MM1S cells with 50μM KDOAM25 for 7 days causes a global increase in H3K4me3 that is evident only when using a quantitative ChIPseq approach as described in the previous chapter and not by the conventional fragments per million normalization approach.

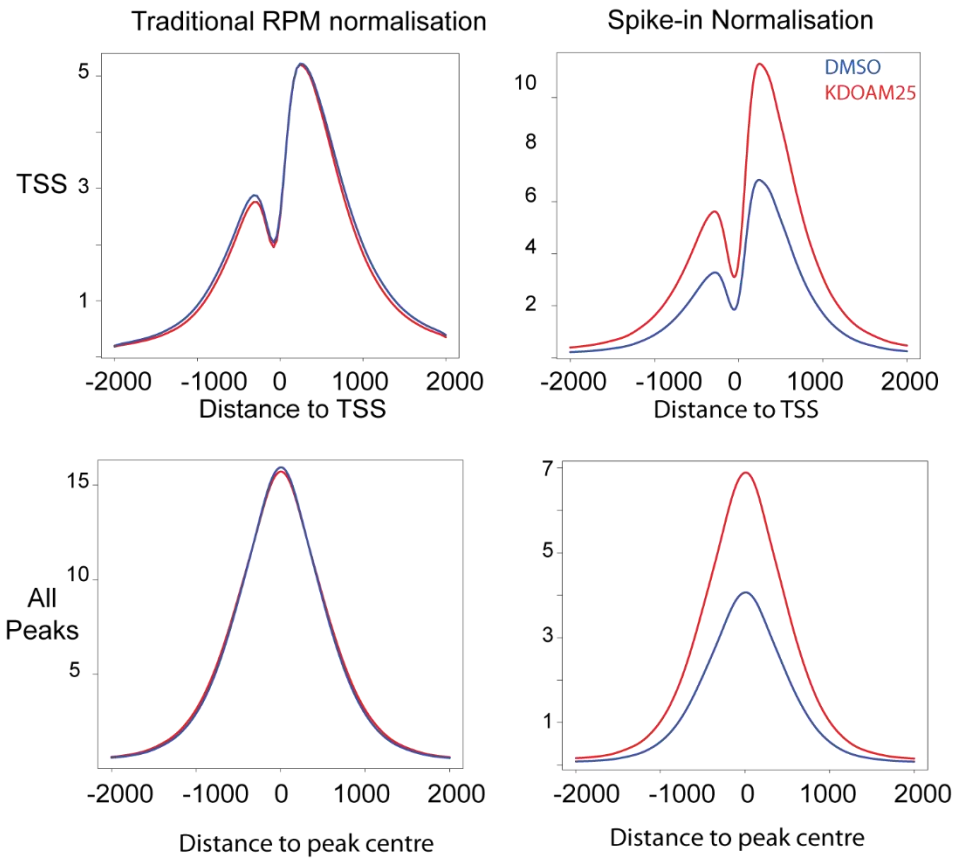


Figure 61 KDOAM25 increases H3K4me3 in MM1S myeloma cells

Data were normalized using either traditional read per million normalization (left) or using spiked-in SF9 chromatin (right). Coverage was determined at either Transcription start sites (TSS) (top) or across all identified peaks (bottom). Data represent the mean coverage of three biological replicates.

The increase in coverage at transcription start sites was seen across many classes of genes including those involved in fundamental cellular function such as beta actin, genes associated with proliferation such as cyclin D and tumour suppressor genes such as CDKN1A (Figure 62)

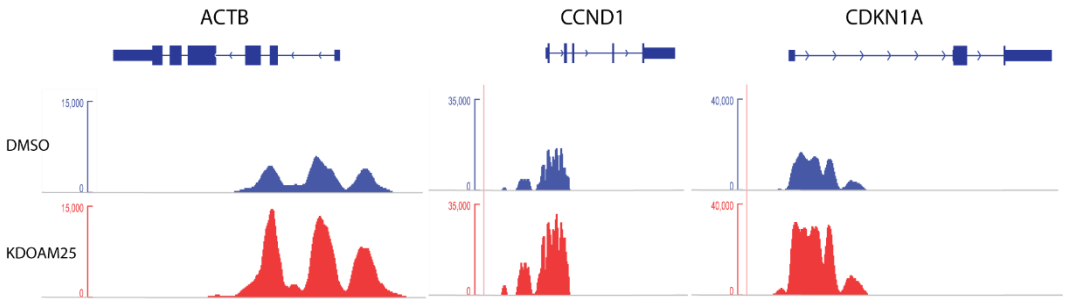


Figure 62 Increased H3K4me3 at transcription start sites in KDOAM25 treated MM1A.

Shown are the profiles for beta-actin, cyclin D1 and CDKN1A all indicating an increase in H3K4me3 at the transcription start site in MM1S cells treated with 50µM KDOAM25.

6.4 DISCUSSION

In this chapter I have demonstrated that the action of a small molecule inhibitor of the KDM5 family shows significant phenotypic difference to the response seen with GSK-J4, an inhibitor that targets both KDM5 and KDM6 enzymes. In contrast to GSK-J4 which rapidly induces apoptosis in all myeloma cell lines tested, the effect of inhibition of KDM5 seems limited to a specific cell line, MM1S, and results in a cell cycle arrest evident only after a delay of 5 days.

The reason why MM1S is sensitive to treatment with inhibitors of KDM5 whereas other myeloma cell lines tested are not, remains unclear. MM1S was derived from a patient with an IgA lambda myeloma whose disease was in the leukaemic phase (Greenstein et al. 2003). A study investigating mutations found in patients with myeloma and myeloma cell lines identified a point mutation in histone methyltransferase 2A (KMT2A), responsible for the trimethylation of H3K4, in the MM1S cell line that is predicted to lead to a loss of function (Leich et al. 2013). An analysis of the COSMIC database of mutations in cancer (Futreal et al. 2004) revealed that in multiple myeloma only one other sample out of fifty, including all the additional cell lines studied, also carried a mutation in KMT2A. This observation invites the speculation that the efficacy of the KDM5 inhibitors in MM1S is related to this mutation.

The different potencies of KDM5-C70 and KDOAM25 in inhibiting MM1S proliferation are difficult to explain. The difference in IC_{50} as measured by an AlphaScreen is low (5nM for KDM5-C70 versus 20nM for KDOAM25) whereas the difference in EC_{50} as measured by cellular proliferation is over 100-fold (200nM compared with 30µM). A possible explanation for this finding is that KDOAM25 does not enter cells as well as predicted or that it suffers from stability issues either in cell culture media or within the cell.

In order to better understand the biological effects of exposure to KDM5 inhibitors in MM1S, an investigation of the changes in H3K4me3 occupancy in cell lines that do not demonstrate cell cycle arrest would be of interest. Correlation with transcriptomic analysis such as RNAseq would also potentially provide insights into the mechanism leading to cell cycle arrest within MM1S cells. An RNAseq experiment was performed using KDOAM25 however it was later discovered that the batch of KDOAM25 that had been used was contaminated with a range of intermediate products of synthesis. When this batch was subsequently tested for its effect on cellular proliferation it was found to be considerably more potent than pure KDOAM25 and therefore it could not be certain exactly what treatment the cells had received so analysis of this data has not been further pursued.

The results of the ChIPseq with KDOAM25 (Figure 61) demonstrate the importance of using the quantitative ChIP methodology when investigating global changes in chromatin occupancy. Using traditional normalization methods the difference in occupancy is obscured yet becomes evident when the spike-in of exogenous chromatin is performed.

Taken together, the data in this chapter demonstrate that the specific inhibition of the KDM5 family of enzymes results in a significantly different phenotype to that observed with dual inhibitors of KDM5 and KDM6 enzymes, such as GSK-J4.

7 DISCUSSION AND FUTURE PERSPECTIVES

In this thesis I have demonstrated that GSK-J4, a small molecule inhibitor of KDM5B, KDM6A and KDM6B is able to inhibit proliferation of a range of cancers that affect bone include multiple myeloma, Ewing sarcoma and chordoma. A similar phenotypic effect is observed using locked nucleic acids to knock down KDM6A and KDM6B directly, resulting also in an indirectly knockdown of KDM5B. Inhibition of KDM5B alone, either by use of a small molecule inhibitor such as KDOAM25 or a locked nucleic acid is not sufficient to reproduce the phenotype.

The phenotypic response to GSK-J4 is characterized by a biphasic response: within two hours there is a rapid induction of a large number of metallothionein genes which is followed after approximately 6 hours by activation of the ATF4 pathway through the eIF2α kinase GCN2. Ectopic expression of a number of metallothioneines using the metallothionein ubergene construct was able on its own to activate the ATF4 pathway, an association that has not been previously documented in the literature. However, there remains uncertainty as to the exact mechanism by which the metallothioneins are induced and how their induction leads to the ATF4 response.

Possible explanations for the induction of metallothioneins has been discussed previously in chapter 3. The added information that was obtained by ChIPseq in chapter 5 confuses the situation as there appears to be an increase in the inhibitory H3K27me3 mark at the 24h time point across the metallothioneine locus despite a very large expression of a number of metallothioneins as determined by RNAseq. In addition, for some individual

metallohthionein genes such as MT1G and MT1H there is increased H3K4me3 at the TSS in GSK-J4 treated cells compared to untreated, whereas for MT1X the level of H3K4me3 is decreased (although in absolute terms still large). This results in the situation that in control cells MT1X has a lower level of H3K27me3, and high H3K4me3 but almost no transcription. This arrangement may be indicative of the metallothioneins as poised, or bivalent, genes that are not actively transcribed but can be rapidly activated in response to a stimulus such as, in the case of metallothioneins, heavy metal intoxication.

In order to clarify the epigenetic regulation of the metallothionein cluster it would be advantageous to further probe the area with other tools to determine the chromatin state. As discussed previously in chapter 5, earlier time points after treatment with GSK-J4 could reveal permissive changes in the H3K4me3 and H3K27me3. The Assay for Transposase Accessible Chromatin followed by sequencing (ATACseq) could be performed to determine if chromatin was open and accessible for binding of key components of transcriptional machinery. ChIPseq using key transcription factors for metallothionein expression such as MTF-1 could also be performed to help dissect its role in the expression of metallothioneins seen with GSK-J4. It would also be of interest to examine DNA methylation in promoter regions of the metallothionein genes and investigate the role of non-coding RNAs in metallothionein regulation. The MT1D pseudogene has been demonstrated to act as a long non-coding RNA and play a role in the pathogenesis of gastric cancer (W. Yu et al. 2014) and the micro RNAs have been demonstrated to alter expression of metallothionein 2A (An et al. 2013). Examination of documented enhancer and promoter regions around the metallothionein cluster (W Lee et al. 2016) could also reveal additional information about control of metallothionein expression.

A further question that remains unanswered is the mechanism by which overexpression of metallothioneins leads to induction of the ATF4 response. Data presented in chapter 3 implicates the kinase GCN2 as being responsible for the activation of ATF4 in cells treated with GSK-J4. GCN2 is activated by detecting uncharged tRNAs (Dong et al. 2000) and uncharged cysteinyl-tRNA has been demonstrated to activate this pathway (X. Yu and Long 2016). Normally uncharged tRNAs would be encountered at times of nutritional deficiency which are unlikely to be met in cell culture conditions due to the excess of amino acids present in cell culture media. A potential explanation arises from the unusual properties of metallothioneins in containing a large percentage of cysteine residues for each molecule and the extremely high level of transcription observed. In chapter 3, a time-course of MT1X expression demonstrated that levels peaked at 12h after exposure to GSK-J4 and were reduced by the 24h time point (Figure 33). Sequencing data presented in chapter 5 reveals that at the 24h time point, a large number of metallothionein genes are still highly up-regulated and that if one sums the individual expression levels measured as transcripts per million, almost 3% of the entire transcriptional output of polyadenylated RNAs is producing metallothioneins. To put this figure into context, at the 24h time point the expression of metallothioneins is 30 times higher than the expression of beta actin and 10 times higher than the expression of GAPDH. The untested expectation would be that this percentage would be even higher earlier in the response to GSK-J4 treatment.

This information regarding metallothionein expression suggests that when cells are exposed to GSK-J4, their requirement for incorporating cysteine residues into protein will be increased. This assumption is based on the observed expression of metallothioneins and the known cysteine composition in metallothioneins of 30% compared to only 1% in proteins on

average (Hormoz 2013). If the rate of overall mRNA production remains constant, the increase in the rate of use of cysteine at the 24h time point can be calculated as

$$Fold\ change\ in\ rate\ of\ cystein\ usage = \frac{rate\ in\ treated}{rate\ in\ control} = \frac{(0.97 * 0.01 + 0.03 * 0.3)}{1 * .01} = 1.87$$

Given the even larger expression of metallothioneins observed at earlier time points, it is likely that this figure will acutely be even higher.

A hypothesis to explain the activation of GCN2 is therefore that as the rate of production of metallothioneins increases, the rate of cysteine utilisation increases and as such the cysteinyl-tRNA synthetase (CARS), responsible for recharging used tRNA, is unable to keep up with the requirement, resulting in uncharged cysteinyl-tRNA and activation of GCN2. This hypothesis could be tested in a number of ways. Firstly, overexpression of CARS should be able to prevent induction of the ATF4 pathway by increasing the maximum rate of cysteinyl-tRNA recharging preventing the uncharged tRNAs from activating GCN2. Secondly, ectopic addition of pre-formed metallothionein not requiring the new incorporation of cysteine residues should not activate the ATF4 pathway.

The current work has largely focused on multiple myeloma with only brief examinations of other cancers affecting bone. Whilst the data available for Ewing sarcoma suggest that the same pathways and mechanism of action of GSK-J4 will be important, these observations remain to be tested. The data available for chordoma are in an even earlier stage of development and is being actively followed. No data to date has been obtained in osteosarcoma looking at the effect of GSK-J4 and this would be a natural extension to the current work.

The importance of GSK-J4 and inhibition of KDM5B, KDM6A and KDM6B also extends beyond the field of cancer biology. The original publication on GSK-J4 examined the ability of the compound to reduce pro-inflammatory changes in a macrophage population (Kruidenier et al. 2012). Current work within the group is examining the role of GSK-J4 in immune cell differentiation and results suggest that in this very different setting the mechanism of action still depends on induction of metallothioneins, an ATF4 response and metabolic changes. GSK-J4 has also been shown to affect chondrocyte differentiation from mesenchymal stem cells (Yapp et al. 2016). It is possible that in these diverse fields and applications, GSK-J4 is acting in a similar way by affecting chromatin remodelling in response to a stimulus due to the inhibition of KDM6B.

In view of the observations above, further study of the mechanism of action of GSK-J4 may deepen our understanding of chromatin biology and appears to be a rich area of future research in many disease fields.

8 REFERENCES

Agger, Karl, Paul A C Cloos, Lise Rudkjaer, Kristine Williams, Gitte Andersen, Jesper Christensen, and Kristian Helin. 2009. "The H3K27me3 Demethylase JMJD3 Contributes to the Activation of the INK4A-ARF Locus in Response to Oncogene- and Stress-Induced Senescence." *Genes & Development* 23 (10): 1171–76. doi:10.1101/gad.510809.

Aihara, Koki, Akitake Mukasa, Kengo Gotoh, Kuniaki Saito, Genta Nagae, Shingo Tsuji, Kenji Tatsuno, et al. 2014. "H3F3A K27M Mutations in Thalamic Gliomas from Young Adult Patients." *Neuro-Oncology* 16 (1): 140–46. doi:10.1093/neuonc/not144.

Akizu, Naiara, Conchi Estarás, Laura Guerrero, Elisa Martí, and Marian A Martínez-Balbás. 2010. "H3K27me3 Regulates BMP Activity in Developing Spinal Cord." *Development (Cambridge, England)* 137 (17): 2915–25. doi:10.1242/dev.049395.

Allfrey, V G, and A E Mirsky. 1964. "Structural Modifications of Histones and Their Possible Role in the Regulation of RNA Synthesis." *Science (New York, N.Y.)* 144 (3618): 559. doi:10.1126/science.144.3618.559.

Amaral, Ana Teresa, Cecilia Garofalo, Roberta Frapolli, Maria Cristina Manara, Caterina Mancarella, Sarah Uboldi, Silvana Di Giandomenico, et al. 2015. "Trabectedin Efficacy in Ewing Sarcoma Is Greatly Increased by Combination with Anti-IGF Signaling Agents." *Clinical Cancer Research : An Official Journal of the American Association for Cancer Research* 21 (6): 1373–82. doi:10.1158/1078-0432.CCR-14-1688.

Amary, M Fernanda, Fitim Berisha, Rafael Mozela, Rebecca Gibbons, Alice Guttridge, Paul O'Donnell, Daniel Baumhoer, Roberto Tirabosco, and Adrienne M Flanagan. 2016. "The H3F3 K36M Mutant Antibody Is a Sensitive and Specific Marker for the Diagnosis of Chondroblastoma." *Histopathology*, July. doi:10.1111/his.12945.

An, Juan, Yuanming Pan, Zhi Yan, Wenmei Li, Jiantao Cui, Jiao Yuan, Liqing Tian, Rui Xing, and Youyong Lu. 2013. "MiR-23a in Amplified 19p13.13 Loci Targets Metallothionein 2A and Promotes Growth in Gastric Cancer Cells." *Journal of Cellular Biochemistry* 114 (9): 2160–69. doi:10.1002/jcb.24565.

Anders, Simon. 2009. "Visualization of Genomic Data with the Hilbert Curve." *Bioinformatics (Oxford, England)* 25 (10). Oxford University Press: 1231–35. doi:10.1093/bioinformatics/btp152.

Anderton, J A, S Bose, M Vockerodt, K Vrzalikova, W Wei, M Kuo, K Helin, et al. 2011. "The H3K27me3 Demethylase, KDM6B, Is Induced by Epstein-Barr Virus and over-Expressed in Hodgkin's Lymphoma." *Oncogene* 30 (17). Macmillan Publishers Limited: 2037–43. doi:10.1038/onc.2010.579.

Andreou, D, S S Bielack, D Carrle, M Kevric, R Kotz, W Winkelmann, G Jundt, et al. 2011. "The Influence of Tumor- and Treatment-Related Factors on the Development of Local Recurrence in Osteosarcoma after Adequate Surgery. An Analysis of 1355 Patients Treated on Neoadjuvant Cooperative Osteosarcoma Study Group Protocols." *Annals of Oncology : Official Journal of the European Society for Medical Oncology / ESMO* 22 (5): 1228–35. doi:10.1093/annonc/mdq589.

Arrowsmith, Cheryl H, James E Audia, Christopher Austin, Jonathan Baell, Jonathan

Bennett, Julian Blagg, Chas Bountra, et al. 2015. “The Promise and Peril of Chemical Probes.” *Nature Chemical Biology* 11 (8): 536–41. doi:10.1038/nchembio.1867.

Atkins, C, Q Liu, E Minthorn, S Y Zhang, D J Figueroa, K Moss, T B Stanley, et al. 2013. “Characterization of a Novel PERK Kinase Inhibitor with Antitumor and Antiangiogenic Activity.” *Cancer Res* 73 (6): 1993–2002. doi:0008-5472.CAN-12-3109 [pii]10.1158/0008-5472.CAN-12-3109.

Attal, Michel, Jean-Luc Harousseau, Anne-Marie Stoppa, Jean-Jacques Sotto, Jean-Gabriel Fuzibet, Jean-François Rossi, Philippe Casassus, et al. 1996. “A Prospective, Randomized Trial of Autologous Bone Marrow Transplantation and Chemotherapy in Multiple Myeloma.” *New England Journal of Medicine* 335 (2). Massachusetts Medical Society : 91–97. doi:10.1056/NEJM199607113350204.

Azad, Nilofer, Cynthia A Zahnow, Charles M Rudin, and Stephen B Baylin. 2013. “The Future of Epigenetic Therapy in Solid Tumours--Lessons from the Past.” *Nat Rev Clin Oncol* 10 (5): 256–66. doi:10.1038/nrclinonc.2013.42.

Bader, Scott, Marion Walker, Brian Hendrich, A Bird, Colin Bird, Martin Hooper, and Andrew Wyllie. 1999. “Somatic Frameshift Mutations in the MBD4 Gene of Sporadic Colon Cancers with Mismatch Repair Deficiency.” *Oncogene* 18 (56). Nature Publishing Group: 8044–47. doi:10.1038/sj.onc.1203229.

Bankevich, Anton, Sergey Nurk, Dmitry Antipov, Alexey A Gurevich, Mikhail Dvorkin, Alexander S Kulikov, Valery M Lesin, et al. 2012. “SPAdes: A New Genome Assembly Algorithm and Its Applications to Single-Cell Sequencing.” *Journal of Computational Biology : A Journal of Computational Molecular Cell Biology* 19 (5):

455–77. doi:10.1089/cmb.2012.0021.

Barcia-Vieitez, Ramiro, and Juan Ignacio Ramos-Martínez. 2014. “The Regulation of the Oxidative Phase of the Pentose Phosphate Pathway: New Answers to Old Problems.” *IUBMB Life* 66 (11): 775–79. doi:10.1002/iub.1329.

Barnes, David J., Edward Hookway, Nick Athanasou, Takeshi Kashima, Udo Oppermann, Simon Hughes, Daniel Swan, et al. 2016. “A Germline Mutation of CDKN2A and a Novel RPLP1-C19MC Fusion Detected in a Rare Melanotic Neuroectodermal Tumor of Infancy: A Case Report.” *BMC Cancer* 16 (1). BioMed Central: 629. doi:10.1186/s12885-016-2669-3.

Barrett, Angela, Bente Madsen, John Copier, Pei Juan Lu, Lucienne Cooper, Angelo G Scibetta, Joy Burchell, and Joyce Taylor-Papadimitriou. 2002. “PLU-1 Nuclear Protein, Which Is Upregulated in Breast Cancer, Shows Restricted Expression in Normal Human Adult Tissues: A New Cancer/testis Antigen?” *International Journal of Cancer. Journal International Du Cancer* 101 (6): 581–88. doi:10.1002/ijc.10644.

Baylin, SB, and JG Herman. 2000. “DNA Hypermethylation in Tumorigenesis: Epigenetics Joins Genetics.” *Trends in Genetics*. http://www.sciencedirect.com/science/article/pii/S016895259901971X.

Behjati, Sam, Patrick S Tarpey, Nadège Presneau, Susanne Scheipl, Nischalan Pillay, Peter Van Loo, David C Wedge, et al. 2013. “Distinct H3F3A and H3F3B Driver Mutations Define Chondroblastoma and Giant Cell Tumor of Bone.” *Nature Genetics* 45 (12). Nature Publishing Group: 1479–82. doi:10.1038/ng.2814.

Berger, Shelley L., Tony Kouzarides, Ramin Shiekhattar, and Ali Shilatifard. 2009. “An

Operational Definition of Epigenetics" 23 (7). Cold Spring Harbor Laboratory Press: 781–83. doi:10.1101/gad.1787609.

Berletch, Joel B, Xinxian Deng, Di Kim Nguyen, and Christine M Disteche. 2013. "Female Bias in Rhox6 and 9 Regulation by the Histone Demethylase KDM6A." *PLoS Genetics* 9 (5): e1003489. doi:10.1371/journal.pgen.1003489.

Betancur, Juan G, and Yukihide Tomari. 2015. "Cryptic RNA-Binding by PRC2 Components EZH2 and SUZ12." *RNA Biology* 12 (9). Taylor & Francis: 959–65. doi:10.1080/15476286.2015.1069463.

Bianconi, Eva, Allison Piovesan, Federica Facchin, Alina Beraudi, Raffaella Casadei, Flavia Frabetti, Lorenza Vitale, et al. 2016. "An Estimation of the Number of Cells in the Human Body." *Annals of Human Biology* 40 (6): 463–71. Accessed June 25. doi:10.3109/03014460.2013.807878.

Bird, A. 2002. "DNA Methylation Patterns and Epigenetic Memory." *Genes & Development*. http://genesdev.cshlp.org/content/16/1/6.short.

Bird, A, A. Bird, A. P. Wolffe, M. Okano, F. Lyko, G.-L. Xu, T. Bestor, et al. 1999. "DNA Methylation de Novo." *Science (New York, N.Y.)* 286 (5448). American Association for the Advancement of Science: 2287–88. doi:10.1126/science.286.5448.2287.

Black, Joshua C., Capucine Van Rechem, and Johnathan R. Whetstine. 2012. "Histone Lysine Methylation Dynamics: Establishment, Regulation, and Biological Impact." *Molecular Cell* 48 (4): 491–507. doi:10.1016/j.molcel.2012.11.006.

Blair, Lauren P, Jian Cao, Mike Ran Zou, Joyce Sayegh, and Qin Yan. 2011. "Epigenetic

Regulation by Lysine Demethylase 5 (KDM5) Enzymes in Cancer." *Cancers* 3 (1): 1383–1404. doi:10.3390/cancers3011383.

Blatch, G L, and M Lässle. 1999. "The Tetratricopeptide Repeat: A Structural Motif Mediating Protein-Protein Interactions." *BioEssays : News and Reviews in Molecular, Cellular and Developmental Biology* 21 (11): 932–39. doi:10.1002/(SICI)1521-1878(199911)21:11<932::AID-BIES5>3.0.CO;2-N.

Blatnik, Matthew, Suzanne R Thorpe, and John W Baynes. 2008. "Succination of Proteins by Fumarate: Mechanism of Inactivation of Glyceraldehyde-3-Phosphate Dehydrogenase in Diabetes." *Annals of the New York Academy of Sciences* 1126 (April). NIH Public Access: 272–75. doi:10.1196/annals.1433.047.

Bracken, Adrian P, Daniela Kleine-Kohlbrecher, Nikolaj Dietrich, Diego Pasini, Gaetano Gargiulo, Chantal Beekman, Kim Theilgaard-Mönch, et al. 2007. "The Polycomb Group Proteins Bind throughout the INK4A-ARF Locus and Are Disassociated in Senescent Cells." *Genes & Development* 21 (5). Cold Spring Harbor Laboratory Press: 525–30. doi:10.1101/gad.415507.

Braunreiter, Chi L, Jeffrey D Hancock, Cheryl M Coffin, Kenneth M Boucher, and Stephen L Lessnick. 2006. "Expression of EWS-ETS Fusions in NIH3T3 Cells Reveals Significant Differences to Ewing's Sarcoma." *Cell Cycle (Georgetown, Tex.)* 5 (23): 2753–59. doi:10.4161/cc.5.23.3505.

Brito, Jose L R, Brian Walker, Matthew Jenner, Nicholas J Dickens, Nicola J M Brown, Fiona M Ross, Athanasia Avramidou, et al. 2009. "MMSET Deregulation Affects Cell Cycle Progression and Adhesion Regulons in t(4;14) Myeloma Plasma Cells."

Haematologica 94 (1). Ferrata Storti Foundation: 78–86. doi:10.3324/haematol.13426.

Brush, Matthew H, Douglas C Weiser, and Shirish Shenolikar. 2003. "Growth Arrest and DNA Damage-Inducible Protein GADD34 Targets Protein Phosphatase 1 Alpha to the Endoplasmic Reticulum and Promotes Dephosphorylation of the Alpha Subunit of Eukaryotic Translation Initiation Factor 2." *Molecular and Cellular Biology* 23 (4): 1292–1303. http://www.ncbi.nlm.nih.gov/pubmed/12556489.

Burdach, Stefan, Stephanie Plehm, Rebekka Unland, Arndt Borkhardt, Martin S. Staege, Carsten Müller-Tidow, and Günther H.S. Richter. 2009. "Epigenetic Maintenance of Stemness and Malignancy in Peripheral Neuroectodermal Tumors by EZH2." *Cell Cycle* 8 (13). Landes Bioscience: 1991–96. doi:10.4161/cc.8.13.8929.

Burnichon, Nelly, Jean-Jacques Brière, Rossella Libé, Laure Vescovo, Julie Rivière, Frédérique Tissier, Elodie Jouanno, et al. 2010. "SDHA Is a Tumor Suppressor Gene Causing Paraganglioma." *Human Molecular Genetics* 19 (15): 3011–20. doi:10.1093/hmg/ddq206.

Cai, Lu. 2004. "Metallothionein as an Adaptive Protein Prevents Diabetes and Its Toxicity." *Nonlinearity in Biology, Toxicology, Medicine* 2 (2). SAGE Publications: 89–103. doi:10.1080/15401420490464367.

Cao, Ru, Yu-Ichi Tsukada, and Yi Zhang. 2005. "Role of Bmi-1 and Ring1A in H2A Ubiquitylation and Hox Gene Silencing." *Molecular Cell* 20 (6): 845–54. doi:10.1016/j.molcel.2005.12.002.

Carafa, Vincenzo, Dante Rotili, Mariantonietta Forgione, Francesca Cuomo, Enrica Serretiello, Gebremedhin Solomon Hailu, Elina Jarho, Maija Lahtela-Kakkonen,

Antonello Mai, and Lucia Altucci. 2016. “Sirtuin Functions and Modulation: From Chemistry to the Clinic.” *Clinical Epigenetics* 8: 61. doi:10.1186/s13148-016-0224-3.

Chan, Kui-Ming, Dong Fang, Haiyun Gan, Rintaro Hashizume, Chuanhe Yu, Mark Schroeder, Nalin Gupta, et al. 2013. “The Histone H3.3K27M Mutation in Pediatric Glioma Reprograms H3K27 Methylation and Gene Expression.” *Genes & Development* 27 (9): 985–90. doi:10.1101/gad.217778.113.

Chargaff, E, R Lipshitz, and C Green. 1952. “Composition of the Desoxypentose Nucleic Acids of Four Genera of Sea-Urchin.” *The Journal of Biological Chemistry* 195 (1): 155–60. http://www.jbc.org/content/195/1/155.short.

Chen, Xu, Weibin Xie, Peng Gu, Qingqing Cai, Bo Wang, Yun Xie, Wen Dong, et al. 2015. “Upregulated WDR5 Promotes Proliferation, Self-Renewal and Chemoresistance in Bladder Cancer via Mediating H3K4 Trimethylation.” *Scientific Reports* 5: 8293. doi:10.1038/srep08293.

Chiaverini, Natalie, and Marc De Ley. 2010. “Protective Effect of Metallothionein on Oxidative Stress-Induced DNA Damage.” *Free Radical Research* 44 (6): 605–13. doi:10.3109/10715761003692511.

Chng, W J, A Dispenzieri, C-S Chim, R Fonseca, H Goldschmidt, S Lentzsch, N Munshi, et al. 2014. “IMWG Consensus on Risk Stratification in Multiple Myeloma.” *Leukemia* 28 (2). Nature Publishing Group: 269–77. doi:10.1038/leu.2013.247.

Chng, Wee J, Shaji Kumar, Scott Vanwier, Greg Ahmann, Tammy Price-Troska, Kim Henderson, Tae-Hoon Chung, et al. 2007. “Molecular Dissection of Hyperdiploid Multiple Myeloma by Gene Expression Profiling.” *Cancer Research* 67 (7). American

Association for Cancer Research: 2982–89. doi:10.1158/0008-5472.CAN-06-4046.

Cipak, L, and S Jantova. 2010. “PARP-1 Inhibitors: A Novel Genetically Specific Agents for Cancer Therapy.” *Neoplasma* 57 (5): 401–5. http://www.ncbi.nlm.nih.gov/pubmed/20568893.

Collins, Shauna M., Courtney E. Bakan, Gina D. Swartzel, Craig C. Hofmeister, Yvonne A. Efebera, Hakju Kwon, Gary C. Starling, et al. 2013. “Elotuzumab Directly Enhances NK Cell Cytotoxicity against Myeloma via CS1 Ligation: Evidence for Augmented NK Cell Function Complementing ADCC.” *Cancer Immunology, Immunotherapy* 62 (12). Springer Berlin Heidelberg: 1841–49. doi:10.1007/s00262-013-1493-8.

Copur, Ömer, and Jürg Müller. 2013. “The Histone H3-K27 Demethylase Utx Regulates HOX Gene Expression in Drosophila in a Temporally Restricted Manner.” *Development (Cambridge, England)* 140 (16): 3478–85. doi:10.1242/dev.097204.

Cuthbert, Graeme L, Sylvain Daujat, Andrew W Snowden, Hediye Erdjument-Bromage, Teruki Hagiwara, Michiyuki Yamada, Robert Schneider, et al. 2004. “Histone Deimination Antagonizes Arginine Methylation.” *Cell* 118 (5): 545–53. doi:10.1016/j.cell.2004.08.020.

Damiano, J S, A E Cress, L A Hazlehurst, A A Shtil, and W S Dalton. 1999. “Cell Adhesion Mediated Drug Resistance (CAM-DR): Role of Integrins and Resistance to Apoptosis in Human Myeloma Cell Lines.” *Blood* 93 (5): 1658–67. http://www.ncbi.nlm.nih.gov/pubmed/10029595.

Dang, Lenny, David W White, Stefan Gross, Bryson D Bennett, Mark A Bittinger, Edward

M Driggers, Valeria R Fantin, et al. 2009. “Cancer-Associated IDH1 Mutations Produce 2-Hydroxyglutarate.” *Nature* 462 (7274): 739–44. doi:10.1038/nature08617.

Dantas Machado, Ana Carolina, Tianyin Zhou, Satyanarayan Rao, Pragya Goel, Chaitanya Rastogi, Allan Lazarovici, Harmen J Bussemaker, and Remo Rohs. 2015. “Evolving Insights on How Cytosine Methylation Affects Protein-DNA Binding.” *Briefings in Functional Genomics* 14 (1): 61–73. doi:10.1093/bfgp/elu040.

Davidovich, Chen, Xueyin Wang, Catherine Cifuentes-Rojas, Karen J Goodrich, Anne R Gooding, Jeannie T Lee, and Thomas R Cech. 2015. “Toward a Consensus on the Binding Specificity and Promiscuity of PRC2 for RNA.” *Molecular Cell* 57 (3). NIH Public Access: 552–58. doi:10.1016/j.molcel.2014.12.017.

De Paepe, C, M Krivega, G Cauffman, M Geens, and H Van de Velde. 2014. “Totipotency and Lineage Segregation in the Human Embryo.” *Molecular Human Reproduction* 20 (7): 599–618. doi:10.1093/molehr/gau027.

DeBerardinis, R J, A Mancuso, E Daikhin, I Nissim, M Yudkoff, S Wehrli, and C B Thompson. 2007. “Beyond Aerobic Glycolysis: Transformed Cells Can Engage in Glutamine Metabolism That Exceeds the Requirement for Protein and Nucleotide Synthesis.” *Proc Natl Acad Sci U S A* 104 (49): 19345–50. doi:0709747104 [pii]10.1073/pnas.0709747104.

Delattre, O, J Zucman, B Plougastel, C Desmaze, T Melot, M Peter, H Kovar, I Joubert, P de Jong, and G Rouleau. 1992. “Gene Fusion with an ETS DNA-Binding Domain Caused by Chromosome Translocation in Human Tumours.” *Nature* 359 (6391): 162–65. doi:10.1038/359162a0.

Delcuve, Geneviève P, Dilshad H Khan, James R Davie, A Groth, W Rocha, A Verreault, G Almouzni, et al. 2012. “Roles of Histone Deacetylases in Epigenetic Regulation: Emerging Paradigms from Studies with Inhibitors.” *Clinical Epigenetics* 4 (1). BioMed Central: 5. doi:10.1186/1868-7083-4-5.

Delhommeau, François, Sabrina Dupont, Véronique Della Valle, Chloé James, Severine Trannoy, Aline Massé, Olivier Kosmider, et al. 2009. “Mutation in TET2 in Myeloid Cancers.” *http://dx.doi.org/10.1056/NEJMoa0810069*. Massachusetts Medical Society .

Denli, Ahmet M, Bastiaan B J Tops, Ronald H A Plasterk, René F Ketting, and Gregory J Hannon. 2004. “Processing of Primary microRNAs by the Microprocessor Complex.” *Nature* 432 (7014): 231–35. doi:10.1038/nature03049.

Dey, A, J Ellenberg, A Farina, A E Coleman, T Maruyama, S Sciortino, J Lippincott-Schwartz, and K Ozato. 2000. “A Bromodomain Protein, MCAP, Associates with Mitotic Chromosomes and Affects G(2)-to-M Transition.” *Molecular and Cellular Biology* 20 (17): 6537–49. http://www.ncbi.nlm.nih.gov/pubmed/10938129.

Di Croce, Luciano, and Kristian Helin. 2013. “Transcriptional Regulation by Polycomb Group Proteins.” *Nature Structural & Molecular Biology* 20 (10): 1147–55. doi:10.1038/nsmb.2669.

DiMartino, Jorge F., and Michael L. Cleary. 1999. “MLL Rearrangements in Haematological Malignancies: Lessons from Clinical and Biological Studies” 106 (3). Blackwell Science Ltd. doi:10.1046/j.1365-2141.1999.01439.x.

Djebali, Sarah, Carrie A. Davis, Angelika Merkel, Alex Dobin, Timo Lassmann, Ali

Mortazavi, Andrea Tanzer, et al. 2012. “Landscape of Transcription in Human Cells.” *Nature* 489 (7414). Nature Publishing Group: 101–8. doi:10.1038/nature11233.

Doerfler, W. 1983. “DNA Methylation and Cene Activity.” *Annual Review of Biochemistry*. http://www.annualreviews.org/doi/pdf/10.1146/annurev.bi.52.070183.000521.

Doñas, Cristian, Macarena Carrasco, Macarena Fritz, Carolina Prado, Gabriela Tejón, Francisco Osorio-Barrios, Valeria Manríquez, et al. 2016. “The Histone Demethylase Inhibitor GSK-J4 Limits Inflammation through the Induction of a Tolerogenic Phenotype on DCs.” *Journal of Autoimmunity*, August. doi:10.1016/j.jaut.2016.07.011.

Dong, J, H Qiu, M Garcia-Barrio, J Anderson, and A G Hinnebusch. 2000. “Uncharged tRNA Activates GCN2 by Displacing the Protein Kinase Moiety from a Bipartite tRNA-Binding Domain.” *Molecular Cell* 6 (2): 269–79. http://www.ncbi.nlm.nih.gov/pubmed/10983975.

Douglas, Dorothea, Jessie Hao-Ru Hsu, Long Hung, Aaron Cooper, Diana Abdueva, John van Doorninck, Grace Peng, Hiro Shimada, Timothy J Triche, and Elizabeth R Lawlor. 2008. “BMI-1 Promotes Ewing Sarcoma Tumorigenicity Independent of CDKN2A Repression.” *Cancer Research* 68 (16). NIH Public Access: 6507–15. doi:10.1158/0008-5472.CAN-07-6152.

Du, Pan, Warren A Kibbe, and Simon M Lin. 2008. “Lumi: A Pipeline for Processing Illumina Microarray.” *Bioinformatics (Oxford, England)* 24 (13): 1547–48. doi:10.1093/bioinformatics/btn224.

Du, Qian, Phuc-Loi Luu, Clare Stirzaker, and Susan J Clark. 2015. “Methyl-CpG-Binding Domain Proteins: Readers of the Epigenome.” *Epigenomics* 7 (6): 1051–73. doi:10.2217/epi.15.39.

Durie, B G, and S E Salmon. 1975. “A Clinical Staging System for Multiple Myeloma. Correlation of Measured Myeloma Cell Mass with Presenting Clinical Features, Response to Treatment, and Survival.” *Cancer* 36 (3): 842–54. http://www.ncbi.nlm.nih.gov/pubmed/1182674.

Eglen, Richard M, Terry Reisine, Philippe Roby, Nathalie Rouleau, Chantal Illy, Roger Bossé, and Martina Bielefeld. 2008. “The Use of AlphaScreen Technology in HTS: Current Status.” *Current Chemical Genomics* 1. Bentham Science Publishers: 2–10. doi:10.2174/1875397300801010002.

Endo, Shinya, Masayuki Amano, Nao Nishimura, Niina Ueno, Shikiko Ueno, Hiromichi Yuki, Shiho Fujiwara, et al. 2016. “Immunomodulatory Drugs Act as Inhibitors of DNA Methyltransferases and Induce PU.1 up-Regulation in Myeloma Cells.” *Biochemical and Biophysical Research Communications* 469 (2): 236–42. doi:10.1016/j.bbrc.2015.11.116.

Estarás, Conchi, Naiara Akizu, Alejandra García, Sergi Beltrán, Xavier de la Cruz, and Marian A Martínez-Balbás. 2012. “Genome-Wide Analysis Reveals That Smad3 and JMJD3 HDM Co-Activate the Neural Developmental Program.” *Development (Cambridge, England)* 139 (15): 2681–91. doi:10.1242/dev.078345.

Esteller, M. 2007. “Cancer Epigenomics: DNA Methylomes and Histone-Modification Maps.” *Nature Reviews Genetics*.

http://www.nature.com/nrg/journal/v8/n4/abs/nrg2005.html.

Etoh, Tsuyoshi, Yae Kanai, Saori Ushijima, Tohru Nakagawa, Yukihiro Nakanishi, Mitsuru Sasako, Seigo Kitano, and Setsuo Hirohashi. 2004. "Increased DNA Methyltransferase 1 (DNMT1) Protein Expression Correlates Significantly with Poorer Tumor Differentiation and Frequent DNA Hypermethylation of Multiple CpG Islands in Gastric Cancers." *The American Journal of Pathology* 164 (2): 689–99. doi:10.1016/S0002-9440(10)63156-2.

Fabregat, I, J Vitorica, J Satrustegui, and A Machado. 1985. "The Pentose Phosphate Cycle Is Regulated by NADPH/NADP Ratio in Rat Liver." *Archives of Biochemistry and Biophysics* 236 (1): 110–18. http://www.ncbi.nlm.nih.gov/pubmed/3966788.

Figueroa, Maria E, Omar Abdel-Wahab, Chao Lu, Patrick S Ward, Jay Patel, Alan Shih, Yushan Li, et al. 2010. "Leukemic IDH1 and IDH2 Mutations Result in a Hypermethylation Phenotype, Disrupt TET2 Function, and Impair Hematopoietic Differentiation." *Cancer Cell* 18 (6): 553–67. doi:10.1016/j.ccr.2010.11.015.

Filippakopoulos, Panagis, and Stefan Knapp. 2014. "Targeting Bromodomains: Epigenetic Readers of Lysine Acetylation." *Nature Reviews Drug Discovery* 13 (5). Nature Publishing Group: 337–56. doi:10.1038/nrd4286.

French, Christopher A, Jeffery L Kutok, William C Faquin, Jeffrey A Toretsky, Cristina R Antonescu, Constance A Griffin, Vania Nose, et al. 2004. "Midline Carcinoma of Children and Young Adults with NUT Rearrangement." *Journal of Clinical Oncology : Official Journal of the American Society of Clinical Oncology* 22 (20): 4135–39. doi:10.1200/JCO.2004.02.107.

Frey, Felice, Thomas Sheahan, Katja Finkl, Gabriele Stoehr, Matthias Mann, Christian Benda, and Jürg Müller. 2016. "Molecular Basis of PRC1 Targeting to Polycomb Response Elements by PhoRC." *Genes & Development* 30 (9): 1116–27. doi:10.1101/gad.279141.116.

Friedmann, David R., and Ronen Marmorstein. 2013. "Structure and Mechanism of Non-Histone Protein Acetyltransferase Enzymes." *FEBS Journal* 280 (22): 5570–81. doi:10.1111/febs.12373.

Fukui, Kenji, and Kenji Fukui. 2010. "DNA Mismatch Repair in Eukaryotes and Bacteria." *Journal of Nucleic Acids* 2010. Hindawi Publishing Corporation: 1–16. doi:10.4061/2010/260512.

Futreal, P. Andrew, Lachlan Coin, Mhairi Marshall, Thomas Down, Timothy Hubbard, Richard Wooster, Nazneen Rahman, and Michael R. Stratton. 2004. "A Census of Human Cancer Genes." *Nature Reviews Cancer* 4 (3). Nature Publishing Group: 177–83. doi:10.1038/nrc1299.

Garnett, Mathew J, Elena J Edelman, Sonja J Heidorn, Chris D Greenman, Anahita Dastur, King Wai Lau, Patricia Greninger, et al. 2012. "Systematic Identification of Genomic Markers of Drug Sensitivity in Cancer Cells." *Nature* 483 (7391): 570–75. doi:10.1038/nature11005.

Gaspar, N., D. S. Hawkins, U. Dirksen, I. J. Lewis, S. Ferrari, M.-C. Le Deley, H. Kovar, et al. 2015. "Ewing Sarcoma: Current Management and Future Approaches Through Collaboration." *Journal of Clinical Oncology* 33 (27). American Society of Clinical Oncology: 3036–46. doi:10.1200/JCO.2014.59.5256.

Genovese, Giulio, Anna K. Kähler, Robert E. Handsaker, Johan Lindberg, Samuel A. Rose, Samuel F. Bakhoum, Kimberly Chambert, et al. 2014. "Clonal Hematopoiesis and Blood-Cancer Risk Inferred from Blood DNA Sequence." *http://dx.doi.org/10.1056/NEJMoa1409405*. Massachusetts Medical Society .

Gerrand, Craig, Nick Athanasou, Bernadette Brennan, Robert Grimer, Ian Judson, Bruce Morland, David Peake, et al. 2016. "UK Guidelines for the Management of Bone Sarcomas." *Clinical Sarcoma Research* 6 (1). BioMed Central: 7. doi:10.1186/s13569-016-0047-1.

Ghoshal, K., J. Datta, S. Majumder, S. Bai, X. Dong, M. Parthun, and S. T. Jacob. 2002. "Inhibitors of Histone Deacetylase and DNA Methyltransferase Synergistically Activate the Methylated Metallothionein I Promoter by Activating the Transcription Factor MTF-1 and Forming an Open Chromatin Structure." *Molecular and Cellular Biology* 22 (23): 8302–19. doi:10.1128/MCB.22.23.8302-8319.2002.

Gil, Jesús, and Gordon Peters. 2006. "Regulation of the INK4b-ARF-INK4a Tumour Suppressor Locus: All for One or One for All." *Nature Reviews. Molecular Cell Biology* 7 (9): 667–77. doi:10.1038/nrm1987.

Goll, Mary Grace, Finn Kirpekar, Keith A Maggert, Jeffrey A Yoder, Chih-Lin Hsieh, Xiaoyu Zhang, Kent G Golic, Steven E Jacobsen, and Timothy H Bestor. 2006. "Methylation of tRNAAsp by the DNA Methyltransferase Homolog Dnmt2." *Science (New York, N.Y.)* 311 (5759): 395–98. doi:10.1126/science.1120976.

González, David, Mirjam van der Burg, Ramón García-Sanz, James A Fenton, Anton W Langerak, Marcos González, Jacques J M van Dongen, et al. 2007. "Immunoglobulin

Gene Rearrangements and the Pathogenesis of Multiple Myeloma." *Blood* 110 (9). American Society of Hematology: 3112–21. doi:10.1182/blood-2007-02-069625.

Görgün, Güllü, Elisabetta Calabrese, Ender Soydan, Teru Hideshima, Giulia Perrone, Madhavi Bandi, Diana Cirstea, et al. 2010. "Immunomodulatory Effects of Lenalidomide and Pomalidomide on Interaction of Tumor and Bone Marrow Accessory Cells in Multiple Myeloma." *Blood* 116 (17). American Society of Hematology: 3227–37. doi:10.1182/blood-2010-04-279893.

Grayson, A R, E M Walsh, M J Cameron, J Godec, T Ashworth, J M Ambrose, A B Aserlind, et al. 2014. "MYC, a Downstream Target of BRD-NUT, Is Necessary and Sufficient for the Blockade of Differentiation in NUT Midline Carcinoma." *Oncogene* 33 (13): 1736–42. doi:10.1038/onc.2013.126.

Greenfield, A, L Carrel, D Pennisi, C Philippe, N Quaderi, P Siggers, K Steiner, et al. 1998. "The UTX Gene Escapes X Inactivation in Mice and Humans." *Human Molecular Genetics* 7 (4): 737–42. http://www.ncbi.nlm.nih.gov/pubmed/9499428.

Greenstein, Stephanie, Nancy L Krett, Yoshihiro Kurosawa, Chunguang Ma, Dharminder Chauhan, Teru Hideshima, Kenneth C Anderson, et al. 2003. "Characterization of the MM.1 Human Multiple Myeloma (MM) Cell Lines." *Experimental Hematology* 31 (4). Elsevier: 271–82. doi:10.1016/S0301-472X(03)00023-7.

Greipp, Philip R, Jesus San Miguel, Brian G M Durie, John J Crowley, Bart Barlogie, Joan Bladé, Mario Boccadoro, et al. 2005. "International Staging System for Multiple Myeloma." *Journal of Clinical Oncology : Official Journal of the American Society of Clinical Oncology* 23 (15): 3412–20. doi:10.1200/JCO.2005.04.242.

Grijzenhout, Anne, Jonathan Godwin, Haruhiko Koseki, Michal Ryszard Gdula, Dorota Szumska, Joanna F. McGouran, Shoumo Bhattacharya, Benedikt M. Kessler, Neil Brockdorff, and Sarah Cooper. 2016. “Functional Analysis of AEBP2, a PRC2 Polycomb Protein, Reveals a Trithorax Phenotype in Embryonic Development and in ESCs.” *Development* 143 (15): 2716–23. doi:10.1242/dev.123935.

Gros, Christina, Jacques Fahy, Ludovic Halby, Isabelle Dufau, Alexandre Erdmann, Jean-Marc Gregoire, Fréderic Ausseil, Stéphane Vispé, and Paola B Arimondo. 2012. “DNA Methylation Inhibitors in Cancer: Recent and Future Approaches.” *Biochimie* 94 (11): 2280–96. doi:10.1016/j.biochi.2012.07.025.

Guo, Huaijian, Mario-Ernesto Cruz-Munoz, Ning Wu, Michael Robbins, and André Veillette. 2015. “Immune Cell Inhibition by SLAMF7 Is Mediated by a Mechanism Requiring Src Kinases, CD45, and SHIP-1 That Is Defective in Multiple Myeloma Cells.” *Molecular and Cellular Biology* 35 (1). American Society for Microbiology: 41–51. doi:10.1128/MCB.01107-14.

Gupta, Rajnish A., Nilay Shah, Kevin C. Wang, Jeewon Kim, Hugo M. Horlings, David J. Wong, Miao-Chih Tsai, et al. 2010. “Long Non-Coding RNA HOTAIR Reprograms Chromatin State to Promote Cancer Metastasis.” *Nature* 464 (7291). Nature Publishing Group: 1071–76. doi:10.1038/nature08975.

Gurevich, Alexey, Vladislav Saveliev, Nikolay Vyahhi, and Glenn Tesler. 2013. “QUAST: Quality Assessment Tool for Genome Assemblies.” *Bioinformatics (Oxford, England)* 29 (8): 1072–75. doi:10.1093/bioinformatics/btt086.

Gutiérrez, Luis, Katarzyna Oktaba, Johanna C Scheuermann, Maria Cristina Gambetta,

Nga Ly-Hartig, and Jürg Müller. 2012. “The Role of the Histone H2A Ubiquitinase Sce in Polycomb Repression.” *Development (Cambridge, England)* 139 (1): 117–27. doi:10.1242/dev.074450.

Han, Leng, Bing Su, Wen-Hsiung Li, and Zhongming Zhao. 2008. “CpG Island Density and Its Correlations with Genomic Features in Mammalian Genomes.” *Genome Biology* 9 (5): R79. doi:10.1186/gb-2008-9-5-r79.

Hanahan, Douglas, and Robert A. Weinberg. 2011. “Hallmarks of Cancer: The Next Generation.” *Cell* 144 (5): 646–74. doi:10.1016/j.cell.2011.02.013.

Hanahan, Douglas, and Robert A Weinberg. 2000. “The Hallmarks of Cancer.” *Cell* 100 (1): 57–70. doi:10.1016/S0092-8674(00)81683-9.

Hancock, Jeffrey D, and Stephen L Lessnick. 2008. “A Transcriptional Profiling Meta-Analysis Reveals a Core EWS-FLI Gene Expression Signature.” *Cell Cycle (Georgetown, Tex.)* 7 (2): 250–56. doi:10.4161/cc.7.2.5229.

Hashimoto, Hideharu, Samuel Hong, Ashok S Bhagwat, Xing Zhang, and Xiaodong Cheng. 2012. “Excision of 5-Hydroxymethyluracil and 5-Carboxylcytosine by the Thymine DNA Glycosylase Domain: Its Structural Basis and Implications for Active DNA Demethylation.” *Nucleic Acids Research* 40 (20): 10203–14. doi:10.1093/nar/gks845.

Hashizume, Rintaro, Noemi Andor, Yuichiro Ihara, Robin Lerner, Haiyun Gan, Xiaoyue Chen, Dong Fang, et al. 2014. “Pharmacologic Inhibition of Histone Demethylation as a Therapy for Pediatric Brainstem Glioma.” *Nature Medicine* advance on (November). Nature Publishing Group, a division of Macmillan Publishers Limited. All Rights

Reserved. doi:10.1038/nm.3716.

Hassa, Paul O, Sandra S Haenni, Michael Elser, and Michael O Hottiger. 2006. “Nuclear ADP-Ribosylation Reactions in Mammalian Cells: Where Are We Today and Where Are We Going?” *Microbiology and Molecular Biology Reviews : MMBR* 70 (3): 789–829. doi:10.1128/MMBR.00040-05.

He, Lin, and Gregory J. Hannon. 2004. “MicroRNAs: Small RNAs with a Big Role in Gene Regulation.” *Nature Reviews Genetics* 5 (7). Nature Publishing Group: 522–31. doi:10.1038/nrg1379.

Heinemann, Bo, Jesper Morten Nielsen, Heidi Rye Hudlebusch, Michael J. Lees, Dorthe Vang Larsen, Thomas Boesen, Marc Labelle, Lars-Ole Gerlach, Peter Birk, and Kristian Helin. 2014. “Inhibition of Demethylases by GSK-J1/J4.” *Nature* 514 (7520). Nature Research: E1–2. doi:10.1038/nature13688.

Heinz, Sven, Christopher Benner, Nathanael Spann, Eric Bertolino, Yin C Lin, Peter Laslo, Jason X Cheng, Cornelis Murre, Harinder Singh, and Christopher K Glass. 2010. “Simple Combinations of Lineage-Determining Transcription Factors Prime Cis-Regulatory Elements Required for Macrophage and B Cell Identities.” *Molecular Cell* 38 (4): 576–89. doi:10.1016/j.molcel.2010.05.004.

Hensel, Tim, Chiara Giorgi, Oxana Schmidt, Julia Calzada-Wack, Frauke Neff, Thorsten Buch, Felix K Niggli, Beat W Schäfer, Stefan Burdach, and Günther H S Richter. 2016. “Targeting the EWS-ETS Transcriptional Program by BET Bromodomain Inhibition in Ewing Sarcoma.” *Oncotarget* 7 (2). Impact Journals, LLC: 1451–63. doi:10.18632/oncotarget.6385.

Hernández-Muñoz, Inmaculada, Anders H Lund, Petra van der Stoop, Erwin Boutsma, Inhua Muijrers, Els Verhoeven, Dmitri A Nusinow, Barbara Panning, York Marahrens, and Maarten van Lohuizen. 2005. "Stable X Chromosome Inactivation Involves the PRC1 Polycomb Complex and Requires Histone MACROH2A1 and the CULLIN3/SPOP Ubiquitin E3 Ligase." *Proceedings of the National Academy of Sciences of the United States of America* 102 (21): 7635–40. doi:10.1073/pnas.0408918102.

Hideshima, Teru, Dharminder Chauhan, Paul Richardson, Constantine Mitsiades, Nicholas Mitsiades, Toshiaki Hayashi, Nikhil Munshi, et al. 2002. "NF-Kappa B as a Therapeutic Target in Multiple Myeloma." *The Journal of Biological Chemistry* 277 (19): 16639–47. doi:10.1074/jbc.M200360200.

Hilbert, David. 1891. "Ueber Die Stetige Abbildung Einer Line Auf Ein Flachenstuck." *Mathematische Annalen* 38 (3). Springer-Verlag: 459–60. doi:10.1007/BF01199431.

Hong, Sunhwa, Young-Wook W Cho, Li-Rong R Yu, Hong Yu, Timothy D Veenstra, and Kai Ge. 2007. "Identification of JmjC Domain-Containing UTX and JMJD3 as Histone H3 Lysine 27 Demethylases." *Proc Natl Acad Sci U S A* 104 (47): 18439–44. doi:10.1073/pnas.0707292104.

Hormoz, Sahand. 2013. "Amino Acid Composition of Proteins Reduces Deleterious Impact of Mutations." *Scientific Reports* 3: 2919. doi:10.1038/srep02919.

Hu-Lieskovan, Siwen, Jeremy D Heidel, Derek W Bartlett, Mark E Davis, and Timothy J Triche. 2005. "Sequence-Specific Knockdown of EWS-FLI1 by Targeted, Nonviral Delivery of Small Interfering RNA Inhibits Tumor Growth in a Murine Model of

Metastatic Ewing's Sarcoma." *Cancer Research* 65 (19): 8984–92. doi:10.1158/0008-5472.CAN-05-0565.

Huang, Fu, Mahesh B Chandrasekharan, Yi-Chun Chen, Srividya Bhaskara, Scott W Hiebert, and Zu-Wen Sun. 2010. "The JmjN Domain of Jhd2 Is Important for Its Protein Stability, and the Plant Homeodomain (PHD) Finger Mediates Its Chromatin Association Independent of H3K4 Methylation." *The Journal of Biological Chemistry* 285 (32): 24548–61. doi:10.1074/jbc.M110.117333.

Hurtubise, Annie, Mark L Bernstein, and Richard L Momparler. 2008. "Preclinical Evaluation of the Antineoplastic Action of 5-Aza-2'-deoxycytidine and Different Histone Deacetylase Inhibitors on Human Ewing's Sarcoma Cells." *Cancer Cell International* 8: 16. doi:10.1186/1475-2867-8-16.

Hutvágner, G, J McLachlan, A E Pasquinelli, E Bálint, T Tuschl, and P D Zamore. 2001. "A Cellular Function for the RNA-Interference Enzyme Dicer in the Maturation of the Let-7 Small Temporal RNA." *Science (New York, N.Y.)* 293 (5531): 834–38. doi:10.1126/science.1062961.

Ibragimova, Ilsiya, Marie E Maradeo, Essel Dulaimi, and Paul Cairns. 2013. "Aberrant Promoter Hypermethylation of PBRM1, BAP1, SETD2, KDM6A and Other Chromatin-Modifying Genes Is Absent or Rare in Clear Cell RCC." *Epigenetics : Official Journal of the DNA Methylation Society* 8 (5): 486–93. doi:10.4161/epi.24552.

Iida, Tetsuo, Isao Suetake, Shoji Tajima, Hiroshi Morioka, Satoshi Ohta, Chikashi Obuse, and Toshiki Tsurimoto. 2002. "PCNA Clamp Facilitates Action of DNA Cytosine

Methyltransferase 1 on Hemimethylated DNA." *Genes to Cells* 7 (10). Blackwell Science Ltd: 997–1007. doi:10.1046/j.1365-2443.2002.00584.x.

Imoto, Akemi, Mami Okada, Toshio Okazaki, Hidero Kitasato, Hideo Harigae, and Shinichiro Takahashi. 2010. "Metallothionein-1 Isoforms and Vimentin Are Direct PU.1 Downstream Target Genes in Leukemia Cells." *The Journal of Biological Chemistry* 285 (14): 10300–309. doi:10.1074/jbc.M109.095810.

Inoue, Shin-Ichi, Mitsuji Moriya, Yusuke Watanabe, Sachiko Miyagawa-Tomita, Tetsuya Niihori, Daiju Oba, Masao Ono, et al. 2014. "New BRAF Knockin Mice Provide a Pathogenetic Mechanism of Developmental Defects and a Therapeutic Approach in Cardio-Facio-Cutaneous Syndrome." *Human Molecular Genetics*, July. doi:10.1093/hmg/ddu376.

Ito, Takumi, Hideki Ando, Takayuki Suzuki, Toshihiko Ogura, Kentaro Hotta, Yoshimasa Imamura, Yuki Yamaguchi, and Hiroshi Handa. 2010. "Identification of a Primary Target of Thalidomide Teratogenicity." *Science (New York, N.Y.)* 327 (5971). American Association for the Advancement of Science: 1345–50. doi:10.1126/science.1177319.

Itsumi, M, S Inoue, A J Elia, K Murakami, M Sasaki, E F Lind, D Brenner, et al. 2015. "Idh1 Protects Murine Hepatocytes from Endotoxin-Induced Oxidative Stress by Regulating the Intracellular NADP(+)/NADPH Ratio." *Cell Death and Differentiation* 22 (11): 1837–45. doi:10.1038/cdd.2015.38.

Jacobs, J J, B Scheijen, J W Voncken, K Kieboom, A Berns, and M van Lohuizen. 1999. "Bmi-1 Collaborates with c-Myc in Tumorigenesis by Inhibiting c-Myc-Induced

Apoptosis via INK4a/ARF." *Genes & Development* 13 (20): 2678–90. http://www.ncbi.nlm.nih.gov/pubmed/10541554.

Jaiswal, Siddhartha, Pierre Fontanillas, Jason Flannick, Alisa Manning, Peter V. Grauman, Brenton G. Mar, R. Coleman Lindsley, et al. 2014. "Age-Related Clonal Hematopoiesis Associated with Adverse Outcomes." *http://dx.doi.org/10.1056/NEJMoa1408617*. Massachusetts Medical Society .

Jang, Moon Kyoo, Kazuki Mochizuki, Meisheng Zhou, Ho-Sang Jeong, John N Brady, and Keiko Ozato. 2005. "The Bromodomain Protein Brd4 Is a Positive Regulatory Component of P-TEFb and Stimulates RNA Polymerase II-Dependent Transcription." *Molecular Cell* 19 (4): 523–34. doi:10.1016/j.molcel.2005.06.027.

Jansson, Martin D., and Anders H. Lund. 2012. "MicroRNA and Cancer." *Molecular Oncology* 6 (6): 590–610. doi:10.1016/j.molonc.2012.09.006.

JASANI, B., and K.W. SCHMID. 1997. "Significance of Metallothionein Overexpression in Human Tumours." *Histopathology* 31 (3). Blackwell Science Ltd: 211–14. doi:10.1046/j.1365-2559.1997.2140848.x.

Jeltsch, Albert. 2016. "On the Enzymatic Properties of Dnmt1: Specificity, Processivity, Mechanism of Linear Diffusion and Allosteric Regulation of the Enzyme." *Epigenetics* 1 (2): 63–66. Accessed June 27. http://www.ncbi.nlm.nih.gov/pubmed/17965604.

Jenuwein, T, and C D Allis. 2001. "Translating the Histone Code." *Science (New York, N.Y.)* 293 (5532): 1074–80. doi:10.1126/science.1063127.

Johansson, Catrine, Anthony Tumber, KaHing Che, Peter Cain, Radosław Nowak, Carina Gileadi, and Udo Oppermann. 2014. “The Roles of Jumonji-Type Oxygenases in Human Disease.” *Epigenomics* 6 (1): 89–120. doi:10.2217/epi.13.79.

Johansson, Catrine, Srikannathasan Velupillai, Anthony Tumber, Aleksandra Szykowska, Edward S Hookway, Radoslaw P Nowak, Claire Strain-Damerell, et al. 2016. “Structural Analysis of Human KDM5B Guides Histone Demethylase Inhibitor Development.” *Nature Chemical Biology* 12 (JUly). Nature Publishing Group, a division of Macmillan Publishers Limited. All Rights Reserved.: 78–80. doi:10.1038/nchembio.2087.

Johnson, David S., Ali Mortazavi, Richard M. Myers, and Barbara Wold. 2007. “Genome-Wide Mapping of in Vivo Protein-DNA Interactions.” *Science* 316 (5830).

Juergens, Christine, Claire Weston, Ian Lewis, Jeremy Whelan, Michael Paulussen, Odile Oberlin, Jean Michon, Andreas Zoubek, Herbert Juergens, and Alan Craft. 2006. “Safety Assessment of Intensive Induction with Vincristine, Ifosfamide, Doxorubicin, and Etoposide (VIDE) in the Treatment of Ewing Tumors in the EURO-E.W.I.N.G. 99 Clinical Trial.” *Pediatric Blood & Cancer* 47 (1). Wiley Subscription Services, Inc., A Wiley Company: 22–29. doi:10.1002/pbc.20820.

Juliano, Celina, Jianquan Wang, and Haifan Lin. 2011. “Uniting Germline and Stem Cells: The Function of Piwi Proteins and the piRNA Pathway in Diverse Organisms.” *Annual Review of Genetics* 45: 447–69. doi:10.1146/annurev-genet-110410-132541.

Kamikawa, Yasunao F, and Mary E Donohoe. 2015. “Histone Demethylation Maintains Prdm14 and Tsix Expression and Represses xIst in Embryonic Stem Cells.” *PloS One*

10 (5). Public Library of Science: e0125626. doi:10.1371/journal.pone.0125626.

Karmodiya, Krishanpal, Arnaud R Krebs, Mustapha Oulad-Abdelghani, Hiroshi Kimura, and Laszlo Tora. 2012. "H3K9 and H3K14 Acetylation Co-Occur at Many Gene Regulatory Elements, While H3K14ac Marks a Subset of Inactive Inducible Promoters in Mouse Embryonic Stem Cells." *BMC Genomics* 13 (1). BioMed Central: 424. doi:10.1186/1471-2164-13-424.

Kawano, Yawara, Michele Moschetta, Salomon Manier, Siobhan Glavey, Güllü T. Görgün, Aldo M. Roccaro, Kenneth C. Anderson, and Irene M. Ghobrial. 2015. "Targeting the Bone Marrow Microenvironment in Multiple Myeloma." *Immunological Reviews* 263 (1): 160–72. doi:10.1111/imr.12233.

Keats, Jonathan J, Christopher A Maxwell, Brian J Taylor, Michael J Hendzel, Marta Chesi, P Leif Bergsagel, Loree M Larratt, et al. 2005. "Overexpression of Transcripts Originating from the MMSET Locus Characterizes All t(4;14)(p16;q32)-Positive Multiple Myeloma Patients." *Blood* 105 (10). American Society of Hematology: 4060–69. doi:10.1182/blood-2004-09-3704.

Kim, Sungeun, Christopher T Denny, and Ron Wisdom. 2006. "Cooperative DNA Binding with AP-1 Proteins Is Required for Transformation by EWS-Ets Fusion Proteins." *Molecular and Cellular Biology* 26 (7): 2467–78. doi:10.1128/MCB.26.7.2467-2478.2006.

Kinsey, Michelle, Richard Smith, and Stephen L Lessnick. 2006. "NR0B1 Is Required for the Oncogenic Phenotype Mediated by EWS/FLI in Ewing's Sarcoma." *Molecular Cancer Research : MCR* 4 (11): 851–59. doi:10.1158/1541-7786.MCR-06-0090.

Kokabu, Shoichiro, Jonathan W Lowery, and Eijiro Jimi. 2016. “Cell Fate and Differentiation of Bone Marrow Mesenchymal Stem Cells.” *Stem Cells International* 2016: 3753581. doi:10.1155/2016/3753581.

Kondo, Motonari. 2010. “Lymphoid and Myeloid Lineage Commitment in Multipotent Hematopoietic Progenitors.” *Immunological Reviews* 238 (1): 37–46. doi:10.1111/j.1600-065X.2010.00963.x.

Kopp, Lisa M, Chengcheng Hu, Beatriz Rozo, Andrea White-Collins, Winston W Huh, Angela Yarborough, Cynthia E Herzog, and Pooja Hingorani. 2015. “Utility of Bone Marrow Aspiration and Biopsy in Initial Staging of Ewing Sarcoma.” *Pediatric Blood & Cancer* 62 (1): 12–15. doi:10.1002/pbc.25212.

Kouzarides, Tony. 2007. “Chromatin Modifications and Their Function.” *Cell*. doi:10.1016/j.cell.2007.02.005.

Krönke, Jan, Namrata D Udeshi, Anupama Narla, Peter Grauman, Slater N Hurst, Marie McConkey, Tanya Svinkina, et al. 2014. “Lenalidomide Causes Selective Degradation of IKZF1 and IKZF3 in Multiple Myeloma Cells.” *Science (New York, N.Y.)* 343 (6168): 301–5. doi:10.1126/science.1244851.

Kruidenier, Laurens, Chun-wa Chung, Zhongjun Cheng, John Liddle, KaHing Che, Gerard Joberty, Marcus Bantscheff, et al. 2012. “A Selective Jumonji H3K27 Demethylase Inhibitor Modulates the Proinflammatory Macrophage Response.” *Nature* 488 (7411). Nature Publishing Group, a division of Macmillan Publishers Limited. All Rights Reserved.: 404–8. doi:10.1038/nature11262.

Kruse-Lösler, Birgit, Christoph Gaertner, Horst Bürger, László Seper, Ulrich Joos, and

Johannes Kleinheinz. 2006. “Melanotic Neuroectodermal Tumor of Infancy: Systematic Review of the Literature and Presentation of a Case.” *Oral Surgery, Oral Medicine, Oral Pathology, Oral Radiology, and Endodontics* 102 (2). Elsevier: 204–16. doi:10.1016/j.tripleo.2005.08.010.

Kumar, Rajiv, Sabrina Angelini, Erna Snellman, and Kari Hemminki. 2004. “BRAF Mutations Are Common Somatic Events in Melanocytic Nevi.” *Journal of Investigative Dermatology* 122 (2): 342–48. doi:10.1046/j.0022-202X.2004.22225.x.

Kung, Johnny T Y, David Colognori, and Jeannie T Lee. 2013. “Long Noncoding RNAs: Past, Present, and Future.” *Genetics* 193 (3): 651–69. doi:10.1534/genetics.112.146704.

Kuo, Alex J, Peggie Cheung, Kaifu Chen, Barry M Zee, Mitomu Kioi, Josh Lauring, Yuanxin Xi, et al. 2011. “NSD2 Links Dimethylation of Histone H3 at Lysine 36 to Oncogenic Programming.” *Molecular Cell* 44 (4): 609–20. doi:10.1016/j.molcel.2011.08.042.

Kurtz, Stefan, Adam Phillippy, Arthur L Delcher, Michael Smoot, Martin Shumway, Corina Antonescu, Steven L Salzberg, et al. 2004. “Versatile and Open Software for Comparing Large Genomes.” *Genome Biology* 5 (2). BioMed Central: R12. doi:10.1186/gb-2004-5-2-r12.

Kuzbicki, Lukasz, Dariusz Lange, Anita Straczynska-Niemiec, and Barbara W Chwirot. 2013. “JARID1B Expression in Human Melanoma and Benign Melanocytic Skin Lesions.” *Melanoma Research* 23 (1): 8–12. doi:10.1097/CMR.0b013e32835d5d6f.

Laird, PW, and R Jaenisch. 1996. “The Role of DNA Methylation in Cancer Genetics and

Epigenetics." *Annual Review of Genetics*. http://www.annualreviews.org/doi/abs/10.1146/annurev.genet.30.1.441.

Landais, I, M Ogliastro, K Mita, J Nohata, M López-Ferber, M Duonor-Cérutti, T Shimada, P Fournier, and G Devauchelle. 2003. "Annotation Pattern of ESTs from Spodoptera Frugiperda Sf9 Cells and Analysis of the Ribosomal Protein Genes Reveal Insect-Specific Features and Unexpectedly Low Codon Usage Bias." *Bioinformatics (Oxford, England)* 19 (18): 2343–50. http://www.ncbi.nlm.nih.gov/pubmed/14668217.

Laubach, Jacob P, Philippe Moreau, Jesús F San-Miguel, and Paul G Richardson. 2015. "Panobinostat for the Treatment of Multiple Myeloma." *Clinical Cancer Research : An Official Journal of the American Association for Cancer Research* 21 (21): 4767–73. doi:10.1158/1078-0432.CCR-15-0530.

Lederer, Damien, Bernard Grisart, Maria Cristina Digilio, Valérie Benoit, Marianne Crespin, Sophie Claire Ghariani, Isabelle Maystadt, Bruno Dallapiccola, and Christine Verellen-Dumoulin. 2012. "Deletion of KDM6A, a Histone Demethylase Interacting with MLL2, in Three Patients with Kabuki Syndrome." *The American Journal of Human Genetics*. Vol. 90. http://www.sciencedirect.com/science/article/pii/S000292971100499X.

Lee, Kenneth K, and Jerry L Workman. 2007. "Histone Acetyltransferase Complexes: One Size Doesn't Fit All." *Nature Reviews. Molecular Cell Biology* 8 (4): 284–95. doi:10.1038/nrm2145.

Lee, W, A Haslinger, M Karin, and R Tjian. 2016. "Activation of Transcription by Two Factors That Bind Promoter and Enhancer Sequences of the Human Metallothionein

Gene and SV40." *Nature* 325 (6102): 368–72. Accessed September 28. doi:10.1038/325368a0.

Lee, William, Sewit Teckie, Thomas Wiesner, Leili Ran, Carlos N Prieto Granada, Mingyan Lin, Sinan Zhu, et al. 2014. "PRC2 Is Recurrently Inactivated through EED or SUZ12 Loss in Malignant Peripheral Nerve Sheath Tumors." *Nature Genetics* 46 (11): 1227–32. doi:10.1038/ng.3095.

Lee, Yong Joo, Myoung-Eun Han, Su-Jin Baek, Seon-Young Kim, and Sae-Ock Oh. 2015. "Roles of DPY30 in the Proliferation and Motility of Gastric Cancer Cells." *PloS One* 10 (7): e0131863. doi:10.1371/journal.pone.0131863.

Leich, E, S Weißbach, H-U Klein, T Grieb, J Pischimarov, T Stühmer, M Chatterjee, et al. 2013. "Multiple Myeloma Is Affected by Multiple and Heterogeneous Somatic Mutations in Adhesion- and Receptor Tyrosine Kinase Signaling Molecules." *Blood Cancer Journal* 3 (2). Nature Publishing Group: e102. doi:10.1038/bcj.2012.47.

LeRoith, Derek, and Charles T Roberts. 2003. "The Insulin-like Growth Factor System and Cancer." *Cancer Letters* 195 (2): 127–37. http://www.ncbi.nlm.nih.gov/pubmed/12767520.

Lewis, Peter W, Manuel M Müller, Matthew S Koletsky, Francisco Cordero, Shu Lin, Laura A Banaszynski, Benjamin A Garcia, Tom W Muir, Oren J Becher, and C David Allis. 2013. "Inhibition of PRC2 Activity by a Gain-of-Function H3 Mutation Found in Pediatric Glioblastoma." *Science (New York, N.Y.)* 340 (6134): 857–61. doi:10.1126/science.1232245.

Ley, Timothy J., Li Ding, Matthew J. Walter, Michael D. McLellan, Tamara Lamprecht,

David E. Larson, Cyriac Kandoth, et al. 2010. “DNMT3A Mutations in Acute Myeloid Leukemia.” *http://dx.doi.org/10.1056/NEJMoa1005143*. Massachusetts Medical Society .

Li, Qian, Lei Shi, Bin Gui, Wenhua Yu, Jiamu Wang, Di Zhang, Xiao Han, Zhi Yao, and Yongfeng Shang. 2011. “Binding of the JmjC Demethylase JARID1B to LSD1/NuRD Suppresses Angiogenesis and Metastasis in Breast Cancer Cells by Repressing Chemokine CCL14.” *Cancer Research* 71 (21): 6899–6908. doi:10.1158/0008-5472.CAN-11-1523.

Li, X., H. Chen, and P. N. Epstein. 2004. “Metallothionein Protects Islets from Hypoxia and Extends Islet Graft Survival by Scavenging Most Kinds of Reactive Oxygen Species.” *Journal of Biological Chemistry* 279 (1). American Society for Biochemistry and Molecular Biology: 765–71. doi:10.1074/jbc.M307907200.

Li, Ying, Mei Liu, Yanjun Zhang, Chun Han, Junhao You, Junlan Yang, Cheng Cao, and Shunchang Jiao. 2013. “Effects of ARHI on Breast Cancer Cell Biological Behavior Regulated by microRNA-221.” *Tumour Biology : The Journal of the International Society for Oncodevelopmental Biology and Medicine* 34 (6): 3545–54. doi:10.1007/s13277-013-0933-6.

Li, Zhi-Wei, Haiming Chen, Richard A Campbell, Benjamin Bonavida, and James R Berenson. 2008. “NF-kappaB in the Pathogenesis and Treatment of Multiple Myeloma.” *Current Opinion in Hematology* 15 (4): 391–99. doi:10.1097/MOH.0b013e328302c7f4.

Liao, Jing, Rahul Karnik, Hongcang Gu, Michael J Ziller, Kendell Clement, Alexander M

Tsankov, Veronika Akopian, et al. 2015. “Targeted Disruption of DNMT1, DNMT3A and DNMT3B in Human Embryonic Stem Cells.” *Nature Genetics* 47 (5): 469–78. doi:10.1038/ng.3258.

Liao, Yang, Gordon K Smyth, and Wei Shi. 2014. “featureCounts: An Efficient General Purpose Program for Assigning Sequence Reads to Genomic Features.” *Bioinformatics (Oxford, England)* 30 (7): 923–30. doi:10.1093/bioinformatics/btt656.

Liu, Zhi, Wei Cao, Longxia Xu, Xi Chen, Yu Zhan, Qian Yang, Sanhong Liu, et al. 2015. “The Histone H3 Lysine-27 Demethylase Jmjd3 Plays a Critical Role in Specific Regulation of Th17 Cell Differentiation.” *Journal of Molecular Cell Biology* 7 (6): 505–16. doi:10.1093/jmcb/mjv022.

Llamas-Velasco, Mar, Luis Requena, Julie Adam, Norma Frizzell, Arndt Hartmann, and Thomas Mentzel. 2016. “Loss of Fumarate Hydratase and Aberrant Protein Succination Detected With S-(2-Succino)-Cysteine Staining to Identify Patients With Multiple Cutaneous and Uterine Leiomyomatosis and Hereditary Leiomyomatosis and Renal Cell Cancer Syndrome.” *The American Journal of Dermatopathology*, April. doi:10.1097/DAD.0000000000000580.

Lokhorst, Henk M., Torben Plesner, Jacob P. Laubach, Hareth Nahi, Peter Gimsing, Markus Hansson, Monique C. Minnema, et al. 2015. “Targeting CD38 with Daratumumab Monotherapy in Multiple Myeloma.” *New England Journal of Medicine* 373 (13). Massachusetts Medical Society: 1207–19. doi:10.1056/NEJMoa1506348.

Loughery, Jayne E P, Philip D Dunne, Karla M O’Neill, Richard R Meehan, Jennifer R

McDaid, and Colum P Walsh. 2011. “DNMT1 Deficiency Triggers Mismatch Repair Defects in Human Cells through Depletion of Repair Protein Levels in a Process Involving the DNA Damage Response.” *Human Molecular Genetics* 20 (16): 3241–55. doi:10.1093/hmg/ddr236.

Love, Michael I, Wolfgang Huber, Simon Anders, I Lönnstedt, T Speed, MD Robinson, GK Smyth, et al. 2014. “Moderated Estimation of Fold Change and Dispersion for RNA-Seq Data with DESeq2.” *Genome Biology* 15 (12). BioMed Central: 550. doi:10.1186/s13059-014-0550-8.

Lu, Guangrong, Vasu Punj, and Preet M. Chaudhary. 2008. “Proteasome Inhibitor Bortezomib Induces Cell-Cycle Arrest and Apoptosis in Cell Lines Derived from Ewing’s Sarcoma Family of Tumors and Synergizes with TRAIL.” *Cancer Biology & Therapy* 7 (4). Landes Bioscience: 603–8. doi:10.4161/cbt.7.4.5564.

Lu, P J, K Sundquist, D Baeckstrom, R Poulsom, A Hanby, S Meier-Ewert, T Jones, et al. 1999. “A Novel Gene (PLU-1) Containing Highly Conserved Putative DNA/chromatin Binding Motifs Is Specifically up-Regulated in Breast Cancer.” *The Journal of Biological Chemistry* 274 (22): 15633–45. http://www.ncbi.nlm.nih.gov/pubmed/10336460.

Ludwig, C, D S Williams, D B Bartlett, S J Essex, G McNee, J W Allwood, E Jewell, et al. 2015. “Alterations in Bone Marrow Metabolism Are an Early and Consistent Feature during the Development of MGUS and Multiple Myeloma.” *Blood Cancer Journal* 5 (10). Nature Publishing Group: e359. doi:10.1038/bcj.2015.85.

Maiso, Patricia, Daisy Huynh, Michele Moschetta, Antonio Sacco, Yosra Aljawai, Yuji

Mishima, John M Asara, et al. 2015. “Metabolic Signature Identifies Novel Targets for Drug Resistance in Multiple Myeloma.” *Cancer Research* 75 (10). American Association for Cancer Research: 2071–82. doi:10.1158/0008-5472.CAN-14-3400.

Maláč, Kamil, and Ivan Barvík. 2013. “Complex between Human RNase HI and the Phosphonate-DNA/RNA Duplex: Molecular Dynamics Study.” *Journal of Molecular Graphics & Modelling* 44 (July): 81–90. doi:10.1016/j.jmgm.2013.05.004.

Mankin, H J, T A Lange, and S S Spanier. 1982. “The Hazards of Biopsy in Patients with Malignant Primary Bone and Soft-Tissue Tumors.” *The Journal of Bone and Joint Surgery. American Volume* 64 (8): 1121–27. http://www.ncbi.nlm.nih.gov/pubmed/7130225.

Mann, Bhupinder S, John R Johnson, Martin H Cohen, Robert Justice, and Richard Pazdur. 2007. “FDA Approval Summary: Vorinostat for Treatment of Advanced Primary Cutaneous T-Cell Lymphoma.” *The Oncologist* 12 (10): 1247–52. doi:10.1634/theoncologist.12-10-1247.

Mardis, Elaine R, Li Ding, David J Dooling, David E Larson, Michael D McLellan, Ken Chen, Daniel C Koboldt, et al. 2009. “Recurring Mutations Found by Sequencing an Acute Myeloid Leukemia Genome.” *The New England Journal of Medicine* 361 (11): 1058–66. doi:10.1056/NEJMoa0903840.

Margoshes, Marvin, and Bert L. Vallee. 1957. “A CADMIUM PROTEIN FROM EQUINE KIDNEY CORTEX.” *Journal of the American Chemical Society* 79 (17). American Chemical Society: 4813–14. doi:10.1021/ja01574a064.

Martinez-Garcia, Eva, and Jonathan D Licht. 2010. “Deregulation of H3K27 Methylation

in Cancer." *Nature Genetics* 42 (2). Nature Publishing Group: 100–101. doi:10.1038/ng0210-100.

Martinez, Victor D., Emily A. Vucic, Kelsie L. Thu, Roland Hubaux, Katey S.S. Enfield, Larissa A. Pikor, Daiana D. Becker-Santos, et al. 2015. "Unique Somatic and Malignant Expression Patterns Implicate PIWI-Interacting RNAs in Cancer-Type Specific Biology." *Scientific Reports* 5 (May). Nature Publishing Group: 10423. doi:10.1038/srep10423.

Marx, Vivien. 2015. "Visualizing Epigenomic Data." *Nature Methods* 12 (6): 499–502. doi:10.1038/nmeth.3409.

Mateos, María-Victoria, Miguel Granell, Albert Oriol, Joaquin Martinez-Lopez, Joan Blade, Miguel T. Hernandez, Jesus Martín, et al. 2016. "Elotuzumab in Combination with Thalidomide and Low-Dose Dexamethasone: A Phase 2 Single-Arm Safety Study in Patients with Relapsed/refractory Multiple Myeloma." *British Journal of Haematology*, July. doi:10.1111/bjh.14263.

May, W A, S L Lessnick, B S Braun, M Klemsz, B C Lewis, L B Lunsford, R Hromas, and C T Denny. 1993. "The Ewing's Sarcoma EWS/FLI-1 Fusion Gene Encodes a More Potent Transcriptional Activator and Is a More Powerful Transforming Gene than FLI-1." *Molecular and Cellular Biology* 13 (12): 7393–98. http://www.ncbi.nlm.nih.gov/pubmed/8246959.

McLaughlin-Drubin, Margaret E, Christopher P Crum, Karl Münger, and K Munger. 2011. "Human Papillomavirus E7 Oncoprotein Induces KDM6A and KDM6B Histone Demethylase Expression and Causes Epigenetic Reprogramming." *Proc Natl Acad Sci*

U S A 108 (5): 2130–35. doi:10.1073/pnas.1009933108.

Mirabella, F, P Wu, C P Wardell, M F Kaiser, B A Walker, D C Johnson, and G J Morgan. 2013. "MMSET Is the Key Molecular Target in t(4;14) Myeloma." *Blood Cancer Journal* 3 (5). Nature Publishing Group: e114. doi:10.1038/bcj.2013.9.

Moreau, Philippe, Michel Attal, Thierry Facon, N. Howlade, A. Noone, M. Krapcho, N. Becker, et al. 2015. "Frontline Therapy of Multiple Myeloma." *Blood* 125 (20). American Society of Hematology: 3076–84. doi:10.1182/blood-2014-09-568915.

Morgan, Gareth J, Brian A Walker, and Faith E Davies. 2012. "The Genetic Architecture of Multiple Myeloma." *Nature Reviews. Cancer* 12 (5): 335–48. doi:10.1038/nrc3257.

Morin, Ryan D, Nathalie A Johnson, Tesa M Severson, Andrew J Mungall, Jianghong An, Rodrigo Goya, Jessica E Paul, et al. 2010. "Somatic Mutations Altering EZH2 (Tyr641) in Follicular and Diffuse Large B-Cell Lymphomas of Germinal-Center Origin." *Nature Genetics* 42 (2): 181–85. doi:10.1038/ng.518.

Morishita, Masayo, Damiaan Mevius, and Eric di Luccio. 2014. "In Vitro Histone Lysine Methylation by NSD1, NSD2/MMSET/WHSC1 and NSD3/WHSC1L." *BMC Structural Biology* 14: 25. doi:10.1186/s12900-014-0025-x.

Murr, Rabih. 2010. "Interplay between Different Epigenetic Modifications and Mechanisms." *Advances in Genetics* 70: 101–41. doi:10.1016/B978-0-12-380866-0.60005-8.

Nakashima, Hiroyuki, Tohru Kimura, Yoshiaki Kaga, Tsunetoshi Nakatani, Yoshiyuki Seki, Toshinobu Nakamura, and Toru Nakano. 2013. "Effects of dppa3 on DNA

Methylation Dynamics during Primordial Germ Cell Development in Mice." *Biology of Reproduction* 88 (5): 125. doi:10.1095/biolreprod.112.105932.

Nakatani, Fumihiko, Kazuhiro Tanaka, Riku Sakimura, Yoshihiro Matsumoto, Tomoya Matsunobu, Xu Li, Masuo Hanada, Takamitsu Okada, and Yukihide Iwamoto. 2003. "Identification of p21WAF1/CIP1 as a Direct Target of EWS-Fli1 Oncogenic Fusion Protein." *The Journal of Biological Chemistry* 278 (17): 15105–15. doi:10.1074/jbc.M211470200.

Nathan, Dafna, Kristin Ingvarsdottir, David E Sterner, Gwendolyn R Bylebyl, Milos Dokmanovic, Jean A Dorsey, Kelly A Whelan, et al. 2006. "Histone Sumoylation Is a Negative Regulator in Saccharomyces Cerevisiae and Shows Dynamic Interplay with Positive-Acting Histone Modifications." *Genes & Development* 20 (8): 966–76. doi:10.1101/gad.1404206.

National Cancer Intelligence Network. 2012. "Bone Sarcoma Incidence and Survival." http://www.wmciu.nhs.uk/documents/ReportR1205_BoneSarcomaIncidenceAndSurvival.pdf.

Nègre, Vincent, Thierry Hôtelier, Anne-Nathalie Volkoff, Sylvie Gimenez, François Cousserans, Kazuei Mita, Xavier Sabau, et al. 2006. "SPODOBASE : An EST Database for the Lepidopteran Crop Pest Spodoptera." *BMC Bioinformatics* 7 (1). BioMed Central: 322. doi:10.1186/1471-2105-7-322.

Neri, Giovanni, and Emanuela Lucci-Cordisco. 2009. "Silent Beginning: Early Silencing of the MED1/MBD4 Gene in Colorectal Tumorigenesis." *http://dx.doi.org/10.4161/cbt.8.2.7647*. Taylor & Francis.

Nguyen, Anh Tram, Olena Taranova, Jin He, and Yi Zhang. 2011. “DOT1L, the H3K79 Methyltransferase, Is Required for MLL-AF9-Mediated Leukemogenesis.” *Blood* 117 (25): 6912–22. doi:10.1182/blood-2011-02-334359.

Nikrad, Malti, Thomas Johnson, Hamsa Puthalalath, Leigh Coultas, Jerry Adams, and Andrew S Kraft. 2005. “The Proteasome Inhibitor Bortezomib Sensitizes Cells to Killing by Death Receptor Ligand TRAIL via BH3-Only Proteins Bik and Bim.” *Molecular Cancer Therapeutics* 4 (3): 443–49. doi:10.1158/1535-7163.MCT-04-0260.

Norris, Robin E, Peter C Adamson, Vu T Nguyen, and Elizabeth Fox. 2014. “Preclinical Evaluation of the PARP Inhibitor, Olaparib, in Combination with Cytotoxic Chemotherapy in Pediatric Solid Tumors.” *Pediatric Blood & Cancer* 61 (1): 145–50. doi:10.1002/pbc.24697.

Nottke, Amanda, Mónica P Colaiácovo, and Yang Shi. 2009. “Developmental Roles of the Histone Lysine Demethylases.” *Development (Cambridge, England)* 136 (6): 879–89. doi:10.1242/dev.020966.

Nowak, Scott J, and Victor G Corces. 2004. “Phosphorylation of Histone H3: A Balancing Act between Chromosome Condensation and Transcriptional Activation.” *Trends in Genetics : TIG* 20 (4): 214–20. doi:10.1016/j.tig.2004.02.007.

Ntziachristos, Panagiotis, Aristotelis Tsirigos, G. Grant Welstead, Thomas Trimarchi, Sofia Bakogianni, Luyao Xu, Evangelia Loizou, et al. 2014. “Contrasting Roles of Histone 3 Lysine 27 Demethylases in Acute Lymphoblastic Leukaemia.” *Nature*, August. Nature Publishing Group. doi:10.1038/nature13605.

Oba, Yasuo, Jun Won Lee, Lori A Ehrlich, Ho Yeon Chung, Diane F Jelinek, Natalie S Callander, Richard Horuk, Sun Jin Choi, and G David Roodman. 2005. "MIP-1alpha Utilizes Both CCR1 and CCR5 to Induce Osteoclast Formation and Increase Adhesion of Myeloma Cells to Marrow Stromal Cells." *Experimental Hematology* 33 (3): 272–78. doi:10.1016/j.exphem.2004.11.015.

Obeng, E A, L M Carlson, D M Gutman, W J Harrington Jr., K P Lee, and L H Boise. 2006. "Proteasome Inhibitors Induce a Terminal Unfolded Protein Response in Multiple Myeloma Cells." *Blood* 107 (12): 4907–16. doi:2005-08-3531 [pii]10.1182/blood-2005-08-3531.

Ohta, Katsuya, Naotsugu Haraguchi, Yoshihiro Kano, Yoshinori Kagawa, Masamitsu Konno, Shimpei Nishikawa, Atsushi Hamabe, et al. 2013. "Depletion of JARID1B Induces Cellular Senescence in Human Colorectal Cancer." *International Journal of Oncology* 42 (4): 1212–18. doi:10.3892/ijo.2013.1799.

Okano, Masaki, Daphne W Bell, Daniel A Haber, and En Li. 1999. "DNA Methyltransferases Dnmt3a and Dnmt3b Are Essential for De Novo Methylation and Mammalian Development." *Cell* 99 (3): 247–57. doi:10.1016/S0092-8674(00)81656-6.

Ono, Ryoichi, Tomohiko Taki, Takeshi Taketani, Masafumi Taniwaki, Hajime Kobayashi, and Yasuhide Hayashi. 2002. "LCX, Leukemia-Associated Protein with a CXXC Domain, Is Fused to MLL in Acute Myeloid Leukemia with Trilineage Dysplasia Having t(10;11)(q22;q23)." *Cancer Research* 62 (14): 4075–80. http://www.ncbi.nlm.nih.gov/pubmed/12124344.

Orlando, David A, Mei Wei Chen, Victoria E Brown, Snehakumari Solanki, Yoon J Choi, Eric R Olson, Christian C Fritz, et al. 2014. “Quantitative ChIP-Seq Normalization Reveals Global Modulation of the Epigenome.” *Cell Reports* 9 (3). Elsevier: 1163–70. doi:10.1016/j.celrep.2014.10.018.

Orthaus, S, K Klement, N Happel, C Hoischen, and S Diekmann. 2009. “Linker Histone H1 Is Present in Centromeric Chromatin of Living Human Cells next to Inner Kinetochore Proteins.” *Nucleic Acids Research* 37 (10): 3391–3406. doi:10.1093/nar/gkp199.

Orum, H, and J Wengel. 2001. “Locked Nucleic Acids: A Promising Molecular Family for Gene-Function Analysis and Antisense Drug Development.” *Curr Opin Mol Ther* 3 (3): 239–43. http://www.ncbi.nlm.nih.gov/entrez/query.fcgi?cmd=Retrieve&db=PubMed&dopt=Citation&list_uids=11497347.

Otani, Junji, Toshiyuki Nankumo, Kyohei Arita, Susumu Inamoto, Mariko Ariyoshi, and Masahiro Shirakawa. 2009. “Structural Basis for Recognition of H3K4 Methylation Status by the DNA Methyltransferase 3A ATRX-DNMT3-DNMT3L Domain.” *EMBO Reports* 10 (11): 1235–41. doi:10.1038/embor.2009.218.

Paget, Stephen. 1889. “The Distribution of Secondary Growths In Cancer of the Breast.” *The Lancet* 133 (3421). Elsevier: 571–73. doi:10.1016/S0140-6736(00)49915-0.

Painuly, Utkarsh, and Shaji Kumar. 2013. “Efficacy of Bortezomib as First-Line Treatment for Patients with Multiple Myeloma.” *Clinical Medicine Insights. Oncology* 7. Libertas Academica: 53–73. doi:10.4137/CMO.S7764.

Palanichamy, Jayanth Kumar, and Dinesh S Rao. 2014. “miRNA Dysregulation in Cancer: Towards a Mechanistic Understanding.” *Frontiers in Genetics* 5. Frontiers Media SA: 54. doi:10.3389/fgene.2014.00054.

Pallante, Pierlorenzo, Antonella Federico, Maria Teresa Berlingieri, Mimma Bianco, Angelo Ferraro, Floriana Forzati, Antonino Iaccarino, et al. 2008. “Loss of the CBX7 Gene Expression Correlates with a Highly Malignant Phenotype in Thyroid Cancer.” *Cancer Research* 68 (16): 6770–78. doi:10.1158/0008-5472.CAN-08-0695.

Palumbo, A., H. Avet-Loiseau, S. Oliva, H. M. Lokhorst, H. Goldschmidt, L. Rosinol, P. Richardson, et al. 2015. “Revised International Staging System for Multiple Myeloma: A Report From International Myeloma Working Group.” *Journal of Clinical Oncology* 33 (26). American Society of Clinical Oncology: 2863–69. doi:10.1200/JCO.2015.61.2267.

Palumbo, Antonio, Asher Chanan-Khan, Katja Weisel, Ajay K. Nooka, Tamas Masszi, Meral Beksac, Ivan Spicka, et al. 2016. “Daratumumab, Bortezomib, and Dexamethasone for Multiple Myeloma.” *New England Journal of Medicine* 375 (8). Massachusetts Medical Society: 754–66. doi:10.1056/NEJMoa1606038.

Pansuriya, Twinkal C, Ronald van Eijk, Pio d’Adamo, Maayke A J H van Ruler, Marieke L Kuijjer, Jan Oosting, Anne-Marie Cleton-Jansen, et al. 2011. “Somatic Mosaic IDH1 and IDH2 Mutations Are Associated with Enchondroma and Spindle Cell Hemangioma in Ollier Disease and Maffucci Syndrome.” *Nature Genetics* 43 (12): 1256–61. doi:10.1038/ng.1004.

Parsons, D Williams, Siân Jones, Xiaosong Zhang, Jimmy Cheng-Ho Lin, Rebecca J

Leary, Philipp Angenendt, Parminder Mankoo, et al. 2008. “An Integrated Genomic Analysis of Human Glioblastoma Multiforme.” *Science (New York, N.Y.)* 321 (5897): 1807–12. doi:10.1126/science.1164382.

Patel, Dinshaw J., and Zhanxin Wang. 2013. “Readout of Epigenetic Modifications.” *http://dx.doi.org/10.1146/annurev-Biochem-072711-165700*. Annual Reviews .

Patel, Nikul, Jennifer Black, Xi Chen, A Mario Marcondes, William M Grady, Elizabeth R Lawlor, and Scott C Borinstein. 2012. “DNA Methylation and Gene Expression Profiling of Ewing Sarcoma Primary Tumors Reveal Genes That Are Potential Targets of Epigenetic Inactivation.” *Sarcoma* 2012. Hindawi Publishing Corporation: 498472. doi:10.1155/2012/498472.

Patra, Krushna C., and Nissim Hay. 2014. “The Pentose Phosphate Pathway and Cancer.” *Trends in Biochemical Sciences* 39 (8): 347–54. doi:10.1016/j.tibs.2014.06.005.

Pertea, Mihaela, Daehwan Kim, Geo M Pertea, Jeffrey T Leek, and Steven L Salzberg. 2016. “Transcript-Level Expression Analysis of RNA-Seq Experiments with HISAT, StringTie and Ballgown.” *Nature Protocols* 11 (9): 1650–67. doi:10.1038/nprot.2016.095.

Petermann, R, B M Mossier, D N Aryee, V Khazak, E A Golemis, and H Kovar. 1998. “Oncogenic EWS-Fli1 Interacts with hsRPB7, a Subunit of Human RNA Polymerase II.” *Oncogene* 17 (5): 603–10. doi:10.1038/sj.onc.1201964.

Prideaux, Steven M., Emma Conway O’Brien, Timothy J. Chevassut, Steven M. Prideaux, Emma Conway O’Brien, and Timothy J. Chevassut. 2014. “The Genetic Architecture of Multiple Myeloma.” *Advances in Hematology* 2014. Hindawi Publishing

Corporation: 1–16. doi:10.1155/2014/864058.

Qi, Jin, Lei Huo, Yiwei Tony Zhu, and Yi-Jun Zhu. 2014. “Absent, Small or Homeotic 2-like Protein (ASH2L) Enhances the Transcription of the Estrogen Receptor α Gene through GATA-Binding Protein 3 (GATA3).” *The Journal of Biological Chemistry* 289 (45): 31373–81. doi:10.1074/jbc.M114.579839.

Qing, Guoliang, Bo Li, Annette Vu, Nicolas Skuli, Zandra E Walton, Xueyuan Liu, Patrick A Mayes, et al. 2012. “ATF4 Regulates MYC-Mediated Neuroblastoma Cell Death upon Glutamine Deprivation.” *Cancer Cell* 22 (5): 631–44. doi:10.1016/j.ccr.2012.09.021.

Quinlan, Aaron R, and Ira M Hall. 2010. “BEDTools: A Flexible Suite of Utilities for Comparing Genomic Features.” *Bioinformatics (Oxford, England)* 26 (6): 841–42. doi:10.1093/bioinformatics/btq033.

Rajkumar, S Vincent. 2016. “Multiple Myeloma: 2016 Update on Diagnosis, Risk-Stratification, and Management.” *American Journal of Hematology* 91 (7): 719–34. doi:10.1002/ajh.24402.

Rajkumar, S Vincent, Meletios A Dimopoulos, Antonio Palumbo, Joan Blade, Giampaolo Merlini, María-Victoria Mateos, Shaji Kumar, et al. 2014. “International Myeloma Working Group Updated Criteria for the Diagnosis of Multiple Myeloma.” *The Lancet Oncology* 15 (12): e538–48. doi:10.1016/S1470-2045(14)70442-5.

Rajkumar, S Vincent, Susanna Jacobus, Natalie S Callander, Rafael Fonseca, David H Vesole, Michael E Williams, Rafat Abonour, et al. 2010. “Lenalidomide plus High-Dose Dexamethasone versus Lenalidomide plus Low-Dose Dexamethasone as Initial

Therapy for Newly Diagnosed Multiple Myeloma: An Open-Label Randomised Controlled Trial." *The Lancet. Oncology* 11 (1): 29–37. doi:10.1016/S1470-2045(09)70284-0.

Ramaglia, Maria, Velia D'Angelo, Adriana Iannotta, Daniela Di Pinto, Elvira Pota, Maria Carmen Affinita, Vittoria Donofrio, et al. 2016. "High EZH2 Expression Is Correlated to Metastatic Disease in Pediatric Soft Tissue Sarcomas." *Cancer Cell International* 16 (1). BioMed Central: 59. doi:10.1186/s12935-016-0338-x.

Rao, Mahadev, Nachimuthu Chinnasamy, Julie A Hong, Yuwei Zhang, Mary Zhang, Sichuan Xi, Fang Liu, Victor E Marquez, Richard A Morgan, and David S Schrump. 2011. "Inhibition of Histone Lysine Methylation Enhances Cancer-Testis Antigen Expression in Lung Cancer Cells: Implications for Adoptive Immunotherapy of Cancer." *Cancer Research* 71 (12): 4192–4204. doi:10.1158/0008-5472.CAN-10-2442.

Ren, Xiaojun, Claudius Vincenz, and Tom K. Kerppola. 2008. "Changes in the Distributions and Dynamics of Polycomb Repressive Complexes during Embryonic Stem Cell Differentiation." 28 (9). American Society for Microbiology. doi:10.1128/MCB.00949-07.

Richter, Günther H S, Stephanie Plehm, Annette Fasan, Sabine Rössler, Rebekka Unland, Idriss M Bennani-Baiti, Marc Hotfilder, et al. 2009. "EZH2 Is a Mediator of EWS/FLI1 Driven Tumor Growth and Metastasis Blocking Endothelial and Neuro-Ectodermal Differentiation." *Proceedings of the National Academy of Sciences of the United States of America* 106 (13): 5324–29. doi:10.1073/pnas.0810759106.

Riggi, Nicolò, Mario-Luca Suvà, Domizio Suvà, Luisa Cironi, Paolo Provero, Stéphane Tercier, Jean-Marc Joseph, et al. 2008. "EWS-FLI-1 Expression Triggers a Ewing's Sarcoma Initiation Program in Primary Human Mesenchymal Stem Cells." *Cancer Research* 68 (7). American Association for Cancer Research: 2176–85. doi:10.1158/0008-5472.CAN-07-1761.

Rose, Nathan R., and Robert J. Klose. 2014. "Understanding the Relationship between DNA Methylation and Histone Lysine Methylation." *Biochimica et Biophysica Acta* 1839 (12): 1362–72. doi:10.1016/j.bbagrm.2014.02.007.

Rotem, Assaf, Oren Ram, Noam Shoresh, Ralph A Sperling, Alon Goren, David A Weitz, and Bradley E Bernstein. 2015. "Single-Cell ChIP-Seq Reveals Cell Subpopulations Defined by Chromatin State." *Nature Biotechnology* 33 (11): 1165–72. doi:10.1038/nbt.3383.

Saito, Motoki, and Fuyuki Ishikawa. 2002. "The mCpG-Binding Domain of Human MBD3 Does Not Bind to mCpG but Interacts with NuRD/Mi2 Components HDAC1 and MTA2." *The Journal of Biological Chemistry* 277 (38): 35434–39. doi:10.1074/jbc.M203455200.

Sakaki, Hirotsugu, Masashi Okada, Kenta Kuramoto, Hiroyuki Takeda, Hikaru Watarai, Shuhei Suzuki, Shizuka Seino, et al. 2015. "GSKJ4, A Selective Jumonji H3K27 Demethylase Inhibitor, Effectively Targets Ovarian Cancer Stem Cells." *Anticancer Research* 35 (12): 6607–14. http://www.ncbi.nlm.nih.gov/pubmed/26637876.

Saksouk, Nehmé, Elisabeth Simboeck, Jérôme Déjardin, A Eymery, M Callanan, C Vourc'h, MG Schueler, et al. 2015. "Constitutive Heterochromatin Formation and

Transcription in Mammals." *Epigenetics & Chromatin* 8 (1). BioMed Central: 3. doi:10.1186/1756-8935-8-3.

Sánchez-Romero, María A, Ignacio Cota, and Josep Casadesús. 2015. "DNA Methylation in Bacteria: From the Methyl Group to the Methylome." *Current Opinion in Microbiology* 25 (June): 9–16. doi:10.1016/j.mib.2015.03.004.

Sankar, S, R Bell, B Stephens, R Zhuo, S Sharma, D J Bearss, and S L Lessnick. 2013. "Mechanism and Relevance of EWS/FLI-Mediated Transcriptional Repression in Ewing Sarcoma." *Oncogene* 32 (42). NIH Public Access: 5089–5100. doi:10.1038/onc.2012.525.

Sankar, Savita, and Stephen L. Lessnick. 2011. "Promiscuous Partnerships in Ewing's Sarcoma." *Cancer Genetics* 204 (7): 351–65. doi:10.1016/j.cancergen.2011.07.008.

Schilder, R J, L Hall, A Monks, L M Handel, A J Fornace, R F Ozols, A T Fojo, and T C Hamilton. 1990. "Metallothionein Gene Expression and Resistance to Cisplatin in Human Ovarian Cancer." *International Journal of Cancer* 45 (3): 416–22. http://www.ncbi.nlm.nih.gov/pubmed/2307530.

Schroeder, Andreas, Odilo Mueller, Susanne Stocker, Ruediger Salowsky, Michael Leiber, Marcus Gassmann, Samar Lightfoot, et al. 2006. "The RIN: An RNA Integrity Number for Assigning Integrity Values to RNA Measurements." *BMC Molecular Biology* 7 (1). BioMed Central: 3. doi:10.1186/1471-2199-7-3.

Schuettengruber, B, A M Martinez, N Iovino, and G Cavalli. 2011. "Trithorax Group Proteins: Switching Genes on and Keeping Them Active." *Nat Rev Mol Cell Biol* 12 (12): 799–814. doi:nrm3230 [pii]10.1038/nrm3230.

Schulz, Marcel H, David Weese, Manuel Holtgrewe, Viktoria Dimitrova, Sijia Niu, Knut Reinert, and Hugues Richard. 2014. “Fiona: A Parallel and Automatic Strategy for Read Error Correction.” *Bioinformatics (Oxford, England)* 30 (17): i356-63. doi:10.1093/bioinformatics/btu440.

Schwartz, Yuri B., and Vincenzo Pirrotta. 2013. “A New World of Polycombs: Unexpected Partnerships and Emerging Functions.” *Nature Reviews Genetics* 14 (12). Nature Publishing Group: 853–64. doi:10.1038/nrg3603.

Schwartzentruber, Jeremy, Andrey Korshunov, Xiao-Yang Liu, David T W Jones, Elke Pfaff, Karine Jacob, Dominik Sturm, et al. 2012. “Driver Mutations in Histone H3.3 and Chromatin Remodelling Genes in Paediatric Glioblastoma.” *Nature* 482 (7384): 226–31. doi:10.1038/nature10833.

Scibetta, Angelo G, Samantha Santangelo, Julia Coleman, Debbie Hall, Tracy Chaplin, John Copier, Steve Catchpole, Joy Burchell, and Joyce Taylor-Papadimitriou. 2007. “Functional Analysis of the Transcription Repressor PLU-1/JARID1B.” *Molecular and Cellular Biology* 27 (20): 7220–35. doi:10.1128/MCB.00274-07.

Scott, Clare L, Jésus Gil, Eva Hernando, Julie Teruya-Feldstein, Masako Narita, Dolores Martínez, Tapio Visakorpi, et al. 2007. “Role of the Chromobox Protein CBX7 in Lymphomagenesis.” *Proceedings of the National Academy of Sciences of the United States of America* 104 (13): 5389–94. doi:10.1073/pnas.0608721104.

Shankar, Ganesh M, Nina Lelic, Corey M Gill, Aaron R Thorner, Paul Van Hummelen, Jeffrey H Wisoff, Jay S Loeffler, et al. 2016. “BRAF Alteration Status and the Histone H3F3A Gene K27M Mutation Segregate Spinal Cord Astrocytoma Histology.” *Acta*

Neuropathologica 131 (1): 147–50. doi:10.1007/s00401-015-1492-2.

Shpargel, Karl B, Toru Sengoku, Shigeyuki Yokoyama, and Terry Magnuson. 2012. "UTX and UTY Demonstrate Histone Demethylase-Independent Function in Mouse Embryonic Development." *PLoS Genetics* 8 (9): e1002964. doi:10.1371/journal.pgen.1002964.

Sidrauski, C, D Acosta-Alvear, A Khoutorsky, P Vedantham, B R Hearn, H Li, K Gamache, et al. 2013. "Pharmacological Brake-Release of mRNA Translation Enhances Cognitive Memory." *Elife* 2: e00498. doi:10.7554/eLife.0049800498 [pii].

Siegel, D S, P Richardson, M Dimopoulos, P Moreau, C Mitsiades, D Weber, J Houp, et al. 2014. "Vorinostat in Combination with Lenalidomide and Dexamethasone in Patients with Relapsed or Refractory Multiple Myeloma." *Blood Cancer Journal* 4 (2). Nature Publishing Group: e182. doi:10.1038/bcj.2014.1.

Singhal, Seema, Jayesh Mehta, Raman Desikan, Dan Ayers, Paula Roberson, Paul Eddlemon, Nikhil Munshi, et al. 1999. "Antitumor Activity of Thalidomide in Refractory Multiple Myeloma." *New England Journal of Medicine* 341 (21). Massachusetts Medical Society : 1565–71. doi:10.1056/NEJM199911183412102.

Slany, Astrid, Verena Haudek-Prinz, Anastasia Meshcheryakova, Andrea Bileck, Wolfgang Lamm, Christoph Zielinski, Christopher Gerner, and Johannes Drach. 2014. "Extracellular Matrix Remodeling by Bone Marrow Fibroblast-like Cells Correlates with Disease Progression in Multiple Myeloma." *Journal of Proteome Research* 13 (2). American Chemical Society: 844–54. doi:10.1021/pr400881p.

Smith, Richard, Leah A Owen, Deborah J Trem, Jenny S Wong, Jennifer S Whangbo,

Todd R Golub, and Stephen L Lessnick. 2006. “Expression Profiling of EWS/FLI Identifies NKX2.2 as a Critical Target Gene in Ewing’s Sarcoma.” *Cancer Cell* 9 (5): 405–16. doi:10.1016/j.ccr.2006.04.004.

Spahn, Laura, Robert Petermann, Christine Siligan, Johannes A Schmid, Dave N T Aryee, and Heinrich Kovar. 2002. “Interaction of the EWS NH2 Terminus with BARD1 Links the Ewing’s Sarcoma Gene to a Common Tumor Suppressor Pathway.” *Cancer Research* 62 (16): 4583–87. http://www.ncbi.nlm.nih.gov/pubmed/12183411.

Stanton, Robert C. 2012. “Glucose-6-Phosphate Dehydrogenase, NADPH, and Cell Survival.” *IUBMB Life* 64 (5): 362–69. doi:10.1002/iub.1017.

Steffen, Philipp A., and Leonie Ringrose. 2014. “What Are Memories Made of? How Polycomb and Trithorax Proteins Mediate Epigenetic Memory.” *Nature Reviews Molecular Cell Biology* 15 (5). Nature Publishing Group: 340–56. doi:10.1038/nrm3789.

Stein, C A, J Bo Hansen, Johnathan Lai, SiJian Wu, Anatoliy Voskresenskiy, Anja Høg, Jesper Worm, et al. 2010. “Efficient Gene Silencing by Delivery of Locked Nucleic Acid Antisense Oligonucleotides, Unassisted by Transfection Reagents.” *Nucleic Acids Research* 38 (1). Oxford University Press: e3. doi:10.1093/nar/gkp841.

Sterner, D. E., and S. L. Berger. 2000. “Acetylation of Histones and Transcription-Related Factors.” *Microbiology and Molecular Biology Reviews* 64 (2). American Society for Microbiology: 435–59. doi:10.1128/MMBR.64.2.435-459.2000.

Sturm, Dominik, Hendrik Witt, Volker Hovestadt, Dong-Anh Khuong-Quang, David T W Jones, Carolin Konermann, Elke Pfaff, et al. 2012. “Hotspot Mutations in H3F3A and

IDH1 Define Distinct Epigenetic and Biological Subgroups of Glioblastoma." *Cancer Cell* 22 (4): 425–37. doi:10.1016/j.ccr.2012.08.024.

Subramaniam, Dharmalingam, Ravi Thombre, Animesh Dhar, and Shrikant Anant. 2014. "DNA Methyltransferases: A Novel Target for Prevention and Therapy." *Frontiers in Oncology* 4 (May). Frontiers: 80. doi:10.3389/fonc.2014.00080.

Suzuki, MM, and A Bird. 2008. "DNA Methylation Landscapes: Provocative Insights from Epigenomics." *Nature Reviews Genetics*. http://www.nature.com/nrg/journal/v9/n6/abs/nrg2341.html.

Takahashi, Shinichiro. 2015. "Positive and Negative Regulators of the Metallothionein Gene (Review)." *Molecular Medicine Reports* 12 (1). Spandidos Publications: 795–99. doi:10.3892/mmr.2015.3459.

Tanaka, K, T Iwakuma, K Harimaya, H Sato, and Y Iwamoto. 1997. "EWS-Fli1 Antisense Oligodeoxynucleotide Inhibits Proliferation of Human Ewing's Sarcoma and Primitive Neuroectodermal Tumor Cells." *Journal of Clinical Investigation* 99 (2). American Society for Clinical Investigation: 239–47. doi:10.1172/JCI119152.

Toretsky, Jeffrey A, Verda Erkizan, Amy Levenson, Ogan D Abaan, Jeffrey D Parvin, Timothy P Cripe, Anna M Rice, Sean Bong Lee, and Aykut Uren. 2006. "Oncoprotein EWS-FLI1 Activity Is Enhanced by RNA Helicase A." *Cancer Research* 66 (11): 5574–81. doi:10.1158/0008-5472.CAN-05-3293.

Turc-Carel, Claude, Alain Aurias, Francine Mugneret, Sarab Lizard, Isabelle Sidaner, Christian Volk, Jean Paul Thiery, et al. 1988. "Chromosomes in Ewing's Sarcoma. I. An Evaluation of 85 Cases and Remarkable Consistency of t(11;22)(q24;q12)."

Cancer Genetics and Cytogenetics 32 (2). Elsevier: 229–38. doi:10.1016/0165-4608(88)90285-3.

Uren, A, M S Merchant, C J Sun, M I Vitolo, Y Sun, M Tsokos, P B Illei, et al. 2003. "Beta-Platelet-Derived Growth Factor Receptor Mediates Motility and Growth of Ewing's Sarcoma Cells." *Oncogene* 22 (15): 2334–42. doi:10.1038/sj.onc.1206330.

Vaissière, Thomas, Carla Sawan, and Zdenko Herceg. 2008. "Epigenetic Interplay between Histone Modifications and DNA Methylation in Gene Silencing." *Mutation Research/Reviews in Mutation Research* 659 (1): 40–48. doi:10.1016/j.mrrev.2008.02.004.

Vallet, S, S Pozzi, K Patel, N Vaghela, M T Fulciniti, P Veiby, T Hideshima, et al. 2011. "A Novel Role for CCL3 (MIP-1α) in Myeloma-Induced Bone Disease via Osteocalcin Downregulation and Inhibition of Osteoblast Function." *Leukemia* 25 (7): 1174–81. doi:10.1038/leu.2011.43.

van Haaften, Gijs, Gillian L Dalgliesh, Helen Davies, Lina Chen, Graham Bignell, Chris Greenman, Sarah Edkins, et al. 2009. "Somatic Mutations of the Histone H3K27 Demethylase Gene UTX in Human Cancer." *Nature Genetics* 41 (5): 521–23. doi:10.1038/ng.349.

van Heesch, Sebastiaan, Wigard P Kloosterman, Nico Lansu, Frans-Paul Ruzius, Elizabeth Levandowsky, Clarence C Lee, Shiguo Zhou, et al. 2013. "Improving Mammalian Genome Scaffolding Using Large Insert Mate-Pair next-Generation Sequencing." *BMC Genomics* 14 (1). BioMed Central: 257. doi:10.1186/1471-2164-14-257.

van Maldegem, Annemiek M., Judith V.M.G. Bovée, Elleke F.P. Peterse, Pancras C.W.

Hogendoorn, and Hans Gelderblom. 2016. “Ewing Sarcoma: The Clinical Relevance of the Insulin-like Growth Factor 1 and the Poly-ADP-Ribose-Polymerase Pathway.” *European Journal of Cancer* 53: 171–80. doi:10.1016/j.ejca.2015.09.009.

Varettoni, M., A. Corso, G. Pica, S. Mangiacavalli, C. Pascutto, and M. Lazzarino. 2010. “Incidence, Presenting Features and Outcome of Extramedullary Disease in Multiple Myeloma: A Longitudinal Study on 1003 Consecutive Patients.” *Annals of Oncology* 21 (2). Oxford University Press: 325–30. doi:10.1093/annonc/mdp329.

Varriale, Annalisa, and Giorgio Bernardi. 2010. “Distribution of DNA Methylation, CpGs, and CpG Islands in Human Isochores.” *Genomics* 95 (1): 25–28. doi:10.1016/j.ygeno.2009.09.006.

Viré, Emmanuelle, Carmen Brenner, Rachel Deplus, Loïc Blanchon, Mario Fraga, Céline Didelot, Lluis Morey, et al. 2006. “The Polycomb Group Protein EZH2 Directly Controls DNA Methylation.” *Nature* 439 (7078): 871–74. doi:10.1038/nature04431.

Voigt, Philipp, Wee-Wei Tee, and Danny Reinberg. 2013. “A Double Take on Bivalent Promoters.” *Genes & Development* 27 (12): 1318–38. doi:10.1101/gad.219626.113.

Waddington, C. 1942. “The Epigenotype.” *Endeavour* 1: 18–19.

Waldron, Kevin J., and Nigel J. Robinson. 2009. “How Do Bacterial Cells Ensure That Metalloproteins Get the Correct Metal?” *Nature Reviews Microbiology* 7 (1). Nature Publishing Group: 25–35. doi:10.1038/nrmicro2057.

Walport, Louise J, Richard J Hopkinson, Melanie Vollmar, Sarah K Madden, Carina Gileadi, Udo Oppermann, Christopher J Schofield, and Catrine Johansson. 2014.

"Human UTY(KDM6C) Is a Male-Specific Nϵ-Methyl Lysyl-Demethylase." *The Journal of Biological Chemistry*, May. doi:10.1074/jbc.M114.555052.

Wang, Hengbin, Liangjun Wang, Hediye Erdjument-Bromage, Miguel Vidal, Paul Tempst, Richard S Jones, and Yi Zhang. 2004. "Role of Histone H2A Ubiquitination in Polycomb Silencing." *Nature* 431 (7010): 873–78. doi:10.1038/nature02985.

Wapenaar, Hannah, and Frank J Dekker. 2016. "Histone Acetyltransferases: Challenges in Targeting Bi-Substrate Enzymes." *Clinical Epigenetics* 8: 59. doi:10.1186/s13148-016-0225-2.

Watson, D K, L Robinson, D R Hodge, I Kola, T S Papas, and A Seth. 1997. "FLI1 and EWS-FLI1 Function as Ternary Complex Factors and ELK1 and SAP1a Function as Ternary and Quaternary Complex Factors on the Egr1 Promoter Serum Response Elements." *Oncogene* 14 (2): 213–21. doi:10.1038/sj.onc.1200839.

Watson, J. D., and F. H. C. Crick. 1953. "Molecular Structure of Nucleic Aids: A Structure for Deoxyribose Nucleic Acid." *Nature* 171 (4356): 737–38. doi:10.1176/appi.ajp.160.4.623.

West, Adrian K, Juan Hidalgo, Donnie Eddins, Edward D Levin, and Michael Aschner. 2008. "Metallothionein in the Central Nervous System: Roles in Protection, Regeneration and Cognition." *Neurotoxicology* 29 (3). NIH Public Access: 489–503. doi:10.1016/j.neuro.2007.12.006.

West, Alison C., Ricky W. Johnstone, CA Olsen, MJ Tan, S Spange, T Wagner, T Heinzel, et al. 2014. "New and Emerging HDAC Inhibitors for Cancer Treatment." *Journal of Clinical Investigation* 124 (1). American Society for Clinical Investigation: 30–39.

doi:10.1172/JCI69738.

Wetzel, Joshua, Carl Kingsford, and Mihai Pop. 2011. “Assessing the Benefits of Using Mate-Pairs to Resolve Repeats in de Novo Short-Read Prokaryotic Assemblies.” *BMC Bioinformatics* 12: 95. doi:10.1186/1471-2105-12-95.

Wong, Ping-Pui, Fabrizio Miranda, KaYi V Chan, Chiara Berlato, Helen C Hurst, and Angelo G Scibetta. 2012. “Histone Demethylase KDM5B Collaborates with TFAP2C and Myc to Repress the Cell Cycle Inhibitor p21(cip) (CDKN1A).” *Molecular and Cellular Biology* 32 (9): 1633–44. doi:10.1128/MCB.06373-11.

Wu, Xudong, Jens Vilstrup Johansen, and Kristian Helin. 2013. “Fbxl10/Kdm2b Recruits Polycomb Repressive Complex 1 to CpG Islands and Regulates H2A Ubiquitylation.” *Molecular Cell* 49 (6): 1134–46. doi:10.1016/j.molcel.2013.01.016.

Wu, Yansheng, Li Zhang, Yang Wang, Hui Li, Xiubao Ren, Feng Wei, Wenwen Yu, et al. 2014. “Long Noncoding RNA HOTAIR Involvement in Cancer.” *Tumour Biology : The Journal of the International Society for Oncodevelopmental Biology and Medicine*, August. doi:10.1007/s13277-014-2523-7.

Xiang, Yang, Ziqi Zhu, Gang Han, Xiaolei Ye, Bo Xu, Zhouchun Peng, Yuanjun Ma, et al. 2007. “JARID1B Is a Histone H3 Lysine 4 Demethylase up-Regulated in Prostate Cancer.” *Proceedings of the National Academy of Sciences of the United States of America* 104 (49): 19226–31. doi:10.1073/pnas.0700735104.

Xiao, Mengtao, Hui Yang, Wei Xu, Shenghong Ma, Huaipeng Lin, Honguang Zhu, Lixia Liu, et al. 2012. “Inhibition of α-KG-Dependent Histone and DNA Demethylases by Fumarate and Succinate That Are Accumulated in Mutations of FH and SDH Tumor

Suppressors." *Genes & Development* 26 (12). Cold Spring Harbor Laboratory Press: 1326–38. doi:10.1101/gad.191056.112.

Xie, Bingteng, Heng Zhang, Renyue Wei, Qiannan Li, Xiaogang Weng, Qingran Kong, and Zhonghua Liu. 2016. "Histone H3 Lysine 27 Trimethylation Acts as an Epigenetic Barrier in Porcine Nuclear Reprogramming." *Reproduction (Cambridge, England)* 151 (1): 9–16. doi:10.1530/REP-15-0338.

Xie, Mingchao, Charles Lu, Jiayin Wang, Michael D McLellan, Kimberly J Johnson, Michael C Wendl, Joshua F McMichael, et al. 2014. "Age-Related Mutations Associated with Clonal Hematopoietic Expansion and Malignancies." *Nature Medicine* 20 (12). Nature Publishing Group: 1472–78. doi:10.1038/nm.3733.

Xie, Zhigang, Jayantha Gunaratne, Lip Lee Cheong, Shaw Cheng Liu, Tze Loong Koh, Gaofeng Huang, Walter P Blackstock, and Wee Joo Chng. 2013. "Plasma Membrane Proteomics Identifies Biomarkers Associated with MMSET Overexpression in T(4;14) Multiple Myeloma." *Oncotarget* 4 (7). Impact Journals, LLC: 1008–18. doi:10.18632/oncotarget.1049.

Xue, Wei, Jiong-Tang Li, Ya-Ping Zhu, Guang-Yuan Hou, Xiang-Fei Kong, You-Yi Kuang, Xiao-Wen Sun, et al. 2013. "L_RNA_scaffolder: Scaffolding Genomes with Transcripts." *BMC Genomics* 14 (1). BioMed Central: 604. doi:10.1186/1471-2164-14-604.

Yamaguchi, Hirohito, and Mien-Chie Hung. 2014. "Regulation and Role of EZH2 in Cancer" 46 (3). Korean Cancer Association. http://www.ncbi.nlm.nih.gov/pubmed/25038756.

Yang, Liubin, Rachel Rau, and Margaret A. Goodell. 2015. “DNMT3A in Haematological Malignancies.” *Nature Reviews Cancer* 15 (3). Nature Publishing Group: 152–65. doi:10.1038/nrc3895.

Yapp, Clarence, Andrew J Carr, Andrew Price, Udo Oppermann, and Sarah J B Snelling. 2016. “H3K27me3 Demethylases Regulate in Vitro Chondrogenesis and Chondrocyte Activity in Osteoarthritis.” *Arthritis Research & Therapy* 18 (1): 158. doi:10.1186/s13075-016-1053-7.

Yee, D, R E Favoni, G S Lebovic, F Lombana, D R Powell, C P Reynolds, and N Rosen. 1990. “Insulin-like Growth Factor I Expression by Tumors of Neuroectodermal Origin with the t(11;22) Chromosomal Translocation. A Potential Autocrine Growth Factor.” *The Journal of Clinical Investigation* 86 (6). American Society for Clinical Investigation: 1806–14. doi:10.1172/JCI114910.

Yoon, Jung-Hoon, Shigenori Iwai, Timothy R O’Connor, and Gerd P Pfeifer. 2003. “Human Thymine DNA Glycosylase (TDG) and Methyl-CpG-Binding Protein 4 (MBD4) Excise Thymine Glycol (Tg) from a Tg:G Mispair.” *Nucleic Acids Research* 31 (18): 5399–5404. http://www.ncbi.nlm.nih.gov/pubmed/12954776.

Yoshida, H, T Matsui, A Yamamoto, T Okada, and K Mori. 2001. “XBP1 mRNA Is Induced by ATF6 and Spliced by IRE1 in Response to ER Stress to Produce a Highly Active Transcription Factor.” *Cell* 107 (7): 881–91. http://www.ncbi.nlm.nih.gov/pubmed/11779464.

Yu, Wenjun, Yongxia Qiao, Xun Tang, Lifang Ma, Yulan Wang, Xiao Zhang, Wenhao Weng, et al. 2014. “Tumor Suppressor Long Non-Coding RNA, MT1DP Is

Negatively Regulated by YAP and Runx2 to Inhibit FoxA1 in Liver Cancer Cells." *Cellular Signalling* 26 (12): 2961–68. doi:10.1016/j.cellsig.2014.09.011.

Yu, Xinlei, and Yun Chau Long. 2016. "Crosstalk between Cystine and Glutathione Is Critical for the Regulation of Amino Acid Signaling Pathways and Ferroptosis." *Scientific Reports* 6. Nature Publishing Group: 30033. doi:10.1038/srep30033.

Yu, Y, F Xu, H Peng, X Fang, S Zhao, Y Li, B Cuevas, et al. 1999. "NOEY2 (ARHI), an Imprinted Putative Tumor Suppressor Gene in Ovarian and Breast Carcinomas." *Proceedings of the National Academy of Sciences of the United States of America* 96 (1): 214–19. http://www.ncbi.nlm.nih.gov/pubmed/9874798.

Yu, Yinhua, Satoshi Fujii, Jiuhong Yuan, Robert Z Luo, Lin Wang, Jiaju Bao, Mitsutaka Kadota, et al. 2003. "Epigenetic Regulation of ARHI in Breast and Ovarian Cancer Cells." *Annals of the New York Academy of Sciences* 983 (March): 268–77. http://www.ncbi.nlm.nih.gov/pubmed/12724231.

Zagar, T. M., T. J. Triche, and T. J. Kinsella. 2008. "Extraosseous Ewing's Sarcoma: 25 Years Later." *Journal of Clinical Oncology* 26 (26). American Society of Clinical Oncology: 4230–32. doi:10.1200/JCO.2008.16.5308.

Zhang, Y, and D Reinberg. 2001. "Transcription Regulation by Histone Methylation: Interplay between Different Covalent Modifications of the Core Histone Tails." *Genes & Development* 15 (18): 2343–60. doi:10.1101/gad.927301.

Zhao, Hongbo, and Taiping Chen. 2013. "Tet Family of 5-Methylcytosine Dioxygenases in Mammalian Development." *Journal of Human Genetics* 58 (7). NIH Public Access: 421–27. doi:10.1038/jhg.2013.63.

Zhao, Rui, Tetsuya Nakamura, Yu Fu, Zsolt Lazar, and David L Spector. 2011. "Gene Bookmarking Accelerates the Kinetics of Post-Mitotic Transcriptional Re-Activation." *Nature Cell Biology* 13 (11): 1295–1304. doi:10.1038/ncb2341.

Zheng, Yi-Chao, Jinlian Ma, Zhiru Wang, Jinfeng Li, Bailing Jiang, Wenjuan Zhou, Xiaojing Shi, Xixin Wang, Wen Zhao, and Hong-Min Liu. 2015. "A Systematic Review of Histone Lysine-Specific Demethylase 1 and Its Inhibitors." *Medicinal Research Reviews* 35 (5): 1032–71. doi:10.1002/med.21350.

Zwerner, J P, J Joo, K L Warner, L Christensen, S Hu-Lieskovan, T J Triche, and W A May. 2008. "The EWS/FLI1 Oncogenic Transcription Factor Deregulates GLI1." *Oncogene* 27 (23). Nature Publishing Group: 3282–91. doi:10.1038/sj.onc.1210991.

9 APPENDICES

9.1 LIST OF PRIMERS

Gene Symbol	Forward Primer	Reverse Primer
ACO1	GCATGACCTGCATTGGCAAC	GGTGTTGGGGTGAACTCGAC
ACO2	CGCAAACGACTGAACCGGC	GGTACGACTTGCCTCGCTCA
ACTB	GGATGCAGAAGGAGATCACTG	CGATCCACACGGAGTACTTG
ALDH18A1	TGTTGGCCACCTTGGAACCT	TCTCATCACGCTGGTCCGTC
ASNS	GGAAGACAGCCCCGATTTACT	AGCACGAACTGTTGTAATGTCA
ASS1	TCCGTGGTTCTGGCCTACA	GGCTTCCTCGAAGTCTTCCTT
ATF3	CCCTGAAGCCATTGGAGAGC	CCTCCCGCCTTGATGGTTCT
ATF4	ATGACCGAAATGAGCTTCCTG	GCTGGAGAACCCATGAGGT
ATF5	GGAGTGGCGACAGGATAGAGCT	CCTGTAGGATATGGGTCCCCTTC
CAD	CCATGCACTAGACAGCCAAGA	CGGCTCAGTGTGGATACGAC
CCNA1	GGTCCCGATGCTTGTCAGAT	GCTGGAGGGAAGGCATTTTC
CCNB2	ACTGCTCTGCTCTTGGCTTC	AAGTGTAGTGGCAAGGGTCG
CCNB3	GACCTTGTCCCGCTACATCT	TGTCTGACCAAGGGGTGAAG
CCNC	ATCTCAGCACCTCCAAGGGT	GTGCAAACCCGTTCCTATCG
CCND1	CCTCGGTGTCCTACTTCAAATGT	CTCCTCGCACTTCTGTTCCTC
CCND2	ACTTGTGATGCCCTGACTGAGC	ATCCCGCACGTCTGTAGGGG
CCND3	GACCTGGCTGCTGTGATTGC	ATGGATGGCGGGTACATGGC
CCNE1	CAGGGAGCGGGATGCGAA	TCGCCGTCCTGTCGATTTTG
CCNE2	TGTCAAGACGAAGTAGCCGT	GTTTCTTGGTGACCTCCTCTCT
CCNF	CAGCGGTTTGAGGACAAGCG	TCTCCCGCTTCCGTTTGGTT
CCNG1	TCCAAGCACAGAAGTGTGTAGAGT	CGTGCAGTACGCCCAGAAAC
CCNG2	GGGGTCCAACTTCTCGGGTT	CTCCGGGGTAGCCTCAATCA
CCNI	TGGCCTGCAACCAACTTCTG	TGCCACAAGCTCCCGACAAT
CCNK	CTTGCCTGAAGCGAGGGGATT	GGCTTTGTGTGGTCCAGGTTT
CCNO	GCCACAAGTGACGGCGGAA	GCACAGCGACTCGAAGGAGA
CCNY	GCCAACTGGAAGCGGATTGT	CGCTCTAGCTCGTTCATGTCCT
CDC25B	CCCGCATGTGCCGTTTCATC	TGGTTCATGGGCCGGTAGTC
CDK2	CTGCTCCAGGGCCTAGCTTT	ACAGGGTCACCACCTCATGG
CDK4	AGCTGGTCACATGGTGAGGG	CGGAGCCGGTTCCTACGG
CDK6	AGAGCACCCGAAGTCTTGCT	GGGAGTCCAATCACGTCCAAGAT
CDKN1C	CGTTCATGTAGCAGCAACCG	ACCAGTGTACCTTCTCGTGC
CDKN2A	ACCAGAGGCAGTAACCATGC	AAACTACGAAAGCGGGGTGG
CDKN2B	CCGACCGGGAATAACCTTCC	AAAAGCAAACGACCCCTGGA
CDKN2C	AACGAGTTGGCGTCCGCAG	CAGTCTCCTGGCAATCTCGGG
CHAC1_t1	TCCCCAAGATGCTCCTGACC	TTCAAGGTTGTGGCCGGAGA

CHAC1_t2	CGACTTCGCCTACAGCGACA	CAGGGTTCTGCTCCCCTTGC
CHAC1_tot	GACAGACTTGCGACCGCTTG	TGCCCACCACACCAACATGG
CPS1	CATCCAGCAATCATTCCGGC	AGTCTGATGTGGCTTCCGTG
CS	CATGGGTCAAAGCCGGTTGC	GGGCAGAGTCCTGGTTTGCT
CTH	GAAAGCCTTGCTGAGCTTCCG	TTCCACTTGGAGGGTGTGCT
DDIT3	ATGAACGGCTCAAGCAGGAA	GCAGATTCACCATTCGGTCAA
DDIT4	TCGGAGCATCACTACTGACCTGTTG	AACGCAGCTGCCAGGTGTAATTTT
DLAT	TTCCTGGCTCCTTCACCACC	GGTTAATTGCGGCCGAGTGG
DLD	GGACTTTCTGCAGTGCCTCTGA	AGCAACATATCCTCCAGGACCAG
DLST	CCATCACCAGCAAATGGCGT	GCTTGGCCTTAGCAGGAGCA
DNAJB9	GCTACTCCCCAGTCAATTTTCA	CCGATTTTGGCACACCTAAGAT
DNAJC3	TGTGTTTGGGATGCAGAACTAC	TCTTCAACTTTGACGCAGCTT
FH	GGTTCTGGTCCTCGGTCAGG	ATGTCCATTGCTGCCTCCGA
G6PD	CTCCTACCAGCGCCTCAACA	TCCACGATGATGCGGTTCCA
GAPDH	GAAGGTGAAGGTCGGAGTC	GAAGATGGTGATGGGATTTC
GLS1	CCAGAAGGCACAGACATGGT	ACCACCATTAGCCAGTGTCG
GLS2	GGCCATGTGGATCGCATCTT	ACAGGTCTGGGTTTGACTTGG
GLUD1	AAGTCCGTCCTCCCCGTTAG	CGACTAGGGAGGAAGGGTCC
GLUL	GCTGGCGTGGTCCTAGTTTA	CCAAGAGGCTGTAAGGGTGG
GOT1	GGCCAGCACCCTCTCTAACC	CCAGGTCCCAGGGGTTTTGA
GOT2	GGTGATAAGGATGCCTGGGCT	AAGGCTCCTACACGCTCACC
GPT1	AACTGTCCCCAGCTCCTTCAG	ACAGCTGGGTCTGGCTTAGT
GPT2	CTACCAGGGGCGACAGGGTT	GGACTCCAGCGTGAGGATGC
GSS	ACCGTTCGCGGAGGAAAGG	AGCAATACTCCCTCAGCCAGG
H6PD	CCCCACCTTCTGGGATGTTAGC	TAGCCAGGTCCCCAGTTGCT
HSD11B1	CTTGGAGCAGCCTCAGCACA	TGCTTGGGCAACAAATTGCTCT
IDH1	ACCCCAAGACCTGCTAACGG	GTTTATCGCCTGCCAGACAGC
IDH2	CTGGTGATGTTTCTGATGCCGAC	GTTTGGGAGCCCGAGGTCAA
IDH3G	TGAAACAGCTACGAGGAACACC	GGTAGGGTGCGAGGGGAAC
INHBE	CTCTGCCCTCTAGTGGCTTGA	CGCCTCGGTTGTCCAGTAA
KDM5A	GTCTAAAGTGGGTAGTCGCTTG	GTTTGGGTATCAGTGCTGAGAA
LDHA	AGGTGGAGGTTGTGCATGTT	CGTCAGAGGTGGCAGAACTA
MDH1	TTGCCGCAGTGACCCAGTAA	CGTCGCATTTTGTCCTCCCG
MDH2	CTGAGCCACATCGAGACCAAAGC	CATGCCTGGCTTTCTGGGGAC
ME1	GCTTGGGAGACCTTGGCTGTA	ATTCATCCCTCCGCAAGCTGT
ME2	AGGTGCTGGCCGTCTTTTCA	ACTGGCAAACAAACACCTGCC
ME3	AGACTTCGCCAATGCCAATGC	GCAGAGCAGCCAAGATCCCT
Mt1X	ACGCTTTTCATCTGTCCCGC	GGGTCCATTTCGAGGCAAGG
OGDH	GGGGAGGGCTACGTGTTGAC	TCAGCTCCACCCGAATGAGG
PC	AATGGATTGAGCCGGGCAGA	CACCCTTGGCAGGTCCTTCA
PCK2	GCCATCATGCCGTAGCATC	AGCCTCAGTTCCATCACAGAT
PDHA1	CAGGCAAGCAGAGTGCTGGTA	TCCATTCGGCGTACAGTCTGC
PDHA2	CTGCCATCTACAGCACTCCGT	GAGGAGTTACGGGATGCCAC

PDHB	CCTTCAATTTCTCCATGCAAGCCA	CTGAAGGCCACCAGACATGTAG
PDHX	CGAGGCCGCAAATGCAATCA	AGCGGTGCCTTTAGGTCTCT
PFKB4	CAACATCGTGCAAGTGAAACTG	GACTCGTAGGAGTTCTCATAGCA
PGD	TGGGAACCATCTCCTTGCGG	TCAGAGTGCGCAAACACCCT
PGLS	TGAGACAGGCATTCCAAGGGG	TCGGGGAGTCACTGATGGGA
PSAT1	TGCCGCACTCAGTGTTGTTAG	GCAATTCCCGCACAAGATTCT
PSPH	GAGGACGCGGTGTCAGAAAT	GGTTGCTCTGCTATGAGTCTCT
RGS16	ACCATCCTGCCTACTACGTGC	TCTTTGGCTCTCTCCAGGCAG
RPIA	ACTTTGGGATGCAGGATGGCT	TACGTCCACCTTGGCTGTGG
SDHA	GGGGAAGAAGGAGTACATTGAAGG	AAGAGCTGTGCCCAGTTTTATCA
SDHB	AGGCAACACTCTAGCTTGCAC	TACTGCTGCTTGCCTTCCTGA
SDHC	ACAGCTTGCCTACTCTCGGC	AAGGAGCCAAAAGCTGACCCT
SDHD	GAACGAGATGGCGGTTCTCTG	GCTGCACTCCACACCATTCTG
SESN2	CCTCCTACTTGCCATTCACCCATC	GCTGCCCAACAGAACAGGCTTT
SLC1A3	CCGCTGTCATTGTGGGTACA	GACTACAGCTCGCATTCCCA
SLC1A5	CACTGAGGAAGGAAACCCCC	TCCAGTGTCCAAAGAGCACC
SLC25A1	GCCTGGATGTGGCCATAGTGT	AGGGGCCTTTTGGCACTACT
SLC37A4	GTGGGTGCTCTCCACTGGTT	GCTGCGATGCTGCCTACAAG
SLC38A1	CCCGTCAGTCCTGCCAATTT	CGGACTGCACGTTGTCATAGA
SLC38A2	CCGGGGTGCCGCTATAACC	TGTCAAGGGAAAGGCGCGA
SLC39A10	CCTGCTTTCCTTGCTAGGCG	CACCCTGAGAATGGGGCAGT
STC2	ACAACCCCGTCTGATCTCAGAATTG	CAGGTCCTGTTGCCTAAATCCGTAG
SUCLG1	GCCATTCCCGCTGTTTCGTG	CAAGGGTTGCGGTCATACGC
SUCLG2	TTCAGCCATTGACCTGGAGGA	GGACAAAGACATCACTTCTTGGC
TALDO1	ACAAGGAAGCTGGGATCAGCA	GGGGAGATGAGGGTCACACC
TKT	ACCGCCTACGTATCAGCTCC	ATGGCCCTTGGAGAGCACAA

9.2 CODE FOR HEATMAP FUNCTION

```
qPCRheatmap<-function(data, limit=0, colbot="blue", colmid="white", coltop="red", dendro=F, cellwidth=20, divisions=200, ...)
{

    if (limit==0) {

    toplimit<-max(na.omit(data))

    bottomlimit<-min(na.omit(data))

    logtoplimit<-log10(toplimit)

    logbottomlimit<-log10(bottomlimit)

    if(logtoplimit>abs(logbottomlimit))

    {logbottomlimit<-(log10(toplimit)*-1.0001)

      bottomlimit<-10^logbottomlimit}

    else

    {logtoplimit<-(log10(bottomlimit)*-1.0001)

     toplimit<-10^logtoplimit}}

  else

  {if(limit<1) #sets it to calculate the limits based on a downregulation {

      bottomlimit<-limit*1.0001

      logbottomlimit<-log10(bottomlimit)

      logtoplimit<-logbottomlimit*-1.0001

      toplimit<-10^logtoplimit}

    else #based on an upregulation

    {toplimit<-limit*1.0001

      logtoplimit<-log10(toplimit)

      logbottomlimit<-logtoplimit*-1.0001

      bottomlimit<-10^logbottomlimit}}

    if (dendro==F){dendro<-0}

  else{dendro<-50}

  data[data>=toplimit]<-toplimit

  data[data<=bottomlimit]<-bottomlimit

  breaks<-seq(logbottomlimit,logtoplimit,(logtoplimit-(logbottomlimit))/divisions)

  breaks_legend<-breaks[seq(1,length(breaks),50)]

  colors=colorpanel(length(breaks), colbot, colmid, coltop)

  edpheatmap(log10(data),      breaks=breaks,      color=colors,      cellwidth=cellwidth,      legend_breaks=breaks_legend,
legend_labels=signif(10^breaks_legend,digits=2), treeheight_row=dendro, treeheight_col=dendro, ...)}
```

9.3 H3K4ME3 PEAKS NEAR TRANSCRIPTION START SITES NOT DOWNREGULATED

Chr	Start	End	Distance to TSS	Gene Name	Chr	Start	End	Distance to TSS	Gene Name
chr1	34208	34350	1802	FAM138A	chr11	123937677	123937822	-1868	OR4D5
chr1	494149	494324	1209	LOC100132287	chr12	10129853	10130086	300	CLEC7A
chr1	629456	632588	1391	MIR6723	chr12	23177215	23177402	1672	LOC101928441
chr1	632961	634868	-1501	MIR6723	chr12	57231161	57231485	957	SHMT2
chr1	6723284	6723434	-1386	LOC100505887	chr12	57455501	57455759	317	INHBE
chr1	10795295	10795448	1305	CASZ1	chr12	113335571	113335729	-530	SLC8B1
chr1	12887402	12887635	-1317	PRAMEF4	chr12	116910744	116910850	-159	FBXW8
chr1	13175214	13175334	-7	PRAMEF9	chr12	127883307	127883507	1790	FLJ37505
chr1	14944555	14944686	-1299	KAZN	chr13	23891339	23891484	1958	C1QTNF9B-AS1
chr1	16048659	16048785	-40	CLCNKB	chr13	35478596	35478780	1939	NBEA
chr1	16513729	16513962	440	RNU1-3	chr13	57146810	57147011	-578	PRR20E
chr1	16646260	16646405	758	MST1P2	chr13	57148246	57148370	820	PRR20B
chr1	16646998	16647169	1509	MST1P2	chr13	57162306	57162444	1743	PRR20D
chr1	16666367	16666624	453	RNU1-4	chr13	99257913	99258092	426	GPR18
chr1	16718164	16718296	1927	ESPNP	chr13	111184925	111185040	-1844	ARHGEF7
chr1	16732445	16732664	1907	FAM231A	chr13	113751906	113752029	-878	LINC00552
chr1	16733511	16733632	890	FAM231A	chr14	19434406	19434547	-135	POTEG
chr1	16740296	16741121	192	RNU1-4	chr14	23955142	23955366	-142	DHRS4-AS1
chr1	16895770	16896596	203	RNU1-4	chr14	64503775	64503915	0	ZBTB25
chr1	17012758	17012875	-844	ATP13A2	chr14	72985429	72985580	1452	ZFYVE1
chr1	21294649	21294825	1447	LOC100506801	chr14	73559911	73560045	-1031	HEATR4
chr1	22451677	22451805	-110	ZBTB40	chr14	75279871	75280046	1180	FOS
chr1	28260614	28261645	1677	SESN2	chr14	100894511	100894621	-204	MEG8
chr1	30740095	30740195	-913	MIR4420	chr14	104119062	104119162	-1609	MIR203B
chr1	40692155	40692268	50	NFYC-AS1	chr15	20507696	20507892	-1614	HERC2P3
chr1	47231974	47232077	-136	TAL1	chr15	20940654	20940785	281	LINC01193
chr1	47314166	47314519	-195	STIL	chr15	21502889	21503072	17	NF1P2
chr1	61077256	61077543	125	NFIA	chr15	21514267	21514496	422	MIR5701-1
chr1	68499041	68499306	-1952	DEPDC1	chr15	21940180	21940320	28	NF1P2
chr1	70412265	70412664	1246	CTH	chr15	21951554	21951770	420	MIR5701-2
chr1	71081276	71081400	14	ZRANB2-AS2	chr15	23157920	23158039	639	GOLGA8DP
chr1	74590402	74590614	773	ERICH3-AS1	chr15	23355343	23355591	719	GOLGA8S
chr1	93447330	93447438	-747	FNBP1L	chr15	24168891	24169006	958	PWRN2
chr1	108450032	108450267	-133	NBPF6	chr15	28323677	28323879	-1626	HERC2
chr1	113390222	113390361	-562	MAGI3	chr15	30083748	30083942	890	GOLGA8J
chr1	113950698	113950846	-373	HIPK1	chr15	30571352	30571485	-1137	ULK4P1
chr1	117059979	117060198	-239	TTF2	chr15	30573233	30573335	729	ULK4P2
chr1	120436514	120436695	253	NBPF8	chr15	32455505	32455682	41	GOLGA8O
chr1	143421299	143421520	1183	LOC645166	chr15	34389160	34389336	552	GOLGA8A
chr1	143423674	143423786	954	LOC645166	chr15	34535382	34535551	555	GOLGA8B

chr1	143792061	143792170	-380	LOC388692	chr15	40107096	40107218	-719	BMF
chr1	144246891	144247152	1184	LOC645166	chr15	40953948	40956092	1582	CHAC1
chr1	144248821	144249009	-710	LOC645166	chr15	43826701	43826815	-156	WDR76
chr1	144274950	144275193	1691	LOC101060524	chr15	74995471	74995570	-15	SCAMP5
chr1	144691174	144691444	1695	LOC101060524	chr15	75258964	75259095	471	GOLGA6C
chr1	144716986	144717555	-901	LOC645166	chr15	81135853	81135996	1621	CFAP161
chr1	144719181	144719491	1165	LOC645166	chr15	84516074	84516236	692	GOLGA6L4
chr1	145707992	145708203	-697	PDZK1	chr15	89243779	89243930	-109	FANCI
chr1	145994562	145994787	1048	TXNIP	chr15	89574997	89575245	-466	TICRR
chr1	148890313	148890484	946	PDE4DIP	chr15	101972369	101972667	-1006	MIR6859-3
chr1	149700608	149700780	-410	LOC388692	chr15	101974962	101975169	1541	MIR6859-4
chr1	149841085	149841615	-157	HIST2H3C	chr16	1333333	1333539	-169	BAIAP3
chr1	149852191	149852732	-158	HIST2H3A	chr16	2830227	2830364	123	ZG16B
chr1	149888309	149888478	-477	HIST2H2AB	chr16	8962603	8962708	829	USP7
chr1	151788845	151788981	1621	TDRKH	chr16	14929369	14929493	-1389	MIR6770-2
chr1	152910355	152910575	1902	IVL	chr16	15395402	15395533	-287	MPV17L
chr1	153040109	153040352	888	SPRR2D	chr16	16304716	16304842	-1591	MIR3670-2
chr1	153070587	153070727	951	SPRR2B	chr16	16324158	16324322	-348	MIR6511A3
chr1	153416532	153416638	61	S100A7A	chr16	16328388	16328505	-859	MIR6770-2
chr1	155244601	155244942	91	GBA	chr16	18405427	18405551	273	MIR3670-1
chr1	156126040	156126203	4	LMNA	chr16	18412105	18412234	-192	MIR3179-4
chr1	156642487	156642685	638	BCAN	chr16	18413166	18413273	-1242	MIR3179-4
chr1	160740064	160740202	1076	SLAMF7	chr16	18489877	18489998	-1572	MIR3670-3
chr1	161525630	161525774	1162	HSPA6	chr16	18495703	18495889	-1220	MIR3179-2
chr1	161607113	161607405	1200	HSPA7	chr16	21865833	21865937	850	LOC100190986
chr1	169628950	169629163	1083	SELP	chr16	22513221	22513460	-183	NPIPB5
chr1	201375781	201375947	1836	TNNT2	chr16	27427328	27427534	173	IL21R
chr1	201419717	201419844	1966	TNNI1	chr16	28637732	28637913	-539	NPIPB8
chr1	228621086	228621305	331	MIR7641-2	chr16	28751837	28752155	-439	NPIPB9
chr1	228627602	228627814	558	RNA5S9	chr16	34158449	34158595	1514	LINC00273
chr10	282242	282389	-229	MIR7641-2	chr16	56633113	56633344	606	MT1M
chr10	42999437	42999540	1925	MIR5100	chr16	56666824	56667995	656	MT1G
chr10	45972583	45972711	194	TIMM23	chr16	56670138	56671267	888	MT1H
chr10	46877933	46878034	1309	FRMPD2B	chr16	68083699	68083828	-1603	NFATC3
chr10	68720872	68721020	-198	CCAR1	chr16	70687214	70687424	-1268	MTSS1L
chr10	84138972	84139139	-374	GHITM	chr16	87384011	87384124	-274	FBXO31
chr10	114043233	114043456	-703	ADRB1	chr16	90008130	90008480	1816	DBNDD1
chr11	799799	799954	-1607	SLC25A22	chr17	3399401	3399550	-1065	OR1E1
chr11	1410241	1410504	-71	BRSK2	chr17	6756141	6756714	590	XAF1
chr11	10509254	10509663	-282	MTRNR2L8	chr17	16690099	16690202	-175	CCDC144A
chr11	13962076	13962289	-455	SPON1	chr17	19094121	19094268	981	LOC79999
chr11	19240994	19241258	-166	E2F8	chr17	19111888	19111989	698	SNORD3D
chr11	28477216	28477396	242	MIR8068	chr17	19220307	19220440	991	LOC79999

chr11	32795733	32795888	-1152	CCDC73	chr17	27416364	27416482	-1582	TBC1D3P5
chr11	59424465	59424620	-1589	OR5A2	chr17	29042416	29042598	-393	PIPOX
chr11	59756125	59756263	1135	STX3	chr17	35558906	35559054	-889	SLFN14
chr11	61104091	61104303	1739	CD5	chr17	36177712	36178237	-1350	TBC1D3B
chr11	61204976	61205152	1551	PGA3	chr17	36324762	36325249	1121	TBC1D3G
chr11	61221589	61221809	-650	PGA4	chr17	36389560	36390060	-1373	TBC1D3H
chr11	61357280	61357379	-440	CYB561A3	chr17	36441120	36441222	-1648	TBC1D3F
chr11	62882756	62883118	1238	SLC3A2	chr17	37924173	37924323	-212	TBC1D3
chr11	63973730	63973939	-773	COX8A	chr17	37924760	37924909	362	TBC1D3K
chr11	64996998	64997192	-50	BATF2	chr17	37925317	37925836	1104	TBC1D3K
chr11	65612596	65612721	1591	MAP3K11	chr17	38003143	38003348	-748	TBC1D3C
chr11	69082800	69082900	-326	MIR3164	chr17	38004900	38005407	1120	LOC101060389
chr11	75560128	75560245	-1870	SERPINH1	chr17	38127065	38127280	-782	TBC1D3H
chr11	111918769	111918955	-15	C11orf52	chr17	38128905	38129317	1141	TBC1D3E
chr11	119341635	119341741	-805	C1QTNF5	chr17	39165015	39165114	1097	ARL5C
chr11	119422204	119422345	288	THY1	chr17	40418223	40418384	-353	TOP2A
chr17	43294982	43295185	1532	RNU2-1	chr17	43229629	43229900	-753	LINC00854
chr17	45519245	45519954	924	LRRC37A4P	chr17	43250025	43250587	1713	RNU2-1
chr17	49678234	49678393	-150	SPOP	chr3	39406263	39406539	-288	RPSA
chr17	49764307	49764522	-258	FAM117A	chr3	49007153	49007313	29	WDR6
chr17	81891811	81891991	-26	ANAPC11	chr3	52533755	52533915	-58	NT5DC2
chr17	83225953	83226135	-853	RPL23AP87	chr3	59050151	59050267	-220	C3orf67
chr18	106793	111272	-33	ROCK1P1	chr3	125967453	125967571	-1632	ROPN1B
chr18	111973	112503	101	MIR8078	chr3	127598103	127598323	-144	MCM2
chr18	596669	596892	-218	CLUL1	chr3	137762642	137762821	-1561	SOX14
chr18	5296117	5296233	20	ZBTB14	chr3	140941465	140941703	-236	SLC25A36
chr18	7117049	7117167	706	LAMA1	chr3	141486870	141486981	-122	RASA2
chr18	21612029	21612136	-187	SNRPD1	chr3	183548401	183548578	-246	KLHL6-AS1
chr18	46963331	46963464	1011	TCEB3CL	chr3	183557576	183557729	-1941	KLHL6
chr18	46964076	46964596	72	TCEB3CL	chr3	195881041	195881354	1198	MIR6829
chr18	46964962	46965712	-693	TCEB3CL2	chr3	196503833	196503943	-120	RNF168
chr18	46966036	46966382	-1565	TCEB3CL2	chr3	196505519	196505669	-1826	RNF168
chr18	47021486	47025226	571	TCEB3CL	chr3	198040493	198040646	-1102	LMLN-AS1
chr18	47029360	47030881	-42	TCEB3C	chr4	337003	337118	-747	ZNF141
chr18	47034856	47035210	584	TCEB3B	chr4	8582250	8582386	1828	GPR78
chr18	79069145	79069273	-66	ATP9B	chr4	9248027	9248178	-528	USP17L11
chr18	79679191	79679368	-522	CTDP1	chr4	10020886	10021031	532	SLC2A9
chr19	851464	851626	-746	ELANE	chr4	20699967	20700348	-256	PACRGL
chr19	2281210	2281730	712	C19orf35	chr4	88378889	88379096	253	HERC6
chr19	3721673	3721968	121	TJP3	chr4	88699165	88699354	-1387	NAP1L5
chr19	4125654	4125779	-1587	MAP2K2	chr4	102828194	102828372	-103	UBE2D3
chr19	9912970	9913114	663	OLFM2	chr4	138240409	138240546	1872	SLC7A11
chr19	11539127	11539241	467	CNN1	chr4	138241341	138241693	832	SLC7A11

chr19	12705550	12705655	916	SNORD41	chr5	7394981	7395132	-1174	ADCY2
chr19	19192732	19192959	79	RFXANK	chr5	8461964	8462088	1101	MIR4458
chr19	19668707	19668941	36	ZNF101	chr5	14652974	14653112	-661	SNORD141A
chr19	34898766	34898894	113	LINC00904	chr5	16177750	16177960	1933	40603
chr19	35490610	35490736	-142	KRTDAP	chr5	21885232	21885452	888	SNORA105A
chr19	35628853	35628969	-167	RBM42	chr5	33934599	33934704	-1735	RXFP3
chr19	36309987	36310148	-1276	LOC100134317	chr5	80651210	80651501	-320	MTRNR2L2
chr19	39412236	39412457	-764	PLEKHG2	chr5	95646843	95647015	50	RFESD
chr19	43024578	43024739	1821	PSG11	chr5	103562780	103562907	-42	NUDT12
chr19	43081448	43081588	1223	PSG2	chr5	127517255	127517384	-290	PRRC1
chr19	43780754	43780988	386	KCNN4	chr5	141403553	141403696	671	PCDHGA9
chr19	44844758	44844920	-1297	PVRL2	chr5	175679873	175680046	-1502	HRH2
chr19	46298897	46299019	582	HIF3A	chr5	181367414	181367537	188	OR4F16
chr19	46783738	46784217	900	SLC1A5	chr6	4428045	4428291	166	MIR7641-2
chr19	47228816	47229682	1945	BBC3	chr6	26027154	26027387	-18	HIST1H4B
chr19	47907867	47908073	292	SNAR-A13	chr6	27146663	27146794	130	HIST1H2BK
chr19	47908690	47908859	1096	SNAR-A13	chr6	30717233	30717473	328	MDC1
chr19	47911166	47911548	-1694	SNAR-C5	chr6	31739938	31740258	150	MSH5
chr19	47913201	47913414	256	SNAR-C2	chr6	32037482	32037640	-755	CYP21A2
chr19	47914035	47914288	1110	SNAR-C2	chr6	32038102	32038307	-112	CYP21A2
chr19	47918619	47918881	321	SNAR-A2	chr6	32130302	32130406	-64	FKBPL
chr19	47919480	47919742	1182	SNAR-A2	chr6	36837581	36837798	1755	CPNE5
chr19	47920118	47920219	1739	SNAR-A2	chr6	104859976	104860086	-112	HACE1
chr19	47922727	47922874	-979	SNAR-A6	chr6	104940095	104940229	365	LINC00577
chr19	47924014	47924277	366	SNAR-A10	chr6	147202572	147202808	-1668	STXBP5
chr19	47924733	47925058	1116	SNAR-A10	chr6	150867065	150867166	782	MTHFD1L
chr19	47925450	47925563	1727	SNAR-A10	chr6	159761766	159761926	-111	ACAT2
chr19	47929707	47929909	990	SNAR-C2	chr6	159779593	159779767	701	SNORA20
chr19	47933154	47933366	-921	SNAR-A2	chr7	1740289	1740437	1947	ELFN1-AS1
chr19	47935224	47935408	1135	SNAR-A1	chr7	2511751	2511865	-721	LFNG
chr19	47938403	47938571	-1054	SNAR-C4	chr7	2688980	2689138	857	AMZ1
chr19	47939021	47939124	-469	SNAR-C4	chr7	30773096	30773312	1787	FAM188B
chr19	47939733	47940041	346	SNAR-C4	chr7	31053234	31053348	830	ADCYAP1R1
chr19	47943426	47944039	-1190	SNAR-A13	chr7	32496872	32497043	1531	AVL9
chr19	47944493	47944810	-271	SNAR-A13	chr7	63303658	63303839	308	ZNF733P
chr19	47950513	47950636	278	SNAR-C3	chr7	74658442	74658543	827	GTF2I
chr19	47951504	47951743	1327	SNAR-C3	chr7	75394923	75395102	401	LOC100101148
chr19	47954696	47954849	-910	SNAR-C1	chr7	102355325	102355549	1007	SPDYE6
chr19	47957366	47957511	1756	SNAR-C5	chr7	102479892	102480014	-1019	POLR2J
chr19	49019289	49019439	120	LOC101059948	chr7	102480727	102480897	-1878	POLR2J
chr19	49044632	49044807	874	CGB5	chr7	102550657	102550845	-481	SPDYE2B
chr19	49048114	49048333	888	CGB8	chr7	102551744	102551904	592	SPDYE2
chr19	50127767	50128005	636	SNAR-A14	chr7	102573504	102573666	-964	POLR2J3

chr19	50133120	50133348	630	SNAR-B2	chr7	102649769	102649945	-468	SPDYE2
chr19	50133674	50133861	97	SNAR-B2	chr7	102650924	102651030	652	SPDYE2B
chr19	50134463	50134641	-688	SNAR-B1	chr7	116288003	116288110	-1329	LOC102724434
chr19	50138515	50138722	619	SNAR-B2	chr7	159006924	159007069	-1358	LINC00689
chr19	50139052	50139186	118	SNAR-B2	chr8	7972508	7972946	526	USP17L8
chr19	50330716	50330911	-1436	KCNC3	chr8	7977150	7977406	707	USP17L3
chr19	51629632	51629734	791	SIGLEC5	chr8	12128557	12128762	638	LOC392196
chr19	52821526	52821680	66	ZNF28	chr8	12137488	12137610	1211	USP17L2
chr19	54222289	54222458	714	LILRB3	chr8	12138011	12138470	520	USP17L2
chr19	54243491	54243702	-828	LILRA6	chr8	12378451	12378739	1194	LOC649352
chr19	55069182	55069394	258	RDH13	chr8	12419057	12419212	-1102	FAM90A25P
chr19	55769729	55769905	-1988	RFPL4AL1	chr8	19313495	19313605	-20	SH2D4A
chr19	56176249	56176433	321	GALP	chr8	22132834	22132974	-1852	HR
chr19	56226584	56226765	1616	ZSCAN5A	chr8	22877632	22877748	-282	LOC101929237
chr2	70977022	70977168	-1350	ANKRD53	chr8	55763768	55763872	160	TMEM68
chr2	74516228	74516405	1847	TLX2	chr8	81722206	81722395	-996	ZFAND1
chr2	91658623	91658763	1256	LOC654342	chr8	85653925	85654141	1643	REXO1L2P
chr2	113498764	113498884	-260	FOXD4L1	chr8	85660773	85660978	1638	REXO1L2P
chr2	131800477	131800687	1079	C2orf27B	chr8	85714255	85717956	1261	REXO1L2P
chr2	132256973	132257204	-8	MIR663B	chr8	85732208	85739559	-415	REXO1L2P
chr2	166487097	166487207	-181	SCN7A	chr8	123396750	123396933	-376	ATAD2
chr2	190647300	190647445	-1750	NAB1	chr8	124040559	124040757	124	FER1L6-AS1
chr2	233713705	233713898	809	UGT1A5	chr8	130086667	130086810	-1970	ASAP1-IT2
chr2	233758575	233758688	-1642	UGT1A1	chr8	141421837	141422012	536	PTP4A3
chr20	23365791	23365945	1505	GZF1	chr8	143038892	143039002	-262	C8orf31
chr20	26208180	26208566	-95	MIR663A	chr8	144607465	144607639	-1857	ARHGAP39
chr20	26209188	26209605	-163	MIR663AHG	chr9	35489119	35489233	-776	RUSC2
chr20	26210911	26211091	-1768	MIR663AHG	chr9	63016202	63016393	-1698	LOC101928381
chr20	32819727	32819848	-106	MAPRE1	chr9	63019013	63019141	1082	LOC101928381
chr20	50731226	50731337	-263	PARD6B	chr9	63821493	63821672	-1928	MIR4477A
chr20	60476728	60476836	-1329	MIR4533	chr9	64747017	64747129	-1707	LOC101928381
chr20	63217322	63217426	-1188	YTHDF1	chr9	65789334	65789531	-1689	LOC101928381
chr21	8203873	8203982	-1388	MIR6724-2	chr9	68302440	68302577	-359	FOXD4L3
chr21	8206334	8207088	1396	MIR6724-3	chr9	74952862	74952986	-38	C9orf40
chr21	8207436	8207977	-767	MIR3648-1	chr9	85742128	85742268	-169	AGTPBP1
chr21	8208359	8209171	-79	MIR3687-1	chr9	97922604	97922730	-97	TRMO
chr21	8209508	8209760	3	RNA18S5	chr9	114330054	114330206	341	ORM2
chr21	8211813	8212063	-634	RNA5-8S5	chr9	130445791	130446489	1433	ASS1
chr21	8212491	8213364	355	RNA5-8S5	chrX	12791170	12791296	-122	PRPS2
chr21	8248829	8249049	-566	MIR6724-2	chrX	49333334	49333435	1758	GAGE2E
chr21	8251140	8251300	-1012	MIR663A	chrX	106640859	106641013	1122	MIR548AN
chr21	8251624	8252166	-337	MIR663A	chrX	135855523	135855675	-1061	CT45A2
chr21	8252794	8253406	868	MIR663A	chrX	153447767	153447886	-1339	TREX2

chr21	8389386	8390137	1399	MIR6724-2	chrX	153903868	153904005	-1139	AVPR2
chr21	8390483	8391986	-1432	RNA18S5	chr22	15690011	15690154	56	POTEH
chr21	8392557	8392795	10	RNA18S5	chr22	19178766	19178922	19	SLC25A1
chr21	8394842	8395095	-639	RNA5-8S5	chr22	20268460	20268677	-275	RTN4R
chr21	8395554	8396184	262	RNA5-8S5	chr22	22645303	22645430	746	GGTLC2
chr21	8431989	8432176	-448	MIR6724-4	chr22	23431645	23431803	-1840	LOC101929374
chr21	8433876	8434187	809	RNA45S5	chr22	28742470	28742624	492	HSCB
chr21	8436118	8436294	-670	RNA18S5	chr22	30356456	30356588	-116	CCDC157
chr21	8438981	8439201	-732	RNA5-8S5	chr22	35649936	35650069	1625	APOL6
chr21	8987015	8987283	150	MIR3648-2	chr22	36029097	36029223	-623	RBFOX2
chr21	8988100	8988211	785	MIR3687-2					
chr21	42008419	42008593	-688	ZNF295-AS1					

9.4 PUBLICATIONS

Inagaki, Y, **E Hookway**, K A Williams, A B Hassan, U Oppermann, Y Tanaka, and E Soilleux. 2016. "Dendritic and Mast Cell Involvement in the Inflammatory Response to Primary Malignant Bone Tumours." *Clinical Sarcoma Research* 6 (1). BioMed Central: 1–8. doi:10.1186/s13569-016-0053-3.

Inagaki, Y., T. G. Kashima, **E. S. Hookway**, Y. Tanaka, A. B. Hassan, U. Oppermann, and N. A. Athanasou. 2015. "Dentine Matrix Protein 1 (DMP-1) Is a Marker of Bone Formation and Mineralisation in Soft Tissue Tumours." *Virchows Archiv*, January. doi:10.1007/s00428-014-1706-3.

Johansson, Catrine, Srikannathasan Velupillai, Anthony Tumber, Aleksandra Szykowska, **Edward S Hookway**, Radoslaw P Nowak, Claire Strain-Damerell, et al. 2016. "Structural Analysis of Human KDM5B Guides Histone Demethylase Inhibitor Development." *Nature Chemical Biology* 12 (JUly). Nature Publishing Group, a division of Macmillan Publishers Limited. All Rights Reserved.: 78–80. doi:10.1038/nchembio.2087.

Inagaki, Yusuke, **Edward S. Hookway**, Takeshi G. Kashima, Mitsuru Munemoto, Yasuhito Tanaka, Andrew Bassim Hassan, Udo Oppermann, and Nick A. Athanasou. 2016. "Sclerostin Expression in Bone Tumours and Tumour-like Lesions." *Histopathology* 69 (3): 470–78. doi:10.1111/his.12953.

Cheng, X., **E. S. Hookway**, T. Kashima, U. Oppermann, A. Galione, and N. A. Athanasou. 2014. "The Role of Calcium and Nicotinic Acid Adenine Dinucleotide Phosphate (NAADP) in Human Osteoclast Formation and Resorption." *Calcified Tissue International* 96 (1): 73–79. doi:10.1007/s00223-014-9939-3.

Barnes, David J., **Edward Hookway**, Nick Athanasou, Takeshi Kashima, Udo Oppermann, Simon Hughes, Daniel Swan, et al. 2016. "A Germline Mutation of CDKN2A and a Novel RPLP1-C19MC Fusion Detected in a Rare Melanotic Neuroectodermal Tumor of Infancy: A Case Report." *BMC Cancer* 16 (1). BioMed Central: 629. doi:10.1186/s12885-016-2669-3.